UNIVERSITÀ DEGLI STUDI DI NAPOLI "FEDERICO II"

FACOLTÀ DI INGEGNERIA

Dipartimento di Ingegneria dei Materiali e della Produzione

DOTTORATO DI RICERCA IN

INGEGNERIA DEI MATERIALI E DELLE STRUTTURE

XXIII CICLO

EPOXY-BASED ORGANIC-INORGANIC HYBRID MATERIALS BY SOL-GEL METHOD: CHEMICAL TAILORING AND MULTI-SCALE CHARACTERIZATION.

Ph.D. dissertation
by
Filomena Piscitelli

Tutor: Ch.mo Prof. Giuseppe Mensitieri
Egr. Dr. Marino Lavorgna

Coordinatore: Ch.mo Prof. Domenico Acierno

TRIENNIO 2007/2010

Per te mamma

Contents

List of Figures

Abstract

The epoxy resins are organic matrices with excellent heat, moisture, and chemical resistance and good adhesion to many substrates, therefore they are mostly applied in the field of coatings, adhesives, casting, composites, laminates and encapsulation of semiconductor devises. However, due to their low mechanical properties and high coefficient of thermal expansion value compared with inorganic materials, the epoxy resins cannot meet all the requirements, especially for the electrical and structural applications such as epoxy molding compounds. Thus organic/inorganic materials are frequently employed in order to overcome this limitation. Two separated routes can be followed in order to prepare these hybrid/nanocomposite materials, either the addition of preformed inorganic particles, i.e. layered silicates montmorillonite (MMT), or the in situ growth of siloxane clusters, since both MMT and silica particles are commonly used for the reinforcement of epoxy matrix to lower shrinkage on curing, to decrease coefficient of thermal expansion, to improve thermal conductivity and barrier properties, and to meet mechanical requirements. In order to prepare epoxy based hybrids/nanocomposites materials, the sol-gel method is widely used either to modify preformed nanoparticles (i.e. MMT) or to synthesize siloxane clusters. Therefore, in this study, both organo-siloxane clusters and silylated MMT by sol-gel method were used to prepare epoxy-based hybrids/(nano)composites. Considerable attention was given to the use of coupling agents to make compatible the organic matrix and the inorganic particles and improve the interfacial interactions providing chemical bonds between them. In details the surface modification of Na-MMT was done by the silylation reaction with three different aminosilanes, namely:

- 3-aminopropyltriethoxysilane (A1100);
- N-(2-aminoethyl)-3-aminopropyltrimethoxysilane (A1120);
- 3-[2-(2-aminoethylamino)ethylamino]-propyl-trimethoxysilane (A1130).

The effects on the Na-MMT d-spacing of three aminosilanes with different chain length were studied in details by combining experimental and computational techniques. Additionally, different routes in terms of reaction temperature and aminosilane concentration was followed to the aim to correlate the final d-spacing between silicates layers and the process parameters. Therefore, with silylated A1100 and A1120 MMT several epoxy-based composites were prepared employing two different dispersion methods, namely the sonication (S) and a combination of sonication and high energy ball-milling (SB). The effect of both the silylation reaction parameters and the dispersion method on the mechanical and thermal properties of composites was evaluated. It was found that the silylation reaction of Na-MMT with aminosilanes is a valuable approach to enhance the interactions between the epoxy matrix and the fillers by means of both the covalent bonds due to the cross-linking reaction and the hydrogen bonding with the hydroxyl groups of opened oxirane rings. In fact, the silylated MMTs provide composites with improved mechanical properties with respect the pristine Na-MMT in terms of increased Tg and elastic modulus in the rubbery region. This improvements is more evident in the sonicated composites since the combination of sonication and ball milling makes compact the interlayer spacing and partially destroys the original layers structures. Additionally the silylated clay composites highlighted an increased fire resistance compared to the pristine epoxy resin as well as to the Na-MMT composite.

The effect of both the coupling agent and sol-gel process parameters on the organo-siloxane domains morphology and mechanical properties of epoxy-based hybrids was evaluated. It was found that the use of large amount of γ-Glycidoxypropyltrimethoxysilane (GOTMS) as coupling agent represents an available route to tailor the mechanical and thermal properties of epoxy-based hybrids samples. In details, we demonstrated that a suitable choice of functionalized siloxane monomers, amine hardener and reaction conditions leads to the formation of nano-heterogeneous networks with well-organized cage-like structures, up to nearly homogeneous bicontinuous systems. In fact under particular process parameters GOTMS molecules are able to spontaneously arrange to form structures similar to polyhedral oligomeric silsesquioxane POSS units with well established architecture. Therefore, as the siloxane amount increases the number of cages become high enough to make them bonded with the amine hardener Jeffamine D230. Thus the distance between two neighbouring cages will be determined only by the length of the amine hardener which links them. This ordered arrangement highlighted as distance correlation peak in the SAXS patterns profile of hybrids samples at high siloxane content becomes responsible of the improved thermal and mechanical properties of hybrids samples. In particular, the co-continuous organic-inorganic structure is demonstrated with the achievement of films instead of powders in the pyrolysis experiments. It also affects the viscous-elastic behaviour causing both the Tg and the elastic modulus to increase. Moreover the symmetric shape of the loss factor peak speaks in favour of siloxane structure homogenously dispersed throughout the organic matrix. Whereas the increase of the Tg's value highlights the strong evidence of hindrance the polymeric chains movements during the glass

transition. Hence, only the high siloxane content assures the clusters to be bonded highlighting the improved mechanical properties.

To the best of our knowledge it is the first time such cage-like clusters bonded by Jeffamine D230 molecules could be detected assuring the Tg to increase without any phase separation.

Moreover, the effect of two amine hardeners, namely MXDA and Jeffamine D230 on the inorganic network morphology and then on the mechanical and thermal properties of hybrid samples was also evaluated. It was found that MXDA is an organic cross-linker faster than the Jeffamine D230, therefore in the MXDA-based hybrids the organic grows more rapidly than the inorganic network, leaving out the GOTMS siloxanes monomers, as the high content of T0 units in MXDA-based hybrids proved. The presence of T0 units is detrimental in the cured hybrids samples, since it causes a dramatic reduction in Tg values. On the contrary, in the Jeffamine-based samples the Tg is markedly increased with respect to the neat epoxy due to their particular organic-inorganic morphology. In fact the Jeffamine is able to bond two neighbouring siloxane cages building up a co-continuous organic-inorganic structure, as the siloxane amount increases.

Keywords

Sol-gel, organic-inorganic hybrids, MMT-silylation, coupling agent, epoxy-based nanocomposites, siloxane structures, SAXS, GOTMS, aminosilanes.

Acknowledgements

First of all, I would like to sincerely thank the persons who supervised this work, Dr. Marino Lavorgna and Prof. Giuseppe Mensitieri, for their friendship, availability and constructive guidance.

I would like to thank Prof. Jocelyne Galy (INSA de Lyon, Ingènierie des Matériaux Polymère, Laboratoire des Matériaux Macromolèculaires, Villeurbanne, France) who hosted me in her laboratory, for her friendship and precious help during my stage in France.

Moreover, I would like to thank Prof. Sabrina Pricl and Dr. Paola Posocco (Università di Trieste, Italy) for the dynamic molecular simulations.

I express my deep sense of gratitude to Dr. Fernande Boisson (INSA de Lyon, Ingènierie des Matériaux Polymère) and Riccardo Spaccini (Università di Agraria Portici (Na)) for their NMR spectral measurements and valuable discussions.

I would also like to thank Dr. Giuseppina Barra, Dr. Valentina Romeo and Ms. Anna Aliberti, for their assistance in the experimental work. I am very grateful.

I wish to express my sincere gratitude to all my friends of laboratory (in Portici and in Lyon), for the enjoyable time spent together and the interesting scientific discussions.

Finally, a special thanks to my parents, to Gianluca, Lisa and Chiara, for their lovely supporting.

Epoxy-based Organic-Inorganic Hybrid materials by sol-gel method: chemical tailoring and multi-scale characterization.

Aims and objectives of the study

Hybrid materials, that include organic and inorganic components intimately dispersed, have been widely studied in the past but both the in-situ growth and the chemical modification of the inorganic component to improve the interfacial interactions are very recent techniques. The primary aim of this project is to provide the basis for the development of hybrids/nanocomposites epoxy-based, by using the sol-gel method, giving considerable attention to the use of coupling agents in both the modification of preformed filler and the in situ synthesis of siloxane clusters. The ultimate objective is to develop epoxy-based hybrids/nanocomposites with improved thermal and mechanical properties with respect to the neat epoxy system.

The interfacial interaction between the organic matrix and the inorganic filler was allowed by following two routes:

1) Silylation reaction of Na-MMT with different aminosilanes.

2) In situ preparation of siloxane clusters by using TEOS and GOTMS as precursors.

Chapter 1: Epoxy resins

1.1 Properties and Applications

In the field of the organic chemistry, the term "epoxy" is referred generally to molecule's functional groups consisting of oxirane rings:

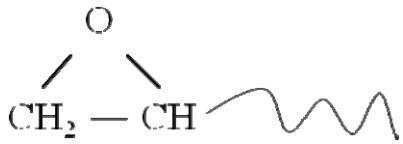

These chemical groups are very reactive. The bond angles C-O-C, O-C-C and H-C-H in ethylene oxide, for example, have been calculated by electron diffraction and by microwave spectroscopy to be ~61°, ~59° and ~116°. The former two values are far below the theoretical bond angles (120°). These strained bond angles in the ring cause the three-membered ring to be unstable, giving rise to the high reactivity of these functional groups. The capability of the oxirane group to undergo a large variety of addition and polymerisation reactions has been exploited for the production of many different thermoplastic and thermosetting epoxy resins. Epoxy resins are compounds containing a minimum of two functional groups so that they can be converted into hard and infusible products through the formation of networks. In order to convert epoxy resins into hard, infusible thermoset networks it is necessary to use crosslinking agents, also referred to as hardeners or curing agents. They may either initiate the curing reactions through their catalytic activity (catalytic hardeners) or may react with the epoxy monomer via a polyaddition/copolymerization reaction. The reactivity

of the epoxy functionality, due to the strained ring, makes possible the use of a wide variety of curing agents. These can have a considerable effect on the properties of the crosslinked products. Epoxy resins were first offered commercially in 1946 and are now used in a wide variety of industries. What makes epoxies superior to other resins, are their mechanical and electrical properties as well as thermal and chemical resistance. These characteristics are responsible for a large range of applications of epoxy resins as protective coatings or in structural applications, such as laminates and composites, tooling, moulding, casting, adhesives and others. In addition to the curing agent in an epoxy resin formulation, other substances may be employed to modify the properties of the polymer. Fillers, for example, are the most common additives used in epoxy formulations to improve mechanical properties, such as modulus and strength. Solvents, diluents, plasticizers and accelerators, sometimes are included in the formulation. One of the most important applications of epoxy resins is for protective coatings, although a decorative function may also be required in some products. Protective coatings account for nearly 50% of the total consumption of the epoxy resins in the USA. These products are durable and provide outstanding adhesion to many substrates (glass, metals, wood). They may also have a very specialised function, such as corrosion prevention or anti-fouling properties. Solvent-resistant and corrosion-resistant films can be obtained, for example, by curing low molecular weight epoxies with aliphatic polyamines. These products are best suited for marine and maintenance coatings where corrosion resistance is required. Higher molecular weight, solid epoxy resins are used in industrial coatings when maximum resistance to solvents and corrosive agents is required, as for example, in appliances, coil primers and in automotive body panels. Powder coatings also represent an important segment of

the market, which continues to increase at a considerable rate. The need to develop more specialised coatings for highly aggressive environments such as nuclear waste management, oil recovery pipes, pulp and paper mills and others, will provide opportunities to sustain the growth pattern of epoxy resins and research in this area. The fastest growth over the past decade has been in laminates and composites. The rapid expansion of the electronics industry has stimulated the demand for high performance thermosetting resins. In this context epoxy reins constitute the workhorse encapsulant and underfill agent in the mounting of chip assemblies to printed circuit boards. Furthermore, the printed circuit itself is generally an epoxy/glass fibre composite. Composites based on advanced epoxy matrices find increasing usage in the transportation industry, particularly in very specialised areas such as in military and commercial aircraft industry, in aerospace applications, in the marine and automotive sectors, that is whenever high strength-to-weight ratio and outstanding resistance to extreme service conditions are required. For instance, epoxy-based composites are the materials of choice in airframe construction: approximately 60 % of the total external surface area, or 19 % of the total weight of the US Navy aircrafts consists of an epoxy- carbon fibre composite [1] The presence of epoxy resin, in these restricted but highly profitable segments of the market, is growing at a steady rate, and is expected to increase further in the near future.

1.2 Hardeners

Among the wide variety of hardeners available nowadays, the main types are: a) aliphatic amines, b) aromatic amines, c) acids and anhydrides.

A) The first group includes PACM (para-aminecycloexanemethane), EDA (ethylenediamine), diethylene triamine (DETA), triethylenetetramine (TETA), the Jeffamine D230 and Metaxylilene diamine (MXDA).

The structures of the mentioned curing agents are shown below.

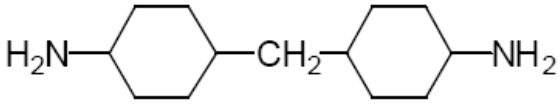

PACM

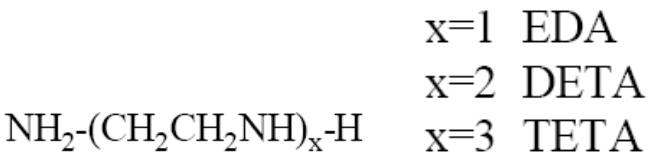

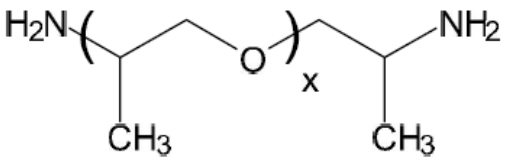

$x \approx 2.5$

The Jeffamine D230 is a polyetheramine characterized by repeating oxypropylene units in the backbone. As shown, the Jeffamine D230 is a bifunctional primary amine with an average molecular weight of about 230.

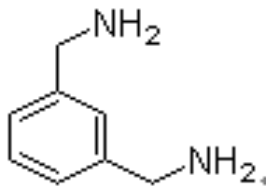

The MXDA is widely used as epoxy resin curing agent for civil engineering adhesives, industrial maintenance coatings for metal, coating for self-leveling industrial flooring and so on.

It is argued that the reaction rate of primary and secondary aliphatic amines is faster than cycloaliphatic and aromatic poly-amines, particularly at room temperature [2].

The simplified reaction between amine and epoxy resins is shown below.

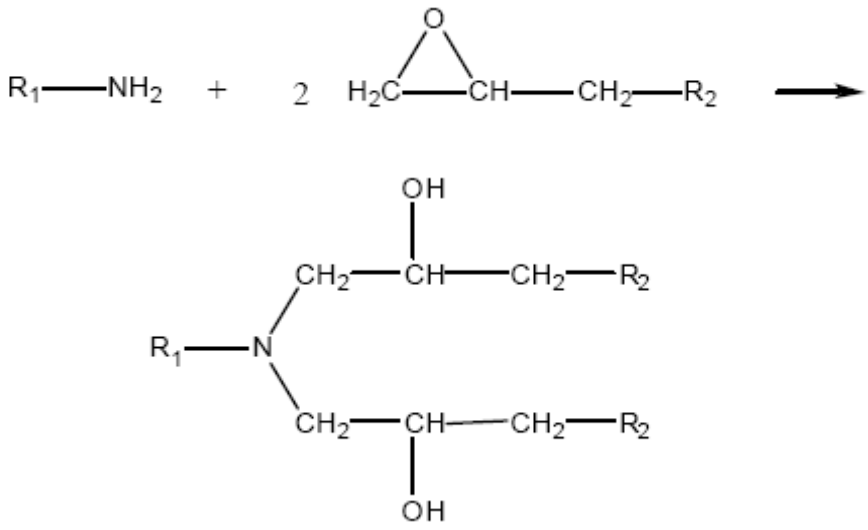

When the epoxy and the amine compounds are multifunctional, the resulting product is a three-dimensional network, as shown below.

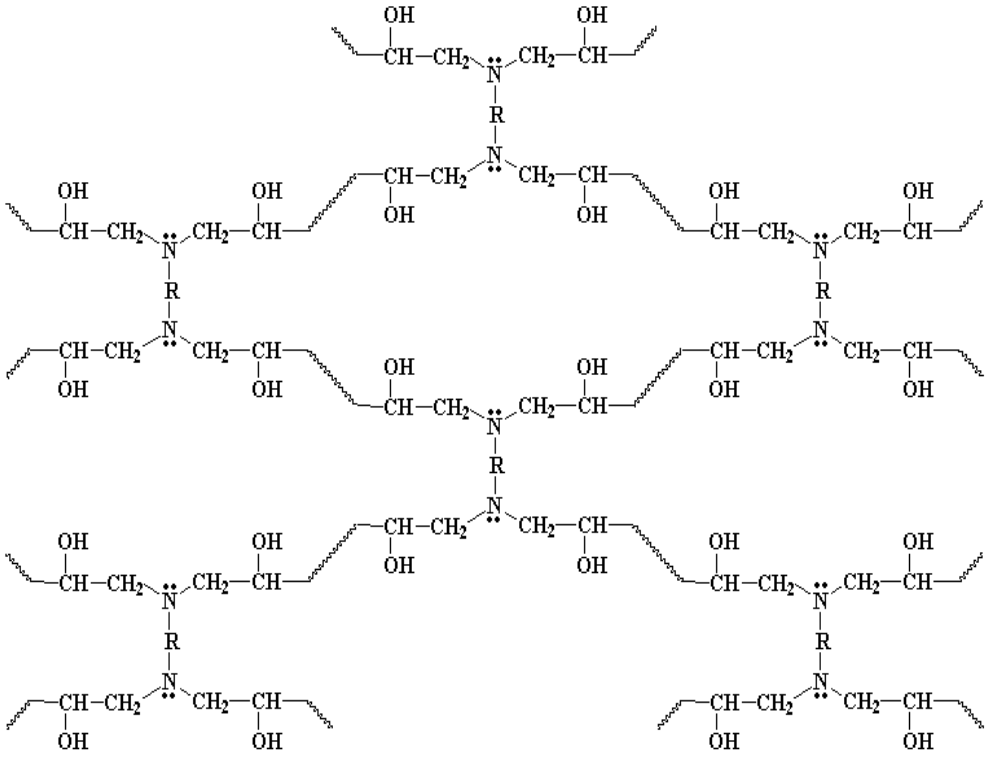

It is well known that the presence of hydroxyl-containing compounds considerably promotes the interactions of epoxy groups with amines and other nucleophilic reagents [3-6]. The reaction proceeds through a trimolecular transition state initially suggested by Smith [7-8].

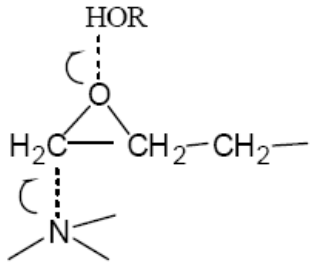

Hence, the hydroxyl groups generated during cure accelerate the reaction, which accounts for the autocatalytic nature of the curing process. Hydroxylic accelerators or hydrogen donors capable of catalyzing the amine epoxy reaction in decreasing order of efficiency are: -OH (Ar » PhCH2 > RCH2 > H); - CO2H; -SO3H; - CONH2; - SO2NH2. Ethylenediamines are highly reactive due to their unhindered polyfunctional nature [3, 9-12], and give rise to tightly cross-linked networks owing to the short distance between the active sites. For this reason, the cured resins exhibit excellent solvent resistance and mechanical strength, but limited flexibility. The low molecular weight of these hardeners is responsible for low viscosity, high vapor pressures, making these compounds corrosive, irritant to the skin and generally toxicologically dangerous. These products are also hygroscopic and have poor miscibility with epoxy resins [11-12]. A technique to overcome these limitations, consists in reacting the ethylenediamine with carboxylic acids. Condensation of the higher homologues of the ethylenediamine series with dimerised or polymerised unsaturated fatty acids, leads to the widely used family of curing agents known as polyamides [14-15]. They exhibit different molecular weights, physical form, amine content and reactivity, but all have low volatility. By adjusting the system's stoichiometry, the final properties of the cured resins may be varied from hard and rigid at below stoichiometry to flexible and soft around or above stoichiometry. The disadvantage of these curing agents is their reduced reactivity, particularly at room temperature, and their tendency to give rise to greasy products because of their exudation to the surface. Addition of tertiary amines, phenolic amines or co-curing agents can help to reduce the severity of these effects [14].

B) To the second group, the aromatic polyamines [16-17], belong a very important class of hardeners for epoxy resin. Examples are shown below:

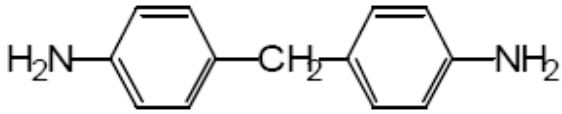

DDM - 4,4'-diaminophenylmethane

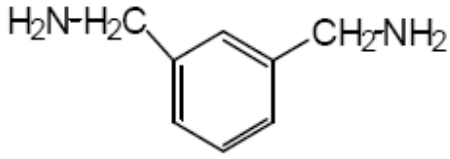

MDP - Meta-phenylenediamine

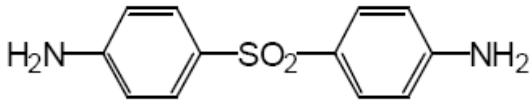

DDS - 4,4'-diaminophenylsulfone

These are less basic than aliphatic or cycloaliphatic polyamines and react slowly with the oxirane ring. Therefore they are used for curing processes at elevated temperatures (heat-cured hardeners) and, even in these conditions, require long periods to obtain the best results [3, 18-19]. However, all resin systems cured in this way provide excellent resistance to a wide variety of chemicals, including organic and inorganic acids, coupled with an outstanding temperature stability, due to the high values of the glass transition temperature. Therefore these hardeners are preferred whenever the materials are subjected to severe conditions

during their service life. Most of the aromatic amines are solids at room temperature and, are transformed to liquid substances by melting or by the formation of eutectic mixtures or less frequently, by blending with liquid cycloaliphatic polyamines [3, 10-12, 16, 20]. In this class of hardeners, MPD provides the highest cross-link density and the best solvent resistance [16]. The low polarity of DDM makes it an excellent curing agent for electrical and electronic applications. In fact it imparts to the resin elevated electrical insulation properties, combined with high retention of mechanical properties, even under conditions of high humidity [17]. DDM is still the most widely used of the aromatic amines, but it has been recently identified as an animal carcinogen and potential human carcinogen [21] and, for many applications is being replaced by other types of curing agents. 4,4'-DDS has the main advantage of providing the highest temperature stability, it has become the standard curing agent for specialised epoxy resins in high temperature tooling and high performance military and aerospace laminating applications [10-11, 22-23]. 3,3'-DDS, despite its reduced heat resistance compared with its 4,4', analogue, has been adopted in certain aerospace laminating applications because of its enhanced honeycomb peel strength [3, 12].

C) Another class of curing agents for epoxy resin consists of carboxylic acids and their anhydrides. They react at high temperatures and require prolonged periods to reach completion, but provide resins with good dimensional stability and insulating and optical properties [11-12, 24-26]. The curing mechanism is more complex than that of the amines, since a number of competing side reactions may occur, especially in the presence of accelerators. The uncatalysed reaction mechanism is initiated by the opening of the anhydride ring by a

hydroxyl group present on the epoxy backbone, with the formation of a half-ester carboxylic acid group. This functionality reacts with an epoxy group to form a di-ester alcohol, which can continue the polymerization process either by esterification with another anhydride group or by etherification with an epoxy ring. The latter reaction is favored and, indeed, in normal conditions only 0.85 equivalents of anhydride are required to provide optimum cross-link densities and properties. Lewis bases such as tertiary amines and imidazoles are widely used as anhydride accelerators [27-28]. The mechanism involves the anhydride ring opening with the formation of internal salts (betaines), which initiate the curing process. The resulting carboxylate ions react with an epoxy group to form alkoxide ester, which in turn react with further anhydride molecules to form carboxylate anion functional esters. Iteration of this sequence leads to the formation of a cross-linked polyester [29-31].No etherification reactions are involved in this mechanism. Lewis acids such as BF3-amine complexes, are also catalysts for the epoxyanhydride reaction, although a fully satisfactory mechanism remains to be proposed. The most important dicarboxylic acid anhydrides used as epoxy hardeners are cycloaliphatic, with the notable exception of phthalic anhydride (PA). PA is the least expensive but has the disadvantage of being difficult to handle due to its tendency to sublime; its hydrogenated derivatives hexahydrophthalic anhydride (HHPA) and tetrahydrophthalic anhydride (THPA) are used extensively for electrical applications [3, 11-12, 20].

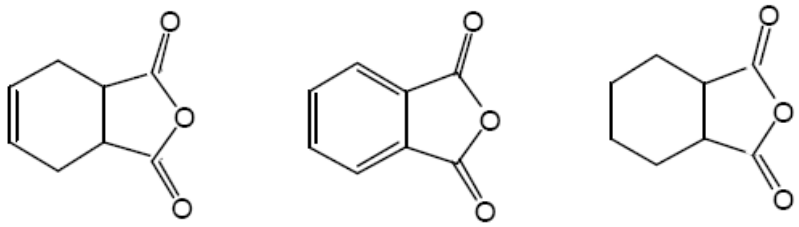

THPA PA HHPA

HHPA, is a low melting point liquid which does not sublime and forms low viscosity liquid eutectic mixtures with the epoxy resins. THPA, gives products with properties very similar to HHPA, but darker in color. The methyl derivatives of the above compounds also find applications in filament wounding pipe manufacture, electrical casting, encapsulation and impregnation.

1.3 Types of epoxy resins

This very important class of materials was first discovered by P. Castan [9] in Switzerland and, independently, by S. Greenlee [32] in the United States in the early 1940s. The new materials immediately showed very interesting characteristics and soon after their discovery were patented and commercialised. The earliest epoxy resins introduced on the market were the reaction products of bisphenol A and epichlorohydrin and this is still the major route for the manufacture of the resins, represented by the formula below, available today:

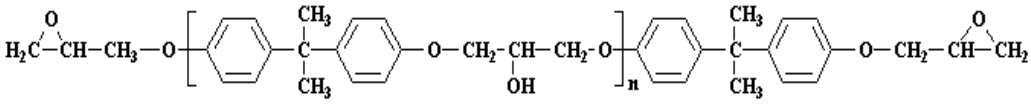

A very large number of hydroxyl compounds have been reacted with epichloridrin to synthesise new epoxy resins but, the most important phenol used today remains bisphenol A, originally studied by Castan. The more important precursors currently in use are reported below. Particularly interesting are the halogenated phenolic compounds that provide improved flame resistance.

1. Bisphenol-A (BPA)

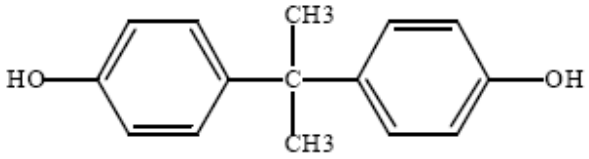

2. Bisphenol-F

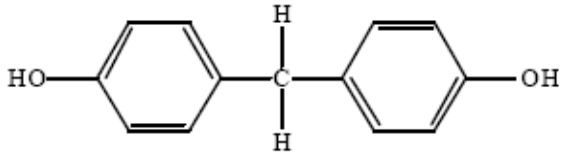

3. Bisphenol-S

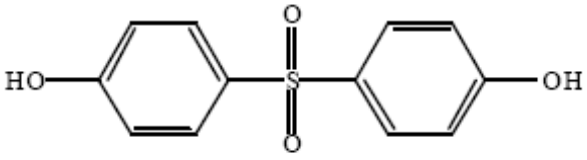

4. Resorcinol

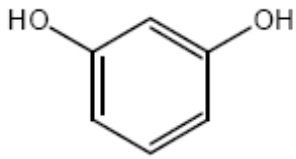

5. Methylolated phenol

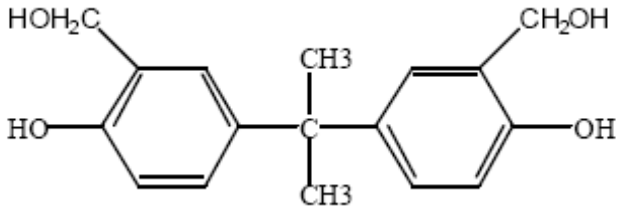

6. Novolacs

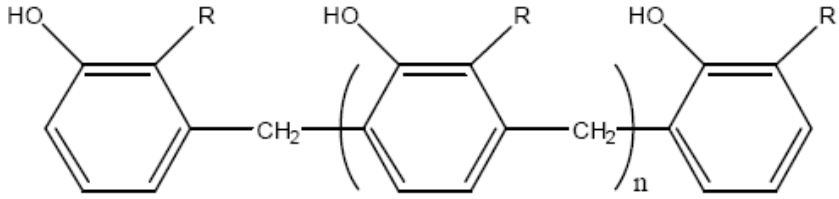

7. Brominated and fluorinated phenols

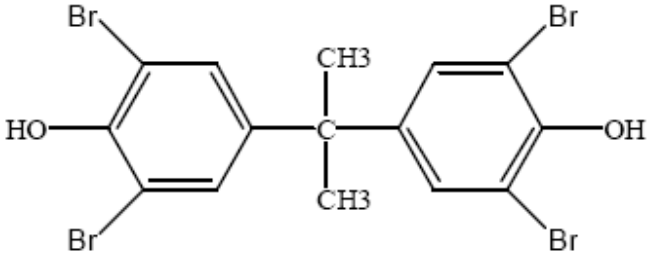

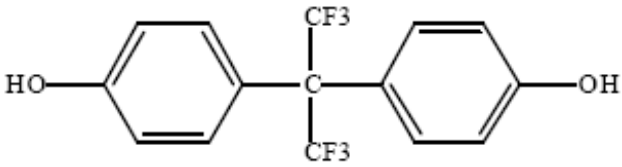

Molecules bearing the amino groups are also reactive towards the epichlorohydrin and have been tested as precursors for epoxy resins. In particular, the resin produced by one of these compounds, 4,4'diamino-diphenylmethane readily shows very interesting properties and has now gained a prominent position in industry [3, 11-12]. The excellent properties of this resin are ultimately due to its high functionality (four epoxy groups per monomer) which produce, upon curing, a very tight network, with an extremely high cross-link density. The structure of this resin is:

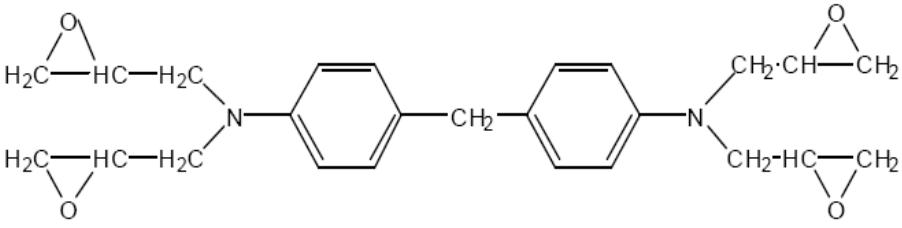

Tetraglycidyl-diaminodiphenylmethane (TGDDM

1.4 References

[1] J. P. Halpin; P. P. Pandolfini; P. J. Bierman; T. J. Kistenmaker; L. W. Hunter; J. S. O'Connor; D. Jablonski; *APL Tech. Dig.,* 18, **1997**, 33.

[2] B.A. Rozenberg; *"Kinetics, T hermodynamics and Mechanism of Reactions of Epoxy Oligomers with Amines"* in *Epoxy Resins, Advances in Polym. Sci. Ser.,* K. Dusek Ed., Springer-Verlag, Berlin, **1986**.

[3] H. Lee; K. Neville; *Handbook of Epoxy Resins,* McGraw-Hill, New York, **1990**.

[4] B. A. Rozenberg; N. S. Enikolopyan; *Polymer,* 25, **1959**, 215.

[5] C. A. May; Y. Tanaka; *Epoxy Resins. Chemistry and Technology,* Decker, NewYork, **1973**.

[6] R. E. Parker; N. S. Isaacs; *Chem. Rev.,* 59, **1959**, 737.

[7] I. T. Smith; *Polymer,* 2, **1961**, 95.

[8] L. J. Gough; I. T. Smith; *J. Appl. Polym. Sci*., 5, **1961**, 86.

[9] P. Castan; *Swiss Patent* 211, 116, **1940**.

[10] J. K. Gillham; *Encyclopaedia of Polymer Science and Technology,* 2nd edn., John Wiley, New York, **1986**, pp. 519-524.

[11] C. A. May; Ed., *Epoxy Resins, Chemistry and Technology,* 2nd. edn., Marcel Dekker Inc., New York, **1988**.

[12] B. Ellis; Ed., *Chemistry and Technology of Epoxy Resins,* Blackie Academic and Professional, Glasgow **1993.**

[13] J. C. Cowan; *US Patent* 2, 450, 940, **1948**.

[14] V. J. Brytus; *Coatings Technology,* 58, **1986**, 44.

[15] F. Richardson; *Pigment and Resin Technology,* May 41-43, **1973**.

[16] J. Philipson; *US Patent 2*, 891, 927, **1959**.

[17] N. V. Seeger; E. E. Fauser; *US Patent* 2, 683, 730, **1954**.

[18] N. St. John; A. G. George; *Polymer,* 33, **1992**, 2679.

[19] L. Xu; J. R. Schlup; *Appl. Spectrosc.,* 50, **1996**, 109.

[20] Ciba-Geigy; *Araldite for Surface Coatings,* Laboratory Manual, Ciba-Geigy Plastics, Cambridge, **1988**.

[21] Aldrich Catalog of Chemicals, **1997**.

[22] R. J. Morgan; E. T. Mones; *J. Appl. Polym. Sci.,* 33, **1987**, 999.

[23] J. Mijovic; J. Kim; J. Slaby; *J. Appl. Polym. Sci,* 29, **1984**, 1449.

[24] J. Bàrtova; K. Bily; P. Marek; *Crosslinked Epoxies,* Sedlacek, B., Kahovec, J., Eds., pp.557-562, de Gruyter, Berlin **1987**.

[25] W. Fisch; W. Hofmann; J. Koskikallio; *J. Appl. Chem.,* 6, **1956**, 429.

[26] W. Fisch; W. Hofmann; *Makromol. Chem.,* 44, **1961**, 8.

[27] R. F. Fischer; *J. Polym. Sci.,* 44, **1960**, 155.

[28] Y. Tanaka; H. Kakiuchi; *J. Polym. Sci.,* A2, **1964**, 3405.

[29] Y. Tanaka; H. Kakiuchi; *J. Appl. Polym. Sci.,* 7, **1963**, 1063.

[30] J. Luston; Z. Manasek; M. Kulickova; *J. Macromol. Sci., Chem. Ed.*, 12, **1978**, 995.

[31] M. K. Antoon; J. L. Koenig; *J. Polym. Sci.,* 19, **1981**, 549.

[32] S.O. Greenlee; *US Patent,* 2, 717, 885, **1955**.

Chapter 2: Sol-Gel Chemistry and Process background

2.1 Introduction

Sol-gel materials encompass a wide range of inorganic and organic-inorganic hybrid materials which share a common preparation strategy: the sol-gel process. It involves the generation of colloidal suspensions, “sols”, which are subsequently converted to viscous gels and then to solid materials. In details, a sol is a dispersion of colloidal particles suspended in Brownian motion within a liquid, whose dimensions, ranging between 1 and 1000 nm, are small enough to ignore the gravity force. The interactions between the particles are dominated by short-range forces (i.e. Van der Waals and superficial charges). Through the polycondensation the sol is converted into a gel, which is a continuous solid structure containing liquid phase. Sol-gel process represents a valid and environmentally sustainable technology to produce bulk glasses or ceramics at low costs without melting of the inorganic precursor phases. It is similar to an organic polymerization in which small molecules form polymeric structures by the loss of substituents. The fact that small molecules are used as precursors for the formation of the crosslinked materials implies several advantages, for example a high control of the purity and composition of the final materials and the use of a solvent based chemistry which offers many advantages for the processing of the materials formed. Contrary to many other procedures used in the production of inorganic materials this is one of the first processes where ambient conditions were applied to produce ceramics. The control over the

preparation of multicomponent systems by a mild reaction method also led to industrial interest in that process [1].

The sol-gel reaction proceeds by two fundamental chemical reactions: the hydrolysis of the alkoxides precursors to introduce a reactive hydroxyl group on the metal and their condensation to form Si-O-Si bonds. These two reactions can be catalysed by acids or basics. In details, the hydrolysis reaction of metal alkoxides M(OR)m where M represent Si, Zr,…etc atoms involves the replacement of alkoxy groups with hydroxyl groups:

$$M(OR)_m + (m-x)H_2O \longrightarrow M(OH)_{m-x}(OR)_x + (m-x)R(OH)$$

For network formation it is necessary that the hydroxyl groups condense with each other eliminating water according to the scheme:

$$\equiv M-OH + \equiv M-OH \longrightarrow \equiv M-O-M\equiv + H_2O$$

The previous two reactions occur simultaneously. Furthermore the presence of partially hydrolyzed molecules allows the reactions between ≡MOH and ROM≡ groups, releasing alcohol instead of water, according to the following scheme:

$$\equiv M-OH + \equiv M-OR \longrightarrow \equiv M-O-M\equiv + ROH$$

Since alkoxides M(OR)m are not miscible with water, the hydrolysis reaction is allowed to occur by using a common solvent, usually the parent alcohol ROH. Then the oxo-metallic network progressively grows from the solution, leading to the formation of oligomers, oxopolymers, colloids (sols or gels), and a solid phase. These reactions can be described as SN2 nucleophilic substitutions and the chemical reactivity of metal alkoxides towards hydrolysis and condensation depends mainly on the electronegativity of the metal ion and the ability to increase its coordination number [2-3]. Silicon has a low electrophilicity and

remains four-coordinated in the monomeric Si(OR)4 alkoxide precursors as well as in silica. Thus, silicon alkoxides are not very reactive. Hydrolysis-condensation reaction rates must be increased using catalyst (acidic, basic or nucleophilic activation). On the other hand, non-silicate metal alkoxides, including transition metals, lanthanides and aluminium are much more reactive than silicon towards nucleophilic reactions. This high chemical reactivity is due to lower electronegativity of the metal as compared to the silicon, and the metal atom's ability to exhibit several coordination states [4]. The coordination expansion spontaneously occurs when the metal alkoxide reacts with water and direct addition of water to transition metal alkoxide leads to uncontrolled precipitation of polydispersed oxide powders. An appropriate choice of the alkoxide, especially the steric hindrance of the alkoxy groups, and of the solvent allows the control of the reactivity towards hydrolysis condensation reactions of M(OR)4 alkoxides. Indeed, the coordination expansion of the metal occurs by solvation or alkoxy bridging leading to less reactive oligomeric species when the steric hindrance effects are limited and when the solvent such as the parent alcohol can solvate the metal [4-5].

The silicon-based sol–gel process is probably the one that has been most investigated; therefore the fundamental reaction principles are discussed using this process as a model system. There are several silicon alkoxides (alkoxysilanes) commercially available, but the most frequently used is tetraethoxysilane (TEOS). The starting sol-gel mixtures of TEOS typically consist of the alkoxide, water and a solvent, often ethanol. To the aim to control the hydrolysis and condensation reactions rates, either an acid or a base must be used as catalyst [2]. The silicon-based sol–gel processes are the predominant process also in the formation of hybrid materials, because of the simple

incorporation of organic groups into the inorganic network using organically modified silanes. Si—C bonds have enhanced stability against hydrolysis in the aqueous media usually used, which is not the case for many metal–carbon bonds, so it is possible to easily incorporate a large variety of organic groups in the network formed. Therefore, in addition to tetralkoxysilanes, other categories of sol-gel precursors include organofunctional alkoxysilanes. Alkyl-substituted alkoxysilanes or organoalkoxysilanes [2] are useful to modify the polymer network because of the presence of the non-hydrolysable groups. They are also used when the introduction of organic matter within the inorganic network is required. These silanes, known as coupling agents, were originally introduced as connectors between organic resin matrices and mineral reinforcement, namely fibres and particulates, to improve bond strength and chemical resistance [6]. The polymer-substrate bond is achieved on one side via the alkoxy component, which attaches the molecule to the mineral surface through condensation with pendant silanols and, on the other side, through interactions of the organofunctional group with the polymer. The occurrence of copolymerisation reactions at the interphase leads to the formation of interpenetrating networks (IPNs) [6-7]. To enable the coupling agent to exert its function, the nature of the organofunctional group is varied according to the chemical nature of the matrix and the service conditions. For example, an epoxy functionalised silane can be used in combination with epoxy resins, while a methacrylate silane is suitable for use with an unsaturated polyester resin [8]. Versatile coupling agents, such as aminosilanes, on the other hand, can be used with several polymers including epoxy resins.

Therefore, a large number of variables influence the amount of hydrolyzed and condensed species and then the structural evolution of silicate polymers: water

content, reaction time, nature of the alkoxide, solvent, pH and thermal history. As a matter of fact, the choice of process parameters affects the microstructure of the produced gels. Moreover, the sol-gel process involves several stages:

- ✓ Hydrolysis of the precursors with the formation of hydroxide species;
- ✓ Condensation with the formation of oxide species;
- ✓ Gelation with the formation of a "spanning cluster" yielding a network which entraps the remaining solution;
- ✓ Ageing with the formation of further crosslinks which change the structure in pore sizes and pore wall strengths;
- ✓ Drying with the loss of solvent and the associated development of capillary stress;
- ✓ Densification with the collapse of the open structure and formation of a dense material.

Any of these phases has a great influence on the properties of the resulting material and the great number of variables involved makes the control of the whole process still very empirical. Therefore a detailed knowledge of the chemical mechanisms, which permits the control of the properties of the final amorphous material at a molecular scale and to synthesize defined structures, is a great challenge for the material scientists.

2.2 Hydrolysis and condensation mechanism

The hydrolysis reaction involves a nucleophilic attack of the water molecule to the central silicon atom of the alkoxysilane, followed by a proton transfer from H2O to an alkoxy group OR, and the exit of an alcohol molecule which is

substituted by the OH group. Often acid or basic catalysis is necessary because of the slow reaction rate of the hydrolysis process.

The hydrolysis mechanisms related to the action of acidic and basic catalysts for tetraethoxysilane were suggested by Aelion et al [9] and successively elaborated by Keefer [10].

In the basic mechanism, the reaction proceeds through a nucleophilic substitution.

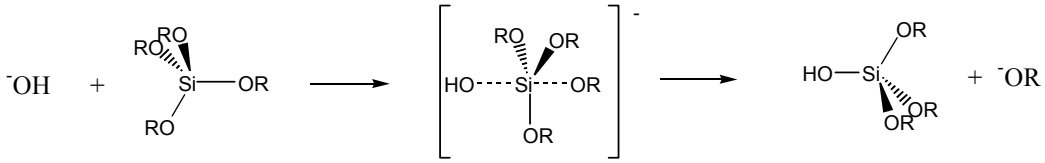

Figure 1 - Mechanism of base-catalysed hydrolysis by nucleophilic substitution (R = H, Et or Si(OR)3)

The hydroxide nucleophile coordinates with the silicon, forming a transient trigonal-bipyramid intermediate; the alkoxide group positioned at the opposite site leaves the intermediate and reacting with water leads to the renewal of the catalyst.

In the acidic catalyzed mechanism the hydrolysis reaction takes place as an electrophilic reaction. The hydronium ion approaches the alkoxysilane molecule to form an activated complex. Afterwards the water molecule becomes the entering specie while one alkoxide group positioned at the opposite side becomes the leaving groups as alcohol.

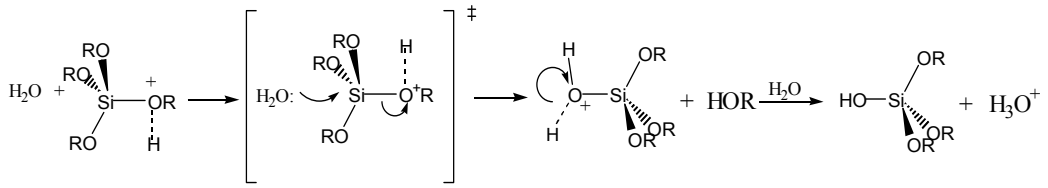

Figure 2 - Mechanism of acid-catalysed hydrolysis by electrophilic reaction

The condensation reaction takes place as soon as some hydrolyzed precursor molecules are present in the solution and it occurs at the same time and with the same reaction path as the hydrolysis, depending on the quantity of water and catalyst present in solution.

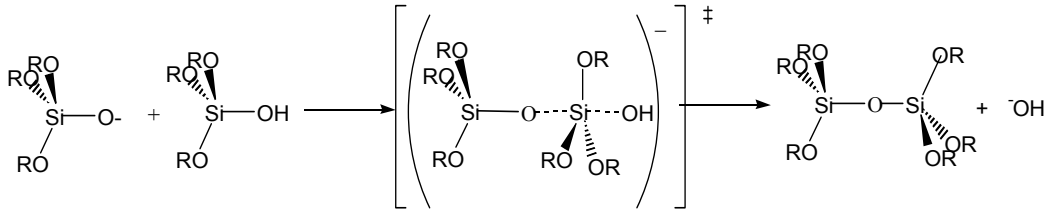

Figure 3 - Mechanism of condensation by nucleophilic substitution.

Condensation in the pH range 3-12 firstly proposed by Iler [11] is a nucleophilic substitution reaction, where a protonated silanol is attacked by a deprotonated silanol (the nucleophile), forming a ≡Si-O-Si≡ bond and displacing a hydroxyl in the process.

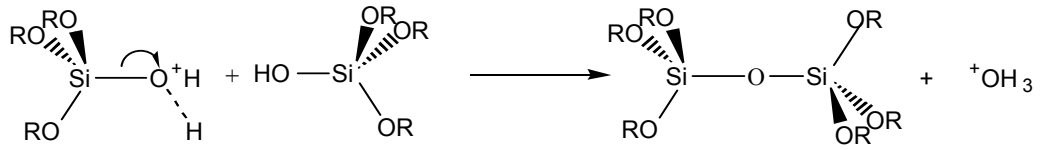

Figure 4 - Mechanism of condensation by electrophilic substitution.

In acid conditions (pH<3), the mechanism of condensation changes from nucleophilic to electrophilic. The SiOH group available is protonated and becomes the electrophile.

All the hydrolysis and condensation reaction showed are reversible.

2.3 Factors affecting hydrolysis/condensation reactions

2.3.1 Nature of catalyst

The nature of the catalyst determines the relative rates of hydrolysis and condensation reactions and therefore it affects the typology of gel in terms of open network structure or dense network structure.

Aelion et al [9] reported that the rate and extent of alkoxide hydrolysis are greatly influenced by the dissociation constant and concentration of the acid or base catalyst. In the presence of HCl the hydrolysis rate is proportional to the concentration of the acid. On the contrary, they found very low rates of reaction with weak acids.

Regarding the hydrolysis under basic conditions with NaOH catalyst, Aelion et al.[9] reported a first order kinetics with respect to TEOS in dilute solution, although at higher concentrations of monomer the reaction was complicated by the formation of insoluble polysilicates. Weaker bases such as NH4OH and pyridine were only effective as catalysts at higher concentrations. Also, in comparison to acid catalyzed hydrolysis, their results revealed a more pronounced dependence of the base catalyzed hydrolysis on solvent nature.

Matejka et al. [12] have studied the effect of catalysts belonging to three different classes of catalysts: acid, neutral and basic, TSA (p-toluensulphonic acid monohydrate), DBTDL (dibutyltindilaurate) and BDMA (benzyldimethylamine) on the condensation of silanes. The catalyzed TEOS polymeric structures were studied with SAXS. Basic catalysts lead to typical

compact structures, while catalysis by TSA and DBTDL (pH neutral) lead to more homogeneous structures and more optically transparent gels, similar to those produced under acid catalysis. This effect is a result of a relatively slower hydrolysis and monomer consumption with respect to the condensation. The monomer is available for condensation even at a late stage, in contrast to the acid catalysis where it is consumed very quickly.

2.3.2 pH of solution

In reactions under basic conditions the hydrolysis steps successive to the first one are faster, since the silanols ((OR)3SiOH) obtained replacing the alkoxy groups on the silicon with hydroxyl group are more acidic and so more prone to be attacked by hydroxide ions [13]. The overall kinetics of the basic catalyzed process are ruled by the formation of the first silanol because this is the slower step. The silanols just generated are immediately used up by fast condensation, leaving no intermediates in the reaction medium [14]. The result of basic catalysis is an aggregation (monomer-cluster) of highly crosslinked sol particles to form gels with large pores between the interconnected particles.

Under acid-catalyzed conditions the hydrolysis reaction is speeded up more efficiently than the condensation reaction producing weakly cross-linked or linear polymers. Condensation involves the attack of silicon atoms carrying protonated silanol species by neutral SiOH nucleophiles. The most basic silanol species are those contained in monomers or weakly branched oligomers so condensation is limited and a bushy network of weakly branched polymers can be obtained.

2.3.3 Water

According to the theoretical models proposed by Bechtold et al. [15] the minimum molar ratio water/alkoxide (r) required for hydrolysis to go to completion is 2. This ratio assures the formation of silicate network Si(O4)1/2, completely void of hydroxyl groups. Otherwise Yoldas [16] showed that with r equal to 4 orthosilicic acid is formed, which has a very large intermolecular separation, and therefore is unable to polymerize.

In practical terms, excess of water ($r > 2$) is expected to cause an increase in the rate of hydrolysis compared to condensation [17]. In acidic conditions, hydrolysis predominates and goes to completion, leading to a decrease in the content of intermediates and to the development of a more cross linked polymer [18]. This behaviour justifies the formation of chain-like aggregates because under low water conditions the condensation of hydrolyzed monomer (whose product is water) is inhibited by a shift of the condensation equilibrium in favour of the reverse reaction, consequently encouraging further hydrolysis [19].

The effects of water in basic conditions are not dissimilar to those for acidic conditions. An excess of water affects hydrolysis more than condensation.

2.3.4 Solvent

An important factor in sol-gel reactions is the type of solvent used. It affects the rates of hydrolysis and condensation and, consequently, also the structural development of the polysiloxane domains. Several types of solvents have also been used such as *polar protic*, (H2O, methanol and formamide), *polar aprotic*, (DMF, THF and acetonitrile), and *non-polar aprotic*, (dioxane).

The polar aprotic solvents inhibit the condensation reactions by deactivating the nucleophile through H-bonding and salvation [20]. Non-polar aprotic solvents, on the other hand, cannot impede the condensation process because they offer no possibilities of either H-bonding or solvation on the negatively charged ions.

Alcoholic solvents, such as ethanol (EtOH) and propanol (PrOH) form azeotropic mixtures with water. The azeotrope, which has a higher vapour pressure than each single component, evaporates first and leaves behind either water or alcohol (depending on their initial amount). If the alcohol is in excess, silanols re-esterify and the water produced is readily removed as part of the azeotrope, thus driving the reverse alkoxylation reaction to completion. Therefore, because the hydrolysis reaction is thermodynamically favourable, the composition of the sol-gel solution should be optimized in order to ensure that water (and not the alcohol) evaporates last [21].

2.3.5 Alkoxide typology

Aelion et al. [9] determined that the rate of hydrolysis decreases with the increasing of the length of the alkyl radical explaining the result as an increase of steric impediment of the longer alkoxy. Condensation is also affected by the nature of the alkyl radical, since the mobility of intermediate species having long non-hydrolysed groups attached to them, is reduced.

The network structure depends strongly on the *functionality* of the monomer. This parameter represents the number of alkoxide groups which are potentially leaving groups. If, indeed, the functionality is equal to 2 such as in structures like $R'_2Si(OR)_2$ only linear or ring aggregates are formed. When the functionality is equal to 1 as in structure like R'_3SiOR it is impossible to produce chain aggregates because the monomers behaves as chain terminators. To obtain high

density network it is important to have monomers with functionality equal to 3 or 4. In this case through the condensation process it is possible to connect densely the monomers and generate colloidal aggregates.

2.4 Aggregation and growth of polyalkoxysilanes

In the reports of Keefer [13], the silicates formed under either basic or acid conditions, are described as fractal in nature. Fractals are structures resulting from random growth processes. They have dilational symmetry and because of this, their appearance remains unchanged after magnification. In mass fractals, the volume occupied grows faster than the mass that generates it. Surface fractals, on the other hand, are highly complex structures with a surface area that increases with mass at a faster rate than normal (Euclidean) objects. Fractal dimensions, in silicate systems, may be determined by X-ray, neutron or light scattering measurements, while the growth of domains can only be simulated by computer models. Typically, fractal geometry describes silica structures on the basis of the relative rates of hydrolysis and condensation [13]. For base-catalyzed reactions, using the *poisoned Eden* model (a reaction-limited monomer-cluster aggregation model), structures range from non-fractal (at high water concentrations), to colloidal (with fractally rough surfaces), to true fractal (polymeric) (at lower water concentrations). In acid-catalyzed systems, where the small particles involved tend to form branched polymers that grow by polymer-polymer interactions, the resultant structures are shown to be true fractal by the *RLCA* (Reaction Limited Cluster-cluster Aggregation) model. The idea that silicic acid monomer can polymerize into siloxane similarly to organic polymers, is rejected by Iler [11]. His classical theory of polymerization of silica [11] involves polymerization of the monomer to first form particles, which then

grow and coalesce with other particles to form weak-lace type of structures. At concentrations above the solubility limit of silica (100-200ppm), $Si(OH)_4$ polymerizes by condensation at rates controlled by either the concentrations of OH^- or H^+ ions in the way discussed previously. The tendency to form ≡Si-O-Si≡ bonds at the expense of silanol groups, leads to the formation of cyclic structures and their subsequent growth by addition of monomer into large three-dimensional polymers. These internal condensation reactions produce compact entities with pendant silanol groups for subsequent growth. Particle size at this point is important because it determines the radius of curvature of the surface that controls the solubility of the particle. Solubility is also determined by the degree of condensation within the particles. The largest and most condensed particles, survive and continue to grow by the Ostwald ripening mechanism. At pH > 7, where silica dissolution and redeposition rates are high, this activity leads to particles of colloidal dimensions. At high pH up to 10.5 and moderate solution concentrations, negative charges on particles cause mutual repulsion and growth *without* aggregation. This is in agreement with results of Aelion et al. [9]. High temperature has a similar effect, since accelerated growth leads to a small number of larger-sized particles [11, 22]. Charges may be reduced by the addition of a coagulant (for example, Na^+ ion of a salt such as Na_2SO_4 or NaCl) in which case aggregation can occur. At too high salt concentrations, precipitation is observed. At low pH, where the rate of polymerisation (and depolymerisation) is slow, particles are very small in size and further growth is discouraged. Under these conditions, the tendency to form networks rather than oversized particles is more pronounced. This effect is due to the low ionic charge on particle surfaces, which allows higher rates of interparticle collisions. Therefore, at a 'high' concentration of SiO2 >1%, aggregation of very small

particles is possible. At pH levels ranging from 5 to 6, there is a rapid simultaneous formation and aggregation of particles, so that the networks formed contain both oligomeric and polymeric species [11]. The above processes and the effects of pH are shown in Figure 5.

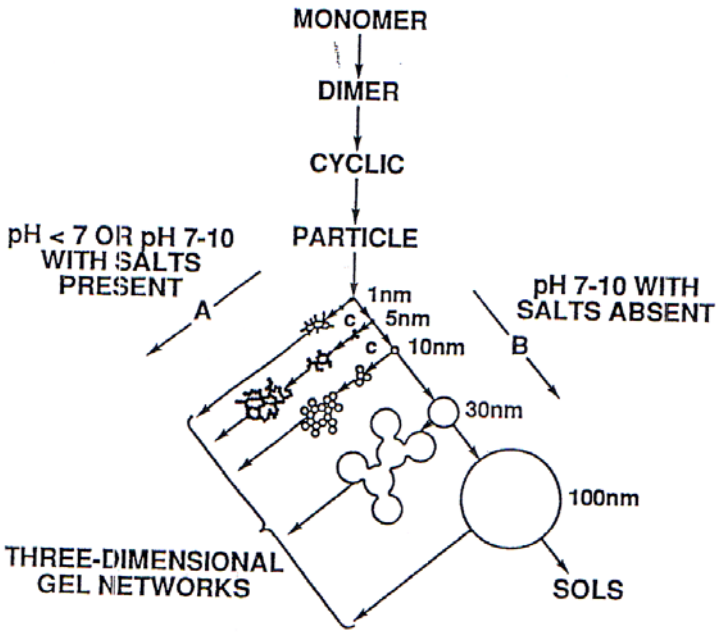

Figure 5 - Schematic representation of polymerization behavior of silica by sol-gel method [11]

Aggregate particles attach to each other through siloxane bonds. These bonds result from the condensation of surface silanol groups and Si-O- ions at the point of contact between the particles. The negative curvature at the point of interparticle contact accounts for the very low local solubility. This pushes the process of further bonding through fast monomer deposition [11]. The hydrogen bond plays an important role because of its link between silanol and siloxane groups of the particle surfaces, directly or through water molecules. H-bonding will be present even up to advanced stages of aging and desiccation [23]. The

process of chain and branch forming is only present in those systems that prevent excessive growth by keeping repulsive charges to low levels. At pH 2, the overall net charge is zero (due to the occurrence of the isoelectric point of silica), but the polymerization is still possible. It is hypothesized by Iler [11] that the negative charge on Si-O- ions, presumably involved in the initial reactions between surface species, is counterbalanced by the positive charge on H+ ions present in the polymerising medium.

2.5 Gelation

The gelation occurs when the repulsive charges located on the surface of siloxane aggregates are low enough to allow aggregation and growth. This condition depends on the pH level. As a result of aggregation into three-dimensional networks, an increasing fraction of the sol becomes occupied by *micro gel regions* [11]. These regions have the same refractive index and density as the surrounding sol, which explains the transparency of the system.

Before the gelation point and under acidic conditions, the precursor of the gel consists of linear or randomly branched polymers, while, under basic conditions this is made up of individual highly branched clusters. At the gelation point, linear chains become entangled while branched clusters impinge on each other [24]. (see Figure 6). The viscosity at this stage increases asymptotically and a transparent gel is formed.

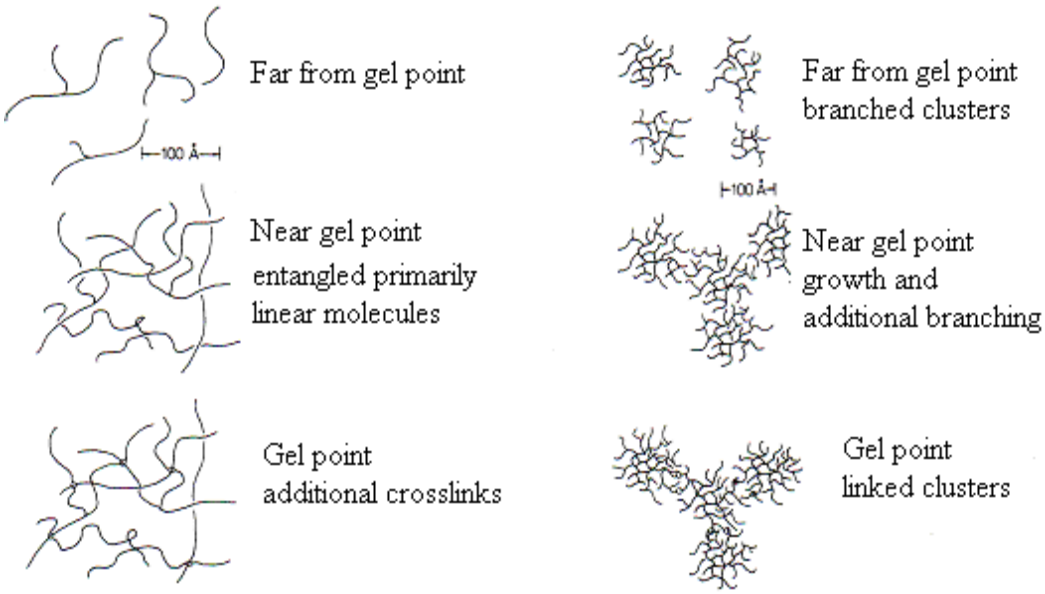

Figure 6 - Gel formation in acid (on the left) and basic catalysed systems (on the right) [2]

2.6 Transition of sol to gel: rheology aspects

Several approaches have been taken to define the gel point. Arbitrary parameters such as the *point* of *no fluidity* [11, 25] are useful measures of gel time, but are not very accurate, and therefore, they cannot give information about viscosity changes taking place. This information, on the other hand, can be accurately provided by rheological measurements. Several authors have reported that the sol-gel transition of acid-catalyzed TEOS solutions takes place in three stages [26-27]. In the first stage, the sol exhibits Newtonian behaviour, so that the viscosity is independent of the shear rate imposed by the measuring instrument. Although the monomer is polymerizing, the formation of aggregate is not dominant and therefore the increase in viscosity is small. During the second stage, a steady increase in viscosity is observed due to the formation of linear

polymers, and at the third stage, a more pronounced increase in viscosity occurs as a result of the formation of three-dimensional networks.

2.7 Ageing and drying of gels

Although the increase in viscosity which accompanies the gelation freezes the systems in a particular structure, after the gel point this frozen-in structure may change appreciably with time depending on the temperature, solvent and pH conditions. The effect of this process, known as ageing [16], consists of shrinkage and stiffening of the material.

The changes in gel structure which can originate from the early stages of its formation are:

- ✓ Gel separation into regions of high and low density because, as the gel point is approached, fluctuations in density grow larger and larger throughout the system;
- ✓ Promotion of additional crosslinking as un-reacted terminal groups (OH and OR) come in contact in regions of higher density;
- ✓ Acceleration of the phase separation process and creation of liquid-solid interfaces (syneresis);

Starting with polymer gels it is expected that the removal of solvent brings shrinkage due to additional cross-linking as un-reacted hydroxyl and alkoxy groups come in contact. The drying process is very important and many of the structural properties of the resulting solid material (i.e. density, elastic properties) depend on the evolution of the system during this phase.

Considering a gel as a network that include a liquid phase (see Figure 7), it is obvious that there is a high interfacial area with a great free energy associated. The decreasing of this energy is the driving force that leads the system to the shrinkage phenomenon.

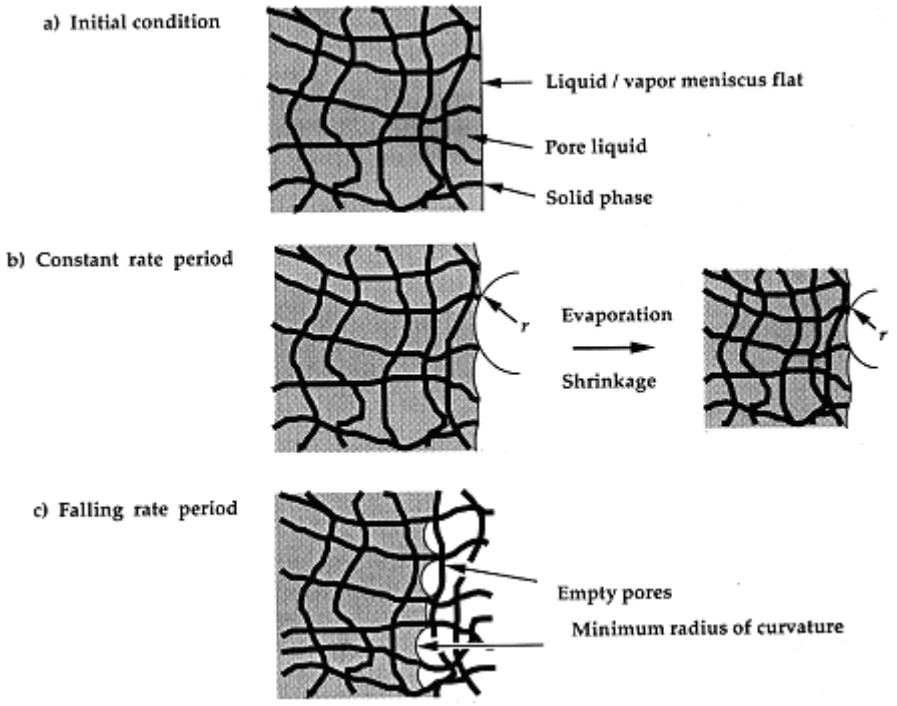

Figure 7 - Drying process. a) the network deforms so easily that little stress is needed to keep it submerged. b) as the network stiffens the pressure increase and the radius of the pores r decrease until it is equal to the radius of the meniscus. c) after this

The evaporation of the liquid from the gel surface, in fact, increases the vapour/solid interface, which has even a greater energy. For this reason the liquid flows from the bulk of the gel to the surface, to cover the dried surface. Because of the evaporation the liquid cannot cover the whole surface without the creation of a meniscus on the pore surface.

The capillary force exerted by the liquid causes the contraction of the solid phase, until the radius of the meniscus is equal to the radius of the pore. At this stage the shrinkage proceeds at a constant rate, and the contraction of the solid phase is equivalent to the volume of the evaporated liquid. After this point the evaporation of the liquid continues moving the liquid-vapour interface towards the bulk of the solid phase leaving a dry solid. This results in an irreversible contraction, because of the further condensation of the un-reacted hydroxyl or alkoxy groups that proceeds during the shrinkage process.

The drying of the gel also produces a pressure gradient in the liquid phase, which leads to differential shrinkage of the network. If the external part shrinks faster than the internal one, tensile stresses arise that tend to fracture the network. The formation of cracks is energetically favourable because at either side of the crack the material can contract more freely. To avoid this phenomenon, a slow evaporation rate of the solvent is required.

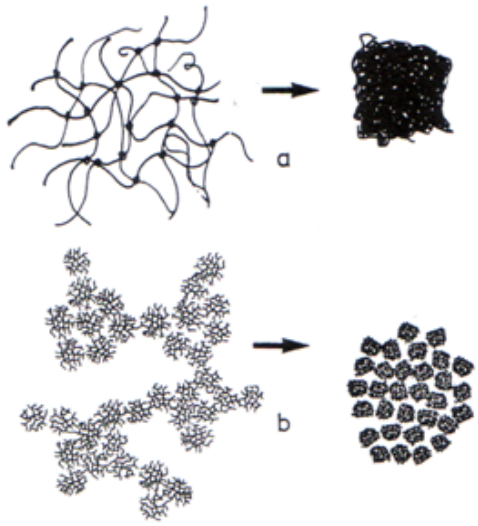

Figure 8 - Representation of desiccation of a) acid b) basic–catalysed [2]

Gels characterized by high density and low pore volume can be formed in weakly crosslinked systems when the rate of condensation is low compared to the rate of solvent removal. Under these conditions the gel's structure can be highly compacted before it is sufficiently crosslinked to be resistant to the densification process. Therefore, as a principle, low pH and low water contents produce dense gels whereas high pH (6 - 10) and high water contents produce gels of high porosity (see Figure 8).

Since large pores lead to lower surface extension and provide wider paths for the evaporation of volatile molecules, the systems obtained through basic catalysis develop lower drying stresses and are less susceptible to fracture [28].

The function of substances such as dimethylformamide [29] as drying control chemical additives is to regulate the relative rates of hydrolysis and condensation, so that larger particles of uniform size are formed. During ageing, a tight size distribution of large pores is achieved that facilitates the expulsion of volatiles, keeping capillary stresses at a safe level [30].

2.8 Densification

The last part of the sol-gel process involves the densification of the dry gel structure to give a glassy material or polycrystalline solid. This evolution of the system occurs under high temperature, and both time and temperature of the thermal treatment can influence the characteristics of the resulting solid material. The transformations involved in this phase of the process are:

- ✓ capillary shrinkage;
- ✓ condensation;

- ✓ structural relaxation;
- ✓ viscous sintering.

The fast evaporation of water and other organics during the thermal treatment causes often the presence of cracks and other structural imperfections. The weight loss and the shrinkage in this phase are not linear and behave differently depending on the temperature, as it is reported on the graph below (Figure 9).

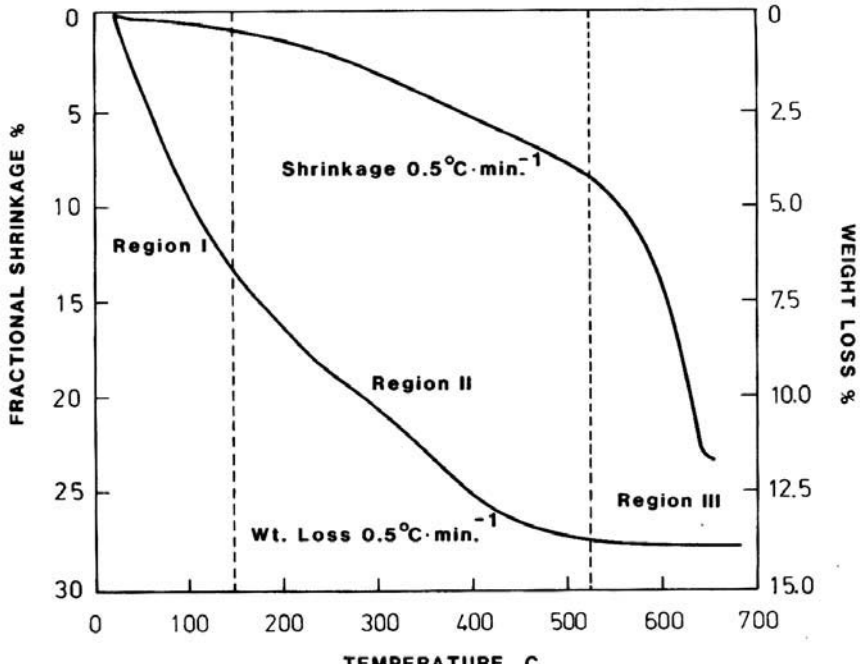

Figure 1 - Shrinkage and weight loss in a gel during the thermal treatment7.

In the first region a small contraction is observed for a great weight loss. The weight loss is due to the evaporation of the water and alcohol still present inside the gel network. The small contraction is due to the increase of the surface energy owing to desorption of the liquids. In the second region the contraction

and the weight loss occur with similar rates. The weight loss is due to the water formed as by-products of the condensation and to the removal of organics, while the contraction is due to a further condensation and to the structural relaxation due to the temperature. In the third region there is contraction without further weight loss, because of the material moves by viscous flow or diffusion to eliminate porosity. The sintering of gels, because of their great interfacial area, can be conducted at temperatures exceptionally low compared to those used for the sintering of ceramic materials. This aspect can be exceptionally interesting with respect to the production of hybrid materials where the presence of an organic phase prevents the utilization of very high temperatures [2].

2.9 References

[1] *Hybrid Materials. Synthesis, Characterization, and Applications* . Edited by Guido Kickelbick Copyright © **2007** Wiley-VCH Verlag GmbH & Co. KGaA, Weinheim.

[2] J. Brinker; G. W. Scherrer; *Sol-gel Science. The Physics and Chemistry of Sol-Gel Processing*, Academic Press, San Diego, CA. **1990.**

[3] J. Livage; M. Henry; C. Sanchez; *Prog. Solid State Chem.,* 18, **1988**, 259-431.

[4] C. Sanchez; F. Ribot; *New J. Chem*., 18, **1994**, 1007-1047.

[5] M. Nabavi; S. Doeuff; C. Sanchez; J. Livage; *J. Non-Cryst. Solids* , 121, **1990**, 31-34.

[6] E. P. Plueddemann; *Silanes and Other Coupling Agents* , K.L. Mittal (eds.), VSP, Utrecht, **1992**, pp.3-19.

[7] G. Tesoro; Y. Wu; *Silanes and Other Coupling Agents* , K.L. Mittal (eds.), VSP, Utrecht, **1992**, pp.215-228.

[8] P. G. Pape; E. P. Plueddemann; *Silanes and Other Coupling Agents,* K.L. Mittal (eds.), VSP, Utrecht, **1992**, pp.105-116.

[9] R. Aelion; A. Loebel; F. Firich; *J. Am. Chem. Soc.*, 72, **1950**, 5705.

[10] K. D. Keefer; *Better ceramics through chemis try, Mat. Res. Soc. Symp., Vol. 32* (Eds.: C. J. Brinker, D. E. Clark, D. R. Ulrich), Elsevier, Pennsylvania, pp. 15, **1984**.

[11] R. K. Iler; *The chemistry of silica*, Wiley, New York, **1979**. Chapter 2, 3.

[12] L. Matejka; K. Dusek; J. Plestil; J. Kriz; F. Ledniky; *Polymer*, 40, **1998**, 171-181.

[13] K. D. Keefer; *Advances in Chemistry Series, Vol.* 224 (Eds.: J. M. Ziegier, F. W. G. Fearon), Am. Chem. Soc., Washington DC, pp. 227-240, **1990**.

[14] R. A. Assink; B. D. Kay; *Polym. Preprints*, 32, **1991**, 506.

[15] M. F. Bechtold; R. D. Vest; L. J. Plambeck; *J. Am. Chem. Soc.* , 90, **1968**, 4590.

[16] B. E. Yoldas; *J. Non-Crystalline Solids,*, 83, **1986**, 375.

[17] C. J. Brinker; K. D. Keefer; D. W. Schaefer; *J. Non-Crystalline Solids*, 48, **1982**, 47.

[18] J. Sanchez; McConnick; *Chem. Proc. of Adv. Mater.* , Wiley, New York, pp. 43, **1992**.

[19] S. Sakka; H. Kozuka; S. Kim; *Ultrastructure. Proc. of Adv. Cer.* (Eds.: J. D. McKenzie, D. R. Ulrich), Wiley, New York, pp. 159, **1988**.

[20] I. Atraki; T. W. Zerda; J. Jonas; *J. Non-Crystalline Solids,* 81, **1986**, 381.

[21] J. Cihlar; *Colloids and Surfaces A, Phys. Eng. Asp.* 70, **1993**, 239.

[22] R. K. Iler; *J. Col. Interf. Sci.,* 75, **1980**, 138.

[23] K. Nassau; K. Raghavachad; *J. Non-Crystalline Solids,* 104, **1988**, 181.

[24] C. J. Brinker; G. W. Scherer; *J. of Non-Crystalline Solids,* 70, **1985**, 301.

[25] M.F. Bechtold; W. Mahier; R.A. Schunn; *J. Poly m. Sci. Polym. Chem. Ed.,* 18, **1980** 2823.

[26] R. Xu; J.A. Pope; J.D. Mackenzie; *J. Nan-Crystallin e Solids,* 106, **1988**, 242.

[27] M. D. Sacks; R. S. Sheu; *J. Non-Crystalline Solids,* 92, **1987**, 383.

[28] M. Yamane; S. Aso; T. Sakaino; *J. Mat. Sci.,* 13, **1978**, 865.

[29] T. Adachi; S. Sakka; *J. Mat. Sci.,* 22, **1987**, 4407.

[30] L. L. Hench; G. Orcel; *J. Non-Crystalline Solids,* 82, **1986**, 1.

Chapter 3: Organic-Inorganic Hybrid Materials

3.1 Introduction

It is well known that organic polymers usually have some superior characteristics with respect to their toughness, flexibility and processability. On the other hand, inorganic materials have high heat resistance and good mechanical and optical properties. Since many of the well-established materials, i.e. metals, ceramics or plastics, cannot fulfill all technological desires, a new class of materials had to be tailored. In regards to projecting new materials, scientists and engineers realized early that mixtures of materials could show superior properties compared with their of pure counterparts. The simplest way to realize such a composite is to incorporate, for instance, inorganic particles into a polymeric matrix, the resulting materials showing improved properties if compared to the neat organic ones. They combine the advantages of the inorganic material (e.g. rigidity, thermal stability) and the organic polymer (e.g., flexibility, dielectric, ductility, and processability). Nowadays, the organic-inorganic materials are regularly used for lightweight materials with advanced mechanical properties, for example in the construction of vehicles of all types or sports equipment. Soon it became evident that decreasing the size of the inorganic units to the same level as the organic building blocks could lead to more homogeneous materials that allow a further fine tuning of materials' properties on the molecular and nanoscale level, generating novel materials that either show characteristics in between the two original phases or even new properties. However, it is worth noting that the

origin of hybrid materials did not take place in a chemical laboratory but in nature. In fact, many natural materials consist of inorganic and organic building blocks distributed on the (macro)molecular or nanoscale. Furthermore, a complex hierarchical order of construction from the nanometer to the millimeter level is regularly found in nature, where every size level of the specific material has its function which benefits the whole performance of the material. Furthermore these different levels of complexity are reached by soft chemical self-assembly mechanisms over a large dimension, which is one of the major challenges of modern materials chemistry. Therefore, hybrid materials or even nanotechnology is not an invention of the last decade but was developed a long time ago. Talking about nanotechnology and nanomaterials, it is necessary first of all to make clear the terms “hybrids” and “nanocomposites”. Commonly the term “hybrids” is more often used if the inorganic units are formed *in situ*, for instance by the sol-gel process [1]. According to this approach both the organic and the inorganic phases are formed together through the simultaneous polymerization of an organic monomer and sol-gel precursors of the inorganic domains. Meanwhile, use of the word “nanocomposites” implies that materials consist of various phases with different compositions, and at least one constituent phase has one dimension less than 100 nm, i.e. nanotubes, layered silicates as montmorillonite (MMT), nanoparticles of metals or metal oxides, and so forth [1]. A gradual transition is implied by the fact that there is no clear borderline between “hybrids” and “nanocomposites”. There are several routes to prepare organic-inorganic hybrids/nanocomposites including intercalation, electrocrystallization, dispersion of preformed particles, sol-gel process, etc. In particular, the sol-gel process with its unique mild processing characteristics and easiness of control is the most common method for preparing hybrid materials.

This process is similar to an organic polymerization starting from molecular precursors resulting in a bulk material. Contrary to many other procedures used in the production of inorganic materials, this is one of the first processes where ambient conditions, i.e. low reaction temperature, were applied to produce ceramics. The control over the preparation of multicomponent systems by a mild reaction method also led to industrial interest in that process. In particular the silicon based sol–gel process was one of the major driving forces what has become the broad field of inorganic–organic hybrid materials. The reason for the special role of silicon was its good processability and the stability of the Si—C bond during the formation of a silica network which allowed the production of organic-modified inorganic networks in one step.

3.2 Types of organic-inorganic hybrids

Depending on the strength or level of interaction two kinds of organic-inorganic hybrid materials can be obtained. In particular Class I hybrid materials are characterized by weak interactions between the two phases (i.e. van der Waals or hydrogen bonds), whereas Class II hybrids evidence strong chemical interactions (i.e. covalent bonds) between the components.

Blends are formed if no strong chemical interactions exist between the inorganic and organic building blocks (see Figure 10 (a)). If an inorganic and an organic network interpenetrate each other without strong chemical interactions, interpenetrating networks (IPNs) are formed (Figure 10 (b)) which is for example the case if the sol-gel material is formed in presence of an organic polymer or vice versa. Both materials described belong the Class I hybrids.

Class II hybrids are formed when the discrete inorganic building blocks, e.g. clusters, are covalently bonded to the organic polymers (Figure 10 (c)) or inorganic and organic polymers are covalently connected with each other (Figure 10 (d)).

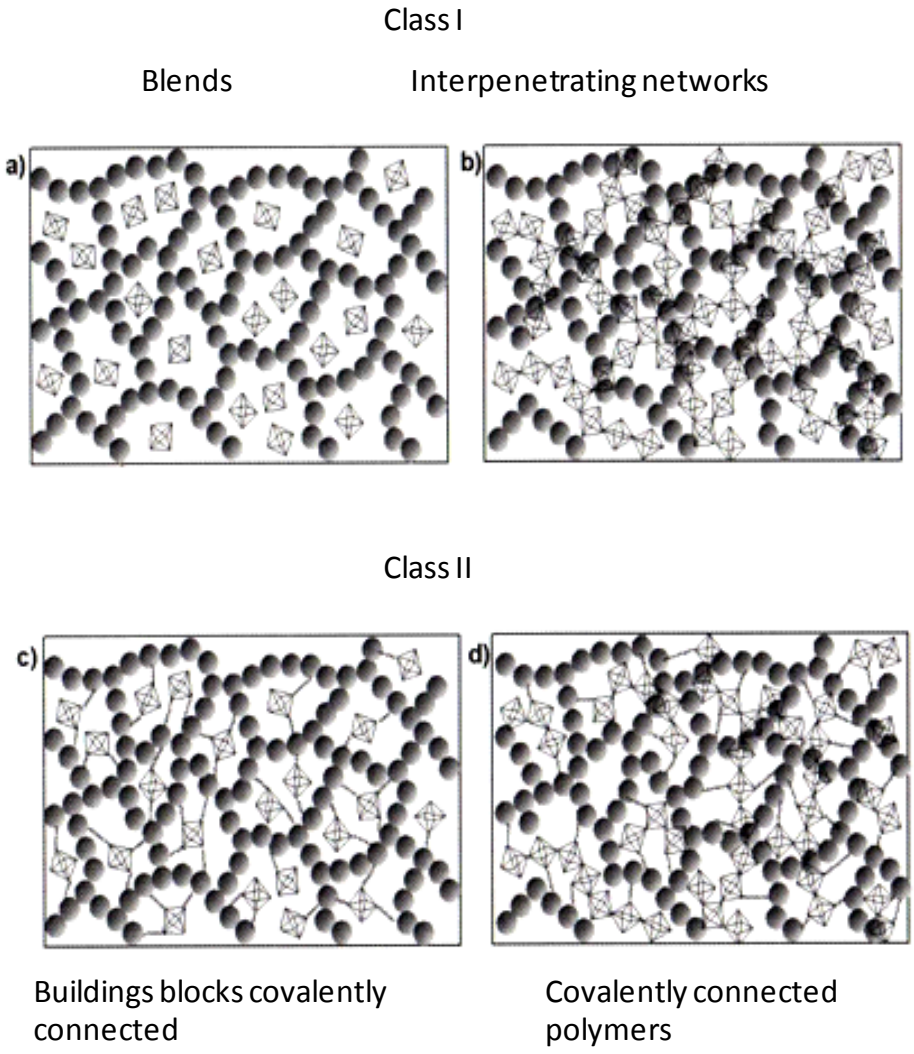

Figure 10 - Schematic representation of the several hybrids typologies. The gray circles represent the monomer of the organic phase while the by-pyramids represent the building blocks of the inorganic phase.

Because of the gradual change in the strength of chemical interactions it becomes clear that there is a steady transition between weak and strong interactions (Scheme 1).

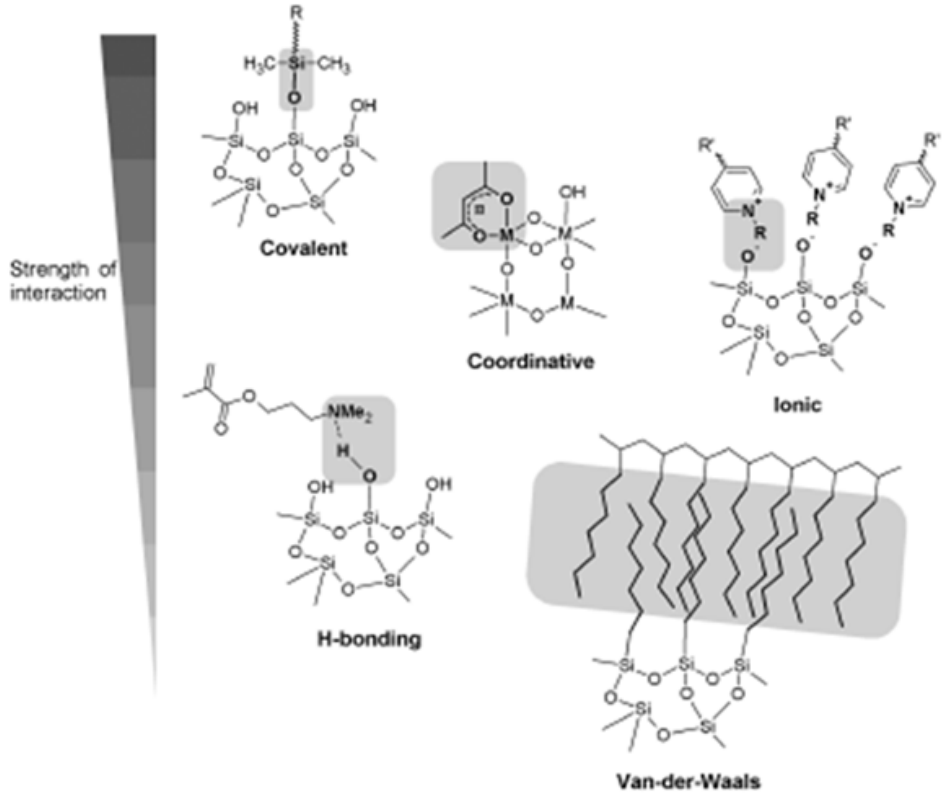

Scheme 1 - Selected interactions typically applied in hybrid materials and their relative strength.

According to the previous classification in this work only epoxy based hybrid/nanocomposite materials of Class II were prepared.

3.3 Interpenetrating Polymer Networks: Phase separation

The morphologies and the properties of the hybrid materials depend on the mechanism and the kinetic of separation between organic and inorganic phases. In particular this effect is much more pronounced for the systems where the inorganic phase is produced starting from a precursor solution (hybrids). In this case the formation of the hybrids involves the formation of the inorganic matrix in presence of the preformed polymer or a mixture of reacting monomers and the resulting morphology can be strongly affected by eventual mechanism of phase separation.

The thermodynamics of a solution containing polymerizing species tells us that mutual solubility among the constituents becomes lower as the average molecular weight of the polymerizing species increases. This is mainly due to the loss of entropy of mixing among the constituents, which leads to the increase of the free energy of mixing:

$$\Delta G = \Delta H - T\Delta S$$

The reduction in mutual solubility caused by polymerization can be contrasted by cooling the system. The free energy of mixing is increased by lowering the temperature. A multicomponent system becomes less stable as the absolute value of the $T\Delta S$ term decreases. In some cases, changes in the polarity of oligomers with the generation and/or consumption of silanol groups may contribute to increase the ΔH term, which will also destabilize the system against

homogeneous mixing. However when the sign of free energy of mixing of the system becomes positive, the thermodynamic driving force for phase separation is generated.

It has often been suggested that phase separation in hybrids takes place by spinodal decomposition [2].

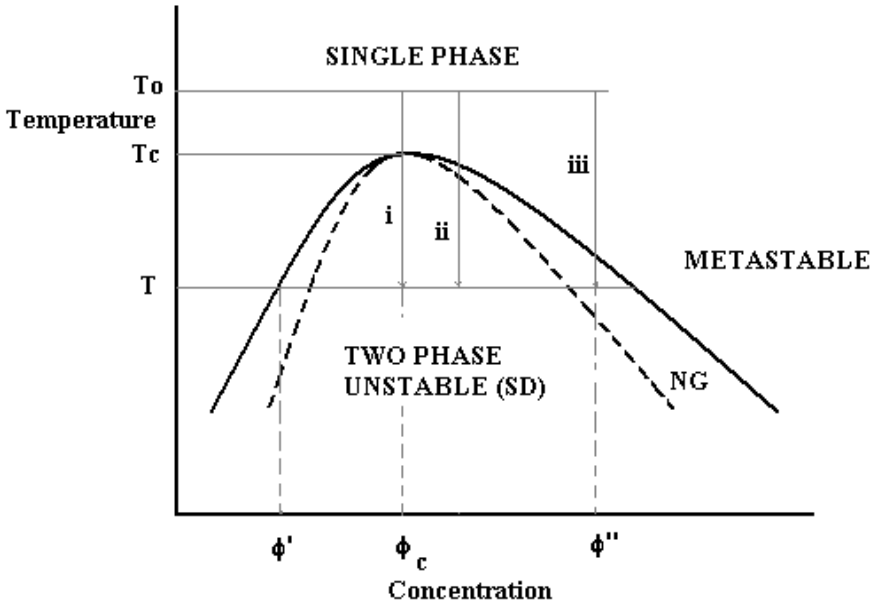

Figure 11 - UCST (Upper Critical Solution Temperature)-type phase diagram

The scheme in the Figure 11 represents a UCST (Upper Critical Solution Temperature)-type phase diagram. The solid curve is known as the binodal and it denotes the border between the thermodynamically stable, single-phase region, from the two-phase region. The dashed curve is known as the spinodal curve and it separates the unstable from the metastable phase-separated region. Two–phase morphologies result by bringing the solution from the single phase region into

the two-phase region by a quenching process equal to a temperature drop of T_0-T. The solution de-mixes, separating into two distinct equilibrium phases of composition ϕ^I and ϕ^{II}. With time, the initial co-continuous phase will be lost to produce a particulate structure where the particles formed are small and uniform in size. Phase continuity may be preserved by rapid cooling, which freezes the morphological features, before the formation of macroscopic domains occurs.

A quenching process into the metastable region (line iii in the Figure 11), brings about phase separation by a mechanism known as Nucleation and Growth (NG), where isolated particles having the equilibrium compositions, appear spontaneously and grow to yield an irregular particle dispersed morphology with a wide distribution of the domain size.

Figure 12 shows a schematic representation of the two phase separation mechanisms: Nucleation and Growth and Spinodal decomposition, as reported by Nakanishi [3].

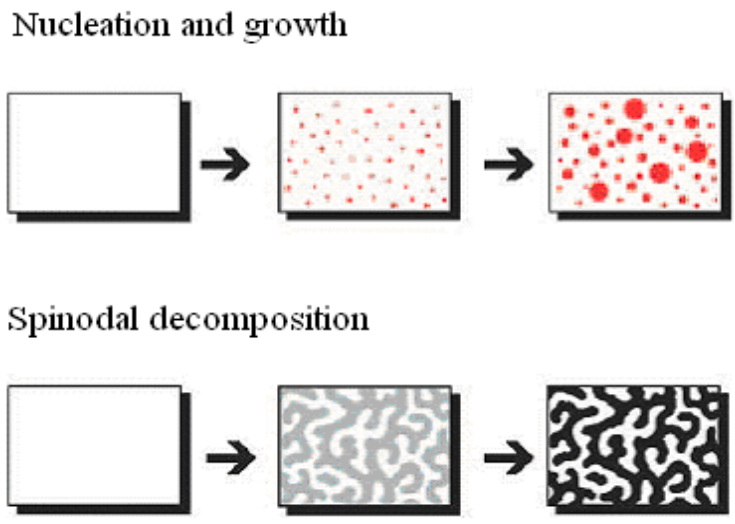

Figure 12 - Nucleation and Growth and Spinodal Decomposition mechanisms [3].

Phase separation between the two components can also take place by a reaction-induced mechanism. In this case the driving force for phase separation arises above a certain molecular weight limit, due to the loss of miscibility between the components. Despite the process goes on isothermally, the quench depth (the difference between T_0 and T) decreases with the molecular weight as a result of a progressive shift of the binodal, as shown in the Figure 13.

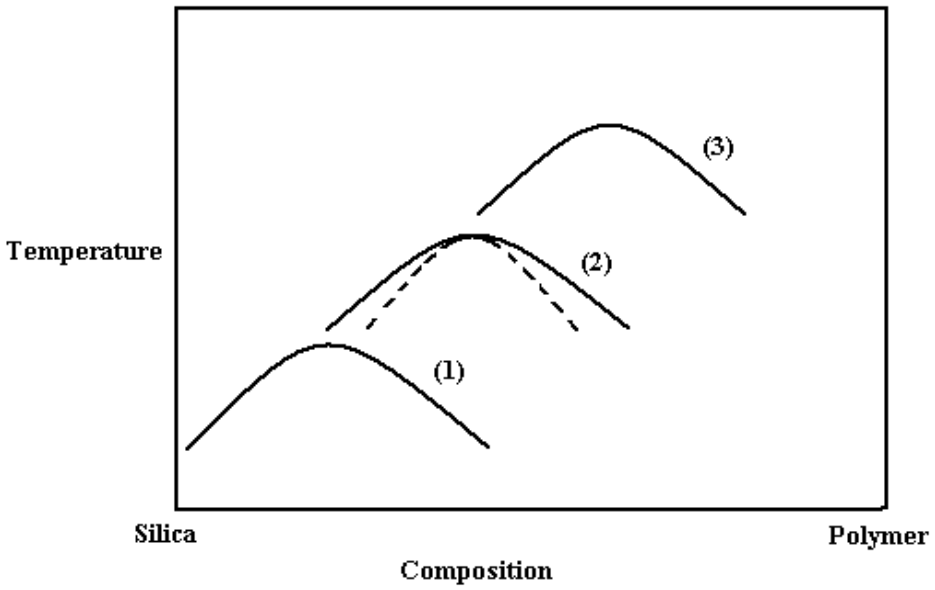

Figure 13 - Binodal curve shifting in reacting systems. The molecular weight increases moving from 1 towards 3.

The diagrams in Figure 11 and Figure 13 can be also used to describe the de-mixing process when the hybrid materials are obtained by casting procedure. In this case the process proceeds isothermally so it is important verify that the casting temperature is above the UCST (upper critical solution temperature) line to avoid phase separation. In reacting systems such as sol-gel systems where silica is growing according the hydrolysis and condensation reactions it is important the upper shift of the UCST line does not cross the isotherm casting

temperature. This represents the necessary condition to produce an Interpenetrating Network Polymer with co-continuous phases. Furthermore the phase separation between organic and inorganic components can be also tailored by using compatibilizating molecules, usually known as coupling agents.

3.4 Use of coupling agents to make compatible organic and inorganic moieties

The transition from the macroscopic world to microscopic, nanoscopic and molecular objects leads, beside the change of physical properties of the material itself, i.e. the so called quantum size effects, to the change of the surface area of the objects. While in macroscopic materials the majority of the atoms is hidden in the bulk of the material it becomes vice versa in very small objects, hence the surface becomes really important when objects become very small. In small nanoparticles (<10nm) nearly every atom is a surface atom that can interact with the environment. One predominant feature of hybrid materials or nanocomposites is their inner interface, which has a direct impact on the materials' properties. A strong interaction between the inorganic nanoparticles and the organic matrix can avoid possible phase separations, which would reach several hundred nanometer length scale leading to materials often opaque. Effects like this are avoided if the reaction parameters are controlled in such a way that the speed of network formation is kept faster than the phase separation reactions. To reduce the tendency of macroscopic phase separation, often caused by the thermodynamic incompatibility of the components, the existence of covalent bonds between organic and inorganic components or strong intermolecular interactions like extensively hydrogen bondings is essential. Therefore, one or both the organic and the inorganic components have to be

modified, in order to render them compatible with each other. This modification consists of adding to either the organic or the inorganic component, functional groups similar in nature of the other constituent. Such modifiers are also known as coupling agents. In the silica-based hybrid materials silane coupling agents are the most used type of modifier agents. They generally have hydrolyzable and organofunctional ends. The general structure of the coupling agents can be represented as $RSiX_3$, where the X represents the hydrolyzable groups, which are typically chloro, ethoxy, or methoxy groups. The organo, R, group can have a variety of functionalities chosen to meet the requirements of the polymer. The functional group X reacts for instance with hydroxyl groups on the SiO2 surface, in preformed silica particles, while the alkyl chain may react with the polymer. Hydrophobic silica can thus be obtained.

Mascia and Kioul [4], used GOTMS (γ-glicidoxypropyl-trimethoxysilane) in their work with polyamic acid solutions in NMP and hydrolyzed solutions of TEOS. Transparency in film cast in solutions with enough GOTMS was found to be a function of mixing time and temperature. The authors attributed the transition of the films from a cloudy to a transparent appearance to the compatibilisation of the polymer and the developing siloxane by trimethoxyl functionalities grafted to the polyamic acid backbone by the coupling agent use. These functionalities are involved in the formation of the inorganic network.

Besides above-described chemical method, grafting of polymers to nanoparticles can also be realized by irradiation. Zhang and co-workers [5-8] have published a series of studies on irradiation-grafted nanosilica-filled nanocomposites. It was found that modification of nanoparticles through graft polymerization was very effective to construct nanocomposites because of (i) an increase in hydrophobicity of the nanoparticles that is beneficial to the filler/matrix

miscibility, (ii) an improved interfacial interaction yielded by the molecular entanglement between the grafting polymer on the nanoparticles and the matrix polymer, and (iii) tailorable structure-properties relationship of the nanocomposites provided by changing the species of the grafting monomers and the grafting conditions since different grafting polymers might bring about different interfacial characteristics.

A different approach to the production of IPN is denoted as the SIPNs (Simultaneous Interpenetrating Polymer Networks) process. In this case the material is produced by performing the sol gel process in combination with free radical polymerization reactions of the polymeric phase. This approach allows the in-situ formation and thus the homogeneous incorporation of polymers that normally would not be miscible. Generally the polymeric phase in these materials is polymethylmethacrylate, PMMA obtained through in situ polymerization starting from the monomer (methylmethacrylate, MMA). In the same cases, whether the sol gel process is performed by using alkoxysilanes bringing at least one polymerizable group, the inorganic phase becomes covalently bounded to polymeric phase. These materials display an improvement of the mechanical behaviour along with better thermomechanical stability [9].

The use of coupling agents allowed to observe the same beneficial effect also in thermoset, i.e. epoxy resin, matrices. In fact in hybrids materials obtained by sol-gel method the simultaneous growth of the organic and inorganic networks by the epoxide cross-linking and silica condensation reactions, respectively, enhance the production of nano structured co-continuous domains, if appropriate coupling agents, which prevent phase separation and allow morphological control, were used [10].

Ochi et al. [11] highlighted the fundamental role of GOTMS to make compatible the two organic and inorganic phase in order to improve the mechanical properties of silica epoxy hybrid materials. In details, they found that in the DGEBA/GOTMS hybrids the storage modulus in the rubbery region increased and the peak area of tanδ curves in the glass transition region decreased, respectively, with the hybridization with small amounts of silica. Moreover, at highest silica content, the tanδ peak in the glass transition region completely disappeared and no other tanδ peaks appeared. Therefore, due to the presence of GOTMS coupling agent strong interactions at the organic/inorganic interface took place and then the silica network was homogeneously dispersed in the epoxy network in a molecular order and consequently the motion of network chains was strongly restricted. Observation using Transmission Electron Microscopy (TEM) revealed that the silica networks are uniformly dispersed in the hybrid samples. These phenomena are also observed in other hybrids [12-13].

3.5 Structure-property relationship for IPN materials

In IPN hybrid materials there is a separate phase known as “interphase” [14] (between the organic and the inorganic phases), which contributes substantially to the overall properties. As the molecular scale morphology plays an important role in achieving macroscopic properties of molecular and supermolecular assemblies, many efforts have been focused on the correlation between structure and property, to the aim to prepare multiphase micro- and nano-heterogeneous systems with desired and tuneable properties.

Wilkes et al. [15] studied PDMS (poly-dimethyl-siloxane)/TEOS hybrids. They were among the first to report the synthesis of hybrids based on PDMS (poly-

dimethyl siloxane) oligomers and silica from TEOS. The embedded inorganic phase conferred rigidity to these materials with a corresponding decrease in ductility. The properties were found to be substantially influenced by the amount of acid catalyst added, leading to a better inter-dispersion of the two phases. The use of a larger amount of TEOS and water, as well as additional thermal treatment [16] gave rise to a more highly cross-linked silica structure, leading to an increase in dynamic modulus.

The variables affecting the structure and properties of hybrids have been discussed by Landry et al. [17] who have examined by Small Angle X-Ray Scattering (SAXS) two different samples of organic-inorganic silica composites, and proposed morphological models to describe them. Triethoxysilane-end capped bisphenol-A epoxy resin (EAS) was reacted with TEOS under slightly basic conditions, and a random copolymer trimethoxysilane-methylmethacrylate (MMA- TMS based hybrid, on the other hand, was better described by co-continuous organic and inorganic phases with a periodic fluctuation of about 4nm. This difference in morphology could be probably examined in the following terms. In the acid catalyzed MMA hybrid the TMOS was expected to form a branched polymer structure. Once most of the solvent was removed, phase separation was likely to occur to form a co-continuous interpenetrating network between the organic polymer and the inorganic polymer phases. A tentative of schematic representation of the morphology is shown in Figure 14.

Figure 14 - Schematic representation of the morphology of a co-continuous interpenetrating network hybrid material. (The shadow area represents the inorganic phase while the continuous lines represent the polymer molecules) [18]

Yano et al. [18] prepared organic-inorganic silica hybrids following two different approaches. One method involved the mixing of organic polymer HPC (hydroxypropyl-cellulose), PVA (poly-vinyl-alcohol) or PVDF (poly-vinylidene-fluoride) with TEOS. For the first two polymers, during the sol-gel process inorganic domains were deposited in the organic matrix due to hydrogen bonding. These bonds are able to avoid the separation between the two phases. The other route followed by these authors, was to introduce triethoxysilyl groups into the organic polymer prior to the sol gel reaction with TEOS involving covalent bonds between the two phases. This time the polymer used was PPO (poly-propylene-oxide end-capped with triethoxysilane).

The experiments conducted on the first type of hybrid material showed that with the increasing amount of TEOS content there was an increase of dynamic modulus. But no change in tanδ was observed, apart from a decrease of the intensity of its peak, because the molecular motions of the organic polymer are

slightly restricted by the deposited silica component. The SAXS profiles of the covalently bonded polymers showed a large sharp peak and its height increased with the TEOS content. This is perhaps due to micro phase separation between silica rich domains and the organic polymer matrix. This time the tanδ peak shifted to higher temperatures due to the molecular motions of the organic polymer being restricted by the silica rich domains. The small silica domains responsible for the low mobility of the organic polymer are visible in the morphology model proposed for the poly(propylene oxide)/silica (PPO/SiO_2) hybrid shown in Figure 15.

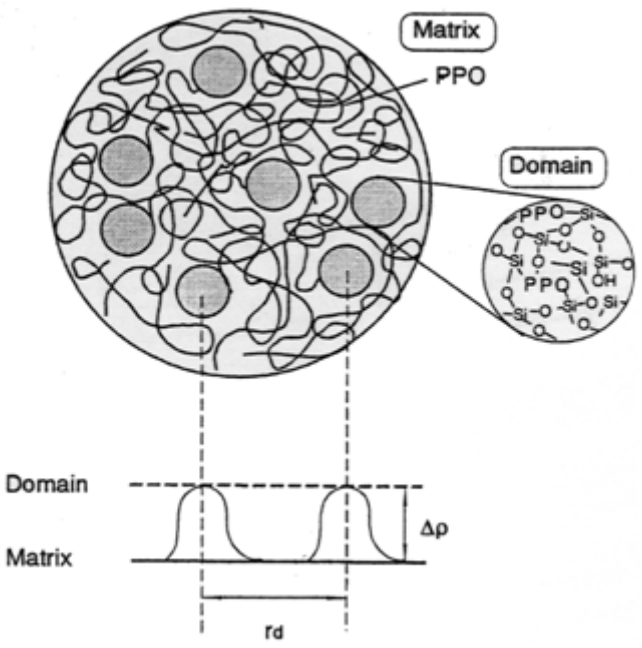

Figure 15 - Morphology model of PPO/SiO2 hybrid where the silica domains are dispersed in the polymer matrix [18].

Recently Mascia et al [19] have prepared nano-composites by casting solutions of both epoxy resin and silica precursors generated both by sol-gel using TEOS and as pre-formed dispersions of 7nm diameter silica particles. For systems obtained from sol-gel, a particulate morphology of the inorganic domains in the resulting films was obtained unless a coupling agent was used. According to this evidence they studied the effect of several coupling agents on the morphology and other properties of the hybrids. In particular, was investigated the effect of the end-chain (mercapto- and amine- type coupling agents) and middle-chain (isocyanate- type coupling agent) functionalisation of the organic matrix (bis-phenol-A type epoxy resin), the chemical nature of the coupling agent and the number of alkoxysilane functionalities. The comparison of the mechanical properties and morphology data of the hybrid systems with respect to the system obtained by mixing the colloidal silica with the polymer has helped in the understanding of the structure of the epoxy-silica hybrids and, also to quantify the interactions between the organic and inorganic phases of the two systems.

3.6 Epoxy-based hybrids and nanocomposites

Since epoxy resins as organic matrix have excellent heat, moisture, and chemical resistance and good adhesion to many substrates, they are mostly applied in the field of coatings, adhesives, casting, potting, composites, laminates and encapsulation of semiconductor devises [20-21]. However, due to their low mechanical properties and high coefficient of thermal expansion (CTE) value compared with inorganic materials, the epoxy resins cannot meet all the requirements of applications, especially for the applications of electrical and structural such as epoxy molding compounds (EMC). Thus organic/inorganic materials are frequently employed in order to overcome this limitation. Two

separated routes can be followed in order to prepare these hybrid/(nano)composite materials, either the addition of preformed inorganic particles, i.e. layered silicates montmorillonite (MMT), or the in situ growth of siloxane clusters, since both MMT and silica particles are commonly used for the reinforcement of epoxy matrix to lower shrinkage on curing, to decrease coefficient of thermal expansion, to improve thermal conductivity and barrier properties, and to meet mechanical requirements. As previously discussed, the intrinsic properties of each component, the shape of fillers, the nature of the interface, and so forth largely affect the properties of hybrid materials [22-23]. It is well known that the load applying on the composites is mainly transferred to the fillers by the interface. Therefore, for excellent properties, strong interfaces between components are needed. Another important factor of fillers for affecting composite properties are their content and size. To enhance the properties, smaller size and larger amount of fillers are required. It has been already reported that the increase of specific surface and fillers contents enhance the mechanical and impact properties of composite [24].

However, when the size of fillers becomes smaller and the fillers content higher, the viscosity of composite resin will be too high to process. In that case, the interfacial strength will be more important factor due to their increasing surface area of fillers. One of the most promising solutions for enhancing processability at high filler-loading system is suggested to be the surface modification of fillers [25]. In general sol-gel method is widely applied either to modify preformed nanoparticles (i.e. MMT) or to synthesize siloxane clusters in order to prepare epoxy based hybrids/nanocomposites materials. Therefore, in this study, to investigate the effect of surface modification on hybrid/nanocomposites properties, especially dynamic mechanical and thermal stability, organo-siloxane

clusters and silylated MMT obtained by sol-gel method were used to prepare epoxy-based hybrid materials.

3.7 Epoxy/silica Hybrids

Ochi et al. [11, 26-27] found that the epoxy/silica nano-hybrids materials, can be prepared by using Biphenol-A type epoxy resin and alkoxysilane as organic and inorganic sources, respectively, and by progressing the sol-gel reaction of the alkoxysilanes during the progress of epoxy curing. By following this route of hybrid preparation, a contemporaneous growth of the two networks are allowed. The epoxy-based hybrid materials exhibited good thermal stability and mechanical properties in the high temperature region even with low silica content (<10wt%). Moreover, the use of GOTMS coupling agent in the epoxy-grafted silicone oligomer hybrid samples [27] showed to enhance the morphological control, since the TEM images highlighted fine silica-rich domains of about 5nm in diameter uniformly dispersed in the cured epoxy matrix. Additionally, the storage modulus in the rubbery region and the peak area of the tanδ curve at the glass transition region increased and decreased, respectively, with the hybridization of organic network. Therefore, the mobility of the epoxy network chains should be considerably suppressed by the hybridization with siloxane structures. Moreover, the introduction of inorganic components in the epoxy resin allowed the coefficient of thermal expansion (CTE) to markedly increase with respect to the neat epoxy system. The thermal decomposition behavior shifted to the high-temperature region with the incorporation of silica network.

Mascia et al. [28] studied the influence of the geometrical configurations of the inorganic phase within an organic matrix on the physical properties of hybrids

materials. To the aim to build up interconnected and chemically bonded organic-inorganic hybrids, two kind of coupling agents were used, namely GOTMS and aminosilanes. In particular, GOTMS was used to functionalize the inorganic particles obtained by TEOS during the sol-gel process, whereas several kinds of aminosilanes, namely Bis-(γ-propyltrimethoxysilane)amine A1170, and Mercapto γ-propyltrimethoxysilane MPTMS, were reacted with Diglycidylether of Bisphenol A (DGEBA) aimed creating siloxanes pendants on the organic chains. They found that the twice functionalization, that is the introduction of coupling agent for both the organic and inorganic components enhance the dispersion of the silica-organosols in the epoxy matrix. Regardless the coupling agent used in the organic component, the hybrid samples exhibit a bicontinuous phase morphology. This comprises three components, respectively an epoxy matrix network, a diffused silica phase and epoxy-silica interphase domains containing a prevalence of alkoxysilane components from the coupling agents used.

Moreover, Matejka et al. [29-31] described the formation, structure and properties of DGEBA-JeffamineD2000-TEOS hybrid materials. They studied the effect of both the catalyst and the synthesis procedure used for the preparation of hybrids materials. In particular they prepared hybrids by using two method, the one-step polymerization, in which all the organic and inorganic component are obliged to react altogether, and the two step polymerization of silica, which consists of prehydrolysis of TEOS in acid medium in the first stage, followed by the build-up of a network in the presence of the amine hardener. The morphology of the network synthesized by the one-step base-catalyzed simultaneous polymerization is the most heterogeneous one, since large siloxane aggregates with a size of about 100-300nm, composed of smaller clusters of 20-70nm in

diameter can be detected. Whereas the two step acid-base polymerization shows smaller siloxane clusters, and then a fine dispersion of inorganic domains. Regardless the preparation procedure, all the hybrid samples highlighted improved dynamic mechanical behavior with respect to the neat epoxy network, in terms of decreased and broadened loss factor tanδ. Furthermore, in the DMA curves of the two-step polymerization hybrids, a new relaxation peak at higher temperature can be observed. This provides evidence of such a phase separation in the epoxy-silica hybrids. In particular, the new relaxation corresponds to the network chains immobilized by interaction with glassy silica domains.

The sol-gel polymerization of organo-trialkoxysilanes $RSi(OR')_3$ under particular reaction parameters results in the formation of polysilsesquioxane POSS cage-like structures. Therefore, Matejka et al. [32] also studied the structural evolution of siloxane cage-like clusters and correlated their morphology to the mechanical behavior of hybrids materials. They found that evolution of the POSS structure is controlled by the competition between intermolecular polycondensation and cyclization. Moreover, because of the incompatibly of the polyhedral POSS framework and pendant organic chains, microphase separation takes place and spontaneous self-organization in cage-like structures occurs. The interphase interaction may contribute to an increase in the glass transition temperature by creating a confined interface layer. The effect, however, is much lower, compared to the interpenetrating networks [29-31]. In fact, the interaction, if any, between the polymeric matrix and the POSS junctions is quite weak. Therefore, the interface interaction is affected by the internal structure of POSS domains, which is determined by the catalysis. Finally, Matejka found that hybrids prepared by silane modified with poly(oxypropylene) acid TSA catalyzed and containing the 64wt% of TEOS

leads to a significant increase both in modulus and Tg. Broadening of the relaxation band corresponds to a broad distribution of immobilized chains. The strength of the interaction and the fraction of confined chains increases with the TEOS content.

3.8 Epoxy/MMT Composites

Because of their unique structure, layered silicates are largely employed in the production of polymer nanocomposites with improved physical properties with respect to the pristine polymeric matrix [33-35]. Enhanced mechanical, thermal and gas-barrier properties can indeed be achieved by adding small amounts of clay (< 5% by weight) to a given polymer, and this in fact opens new avenues in the design and synthesis of a plethora of new, high-performance materials for which an array of advance applications can easily be envisaged.

3.8.1 Structure of layered silicates

The layered silicates used in the nanocomposites belong to the same structural family as the better known minerals talc and mica [36] (i.e. 2:1 phyllosilicates). Montmorillonite (MMT) is one of the layered silicates currently most widely employed in the production of polymer-clay nanocomposites [33-35]. The crystalline structure of MMT is based on a regular arrangement of silicon tetrahedra (SiO_4^{4-}) and aluminum octahedra ($Al(OH)_6^{3-}$), the unit cell containing two tetrahedral and one octahedral layers (Figure 16). MMT layer has permanent negative charge on the surface of its layers because of isomorphous substitutions of Mg^{2+} for Al^{3+} or, rarely, Al^{3+} for Si^{4+} [35]. These negative charges are counterbalanced by the presence of first-group cations such as sodium or potassium, which locate in the proximity of the clay platelets within the gallery

space [33]. Stacking of the layers leads to a regular van der Waals gap between them called the *interlayer* or *gallery*.

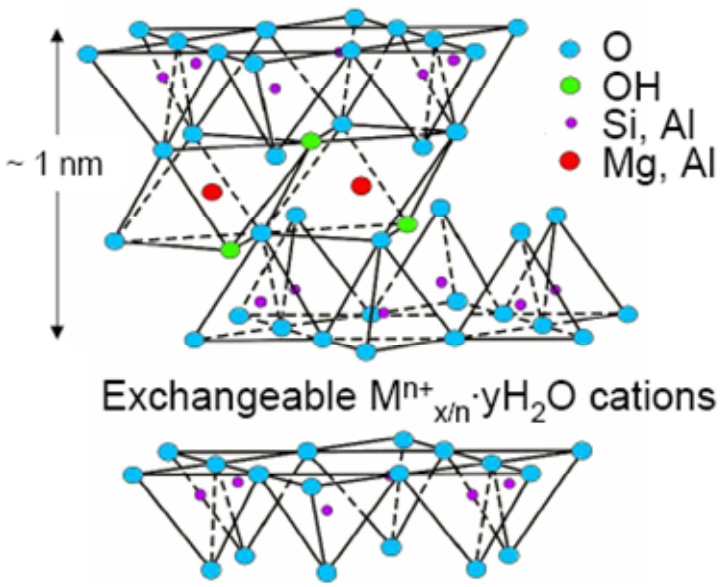

Figure 16 - Structure of the 2:1 layered silicates.

Details on the structure and chemistry for these layered silicates are provided in Figure 16.

All layered silicates are characterized by a large active surface area (700 – 800 m 2 /g in the case of MMT), a moderate negative surface charge (cation exchange capacity) (CEC) and layer morphology, and are regarded as hydrophobic colloids of the constant-charge type. The layer charge indicated by the chemical formula is only to be regarded as an average over the whole crystal because the charge varies from layer to layer (within certain bounds). Only a small proportion of the charge balancing cations are located at the external crystal surface with the majority being present in the interlayer space. The cations are exchangeable for

others in solution. Upon replacing the hydrated metal cation from the interlayers in the pristine layered silicates with organic cations such as an alkylammonium or an alkylphosphonium, the layered silicate attains a hydrophobic/organophillic character and typically results in a larger interlayer spacing. Because the negative charge originates in the silicate layer, the cationic head group of the alkylammonium molecule preferentially resides at the layer surface and the aliphatic tail will radiate away from the surface. The equilibrium layer spacing for an organically modified layered silicate depends both on the cation exchange capacity of the layered silicate, as well as on the chain length of the organic cation.

3.8.2 Morphologies of Polymer/Silicate Nanocomposites

Layered silicates are some examples of layered solids capable of intercalation. Therefore the local and global conformations of the polymers within the host galleries are expected to be dramatically different from those observed in the bulk not only due to the confinement of the polymer chains but also due to specific polymer-surface interactions, normally not observed in the bulk. Hence it is also expected that the local and chain dynamics would be greatly affected by the confinement as well as the polymer-surface interactions.

The structure and properties of the resulting nanostructure can be conveniently mediated by controlling subtle guest–host interactions. Beyond the conventional **phase separated** polymer/silicate composites, for which the polymer and the inorganic host remain immiscible, two types of hybrids are possible (Figure 17): **intercalated** and **exfoliated** or **delaminated** structures. In the intercalated morphology a single, extended polymer chain is intercalated between the host layers resulting in a well ordered multilayer with alternating polymer/inorganic

layers and a repeat distance of a few nanometers. Hence the clay sheets retain a periodic and stacked structure. The intercalation process can be monitored by tracking the increasing long spacing from X-ray scattering, since the galleries must expand to accommodate larger molecules. Whereas in the **exfoliated** or **delaminated** morphology the silicate layers (1 nm thick) are exfoliated and dispersed in a continuous polymer matrix [37-38].

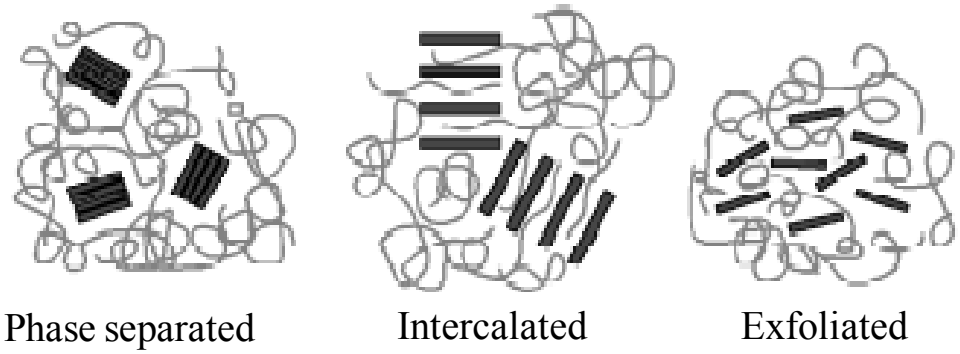

Figure 17 - Schematic representation of different polymer/silicate hybrid structures.

Here the clay sheets are ideally well dispersed and randomized (in orientation) within a matrix of the "coil-like" polymer chains. They have lost their original stacked orientation, and if the structure is truly random then no distinct long spacing should be observable by X-ray scattering. However, literature in the field has a less strict definition of a delaminated hybrid. In most cases in the literature involving delaminated hybrids the clay sheets maintain a considerable amount of order as they tend to remain in a "stacked" structure. Hence it is difficult to distinguish between intercalated and delaminated nanocomposites. In some cases in the literature the only factor which allows distinction between the intercalated and delaminated structure is the spacing between clay sheets (or long period), as both possess stacked–layer structures. In the author's opinion there is a blatant

misuse of the term delaminated (exfoliated) when it is employed to describe a hybrid that displays a clear X-ray peak corresponding to the long spacing of an ordered material. Some researchers improperly utilize wide angle X-ray scattering to monitor the nanocomposite formation, and what they conclude as a disappearance of a correlation peak (evidence of delamination) is really just a convergence of the peak with the main beam. The proper tool to employ, in the author's opinion, is small angle X-ray scattering (SAXS). In fact, this has proven to be an excellent tool to monitor the structure of nanocomposites formed between montmorillonite and epoxies.

3.8.3 Epoxy–Clay composites

As previously discussed, the presence of cations located in the proximity of the clay platelets within the gallery space confers to the pristine structure of, i.e., sodium MMT (Na-MMT) a highly polar nature, and this, in turn, renders this silicate quite incompatible with the vast majority of organic polymers [34-35]. Accordingly, a simple dispersion of Na-MMT in a polymeric matrix will not produce a composite with improved properties compared to the neat macromolecule, because of the poor interfacial interactions between the Na-MMT hydrophilic reaction sites and the highly hydrophobic polymeric chains. Therefore, chemical modification of internal and external Na-MMT platelets plays a crucial role in polymer/clay nanocomposite formation. Several efforts have been done in order to reduce the hydrophilicity of the Na-MMT internal platelets; in particular the cation exchange reaction with a quaternary ammonium salt (see for example the case of Cloisite 30B) represents the most commonly used method to modify clay surface. This modification increases the interlayer spacing and creates a more favourable organophilic environment. However, the

thermal instability of conventional ammonium ion-modified clay is a strong limitation for melt-compounding of polymer/organoclay composites. In fact, most of the alkyl ammonium surfactants are known to undergo a degradation process at temperature at which the plastics are commonly processed [39]. For this reason, the silylation approach involving direct grafting reaction by using a coupling agent has recently attracted much attention, and represents a viable method to make compatible inorganic platelets and organic matrix [40-45]. The presence of broken bonds on the platelet edges are common for layered silicates, and leads to the formation of hydroxyl groups, which can be utilized for chemical modification by silylation reaction. By using an organosilane, it is then possible to covalently bond the organic functional groups onto the layer surface. Importantly, the functionalization of clay minerals with organosilanes can take place at three different sites: at the interlayer space, at the external surface and at the edges [46-47].

In terms of performances of silane-modified MMT nanocomposites, Zhao et al. [48] found that the use of chlorosilane modified clay allowed the improvement of the mechanical behavior of polyethylene (PE)-based nanocomposites determining an increase of both glass transition temperature and elastic modulus in the glassy region. In particular, after trimethylchlorosilane (TMSCl) modification, the OH groups at the edge of clay platelets were reacted and the wetting ability between PE and organoclay was subsequently improved. Moreover, the loss of hydroxyl groups resulted in a decrease of cation exchange capacity (CEC), which caused a reduction in the strength of interaction between the platelets. Both these effects favorably concurred to improve the intercalation of PE into interlayers.

So far the silylation reaction has been widely performed using (3-aminopropyl)trimethoxysilane (A1100), TMSCl and Glycidyl-propyl-triethoxysilane (GPTS) [47] as coupling agents. Among several investigations, it is here mentioned the work of Wang et al. [49], which found that Na-MMT modified by a small amount of A1100 as coupling agent is able to promote a high extent of exfoliation for epoxy/clay nanocomposites. However, to the best of our knowledge, the effects of other aminosilanes on the MMT final basal spacing have not been evaluated yet.

The interfacial interaction between the filler and the epoxy matrix strongly affects the filler morphology within the polymeric network and then the final properties of nanocomposites. In most cases, uniform dispersion [50] or controlled mesoscale association [51] of the nanoparticle is believed to be critical to maximize the epoxy properties improvements. In fact, it is generally believed that the improvement in properties of the clay nanocomposites is directly related to the complete exfoliation of silicate layers in the polymer.

Moreover, depending on the nature of components, namely clay and polymer, the method of preparation (melt, solution or in-situ polymerization) and the processing techniques used, various clay-polymer morphologies as follows phase separated, intercalated or exfoliated structure can be obtained [52].

Koerner et al. [53] found that irrespective of the organically modified MMT (O-MMT) used to prepare the epoxy nanocomposites, conventional processing methodologies as sonication, result in an inhomogeneous distribution of OMMT on the micron scale. Even though alkylammonium which allows the intragallery reactivity to enhance, this only results in extensive swelling of tactoids (interlayer distance of about 10-20nm) and thus retention of layer-layer

correlations, leading to composite micron-scale reinforcing particles, not nano-scale dispersion of individual layers. In contrast, the authors findings highlighted that sub-ambient temperature (cryo) compounding had substantial impact on the ability to reduce tactoid and agglomerate size and increase homogeneity of MMT dispersion. They stated that contrary to the thermal coefficient of thermal expansion and the hardness, the glass transition temperature strongly depends on the extent of OMMT dispersion and interfacial chemistry.

Perrin-Sarazin et al. [54] studied the Ball Milling technique to achieve final clay exfoliation in PP/MMT composites. In details, Ball Milling is a high-energy grinding technique widely used to prepare composites from powders. It is well known to induce several mechanic-chemical changes and structural modifications in clays, leading to great changes in their surface and colloidal properties [55-56]. In the literature, it is recognized that high-energy Ball Milling affects the clay structure by inducing predominant delamination of the platelets at the earlier stages of degradation, breaking the platelets, and finally crushing the structure in the later stages thus leading to the structure amorphization [57-59]. The clay delamination is a crucial issue in the preparation of polymer nanocomposites and as it happens during the early stage of the milling process without even drastic clay structure alteration, it makes the milling a very attractive technique to prepare clay nanocomposites.

In spite of what observed, Giannelis et al. [60] stated that in the MMT polymer composites the edge interactions play a more significant role than degree of exfoliation, a result unique in the field of polymer nanocomposites. They demonstrated that even a combination of polymer/nanofiller compatibility and thermodynamically stable nanofiller dispersion levels may not give rise to reinforcement. These findings provide an important caveat when attempting to

connect structure and properties in polymer nanocomposites, and useful guidance in the design of optimized polymer/layered silicate nanocomposites in particular.

In general, the inter-relationships between mechanical processing, OMMT surface chemistry and the desired property enhancements are not linear and thus must be considered in light of the final application to evaluate the optimal nanocomposite fabrication methodology to achieve maximal benefit.

3.9 References

[1] G. Kickelbick; *Hybrid Materials. Synthe sis, Characterization, and Applications*; Wiley-VCH: Weinheim, Germany, **2007**; Chapter 1.

[2] T. Inoue; *Prog. Polym. Sci.,* 20, **1995**, 119.

[3] K. Nakanishi; *Bull. Chem. Soc. Jpn*., 79, **2006**, 673–691.

[4] A. Kioul; L. Mascia; *J. of Non Crystalline Solids,* 175, **1994**, 169.

[5] C. L. Wu; M. Q. Zhang; M. Z. Rong; K. Friedrich; *Compos. Sci. Technol.,* 65*,* **2005**, 635.

[6] M. Z. Rong; M. Q. Zhang; Y. X. Zheng; H. M. Zeng; R. Walter; K. Friedrich; *J. Mater. Sci. Lett.,* 19*,* **2000**, 1159.

[7] M. Z. Rong; M. Q. Zhang; S. L. Pan; B. Lehmann; K. Friedrich; *Polym. Int.,* 53, **2004**, 176.

[8] M. Z. Rong; M. Q. Zhang; S. L. Pan; K. Friedrich; *J. Appl. Polym. Sci.,* 92, **2004**, 1771.

[9] A. Schwegler; M. Möller; *Macromol. Chem. Phys.,* 199 (9), **1998**, 1859-1864.

[10] L. Prezzi; L. Mascia; *Advances in Polymer Technology* , 24, **2005**, 91-102.

[11] M. Ochi; R. Takahashi; A. Terauchi; *Polymer*, 42, **2001**, 5151-5158.

[12] Q. Hu; E. Marand; *Polymer*, 40, **1999**, 4833.

[13] Z. Ahmad; M. I. Sarwar; S. Wang; J. E. Mark; *Polymer*, 38, **1997**, 4523.

[14] M. S. Whittingham; *Science,* 192, **1976**, 1126.

[15] H. H. Huang; B. Orler; G. L. Wilkes; *Macromolecules,* 20, **1987**, 1322.

[16] G. L. Wilkes; B. Orler; H. H. Huang; *Polym. Preprints,* 26, **1985**, 300.

[17] M. R. Landry; B. K. Coltrain; C. J. T. Landry; *J. Polym. Sci.* , 33, **1995**, 637.

[18] S. Yano; K. Iwata; K. Kurita; *Mater. Sci. and Engin.*, 6, **1998**, 75.

[19] L. Mascia; L. Prezzi; M. Lavorgna; *Polymer Engineering and Science* 48, **2005**, 1039-1048.

[20] J. C. Salomone; *Encyclopedia of polymeric materia ls, vol.3* , New York: CRC Press, **1996**.

[21] W.G. Potter; *Epoxy resins*, New York: Springer, **1970**.

[22] L.E. Nielsen; *Mechanical properties of polymers and composites, vol. 2*, New York: Marcel Dekker, **1974.**

[23] Y. Nakamura; M. Yamaguchi; K. Iko; M. Okubo; T. Matsumoto; *Polymer*, 31, **1990**, 2066.

[24] Y. Nakamura; M. Yamaguchi; M. Okubo; T, Matssummoto; *Journal of Applied Polymer Science* 45, **1992**, 1281.

[25] E.P. Plueddemann; *Silane coupling agents* , New York: Plenum Press, **1982**.

[26] M. Ochi; R. Takahashi; *Journal of P olymer Science: Part B: Polymer Physics* 39, **2001**, 1071.

[27] M. Ochi; T. Matsumura; *Journal of Polymer Science: Part B: Polymer Physics* 43, **2005**, 1631-1639.

[28] L. Mascia; L. Prezzi; B. Haworth; *Journal of Material Science* 41, **2006**, 1145-1155.

[29] L. Matejka; K. Dusek; J. Plestil; J. Kriz; F. Lednicky; *Polymer* 40, **1999**, 171.

[30] L. Matejka; J. Plestil; K. Dusek; *Journal of Non-Crystallin e Solids* 226, **1998**, 114.

[31] L. Matejka; O. Dukh; J. Kolarik; *Polymer*, 41, **2000**, 1449.

[32] L. Matejka; O. Dukh; H. Drahomira; B. Meissner; J. Brus; *Macromolecules* 34, **2001**, 6904-6914

[33] J. Zhang; R. K. Gupta; C. A. Wilkie; *Polymer*, 47, **2006**, 4537.

[34] H. Shi; T. Lan; T. J. Pinnavaia; *Chem. Mater.*, 8, **1996,** 1584.

[35] S. Yariv; H. Cross; in: Dekker M, (Eds), *Clays and Clay Minerals* , New York, **2002**. pp 463-566.

[36] S.D. Burnside; E. P. Giannelis; *Chem Mater*, 7, **1995**, 1597.

[37] R. K. Krishnamoorti, R. A. Vaia, E. P. Giannelis; *Chem Mater*, 8, **1996** 29.

[38] E. P. Giannelis; *Advanced Materials*, 8, **1996**, 29.

[39] L. A. Utracki; *Clay-Containing Polymeric Nanocomposites* , Rapra Technology Limited Press, Shrewsbury, **2004.**

[40] A. Wheeler; J. Wang; J. Baker; L. J. Mathias; *Chem. Mater.*, 17, **2005**, 3012.

[41] N. N. Herrera; J. M. Letoffe; J. L. Putaux; L. David; E. Bourgeat-Lami; *Langmuir*, 20, **2004,** 1564.

[42] A. Y. Park; H. Kwon; A. J. Woo; S. J. Kim; *Adv. Mater.*, 17, **2005,** 106.

[43] N. Herrera; J. Letoffe; J. Reymondc; E. Bourgeat-Lami; *J. Mater. Chem.*, 15, **2005**, 863.

[44] H. He; J. Duchet; J. Galy; J. Gerard; *Colloid. Interface Sci.* , 288, **2005**, 171.

[45] M. Park; I. K. Shim; E. Y. Jung; J. H. Choy; *J. Phys. Chem. Solids* , 65, **2004,** 499.

[46] A. M. Shanmugharaj; K. Y. Rhee; S. H. Ryu; *J. Colloid Inter face Sci.*, 298, **2006,** 854.

[47] A. Di Gianni; E. Amerio; O. Monticelli; R. Bongiovanni; *Appl. Clay Sci.*, 42, **2008**, 116.

[48] C. Zhao; M. Feng; F. Gong; H. Qin; M. Yang; *J. Appl. Polym. Sci.* , 93, **2004,** 676.

[49] K. Wang; L. Wang; J. Wu; L. Chen; C. He; *Langmuir*, 21, **2005,** 3613.

[50] S. J. Park; D. I. Seo; J. R. Lee; D. S. Kim; *Synthesis and characterization of epoxy/clay nanocomposites,* Kongop Hwahak, 12 (2), **2001**, 181-185.

[51] T. D. Fornes; D. R. Paul; *Polymer*, 44, **2003**, 4993-5013.

[52] M. Alexandre; P. Dubois; *Mater. Sci. Eng.*, R 28, **2000**, 1.

[53] H. Koerner; D. Misra; A. Tan; L. Drummy; P. Mirau; R. Vaia; *Polymer*, 47, **2006**, 3426-3435.

[54] F. Perrin-Sarazin; M. Sepehr; S. Bouaricha; J. Denault; *Polymer Engineering and Science*, **2009**, 651-665.

[55] S. Yariv; I. Lapides; *Journal of Mater Synth Process*, 8, **2000**, 223.

[56] E. Kasai; H. Mimura; K. Sugiyama; F. Saito; K. Akiba; Y. Waseda; *Adv. Powder Technol.*, 5, **1994**, 189.

[57] B. Cicel; G. Kranz; *Clay Miner.*, 16, **1981**, 151.

[58] I. Sondi; M. Stubicar; V. Pravdic; *Colloids Surf. A Physicochem. Eng. Asp.*, 127, **1997**, 141.

[59] F. Dellisanti; G. Valdré; *Appl. Clay Sci.*, 28, **2005**, 233.

[60] D. F. Schmidt; E. P. Giannelis; *Chemistry of Ma terials*, 22, **2010**, 167-174.

Chapter 4: Experimental

4.1 Materials

4.1.1 Organic components

4.1.1.1 Diglycidyl ether of bisphenol-A (DGEBA)

A commercially available Diglycidyl ether of bisphenol-A (DGEBA) has been used as main epoxide component, commercially known as Epikote828 obtained from Shell chemicals. These have a number average molecular weight of 370 and 5000 atomic mass units respectively, corresponding to an average degree of polymerisation of 0.1 and 16 expressed in terms of central $CH_2CHOHCH_2$ units per molecule. The Epoxide Equivalent Weight (EEW), the weight of resin in grams which contains one gram-equivalent of epoxy, is 187 g/mol equiv. The general structure is as shown below:

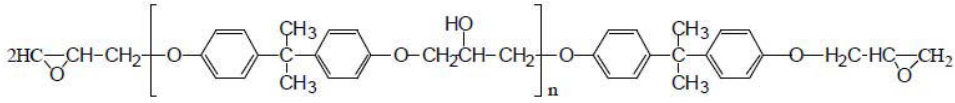

Bisphenol-A epoxy resin

4.1.1.2 1,6 hexanediol Diglycidyl ether

The 1,6 hexanediol Diglycidyl ether is a bifunctional epoxide reactive diluent at EEW = 165 g/mol equiv obtained from Shell chemicals.

4.1.2 Siloxane precursors

4.1.2.1 Silane Coupling agents

Compatibility between the inorganic and the epoxy components is required to obtain a hybrid material with co-continuous phases. To achieve this goal silane coupling agents, namely γ-Glycidoxypropyltrimethoxysilane (GOTMS) and three aminosilanes, 3-aminopropyltriethoxysilane (APTES or A1100), N-(2-aminoethyl)-3-aminopropyltrimethoxysilane (A1120), and 3-[2-(2-aminoethylamino)ethylamino]-propyl-trimethoxysilane (A1130), obtained from GE Advanced Materials, were used. All trifunctional silylating agents had a purity of 98%.

4.1.2.2 Tetraethoxysilane (TEOS)

TEOS was used as silica precursors to generate the siloxane network in the hybrid systems. It was parched from Aldrich, at 98% purity.

4.1.3 Catalyst: Dibutyltin Dilaurate (DBTDL)

DBTDL was used as condensation catalyst in the alkoxysilane solution. It was obtained from Aldrich chemicals with a purity > 95%.

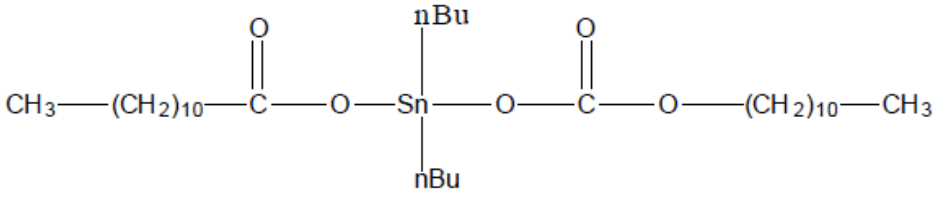

DBTDL

4.1.4 Inorganic components: Montmorillonite

Sodium montmorillonite (Na-MMT) with cationic exchange capacity (CEC) of 92 meq/100g was purchased from Southern Clay Products Inc., USA. Prior to its use, the Na-MMT was dried over night at 90°C *in vacuum* conditions.

4.1.5 Solvents

The solvents used in the hydrolysis and condensation of the silica precursor were distilled water, ethanol and 2-propanol, obtained from Sigma Aldrich. For the silylation reaction of MMT Glycerol purchased from Fluka was used.

4.1.6 Hardeners

The Metaxylilene diamine (MXDA) hardener (obtained by Fluka) has an AEW of 35.56 g/mol equiv.

Jeffamine D230 obtained from Aldrich with a AEW of 54.83 g /mol equiv., with the following structure:

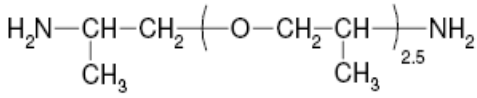

4.2 Silylation reation of Na-MMT

4.2.1 Powders

To perform the silylation reaction of Na-MMT by aminosilanes, three different reaction conditions were used, in which both the reaction temperature and the

amount of the aminosilane were varied, respectively. These experimental routes, referred to, in the following as Procedure 1, 2 or 3, are summarized in Table 1.

Procedure	Amount of Na-MMT in 100 ml of glycerol (g)	Amount of aminosilane in 100 ml of glycerol (g)	Reaction temperature (°C)
1	1	1	80
2	5	20	130
3	5	5	80

Table 1 - Reaction conditions adopted during the silylation process.

1 or 5 grams of dried Na-MMT were added to 100 ml of glycerol, and the resulting suspension was stirred at 60°C for 30' in nitrogen atmosphere. The same procedure was used to dissolve the aminosilane in glycerol. In this work glycerol was selected as the solvent, since, recently, Shanmugharaj et al. [1] verified that, using high surface energy solvents, the interaction between aminosilanes and the edges of the clay platelets is reduced due to low wetting phenomena and, hence, the silane molecules can diffuse and react more efficiently in the mineral galleries.

The resulting Na-MMT dispersion and aminosilane solutions were then mixed, and the grafting reactions were carried out at 80 or 130°C, under constant stirring for 3 h under nitrogen. After cooling, the reaction product was recovered by centrifugation at 13000 rpm, and stabilized at 100°C for 5 h *in vacuum* condition. Excess glycerol was removed by washing each reaction product with water under stirring at 60°C for 1.5 h followed by centrifugation. This washing procedure was repeated three times, and the quantitative elimination of the solvent was confirmed by thermogravimetric analysis. Each resultant product was dried at

80°C under vacuum and then ground to a powder. Procedure 1 was performed on all three aminosilanes, whereas Procedure 2 was carried out only in the case of A1100. In order to study the effect of the two silylation conditions on the final products, the interlayer spacings of the A1100-modified Na-MMTs obtained from the different procedures, i.e. 1 and 2, were compared.

Additionally, in order to determine the degradation temperatures of the silylated Na-MMT, two pastes with water and glycerol as dispersing agents were prepared to be tested by thermogravimetric analysis. In details, the Na-MMT/water paste (***Na-MMT-H2O***) was obtained by dispersing Na-MMT powder in glycerol at 60°C and then following the same procedure illustrated previously for the silylation reaction but without the addition of the aminosilane. The paste with glycerol (***Na-MMT-Gly***) was prepared by dispersing Na-MMT in glycerol at 60°C. After centrifugation, the paste was kept in the oven for 22 h at 60°C *in vacuum* condition.

Once optimized the parameter process the silylation reaction has been carried out following the Procedure 3 and finally the obtained powders were used to prepare ***Epoxy/MMT composites***.

4.3 Preparation of the MMT composites epoxy-based

The epoxy composites were prepared through two different procedures namely sonication mixing (S) and a combination of sonication and high energy ball-milling (SB) which are schematized in Scheme 2.

4.3.1 Sonication mixing (S)

The modified and unmodified clay was first mixed with DGEBA by using the Thinky planetary vacuum mixer for 2 minutes at 2000 rpm. The mixture was then sonicated for 30 minutes (instrument details). Afterwards the hardener MXDA in stoichiometric amount was added and the resulting mixture was degassed for 4 minutes in the planetary vacuum mixer and then poured in special moulds and cured according to the following thermal program: 30°C for 1h, 60°C for 1h, 90°C for 1h, 100°C for 1h, 120°C for 1h and 150°C for 1h. This curing cycle allows the complete conversion of the epoxy groups as confirmed by FTIR analysis (data not reported for sake of brevity). An epoxy control matrix was obtained with this procedure without adding any clays.

4.3.2 Sonication and High Energy Ball-milling (HEBM) mixing (SB)

In this method, the mixture of DGEBA and modified and unmodified clays was first processed by sonication mixing followed by an additional high shear my using a HEBM for 1h at 580 rpm. After that the hardener MXDA was added in stoichiometric amount at the mixture was submitted to the same treatment and thermal curing previously described for sonication mixing procedure. An epoxy control matrix was obtained with this procedure without adding any clays.

In the following the composite materials obtained by including unmodified Na-MMT are simply abbreviated as ***Na-MMT/DGEBA***. The composite materials obtained by using silylated MMT are labeled as ***MMT-A1100*** and ***MMT-A1120*** for samples including clay functionalized respectively with 3-aminopropyltriethoxysilane and N-(3-(trimethoxysilyl)propyl)ethylene-diamine.

Composites with 1 and 3% in weight of inorganic clay content (silicate basis) were prepared. The actual content of inorganic phase (i.e. MMT without the organic moieties) has been calculated by taking into account the organic content due to the moieties introduced by silylation [1]. The percentage of organic amminosilane moieties with respect to the total inorganic mass is 8.1% and 8.8% wt/wt for MMT functionalized respectively with A1100 and A1120 [2-3].

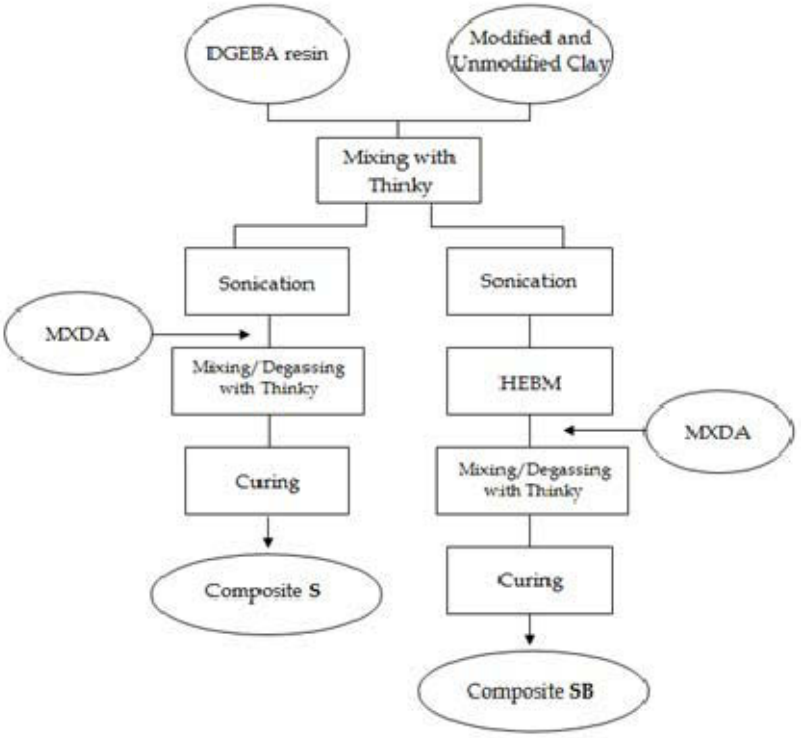

Scheme 2 - Processing methods of epoxy/MMT nanocomposites.

Therefore, since the powders are mentioned as "MMT-x" with x= aminosilane used to functionalize the filler, the corresponding composites were named "***MMT-x y% S***" or "***MMT-x y% SB***", for the sonicated or sonicated-ball-milled samples, respectively, y indicating the powders content.

4.4 Preparation of Epoxy-silica Hybrids

To the aim to study the sol-gel parameters process, several approaches have been attempted. In particular, by using the same hardener (MXDA) the effect of the coupling agent, the solvents and the hydrolysis procedure have been evaluated. In fact, according to the standard sol-gel method the first approach (***Ep-xAP-zSolv-Siy-Sh***) contemplated the pre-hydrolysis procedure in acidic ambient of sol-gel precursors. The APTES coupling agent has been used to functionalize the organic moieties versus the inorganic structures. This approach leads to hybrids with large inorganic particles not well interacting with the organic network. Additionally, the sol-gel procedure solvents retain in the hybrid samples. In order to improve the interfacial interactions between the organic and inorganic moieties, the functionalization of the inorganic structures has been performed by using a second coupling agent GOTMS. Moreover, to eliminate the sol-gel solvents, namely ethyl alcohol and water, the precursors solution has been dried before the addition to the reacting system. In these samples, named ***Ep-xAP-Siy-Ol***, large inorganic particles, even if well bonded to the organic network are present. Hence, to the aim to reduce the inorganic structures dimensions, the ***Ep-xAP-Siy-IS*** approach has been followed. In fact, the so-called "one-step polymerization" [4-6] all the organic and inorganic component are obliged to react altogether, constrains the siloxane structures to be small and well dispersed, with enhanced interfacial interactions due to the GOTMS presence. By using this approach, the siloxane structures become well dispersed in the organic matrix and the extraction of sol-gel pre-hydrolysis solvents has been overcome. However, in spite of the fine inorganic structures the viscous-elastic properties of hybrid samples got worse with respect to the neat epoxy. These results could be ascribed to the retention of developed sol-gel solvents into the reacting system

and to the too opened siloxane structure. Hence the further approach has been attempted, producing the ***Ep-Siy-Mx*** samples. The pre-hydrolysis solvents have been eliminate after mixing with the epoxy resin and an increased amount of GOTMS has been used. This approach assured all sol-gel solvents to be eliminated and enhanced a good dispersion of inorganic structures. This preliminary study was necessary to define both the kind and amount of coupling agent, and the sol-gel process parameters to use. Finally, the effect of the hardener has been evaluated producing the ***Ep-Siy-Je*** samples. Depending on the particular kind of sol-gel procedure and hardener taken into account, different curing cycles have been performed.

4.4.1 Preparation of "Ep-xAP-zSolv-Siy-Sh" hybrids

A three step method has been used. The epoxy resin DGEBA (or a mixing of DGEBA and 1,6 hexanediol diglycidyl ether) has been functionalized with APTES at 70°C in nitrogen atmosphere to avoid the influence of water in the nucleophilic attach of epoxy ring by amine group. The mixture has been allowed to react for 10' after that the reacting mixture has been cooled in ice water in order to avoid the reaction to continue. Meanwhile the siloxane precursors solution has been prepared by mixing at room temperature for 10' Tetraethylorthosilane (TEOS), acidic water (HCl/H2O 2wt%) water and ethyl alcohol as solvent. In detail, the molar ratio between TEOS and water was:

$$TEOS : H_2O = 1 : 3$$

Whereas ethyl alcohol has been added by keeping a weighting ratio twice with respect to the water amount. The pre-hydrolysis solution has been added to the functionalised epoxy resin in order to produce nominal silica content ranging from 2.5 to 15wt%. Finally, a stoichiometric amount of MXDA hardener has

been added taking into account the amount of epoxide groups functionalized before with APTES. The samples have been post-cured for 2h at 150°C after 18h at 23°C. The samples were named ***Ep-xAP-zSolv-Siy-sh***, where x indicates the weight percentage of epoxide groups functionalised with APTES and y the nominal silica content. Finally z represents the weight percentage of 1,6 hexanediol diglycidyl ether added.

4.4.2 Preparation of "Ep-xAP-ySi-Ol" hybrids

The epoxy resin DGEBA has been functionalized in 10' with APTES at 70°C in nitrogen atmosphere and immediately cooled in ice water. The siloxane mixture has been prepared to the aim to produce siloxane oligomers according to Soucek approach [7]. The siloxane precursors solution has been prepared by stirring at 25°C for 24 hours in acidic catalysis TEOS and GOTMS in molar ratio equal to 10. The water and ethyl alcohol (EtOH) have been added in the following molar ratio:

$$TEOS : H_2O = 1 : 2 \text{ and } TEOS : EtOH = 1 : 4$$

By using 0.24 mol of TEOS, 0.1ml of chloride acid at 37wt% has been added. The extraction of solvents has been carried out in a oven at 50°C in vacuum for 5h. Then the siloxane mixture (oligomers) has been added to the functionalised epoxy resin to produce nominal silica content ranging from 5 to 15wt%. Finally, a stoichiometric amount of MXDA hardener has been added taking into account the amount of epoxide groups APTES-functionalized. A post-curing at 150°C after 18h at 23°C has been performed. The samples were named ***Ep-xAP-Siy-Ol***, where x indicates the weight percentage of epoxide groups functionalised with APTES and y the nominal silica content.

4.4.3 Sol-gel in-situ (Ep- xAP-Siy-IS)

DGEBA has been functionalized with APTES at 70°C in nitrogen atmosphere for 10' and then cooled in ice water to immediately stop the functionalization reaction. A siloxane precursors solution has been prepared by mixing at room temperature for 10' TEOS and GOTMS in molar ratio of 10 and the catalyst DBTDL (0.5 wt%) and then added to the functionalized epoxy resin, the final mixture being transparent. Finally, a mixture of water (HCl/H2O 2wt%) in molar ratio [TEOS:H2O = 1:3] and MXDA in stoichiometric amount has been added. The hybrid samples have been post-cured at 150°C after 18h at room temperature. The samples were named ***Ep-xAP-Siy-IS***, where x indicates the weight percentage of epoxide groups functionalised with APTES and y the nominal silica content.

The sol-gel process in the Ep-xAP-Siy-IS approach is base catalyzed because of the presence of MXDA amine hardener. It corresponds to the one-step polymerization carried out by Matejka et al. [4-6] in which all the organic and inorganic component are obliged to react altogether.

4.4.4 Preparation of Ep-Siy-Mx hybrids

A two steps method has been used in order to produce these hybrids, namely the pre-hydrolysis of silica precursors followed by the synthesis of hybrids themselves by mixing the siloxane precursors with epoxy resin DGEBA. In details, a mixture of TEOS and GOTMS in molar ratio of 0.67 have been employed. The hydrolysis reaction has been carried out at 60°C for 4 hours in 2-propanol by using DBTDL as catalyst and the following molar ratio for the water content:

TEOS : H_2O = 1 : 3 and GOTMS : H_2O = 1 : 1.5

A HCl/H2O solution at 2wt% has been employed. The pH of the resulting mixture was about 6-7. Then the reaction products have been mixed at room temperature with the epoxy resin DGEBA, in order to obtain the desired amount of siloxane content. The reaction mixture was concentrated by removing the sol-gel solvents, namely ethanol, 2-propanol and water, by using a rotavapor *in vacuum*. The extraction has been carried out for 15' at 75°C and 30' at 90°C. During the first step at 75°C for three times, a mixture of water and 2-propanol (i.e. 1 ml of H2O + 0.8 ml of 2-Propanol) has been added to the extracting mixture to make complete the hydrolysis and condensation of siloxane moieties. The hybrid mixture was then cooled at room temperature and the hardener MXDA in stoichiometric amount with respect to the overall epoxide content (namely from DGEBA and GOTMS) has been added. The mixture was mechanically stirred and degassed *in vacuum*. The hybrids samples have been cured on aluminium dish to form film with a thickness ranging from 1-3 mm, at 30, 60, 80, 100, 120 and 150°C for 1h during each curing step. The hybrids are labelled as ***Ep-Siy-Mx***, y indicating the actual silica content (i.e. the residual value at 750°C of TGA in air flow thermograms), ranging from 3 to about 20 (Table 2).

Samples	Siloxane content (wt %)
Ep-Mx	-
Ep-Si3- Mx	3.4
Ep-Si7-Mx	7.6
Ep-Si12-Mx	11.7
Ep-Si15-Mx	14.8
Ep-Si20-Mx	21

Table 2 - Ep-Siy-Mx hybrids samples. The corresponding actual siloxane content is listed.

4.4.5 Preparation of Ep-Siy-Je hybrids

TEOS and GOTMS in molar ratio of 0.67 are partly hydrolyzed in 2-propanol by using DBTDL as catalyst, and the following molar ratio for the water content:

TEOS : H_2O = 1 : 3 (mol/mol) and GOTMS : H_2O = 1 : 1.5 (mol/mol)

A solution at 2wt% of HCl in H2O has been employed. The precursors mixture has been stirred at 60°C for 4 hours and then cooled at room temperature. DGEBA has been added and then the solvents has been removed by rotavapor extraction at 40°C for 15'. The hybrid mixture was cooled at room temperature and then the hardener Jeffamine D230 has been added in stoichiometric amount with respect to the both DGEBA and GOTMS epoxide content. The hybrids samples have been cured on aluminium dish to form film with a thickness ranging from 1-3 mm for 4h at 80°C and 12h at 180°C. The hybrids are named ***Ep-Siy-Je***, y indicating the actual silica content (i.e. the residual value at 750°C of TGA in air flow thermograms), ranging from 7 to 22wt% (Table 3).

Samples	Siloxane content (wt %)
Ep-Je	0
Ep-Si7-Je	6.6
Ep-Si12-Je	12.3
Ep-Si18-Je	17.8
Ep-Si22-Je	21.5
Ep-Je	0

Table 3 - Ep-Siy-Je hybrids samples. The corresponding actual siloxane content is listed.

4.5 Characterization Techniques

In this section there is a brief description of the several techniques and experimental conditions adopted in the research to perform a complete understanding of the chemical, physical and thermo-mechanical behaviour of the hybrid/nanocomposites epoxy-based. For a few techniques, generally not usual in the polymer field, the basic principles are also reported.

4.5.1 Fourier Transform Infrared (FT-IR) analysis

Fourier transform infrared (FT-IR) spectra were performed by using a Nicolet FT-IR Fourier transform infrared spectrometer. FTIR spectra were collected over the range 400-4000 cm^{-1} with a resolution of 4 cm^{-1}.

Infrared spectroscopy was used to monitor the aminosilanes grafting process, in the silylation reaction of Na-MMT, on KBr pressed disks containing 1% w/w of inorganic powders. The spectra were acquired in transmission mode.

Moreover, to the aim to follow the epoxide cross-linking reaction, the FT-IR spectra was acquired in transmission mode by leaving a thin film of either the

epoxy matrix or hybrid mixture on a KBr dish. The epoxide groups reduction has been monitored in real time during the samples heating. In order to estimate the conversion degree, α, of epoxide groups with respect to their initial concentration, the following relationship has been applied:

$$\alpha = \frac{C_0 - C_t}{C_0} = 1 - \frac{C_t}{C_0}$$

where C represents the concentration of epoxide groups and the subscripts 0 and t denote, the initial and the generic reaction time t, respectively. According to the Lambert-Beer law, the relation between the conversion degree and the absorbance A (at 916 cm^{-1} for the epoxide group) can be obtained. Furthermore, because of the reduction of film thickness during the curing cycle, a correction of the absorbance area has be done. To this end, the area corresponding to the absorbance of epoxide group must be normalized by using the area of an internal reference. To this end, the stretching of aromatic CH groups at 1509 cm^{-1} has been used, so that the epoxide conversion degree can be assessed according to the following relationship:

$$\alpha = \frac{\overline{A}_0^{916} - \overline{A}_t^{916}}{\overline{A}_0^{916}} \qquad \text{where} \qquad \overline{A}^{916} = \frac{A^{916}}{A^{1509}}$$

Additionally, for the Ep-Siy-Je hybrid samples, due to the high reactivity of the hybrid mixture at 80°C, the relative absorbance area at 25°C has been considered as the first point, i.e. the A_0^{916}.

4.5.2 Gel permeation and chromatography

Gel permeation chromatography (GPC) also known as size exclusion chromatography (SEC) is a chromatographic method in which molecules are separated based on their size. In SEC, a column is packed with a porous materials (typically silica or crosslinked polystyrene) and solvent is forced through the column at rate typically 1ml/min and pressure of 50 to 200 bar. A sample is dissolved in the same solvent that is running through the column and is then introduced into the solvent stream going through the column.

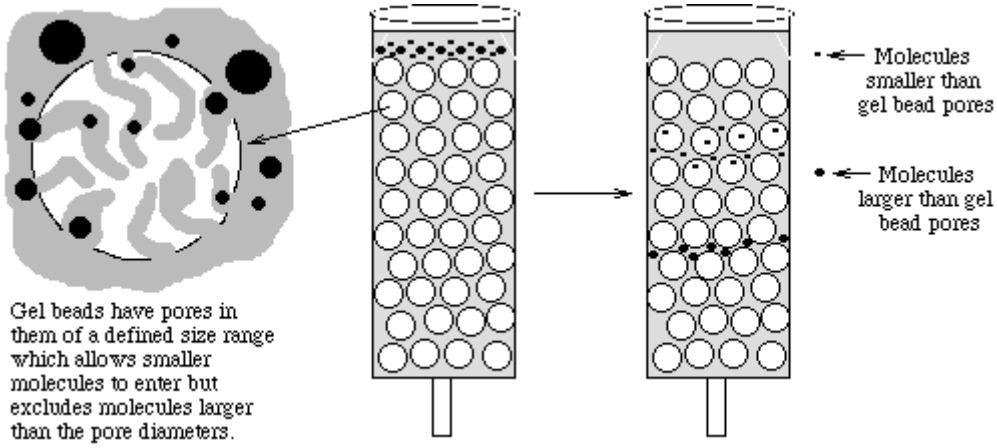

Figure 18 - Schematic working picture of packed column in GPC technique.

A detector monitors the concentration of sample exiting the end of the column. Inside the column, molecules are separated based on their hydrodynamic volume, namely the volume the molecule occupies in a dilute solution. For polymers this can vary greatly with the particular solvent and temperature. By studying the properties of polymers in particular solvents and by calibrating each column setup with samples of known molecular weight, it is possible to get a relative distribution of molecular weights for a given polymer sample. Inside the column, molecules are separated by whether or not they can fit within the pore size of the

packing materials. As a molecule flows through the column it passes by several porous beads. If the molecule can fit inside the pore then it is drawn in by the force of diffusion. There it stays a short while and then moves on. If a molecule cannot fit into a pore then it continues following the solvent flow. For this reason, in GPC column, molecules with larger size will reach the end on the column before molecules with smaller size. The effective range of the column is determined by the pore size of the packing. Any molecules larger than all the pores in a column will be eluted together regardless of their size. Conversely, the smaller molecules can enter the pores more easily and therefore spend more time in these pores, increasing their retention time. Finally, for polymer separations the pore sizes should be on the order of the polymers being analyzed.

According to Matejka, [8] the GPC measures were carried out filling the column with polystyrene-divinylbenzene gel and using THF as eluent. They were used in the Ep-Siy-Je procedure both to assess the inorganic network growth during the sol-gel reaction at 60°C and to follow the cross-linking reactions of DGEBA/siloxane hybrid mixture without the addition of the hardener.

4.5.3 Viscosity measures

The viscosity of reacting epoxy resin with APTES coupling agent was measured at 22°C in a Plexiglas beaker with a static Vibro Viscosimeter A&D model SV-100. The Vibro Viscosimeter measures the viscosity, in real time, by controlling the amplitude of the sensor plates immersed in a sample, specifically the value of viscosity is directly proportional to the driving electrical current needed to vibrate two sensors at a constant frequency of 30 Hz.

4.5.4 Differential Scanning Calorimetry (DSC)

Differential Scanning Calorimetry (DSC) is commonly used to detect transitions and sub-transitions such as melting point and glass transition temperature (T_g) of the polymeric materials.

The DSC measures on solid samples have been performed on a TA Instruments model Q1000. The samples (about 10mg in weight) have been heated in hermetic aluminum pans from -40 to 250°C at a heating rate of 10°C/min. Whereas liquid samples have been analyzed by carrying out the measure suddenly after addition of amine hardener on a TA Instruments model Q20 in the temperature range -120 to 250°C. A second scan, if does, has been done by using the same heating rate.

4.5.5 Dynamic Mechanical Thermal Analysis (DMA)

Dynamic-mechanical measurements were performed on a DMA Q800 of TA Instruments.

For the *Epoxy/MMT* Composites the single cantilever method at a frequency of 1 Hz and 25 μm strain amplitude has been used. Heating of the specimens was performed at 3°C/min in the temperature range from 0°C to 180°C. The samples were dried at 80°C for 24h before testing.

The measure on the *Epoxy/silica Hybrids* have been carried out using a sinusoidal tensional deformation. The samples were heated from -50 to 250°C at a constant hating rate of 3°C/min. The frequency and amplitude of the vibration were adjusted to 1 Hz and ±5μm, respectively.

4.5.6 Thermogravimetric Analysis (TGA)

Thermogravimetric analysis (TGA) was carrying out on a TGA 2950 thermobalance (TA Instruments). Samples were heated from 30 to 750°C at a heating rate of 10°C/min under either nitrogen or air flow. Some results were displayed in terms of first derivative mass loss (DTA).

To the aim to assess the grafting degree of aminosilanes after the silylation reaction on MMT powders, the thermogravimetric analysis in nitrogen flow has been used and the amount of grafted and intercalated aminosilanes was calculated using the following relationship [9]:

$$silane\ grafted\ amount\ (mequiv/g) = \frac{10^3 \times W_{200-600}}{[100 - (W_{200-600})] \times M}$$

where $W_{200\text{-}600}$ corresponds to the mass loss between 200 and 600°C and M (g/mol) is the molecular weight of the grafted silane molecules. The percentage of grafted amount, which corresponds to the percentage of organic aminosilane moieties with respect the total inorganic mass, was calculated as follows:

$$silane\ grafted\ amount\ (\%) = \frac{100 \times W_{200-600}}{100 - W_{200-600}}$$

4.5.7 Cone calorimeter test

Combustion studies were performed by using an oxygen consumption calorimeter (Fire testing technology Limited FFT dual cone calorimeter model) in the vertical orientation mode. The rectangular samples 10x10x5 mm^3 were irradiated with a Heat Flux equal to 35 kW/m^2. Heat release rate (HRR) were measured in triplicate and the results are shown as the average of the curves. It is worth mentioning that usually the HRR measurements with Cone calorimeter are

performed by adopting the horizontal orientation mode. That is the sample is orientated horizontally with respect the irradiating metal jackets. However for epoxy resins, which are characterized by a microstructure intrinsically inhomogeneous, this configuration provides not reliable results. The vertical orientation mode allowing a heat boundary layer to be established around the sample, results a method more reliable and offers the advantage of more reproducible results.

4.5.8 Physical and mechanical properties testing (tensile test)

The tensile properties (tensile strength at break, strain at break and elastic modulus) of the neat epoxy sample and the *Epoxy/MMT Composites* were measured with a SANS CMT universal testing machine in accordance with the ASTM-D638-03 by using a load cell of 1 kN, a crosshead speed of 1 mm/min and an initial pre-load of 0.2 N. The measurements were carried out at room temperature and an average value of five samples was determined.

Mechanical tests on *Epoxy/Silica Hybrids* were performed using a universal testing machine (Instron model 4505), equipped with a temperature control chamber. Values for the Young's modulus were obtained from the tangent of the force/deflection curve using 3-point bending tests, (ASTM D790 method), using rectangular specimens, 60.0x6.0x4.0 mm, and a span/width ratio of 8:1. The measurements were carried out at a cross-head speed of 1 mm/min, at temperatures varying from ambient temperature to 180 °C.

The yield strength was measured in compression on specimens, 60.0x6.0x4.0 mm, loaded along the length. The tests were carried out at different cross-head speeds and in the same temperature range employed for modulus measurements. Due to the absence of a definite maximum in the load/deformation curves the

yield strength was estimated as the stress corresponding to the 5% offset strain from the elastic strain.

Fracture mechanics tests were carried out according to the ASTM D5045-99 standard method. A multiple crack length procedure was used in which single edge notch (SEN) specimens, 60.0x6.0x4.0 mm, with notch length varying from 1.5 to 4.5 mm, extended by 0.2 mm by a razor blade fixed to a micrometer apparatus, were fractured in a three point bending mode at room temperature. At least three samples for each notch length were used. The final length of the notch was measured using an optical microscope after fracturing the specimens.

The critical stress intensity factor, K_c, was calculated according to the following equation:

$$K_c = Y\sigma\sqrt{a}$$

where σ is the stress calculated as the outer skin stress for a rectangular beam in 3-point bending, Y is the compliance calibration factor obtained from the tables quoted in the literature [10] and a in the notch length.

The critical strain energy release rate, G_c, was estimated through the equation,

$$G_c = \frac{U}{BW\phi}$$

where U is the energy at fracture initiation, B and W are the thickness and the width of the specimens, respectively, and ϕ is the correction factor that takes into account the rate of change of compliance (C) with crack length.

$$\phi = C\left[\frac{dC}{d(a/W)}\right]^{-1}$$

The values of ϕ were obtained from the tables reported in literature [11].

4.5.9 Nanoindentation measures

The indentation experiment was performed with a NanoTest^{TM} Platform made by Micro Materials Ltd to evaluate the material's mechanical properties including modulus, hardness and creep behavior. A Berkovich diamond tip with three-side pyramidal geometry is driven to indent the surface of sample. The nano-indentation tests was conducted at a maximum load of 100 mN, with an initial load of 0.02 mN. The load was then held at maximum value for 60 s in order to monitor the creep behavior of neat epoxy and composite samples. Finally the indenter was withdrawn from the sample with the same rate as in the loading cycle until 10mN was reached. At least 20 indents were performed on each sample and the distance between the indentations was about 100 nm to avoid an interaction effect. The Hardness has been evaluated as the indentation maximum load (i.e. 100mN in this experiment) divided by the projected contact area which for a perfectly sharp Berkovich indenter is calculated as:

$$A = 24.56 h_c^2$$

where h_c is the contact depth.

The elastic modulus has been calculated from the reduced elastic modulus by using the following formula:

$$\frac{1}{E_r} = \frac{1-\nu^2}{E} + \frac{1-\nu_i^2}{E_i}$$

where E and ν are the elastic modulus and the Poisson's ratio for the sample respectively, and E_i and ν_i are the same for the indenter. For the case at hand ν has been set equal to 0.35 [12] while for diamond E_i has been set equal to 1140GPa and ν_i to 0.07 [13].

4.5.10 Scanning electronic Microscopy (SEM) and Energy Dispersive Scanning (EDS)

In scanning electron microscopy (SEM) the radiation that interacts with the specimen is a beam of high energy electrons, produced from a filament and accelerated by a high voltage. Three imaging signals can be used back scattered electrons, secondary electrons and X-rays. Characteristic X-rays have well defined energies from different atoms. Thus analytical information can be obtained from an X-ray spectrum. This technique is well known as Energy Dispersive Scanning (EDS). Back scattered electrons are primary beam electrons that have been elastically scattered by the nuclei in the sample and escape from the surface. Thus they can be used to obtain compositional contrast in the sample. Secondary electrons are emitted with low energy from the top few nanometers of the materials. This technique yields topographic images of the sample surface.

Scanning electron microscope (SEM, type Leica S440) was used to observe the morphology of the fracture surface of the samples submitted to tensile tests. A thin layer of gold was sputtered on the fracture surface of specimens, prior to SEM investigation, for providing electrical conductivity.

4.5.11 Wide (WAXS) and Small Angle X-ray Scattering (SAXS)

Macromolecular scale structure is investigated by SAXS method. As known, in addition to the size of the polymers or heterogeneity domains, the SAXS method also gives a geometrical description of the structures using the concept of fractal geometry, because random processes of polymerization or aggregation usually lead to the formation of fractal objects. The fractal structure is characterized by

mass fractal dimension D_m, which is a measure of the compactness or the shape of the fractal object. D_m describes volume distribution of a mass, m, as $m \sim r^{Dm}$, where r is the radius of the fractal object.

The internal structure of the siloxane domains could be extracted by assuming the Multiple Structural Level Model of Beaucage et al [14] which is capable describing scattering functions containing multiple length scales (Guinier regimes) separated by power low scaling regimes (Porod regimes). This approach has been widely applied to scattering data from in situ produced silica/siloxane domains. In particular the Guinier regimes account for the several length scales which constitute the hierarchical structure of the inorganic domain while the power regimes give information about the fractal surface or the fractal mass of the fractal object. A log–log plot of SAXS data, called Porod plot, could give an indication of the fractal nature of inorganic domains, specifically if the system displayed a mass or surface fractal behaviour [15]. The most important parameters extracted from the log-log diagram and used to determine the internal structure of the inorganic domains are either the fractal dimension D_m, or the fractal surface D_s, estimated from the slope of the curve in SAXS profiles and the q values where a discontinuity is observed in the linear behaviour of the SAXS diagram [16]. In detail, if the slope of the scattering curve ranging from 0 to -3, a fractal dimension D_m of the fractal object is extracted. D_m is a measure of the compactness of the inorganic domains and describes volume distribution on the mass fractal [5]; the higher the D_m absolute value, the higher the compactness of the fractal object. On the contrary, if the slope ranging from -3 and -4, information about the fractal surface D_s, as the shape of inorganic domains, could be extracted. Dense smooth particles give a slope of -4. Moreover, the inorganic structure size, L, could be estimated by using the following equation:

$$L=2\pi/qi$$

where *qi* represents the value of the scattering vector in correspondence of the i-change in the slope of the log-log diagram. Whereas, when the SAXS profiles showed the knee shape characteristic of Guinier regime, the gyration radius (Rg), which gives a measure of the mean square distance of the scattering centres within inorganic domains from the centre of gravity [16] was determined. In detail, Rg is related to sizes of inorganic siloxane domains, and was calculated from the slope in the linear region of a plot of *ln(I(q))* versus q^2, according to Guinier's relation [17]:

$$I(q) \propto \exp(-q^2 R_g^2 / 3)$$

Therefore, SAXS measures allowed to estimate both the internal structure and dimension of the siloxane domains of Epoxy/Silica Hybrids

X-ray diffraction experiments were carried out to evaluate the shift of the (001) basal spacing of Na-MMT after the silylation reaction. The intergallery space between the clay platelets is defined as the basal spacing, and is usually denoted as d_{001} since it is derived from the (001) diffraction peak by using Bragg equation. The displacement of the (001) diffraction peak upon silylation was followed by WAXS measurements.

Wide (WAXS) and Small Angle X-ray Scattering (SAXS) were performed using an Anton Paar SAXSess camera equipped with a 2D imaging plate detector. 1.5418Å wavelengths CuKα X-Rays were generated by a Philips PW3830 sealed tube generator source (40kV, 50mA) and slit collimated. All scattering data were dark current and background subtracted, and normalized for the primary beam intensity. Figure 19 shows the image of the apparatus SAXSess by Anton Paar with an example of 2-D SAXS and 1-D SAXS results.

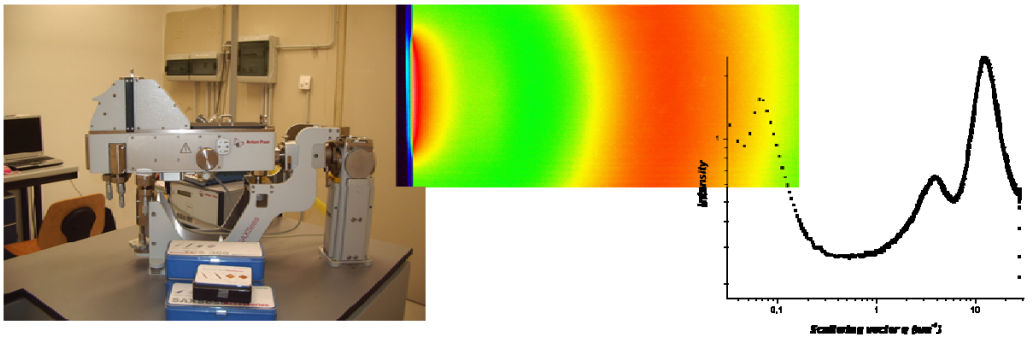

Figure 19 – SAXSess instrument, 2-D SAXS (in the middle) and 1-D SAXS profile (on the right).

4.5.12 Nuclear Magnetic Resonance (NMR) characterization

^{29}Si, ^{13}C, and ^{1}H-NMR spectroscopy are excellent tools for studying local structure at the atomic scale. In the case of epoxy-siloxane hybrids materials, the ^{29}Si-NMR spectroscopy allows to determine the conversion degree of siloxane domains, also during the inorganic condensation. The NMR analysis provides fractions of the structural units Q_i^j, corresponding to Si atoms with *j* hydrolyzed groups (Si-OH) and *i* siloxane bridges (Si-O-Si), as pictured in Figure 20. Distribution of these structure units characterizes the structure topology of silica. The condensation conversion is defined as:

$$\alpha_{Si} = \frac{\sum iQ_i}{4}$$

In the case of trialkoxysilanes GOTMS, the formed siloxane structure is described by the distribution of Ti units, i.e. the structural units with I siloxane bonds –O-Si- attached to the central atom. The conversion is defined as:

$$\alpha_{Si} = \frac{\sum iT_i}{3}$$

Therefore the total siloxane conversion degree is defined as:

$$q = \frac{T_1 + 2T_2 + 3T_3}{3} + \frac{Q_1 + 2Q_2 + 3Q_3 + 4Q_4}{4}$$

The assignment of the NMR bands is as follows: T_0 from -41 to -43 ppm, T_1 from -50 to -52 ppm, T_2 from -59 to -61 ppm, T_3 from -66 to -69 ppm [18], Q_4 at about -109 ppm, Q_3 from -101 ppm, Q_2 from -90 ppm and so on by decreasing of about 10 units meanwhile the siloxane structure become less bridged [19].

The ^{1}H, ^{13}C and ^{29}Si NMR provided information on both the hydrolysis and condensation degree of siloxane precursors and the stability of GOTMS epoxy ring during the pre-hydrolysis reaction mixture at 60°C. To achieve this goal, ^{29}Si, ^{13}C, and ^{1}H-NMR measures on liquid reacting mixture were performed on the un-dilute reaction solutions, by using a glass coaxial tube with the neat solution and deuterated water in two different sites in order to avoid any solvent influence. The ^{29}Si and ^{13}C-NMR spectra were measured in 54-mm at 25°C using a NMR spectrometer at frequencies of 75.4 and 50.6 MHz, respectively. An external standard, HMDS (hexamethyldisoloxane) was used for calibration of the ^{13}C and ^{29}Si scale, the chemical shift of 13C and ^{29}Si having the value of and 6 ppm, respectively, referred to TMS (tetramethylsilane). For measurement of ^{29}Si spectra of isolated fractions, the DEPT pulse sequence was used to increase sensitivity of the measurement. Deuterated water was used as the solvent (in the external site of the coaxial tube) for an internal deuterium block.

Solid-state ^{29}Si-NMR spectroscopy (29Si-CPMAS-NMR) was performed on a Bruker AV-300. NMR spectra were obtained by applying the following parameters: 5000 Hz of rotor spin rate; 5 s of recycle time; 5 ms of contact time; 33 ms of acquisition time; 12500 scans. Samples were packed in 4mm zirconia rotors with KelF caps. The pulse sequence was applied with a 1H ramp to account for the non-homogeneity of the Hartmann-Hahn condition at high spin

rotor rates.Chemical shifts are relative to tetramethylsilane, using an external sample of tetrakis-trimethylsilyl-silane (TTMSS; up-field signal -135.4 ppm) as secondary reference.

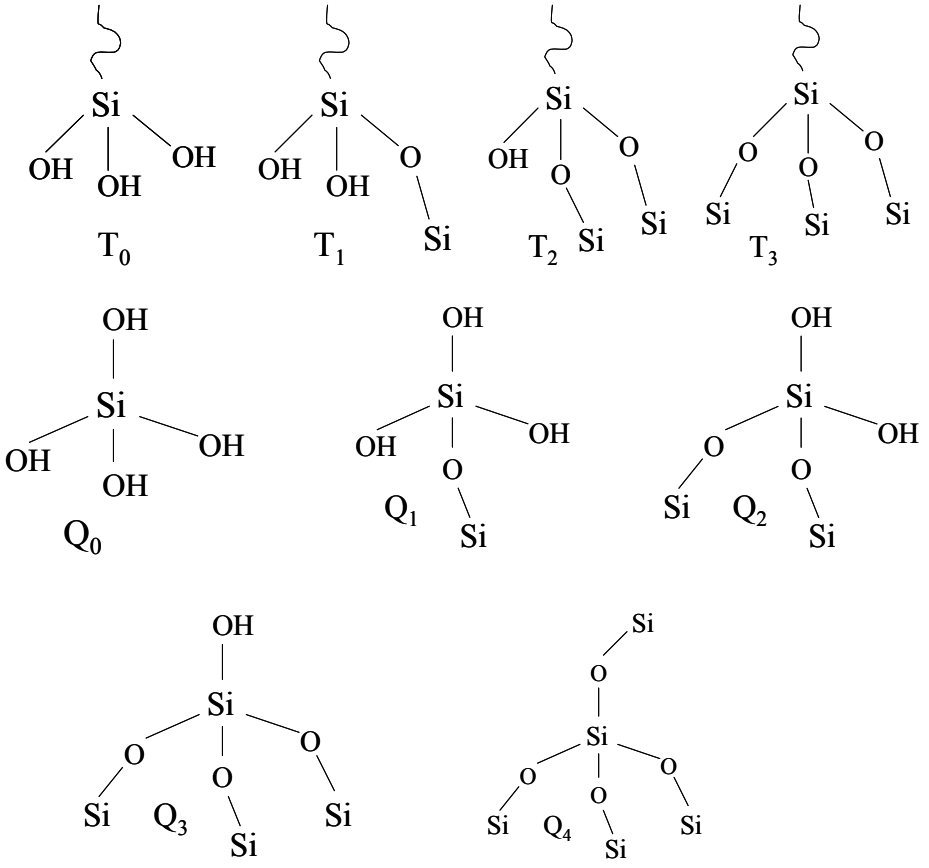

Figure 20 - Structure units in terms of *Ti* and *Qi* for GOTMS and TEOS, respectively.

4.5.13 Molecular Dynamics (MD) analysis

All molecular dynamics (MD) simulations were performed using Materials Studio (v.4.4, Accelrys, San Diego, USA). The starting structure of Na-MMT was taken from previous work [20-24]. The main object of the computational part of this study was the prediction of the basal spacing in the aminosilane functionalized MMT. Since the quantities affecting the MMT basal spacing are highly sensitive to the non-bonded components of the force field (FF) employed (e.g., atomic charges and van der Waals parameters), the ad hoc FF developed by Heinz and coworkers [25-26] was adopted for the optimization of the initial MMT structure and in all subsequent calculations. As demonstrated by Heinz et al. [25-26] for Na-MMT and other phyllosilicates, this accurately derived FF is able to describe, among many other properties, the thermodynamics of surface processes more reliably by reducing deviations of 50-500% in surface and interface energies to less that 10%, thus constituting a fundamental step towards a quantitative modeling of interface processes involving layered silicates.

Accordingly, the resulting lattice of the optimized MMT model was monoclinic, with space group C2/m, and characterized by the following lattice parameters: a = 5.20 Å, b = 9.20 Å, c = 10.13 Å, and $\alpha = 90°$, $\beta = 99°$, $\gamma = 90°$, in excellent agreement with the available literature [26-29].

According to the computational recipe adopted, the molecular models of the aminosilane compounds considered (see Scheme 3) were built and geometry-optimized following a well-validated MD-based protocol [20-24, 30].

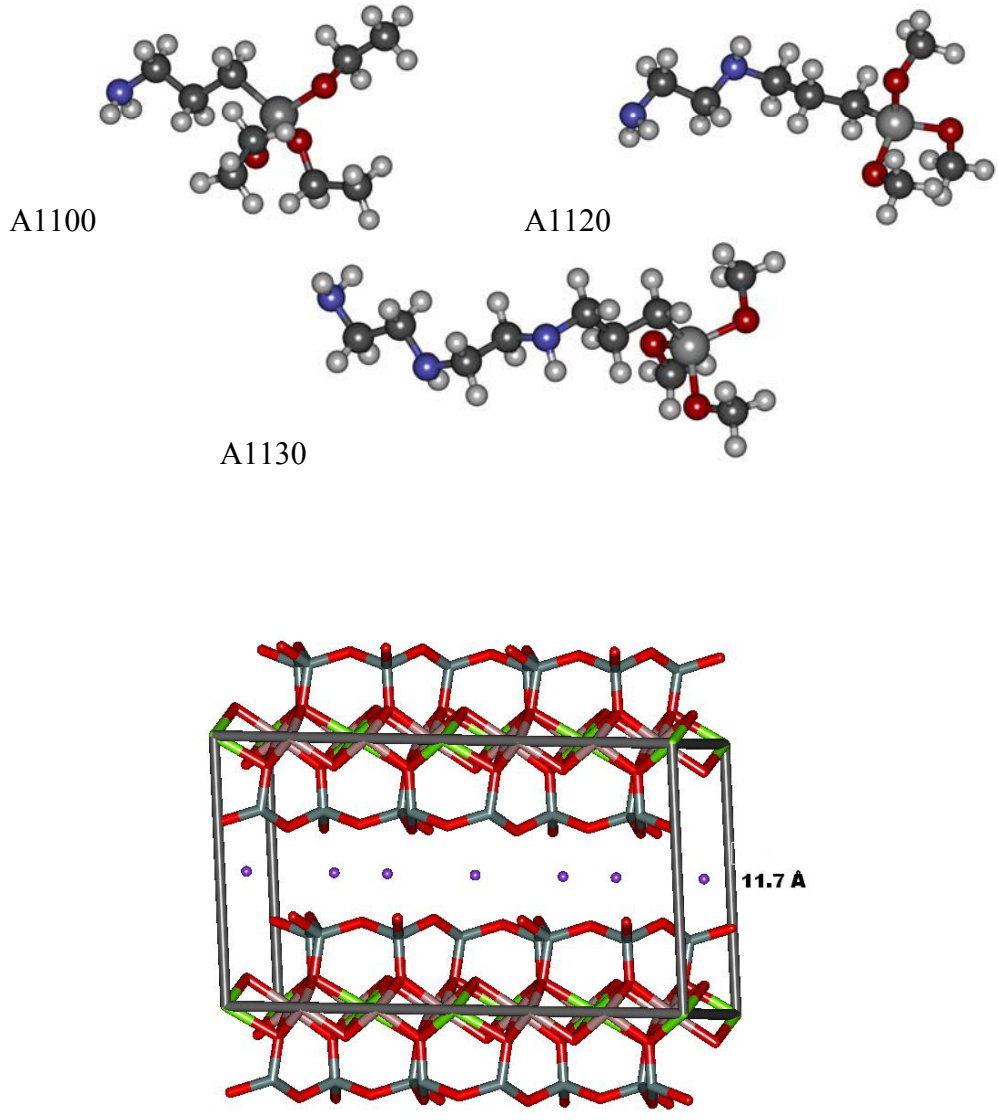

Scheme 3 - Chemical structures of the considered aminosilanes and crystallographic unit cell of MMT. The atom color code is as follows: gray, C; light gray, Si; blue, N; red, O, white, H; purple, Na; green, Al; pink, Mg.

The optimized MMT unit cell model was then modified by grafting the layers with a suitable number of aminosilane molecules [20]. For each aminosilane, three possible options were considered for creating covalent bonds between the

silicon (Si) atoms of the aminosilane and the MMT surface oxygen (O) atoms, as illustrated in Scheme 4.

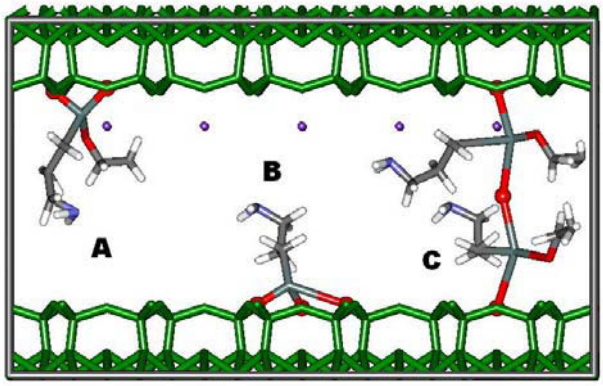

Scheme 4 - Schematic representation of possible covalent bonds formation between the Si atoms of the aminosilane molecules and the MMT surface O atoms. A: two covalent bonds on the same MMT surface; B: three covalent bonds on the same MMT surface; C: two covalent bonds bridging two MMT layers.

The new equilibrium position of the Na^+ counterions on the aminosilane-modified MMT sheets were determined following the procedure suggested by Heinz et al. [26]. Accordingly, half of them were placed 1 nm away on one side, and the remaining half 1 nm from the other side of the MMT layer in 10 different arrangements. Molecular mechanics energy minimizations were then performed to convergence, keeping all other MMT atoms fixed, and the structure with the lowest energy was finally selected for further simulations. In this configuration, the Na^+ ions were found at about 1.8 Å from the center of the surface oxygen atoms, or about 4.8 Å from the central plane of the metal atoms, in excellent agreement with previous simulations [31] and experimental NMR data [32].

Lastly, each aminosilane-MMT unit cell was replicated four times in the a direction, and three times in the b direction, thus yielding a final simulation

supercell for each aminosilane modifier with the following lattice parameters: a = 20.80 Å, b = 27.60 Å, and α = 90°, β = 99°, γ = 90°. The c values in the initial model of aminosilane-MMT supercells were prolonged according to a bi-layer arrangement of each aminosilane molecules.

Molecular mechanics (MM) and molecular dynamics (MD) simulation protocols were then applied, consisting of a preliminary cell energy minimization procedure followed by isobaric-isothermal (NPT) MD runs at 300 K. To avoid crystal structure deformation during minimization, initially both MMT layers were treated as rigid bodies by fixing all cell dimensions except the c axis, whilst all atoms in the interlayer space including the cations were allowed to move without any constraint. Then, in a second minimization round, also movement along the c axis was allowed, leading to a suitable starting interlayer distance for each model. Subsequently, 1 ns NPT MD experiments were performed at 300 K for each system, using the Verlet algorithm and an integration step of 1 fs. Again, both MMT layers were treated as rigid bodies by fixing all cell dimensions except the c axis, leaving all remaining atoms in the interlayer space free to move without any constraint. The Ewald summation method [33] was applied for treating both van der Waals and electrostatic interactions, while temperature was controlled using the Nosé thermostat [34].

The final basal spacing values for each aminosilane-MMT system were extracted from the final part (0.5 ns) of the equilibrated MD trajectory.

Additionally the molecular dynamics (MD) simulation was used to make a theoretical estimation of the length between two neighbouring siloxane cages bonded with Jeffamine D230 in *Ep-Siy-Je* hybrids samples. Here average size oxypropylene monomer unit is introduced (x=2 and x=3) for Jeffamine D230

[35] and two different atomistic models are built chemically linking two alkyl POSS cages and using one Jeffamine D230 molecule, viz. the cages react with two opposite $–NH_2$ groups, namely head-tail attach, or with the same $–NH_2$ group, i.e. head-head attach. Furthermore, with the aim of creating more realistic models, each glycidoxy group is considered reacted with a Jeffamine D230 molecule and, in turn, with a DGEBA chain. These model systems are simulated at 80°C.

4.6 References

[1] A. M. Shanmugharaj; K. Y. Rhee; S. H. Ryu; *J. Colloid Interface Sci.* , 298, 2006, 854.

[2] F. Piscitelli; G. Callegaro; M. Lavorgna; E. Amendola; Proceedings of the 4th International Conference on Times of Polymers (TOP) and Composites, Ischia, Italy, September 21-24, 2008.

[3] D. Acierno; A. D'Amore; L. Grassia, Eds.; University of Naples Federico II: Naples, IT, 2008; pp. 181-183)]

[4] L. Matejka; K. Dusek; J. Plestil; J. Kriz; F. Lednicky; *Polymer* 40, **1999**, 171.

[5] L. Matejka; J. Plestil; K. Dusek; *Journal of Non-Crystalline Solids* 226, **1998**, 114.

[6] L. Matejka; O. Dukh; J. Kolarik; *Polymer*, 41, **2000**, 1449.

[7] K. Zou; M. D. Soucek; *Macromol. Chem. Phys*, 205, **2004**, 2032–2039.

[8] L. Matejka; *Journal of Non-Crystalline Solids,* 270, **2000**, 34-47.

[9] N. N. Herrera; J. M. Letoffe; J. L. Putaux; L. David; E. Bourgeat-Lami; *Langmuir*, 20, **2004,** 1564.

[10] F. Brow; J. Srawley; *ASTM Spec Tech,* 510, **1996**, 13.

[11] E. Plati; J. G. Williams; *Polymer Engineering and Science* , 15, **1975**, 470.

[12] M. Krumova; A. Flores; F.J. Balta Calleja; S. Fakirov; *Colloid Polymer Science*, 280, **2002**, 591.

[13] L. Shen; L. Wang; T. Liu; C. He; *Macr. Materials and Engineering* , 291, **2006**, 1358-1366.

[14] G. Beaucage; T.A. Ukibarri; E.P. Black; D.W. Schaefer; *Multiple Size Scale Structures in Silica-Siloxane Composites Studied by Small-Angle Scattering, in Hybrid Organic-Inorganic Composites* edited by J.E. Mark, CYCLee and PA Bianconi, America Chemical Society, Washington, DC **1995.**

[15] C. S. Betrabet, G. L. Wilkes, *Chem Mater*, 7, **1995,** 535.

[16] M. Xiong; S. Zhou; L. Wu; B. Wang; L. Yang; *Polymer*, 45, **2004,** 8127.

[17] S. Yano; K. Iwata; K. Kurita; *Mater. Sci. Eng. C,* 6, **1998**, 75.

[18] L. Matejka; O. Dukh; J. Brus; W. J. Simonsick; B. Meissner; *Journal of Non-Crystalline Solids,* 270, **2000**, 34-47.

[19] *Colloidal silica, Fundamentals and Applications* , Ed. Martin J. Schick.

[20] M. Fermeglia; M. Ferrone; S. Pricl; *Fluid Phase Equilib.* , 212, **2003,** 315.

[21] R. Toth; A. Coslanich; M. Ferrone; M. Fermeglia; S. Pricl; S. Miertus; E. Chiellini; *Polymer*, 45, **2004,** 8075.

[22] G. Scocchi; P. Posocco; A. Danani; S. Pricl; M. Fermeglia; *Fluid Phase Equilib.*, 261, **2007,** 366.

[23] M. Fermeglia; M. Ferrone; S. Pricl; *Mol. Simul.*, 30, **2004,** 289.

[24] G. Scocchi; P. Posocco; J. W. Handgraaf; J. G. E. M. Fraaije; M. Fermeglia; S. Pricl; *Chem. Eur. J.*, 15, **2009,** 7586.

[25] H. Heinz; U. W. Suter; *J. Phys. Chem. B*, 108, **2004,** 18341.

[26] H. Heinz; H. Koerner; K. L. Anderson; R. A. Vaia; B. L. Farmer; *Chem. Mater.*, 17, **2005,** 5658.

[27] G. Brown; *The X-ray Identification and Crystal Structures of Clay Minerals*, Mineralogical Society Press, London, **1961.**

[28] S. W. Bayley; *Reviews in Minera logy*, Mineralogical Society of America Press, Chelsea, Michigan, **1988**.

[29] S. I. Tsipurski; V. A. Drits; *Clay Miner.*, 19, **1984,** 177.

[30] R. Toth; D. J. Voorn; J. W. Handgraaf; J. G. E. M. Fraaije; M. Fermeglia; S. Pricl; P. Posocco; *Macromolecules*, 42, **2009**, 8260.

[31] E. Hackett; E. Manias; E. P. Giannelis; *Chem. Mater.*, 12, **2000,** 2161.

[32] D. K. Yang; D. B. Zax; *J. Chem. Phys.*, 110, **1999,** 5325.

[33] P. P. Ewald; *Ann. Phys.*, 64, **1921,** 253.

[34] S. Nosé; *Prog. Theor. Phys.*, Suppl. 103, **1991,** 1-46.

[35] J. Brus; M. Spirkova; D. Hlavata; A. Strachota; *Macromolecules*, 37, **2004**, 1346-1357.

Chapter 5: Epoxy/MMT Composites

This chapter is concerned with the main aspects of the *Epoxy/MMT Composites* research and the related experimental results, including their interpretation and evaluation in relation to the objectives.

At first the silylation reaction of sodium montmorillonite (Na-MMT) using

- 3-aminopropyltriethoxysilane (A1100)
- N-(2-aminoethyl)-3-aminopropyltrimethoxysilane (A1120)
- 3-[2-(2-aminoethylamino)ethylamino]-propyl-trimethoxysilane (A1130)

has been described. The effects on the Na-MMT d-spacing of three aminosilanes of different chain length were studied in details by combining experimental and computational techniques.

Therefore, the silylated A1100 and A1120 MMT have been dispersed in DGEBA to prepare several composites. The Metaxylilene diamine (MXDA) has been used as hardener. The effect of both the silylation reaction and the dispersion method on the mechanical and thermal properties of nanocomposites has been evaluated.

5.1 Silylation reaction: preliminary study to evaluate the effect of aminosilanes and process parameters on the basal spacing of Na-MMT.

5.1.1 Fourier Transform Infrared analysis

Infrared spectroscopy was performed in order to identify the presence of the organic moieties on the Na-MMT platelets due to silylation. As pointed out by Zhao et al. [1], the main evidence for the successful intercalation/silylation of the aminoalkylsilanes in the Na-MMT galleries is the presence of C-H and N-H absorbance peaks in the corresponding IR spectra. Figure 21 shows an enlargement of the IR between 3800 and 2500 cm^{-1} for the A1100-MMT sample using the Procedures 1 and 2. In the same Figure, the spectra of the A1100 silane molecule and the pristine Na-MMT are also shown for comparison.

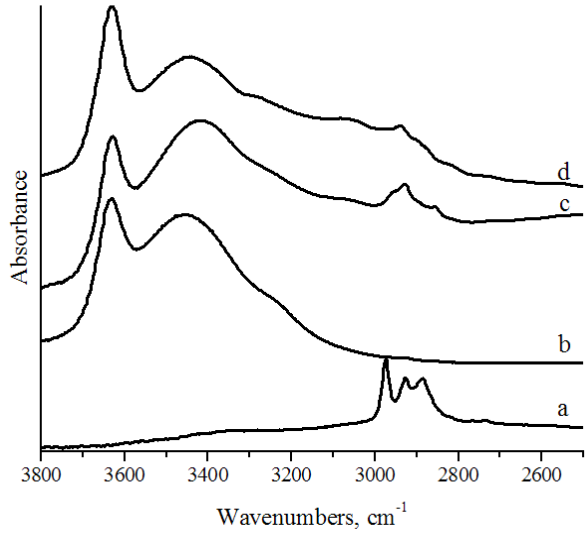

Figure 21 - Infrared spectra of: (a) A1100; (b) pristine Na-MMT; (c) A1100-MMT obtained from Procedure 1; (d) A1100-MMT obtained from Procedure 2

Compared to the neat Na-MMT spectrum, the two functionalized powders show additional peaks which can be attributed to the asymmetric and symmetric stretching vibrations of the methylene groups at 2936 and 2885 cm^{-1}, respectively, thus confirming the presence of the organic moieties on the Na-MMT surface [2-4]. A shoulder at ~3290 cm^{-1} in Figure 21 may be assigned to the stretching of the NH_2 group [5]. It is worth noting that, by increasing the aminosilane concentration and the reaction temperature, both methylene and NH_2 adsorption peaks in Figure 21 become progressively more pronounced, suggesting the presence of a larger amount of intercalated/grafted silane modifiers. No evaluation was performed on the relative intensity of the peaks related to the stretching vibration of isolated or hydrogen bonded OH groups (at 3620 cm^{-1} and 3440 cm^{-1}, respectively), because the possible presence of adsorbed water cannot be ruled out [6].

5.1.2 Thermogravimetric analysis

Thermogravimetric analysis (data not shown) was carried out on the Na-MMT powders prior and after the silylation reaction performed by Procedure 1. The mass losses in the range between 200 and 600°C were used as entry parameters in the following equations:

$$silane\ grafted\ amount\ (mequiv/g) = \frac{10^3 \times W_{200-600}}{[100 - (W_{200-600})] \times M} \quad (1)$$

$$silane\ grafted\ amount\ (\%) = \frac{100 \times W_{200-600}}{100 - W_{200-600}} \quad (2)$$

to evaluate the grafted aminosilane amounts, and the corresponding results are displayed in Table 4. Interestingly, by the application of Procedure 1 the grafted aminosilane amounts increase with increasing of the aminosilane alkyl chain.

		Mass loss[(a)] (%)	Grafted amount (mequiv/g)[(b)]	Grafting amount (%)[(c)]
A1100-MMT	Procedure 1	8.8	0.4 (I=68%; S=32%)	9.6
	Procedure 2	11.4	0.6 (O=21%; I=38%; S=41%)	12.8
A1120-MMT		14.6	0.8	17.1
A1130-MMT		18.8	0.9	23.2

Table 4 - Thermogravimetric analysis of functionalized MMT ([(a)]Mass loss between 200 and 600°C. [(b)]Determined by using Eq. (1). [(c)]Determined by using Eq. (2).).

In order to identify the degraded species, two pastes obtained by dispersing the Na-MMT in water and glycerol, respectively, were analyzed. The results are displayed in terms of first derivative mass loss in Figure 22.

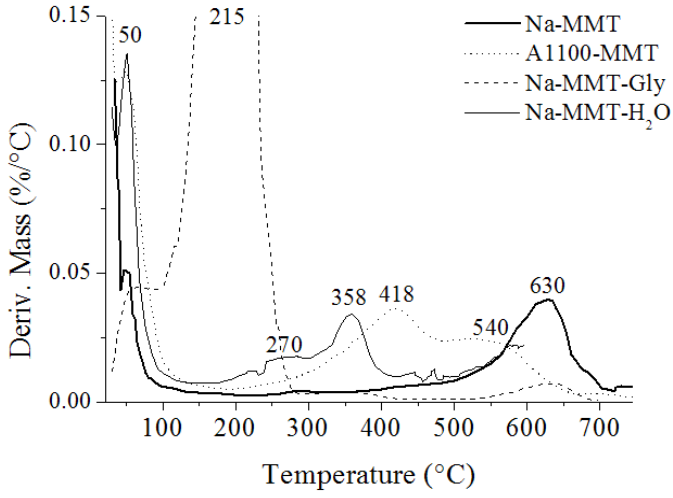

Figure 22 - DTA curves of pristine Na-MMT, functionalized Na-MMT powders, and Na-MMT/water and Na-MMT/glycerol pastes

The pristine Na-MMT shows two peaks at 50 and 630°C corresponding to the physically adsorbed water and the dehydroxylation of the clay, respectively [7-8]. The curve related to the Na-MMT-H_2O paste shows a peak at 50°C related to the loss of physically adsorbed water, whereas the two other peaks at 270 and 358°C (Figure 22) can be sensibly ascribed to the loss of intercalated water. By analogy, the intense peak at 215°C in the Na-MMT-Gly curve could be assigned to the loss of physically adsorbed glycerol, whilst the weak peak at ~350°C could refer to the intercalated glycerol. As for the Na-MMT-H_2O paste, the peak at higher temperature is due to MMT dehydroxylation. The DTG curves of the A1100-MMT system shows the mass loss of physically adsorbed water at 50°C, and other two peaks at 418 and 540°C, respectively. The first one is ascribable to the intercalated aminosilanes, whereas the broad peak at 540°C could be linked to the decomposition of the chemically bound aminosilanes [9]. Due to the consumption of hydroxyl groups belonging to the platelet edges, the Na-MMT dehydroxylation peak at 630°C nearly vanishes for this system. Lastly, the absence of the peak at 215°C related to the physically adsorbed glycerol speaks in favour of the reliability of the applied washing procedure.

With the goal of evaluating the effect of the reaction parameters (i.e. temperature and aminosilane concentration) on the silylation process, the amount of intercalated and grafted aminosilane was assessed by performing TGA analysis on the A1100-MMT systems obtained by using two different reaction routes summarized in Table 1 as Procedure 1 and 2. To eliminate the different contributes due to dissimilar adsorbed amounts of water, the curves shown in Figure 23 A were normalized assigning to each curve the value of 100 to the mass achieved at 150°C. It is worth noting that, as we will discuss later, by increasing both temperature and aminosilane concentration, the quantity of

aminosilanes able to penetrate into the Na-MMT gallery platelets slightly increases. Moreover, the grafted aminosilane amount increased by using the Procedure 2 compared to Procedure 1 (see Table 4). The DTG analysis performed on the A1100-MMT product obtained by Procedure 1 (Figure 23 B)) shows the presence of two peaks at 418 and 540°C, ascribed to the intercalated aminosilanes and chemically bounded aminosilanes, respectively [9].

Interestingly, the A1100-MMT product prepared following Procedure 2 displays a third peak at 310°C, which could be attributed to the aminosilane interacting with the outer surfaces of the clay platelets (see Figure 23 B).

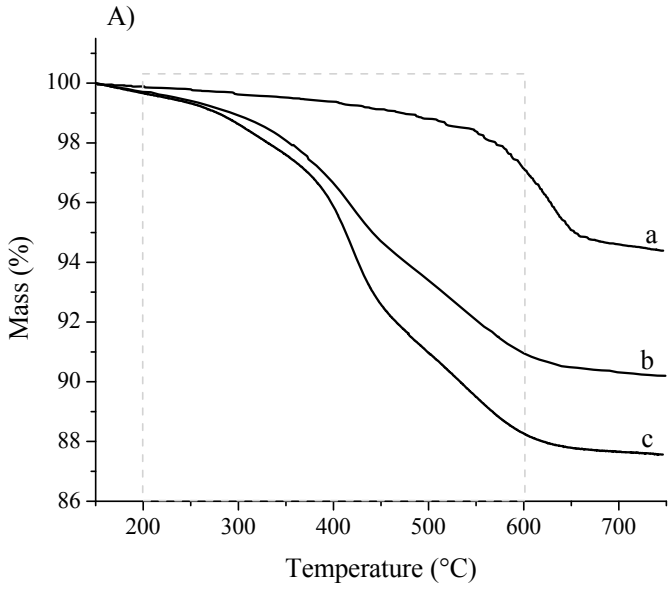

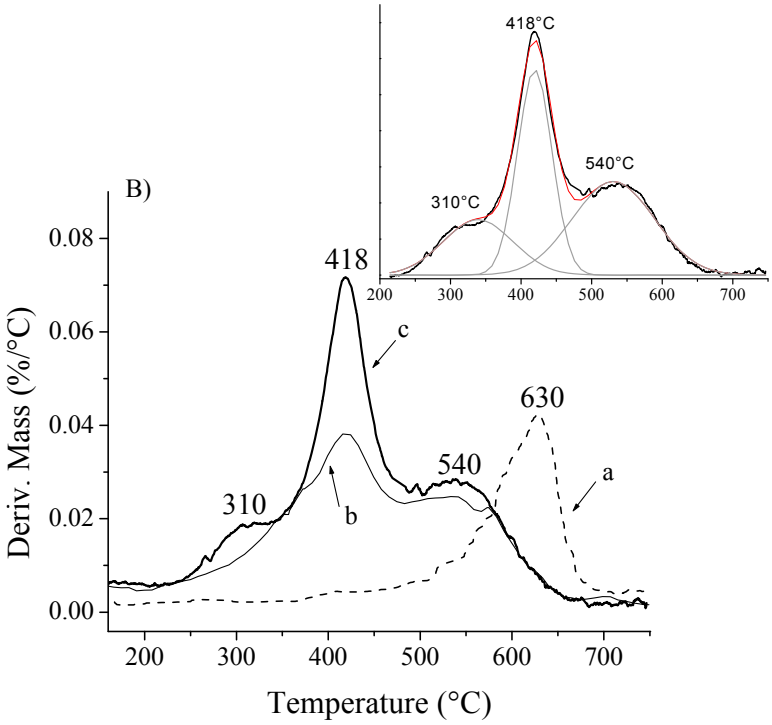

Figure 23 - Thermogravimetric analysis of Na-MMT before and after silylation reaction using two different process parameters: (A) weight losses curve; (B) first derivative of weight losses curve. The inset shows the peak deconvolutions: (a) pristine Na-MMT; (b) A1100-MMT obtained from Procedure 1; (c) A1100-MMT obtained from Procedure 2.

With these peaks assignments in mind, it was possible to quantify each degraded moieties using the deconvolution method of the Origin program. The results of these deconvolutions are summarized in Table 4, where *O* indicates the aminosilane interacting with the outside platelets, and *I* and *S* are the intercalated and chemically bonded aminosilanes, respectively. The results show that higher temperature and aminosilane concentration values lead to an increased amount of chemically bonded silanes with respect to the intercalated species. Moreover, and

perhaps more interestingly, only the A1100-MMT obtained by Procedure 2 displays aminosilanes interacting with the outside platelets.

5.1.3 Wide Angle X-ray Diffraction results and Molecular Dynamics predictions

To quantify the effect of the length of the aminosilane alkyl substituents on the Na-MMT basal spacing, silylation reactions were performed using the three different aminosilanes A1100, A1120 and A1130, and adopting Procedure 1. The X-ray diffraction patterns related to the (001) basal spacing, displayed in Figure 24, show that the introduction of any aminosilane type into the Na-MMT gallery shifts the peak at lower 2θ values compared to the pristine Na-MMT.

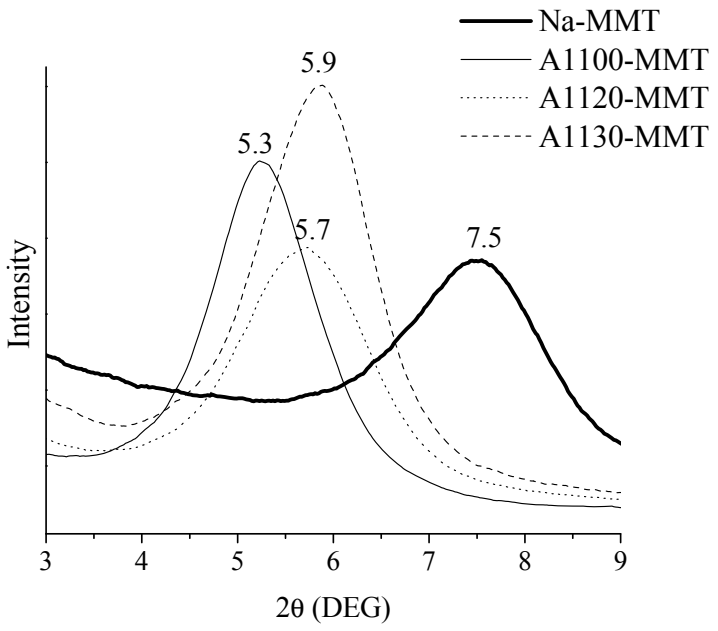

Figure 24 - X-ray diffraction patterns of Na-MMT before and after silylation reaction with different aminosilanes.

This increase of basal spacing is a clear signal that each aminosilane species has been grafted/intercalated in the inter-platelets space of Na-MMT. In detail, the neat Na-MMT shows a peak at 2θ equal to 7.5°, corresponding to a d-spacing value of 11.7Å, whereas the aminosilane-modified MMTs show diffraction peaks at 2θ values between 5.3 and 5.9° (Table 5). Concerning the effect of the alkyl chain length, the A1120-MMT and A1130-MMT systems show lower basal spacing values, 15.3 and 15.0Å, respectively, compared to the A1100-MMT, for which d_{001}= 16.7Å. A major, important conclusion which can be drawn from the analysis of data shown in Table 5 is that the longer the organic chain on the aminosilane molecules, the smaller the d-spacing in the relevant modified MMT, when the process parameters owing to the Procedure 1 have been used to carry out the silylation reaction.

System		2θ (deg)	d-spacing (Å)
Pristine Na-MMT		7.5	11.7
A1100-MMT	Procedure 1	5.3	16.7
	Procedure 2	4.0	22.2
A1120-MMT		5.7	15.3
A1130-MMT		5.9	15.0

Table 5 - d-spacing values for aminosilane-modified MMT estimated by XRD analysis.

To try to find a molecular rationale for the somewhat counterintuitive behavior reported above, molecular dynamics (MD) simulations have been performed on model systems.

Table 6 shows the values of estimated aminosilane-MMT interlayer spacing for all model systems considered (see Scheme 4) as obtained from 1 ns NPT MD

simulations. From these values, and the inspection of the relevant MD trajectories, we can draw some useful considerations.

First of all, independently of the aminosilane chain length, aminosilane molecules bridging two MMT layers (i.e., option C in Scheme 4) result in the lowest *d*-spacing values (see Table 6). From the viewpoint of further employment of aminosilane-MMT systems for polymer intercalation and/or exfoliation, this is the worst case possible, as the distance between MMT sheets is not only practically coincident with that of unmodified MMT (i.e., 11.7 Å), but also the aminosilane molecules act as 'anchoring points", counteracting any eventual macromolecular intercalation/exfoliation. Figure 25 shows an equilibrated MD snapshot of the A1100-MMT/option C system as an example.

System	**d-spacing (Å)**			
	Option A[a]	**Option B[a]**	**Average A and B**	**Option C[a]**
A1100-MMT Procedure 1	17.0	16.2	16.6	11.7
A1100-MMT Procedure 2	21.9	21.7	21.8	11.7
A1120-MMT	15.9	15.3	15.6	11.9
A1130-MMT	15.1	14.8	14.9	11.9

Table 6 - d-spacing values for aminosilane-modified MMT estimated by MD simulations ([a]For the meaning of Options A, B and C, please refer to Scheme 4.).

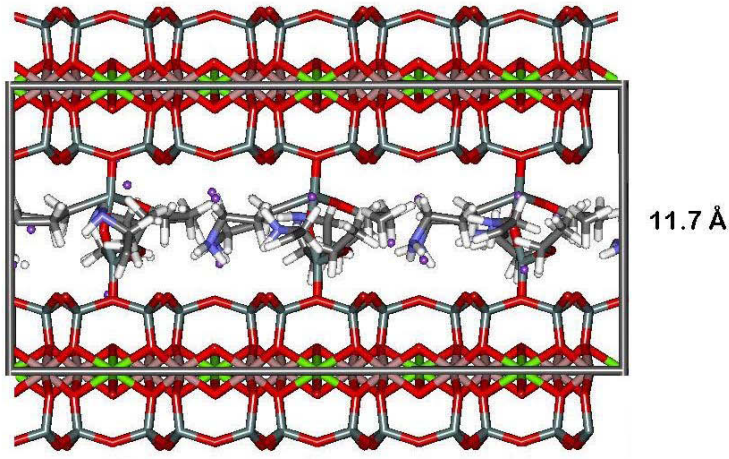

Figure 25 - Equilibrated MD snapshot of the A1100-MMT/option C system (see Scheme 4).

The results obtained for the two alternative bonding options (i.e., A and B in Scheme 4), expressed as average *d*-spacing values (see 3rd column in Table 6), are in excellent agreement with the experimental evidences discussed above. Notably, however, in contrast to common observations during the intercalation of small molecules between the silicate layers, where longer organic chains normally result in higher interlayer spacing, for aminosilane-MMT systems a reverse trend is observed. Indeed, longer aminosilane molecules yield lower *d*-spacing if the silylation reaction has been carried out by using the process parameters of Procedure 1.

A sensible explanation for this coupled experimental/simulation evidence could be hypothesized, keeping in mind that the organic tail of each aminosilane molecule features not only -CH_2 groups, which are hydrophobic, but also one or more -NH_2/NH- groups, which are endowed with hydrophilic character, and capable to originate both intra- and intermolecular hydrogen bonds (see Scheme 3).

Following these lines of reasoning, for the smaller aminosilane molecule A1100, characterized by the presence of a short chain and only one terminal $–NH_2$ group, a mechanism quite similar to that observed for quaternary ammonium salt-modified MMT can be envisaged. Accordingly, the A1100 aminosilane chains are attracted by the surface of clay and, while flattening onto it, provide a screening between the charges of the MMT layers ultimately favoring the weakening of interlayer attraction and, hence, a larger *d*-spacing value.

On the other hand, the other two aminosilane molecules (A1120 and A1130), featuring longer, more mobile chains with one and two –NH groups, respectively, have a strong tendency to interact among themselves (*via* both intermolecular hydrogen bonding and hydrophobic interactions). As a result, their flattening onto the MMT surface is reduced, the charge distribution on the MMT surface is less screened, and the clay sheets do not tend to separate as much as in the case of A1100 chains. Figure 26 (A) and (B) show a comparison between two equilibrated MD snapshots for A1100-MMT and A1120-MMT, respectively, in which the different degree of interactions between the aminosilane chains, resulting in a smaller d-spacing, is well evident.

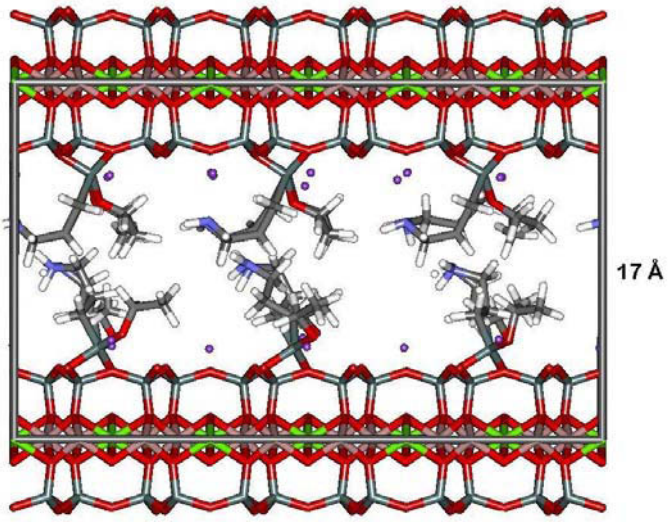

(A)

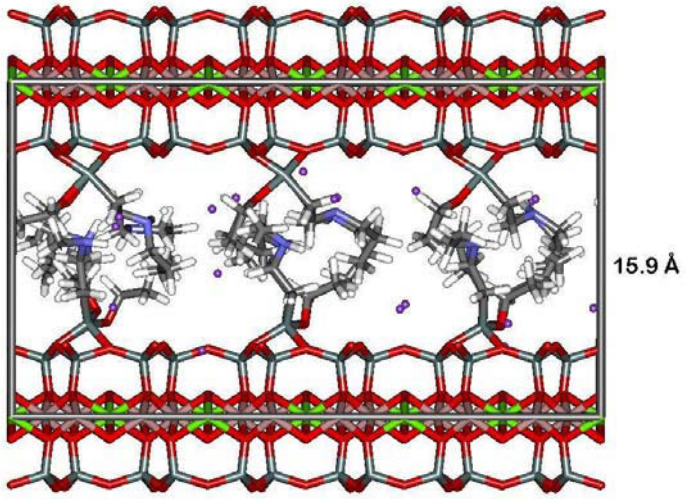

(B)

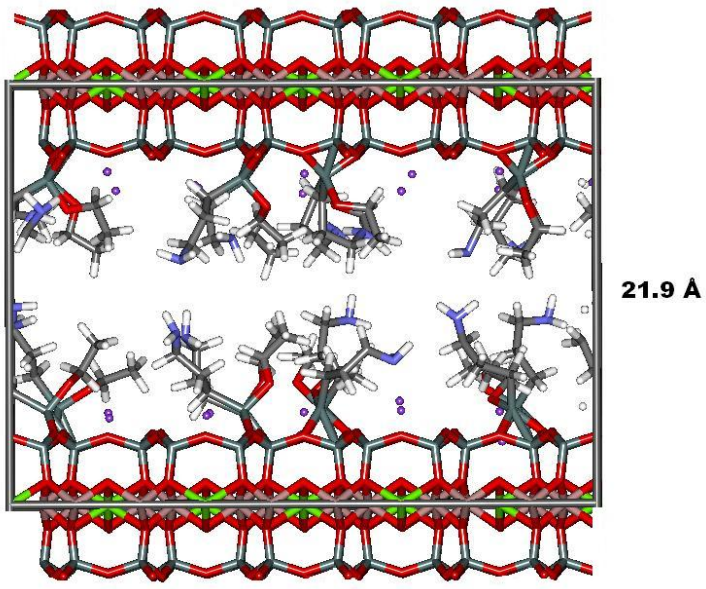

(C)

Figure 26 - Equilibrated MD snapshot of (A) A1100-MMT/option A, reaction Procedure 1, (B) A1120-MMT/option A, and (C) A1100-MMT/option A, reaction Procedure 2 systems (see Scheme 4).

The A1100-MMT system was further selected to check the effect of the preparation procedure adopted. Figure 27 shows the diffraction patterns related to the A1100-MMT obtained by using the Procedures 1 and 2 summarized in Table 4.

For the sake of comparison, the diffraction pattern of the pristine Na-MMT is also reported. In details, the silylation reaction with A1100 by Procedure 2 resulted in a further shift of the (001) diffraction peak up to $2\theta = 4.0°$, corresponding to a d-spacing value of 22.2 Å, with respect to that obtained with the silylation by Procedure 1 (16.7 Å). It is worth noting that the highest reaction temperature and aminosilane concentration (i.e. Procedure 2) allowed obtaining a higher enlargement of the basal spacing. Moreover, the broader (001) diffraction

peak reflects the variety of platelets gallery heights due to the grafted/intercalated products.

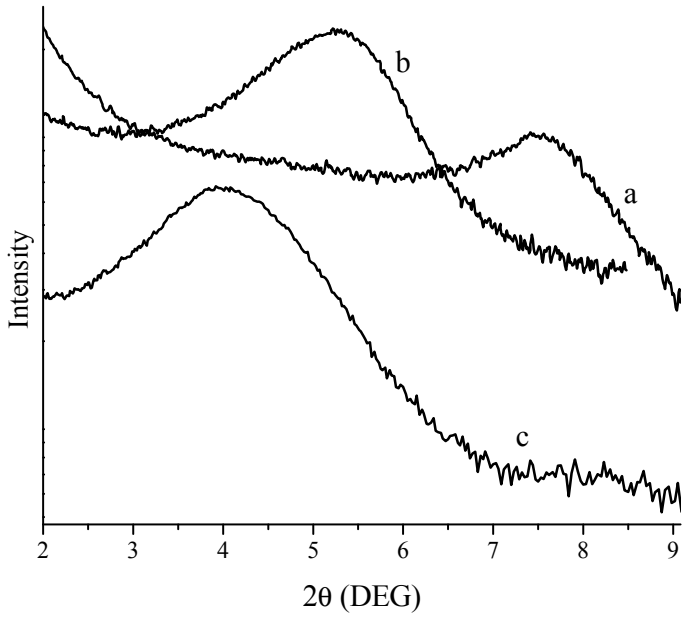

Figure 27 - XRD analyses performed on the Na-MMT before and after silylation reaction carried out using two different process conditions. (a) pristine Na-MMT; (b) A1100-MMT obtained with Procedure 1; (c) A1100-MMT obtained with Procedure 2.

In harmony with the experimental findings, the MD simulations reveal that, upon increasing the number of aminosilane molecules within the clay galleries indeed results in a larger value of the estimated d-spacing, which, in turn, is in excellent agreement with the corresponding experimental evidence (see values in Table 5 and Table 6). Figure 26(C) yields pictorial evidence in support to the numerical value. As can be easily seen by comparing Figure 26(A) and 26(C), when more aminosilane molecules are grafted/intercalated into the clay galleries the surface of the MMT layers is better screened by the silane hydrocarbon chains. Accordingly, the attraction forces among the layers are weakened, and the

resultant distance between them is higher. Not only, but, in the presence of higher silane concentration, the hydrocarbon chains of neighbouring molecules grafted/physical bounded to the same clay layer tend to interact more among themselves than with those laying on the opposite sheet. And this factor further concurs to lessen the overall attraction between facing sheets and, hence, a higher d_{001} value.

5.1.4 Conclusions

Three aminosilanes (A1100, A1120 and A1130) characterized by different lengths of the alkyl chains are used to functionalize the Na-MMT, by following two different routes in terms of reaction temperature and aminosilane concentration (summarized in Table 1 as Procedure 1 and 2). The appearance in the FT-IR spectra of additional peaks at 2936 and 2885 cm^{-1}, attributed to the asymmetric and symmetric stretching vibrations of the methylene groups, respectively, and a shoulder at ~3290 cm^{-1} assigned to the stretching of the NH_2 group, confirm the presence of the organic moieties on the Na-MMT surface. The WAXD analyses show that the introduction of any aminosilane type into the Na-MMT gallery allows the basal spacing to increase with respect to the pristine Na-MMT, which is a clear signal that each aminosilane species has been grafted/intercalated in the inter-platelets space. Moreover, the WAXD analyses highlight the surprising result that by using the process parameters of Procedure 1 the longer the organic chain on the aminosilane molecules, the smaller the d-spacing in the relevant modified MMT. The molecular dynamics simulation explains this result in light of the strong tendency of A1120 and A1130 aminosilanes to interact among themselves by both intermolecular hydrogen bonding and hydrophobic interactions because of the presence of one or two –

NH groups in their organic chains. On the other hand the A1100 molecules, owing only one $–NH_2$ group, provide a better screening between the MMT layers ultimately favouring the weakening of interlayer attraction and, hence, a larger *d*-spacing value. Furthermore the thermogravimetric analyses show that higher temperature and aminosilane concentration values lead to an increased amount of both chemically bonded silanes with respect to the intercalated species and aminosilanes interacting with the outside platelets.

5.2 Silylated-MMT epoxy-based nanocomposites

Keeping in mind the effects caused by the reaction temperature and aminosilane concentration on the actual basal spacing of Na-MMT, the process parameters have been changed in order to give rise a new procedure (listed as Procedure 3 in Table 1), with the goal to increase the Na-MMT basal spacing with the organic chain length of the aminosilane. Therefore, the Procedure 3 has been used to functionalise Na-MMT with A1100 and A1120 aminosilanes, and again the organic chain length has been correlated to the MMT d-spacing. The functionalised powders have been employed to prepare several *Epoxy/MMT Composites.*

5.2.1 Wide Angle X-ray Diffraction characterization of both silylated MMT and epoxy-clay composite.

The WAXS spectra of the silylated MMT with A1100 and A1120 aminosilanes by using the process parameters of the Procedure 3 are reported in Figure 28 as intensity versus the scattering vector, q equal to $q = 2\pi / \lambda sen\theta$ where λ is the wavelength of the X-ray beam and θ is the scattering angle. As far as the

silylated powder spectra are concerned, the peak associated to the interlayer spacing shifts to lower scattering vectors with respect to the pristine Na-MMT, indicating an enlargement of the MMT gallery between the silicate layers. In fact the MMT-A1100 powder shows a diffraction (001) peak shifted to 4.10 nm^{-1}, which corresponds to a interlayer spacing of 15.3Å. The average spacing between the clay layers for MMT-A1120 increases to 18.9 Å. It is worth noting that in the latter instance, a second reflection peak at a basal spacing value of 9.3 Å appears, probably corresponding to the (002) diffraction peak [10]. Clearly the interlayer spacing of MMT increases with the length of aminosilanes. These results indicate that aminosilanes have been grafted/intercalated onto the silicate layer surface and in the silicate gallery of Na-MMT.

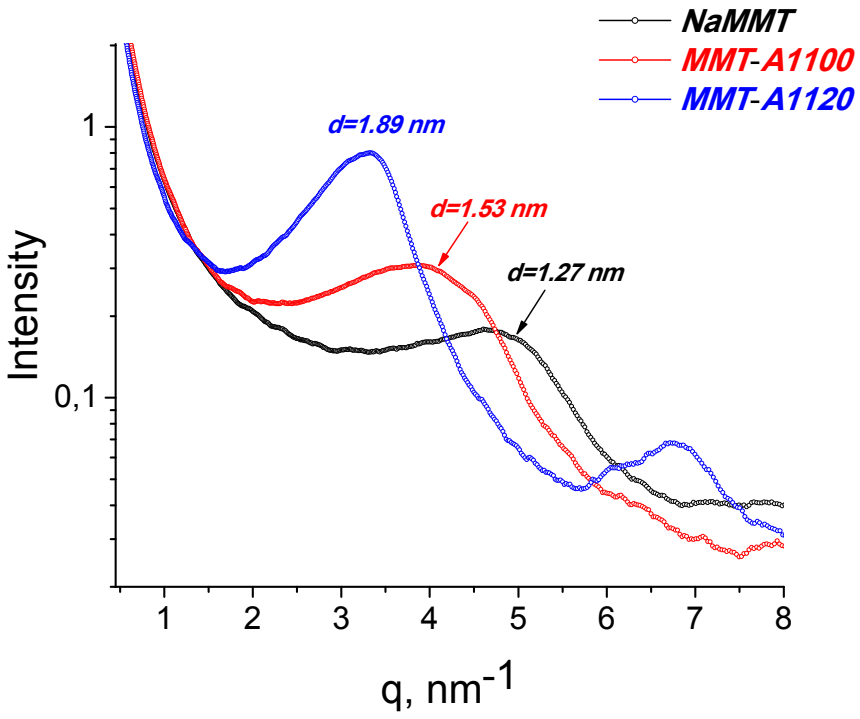

Figure 28 - X-ray diffraction patterns of the pristine and by silylation reaction functionalised Na-MMT powders.

Since the experimental procedures for the preparation of epoxy based composite materials was an *in situ* polymerization achieved through a preliminary mixing step carried out by sonication (S) or a combination of sonication and ball-milling (SB) and a subsequent curing step, it is worth to investigate the morphology of the materials at the two stages of the synthesis, namely before and after curing.

In Figure 29 the spectra of the epoxy pastes obtained by dispersing A1120-MMT powders through both sonication (S) and sonication/ball millng (SB), the spectrum of A1120-MMT powder and the spectrum of the composite A1120-MMT 3% wt/wt SB completely cured are shown.

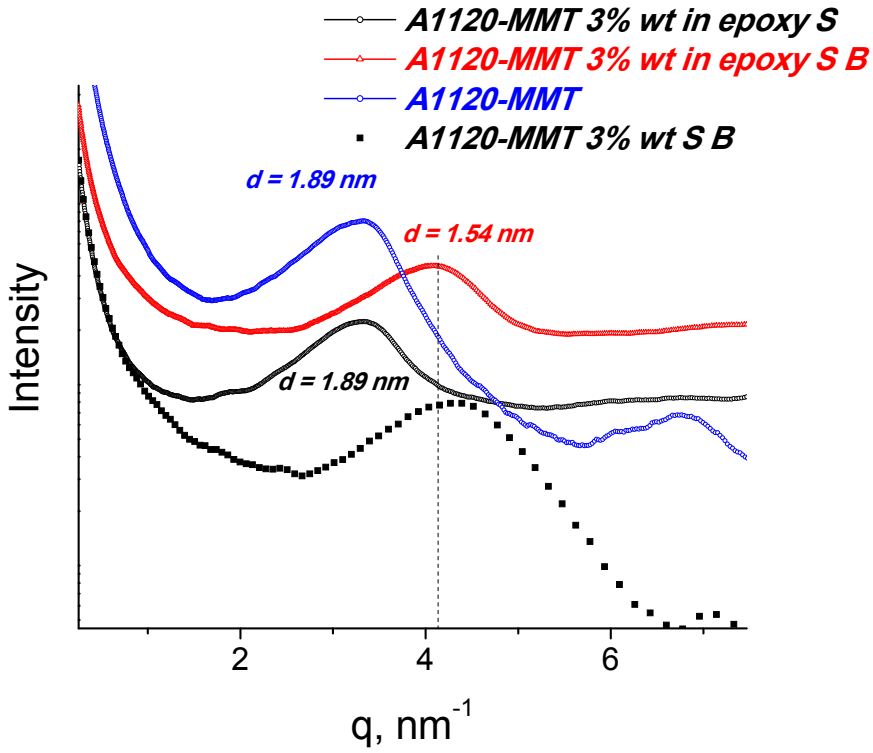

Figure 29 - X-ray diffraction spectra of the uncured pastes A1120-MMT obtained by sonication and sonication/ball-milling mixing procedure compared with the spectra of A1120-MMT powder and A1120-MMT 3% SB composite.

It is worth noting that the sonication mixing procedure does not affect the interlayer spacing of the silylated MMT, whereas the combination of sonication and ball-milling tends to reduce the interlayer spacing, probably through a compactness of the silicate layers.

Similar WAXS spectra have been collected for the pastes obtained by dispersing modified and unmodified MMT in epoxy resin through S and SB mixing procedures and also for cured composites (they are omitted for sake of brevity). The characteristic interlayer spacing for the several materials containing 3% wt/wt of modified and functionalized MMT are reported in Table 7.

	Interlayer Spacing (Å)				
	Powder	**Paste**		**Composite**	
		S	**SB**	**S**	**SB**
Na-MMT	12.7	12.9	13.0	12.6	15.1
A1100-MMT	15.3	17.1	15.7	17.0	14.5
A1120-MMT	18.9	18.9	15.4	18.9	14.8

Table 7 - Interlayer spacing for modified and unmodified clay, pastes and composite materials.

Taking into account that the Van der Waals dimensions of the epoxy monomer are 1.46x0.44x0.35nm [11], it is reasonable to expect that no intercalation occurs in the Na-MMT. In fact by subtracting the layer thickness, equal to 9.6Å, from the interlayer spacing, the remaining separation of 3.1Å is too small to be accessible to the molecular size of epoxy monomer. On the other side, although the silylated clays do not show marked increase of the interlayer spacing upon mixing with DGEBA resins, the remaining separation are compatible with the intercalation of the epoxy monomers between the silicate layers. In particular for

the A1120-MMT clay the remaining separation is 9.3Å which is large enough to host the epoxy monomers [12-13].

Moreover, as reported in Table 7, the sonication mixing procedure allows the penetration of epoxy monomers into MMT gallery only for the clay functionalised with A1100. Thus the interlayer spacing increases from 15.3Å to 17.1Å. Probably in the case of clay modified with A1120 the intermolecular interactions which take place between the amine groups of grafted and intercalated organic moieties prevent the epoxy monomers to enter the silicate galleries [14]. The mixing procedure based on the combination of sonication and ball milling compacts the silicate layers probably due to the pressure extended by the metal balls. The interlayer spacing value decreases without reaching the original value corresponding to the unmodified MMT.

The morphology of Epoxy/MMT composite depends on the competition between intragallery and extragallery cross-linking reactions. Intercalated composites are formed if the curing conditions enhance the intergallery reaction with respect to the extragallery reaction. In fact the higher is the rate of the intergallery reaction the higher is the diffusion of DGEBA monomers into the gallery. This effects is strengthen by the presence of polar moieties inside the galleries which accelerated the cross-linking reaction through a catalytic effect [15].

The interlayer spacing exhibited by the unmodified and functionalized MMTs in the composites are quite comparable with the ones of the epoxy pastes before the curing process. The difficulty in achieving further increase of the interlayer spacing can be ascribed to the sonication mixing which probably promotes the reaction between the amine groups grafted to the edge and the surface of the silicate layers and the epoxy monomers. This cross-linking reaction which

preferentially happens at the exterior of the silicate galleries allows the epoxy gelation time to be locally decreased, the viscosity increased and the silicate layers to be aggregated behaving as compact particles inside the shear field.

In summery the results obtained by the X-Ray diffraction characterization performed on the powders, pastes and composite can be resumed as following:

- ✓ by using the process parameters of the Procedure 3 the interlayer spacing of the modified Na-MMT increases with the length of aminosilanes used for the silylation reaction;
- ✓ during dispersion of modified clays in epoxy resin, the sonication mixing procedure allows the interlayer spacing to increase only for the A1100-MMT clay whereas the ball-milling dispersion method compacts the layered structure of the clays;
- ✓ the cross-linking reaction which takes place during the dispersion of modified MMT in the resin, prevents the intercalation of epoxy monomers in the silicate galleries. Thus retention of layer-layer correlations leads to micron scale reinforcing particles, not nano scale of individual layers;
- ✓ the modified and unmodified MMT clay tactoides result slightly intercalated but well compatibilised with the epoxy matrix.

5.2.2 Dynamic Mechanical Analysis of cured Epoxy/MMT Composites

Typical dynamic-mechanical plots for neat epoxy resin and Epoxy/MMT composite containing 1% wt of unmodified and modified clay, prepared both with S and SB methods, are presented as example in Figure 30 a) and b). The

elastic modulus at 25°C, the modulus at 150°C and the T_g values calculated as maximum of tanδ curves are showed in Table 8.

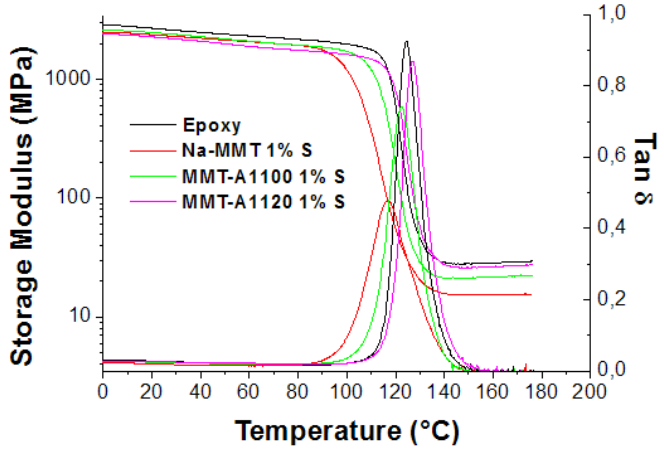

a)

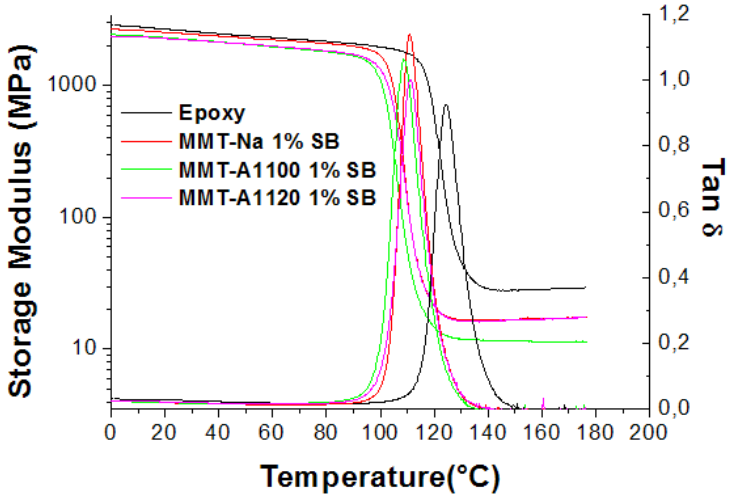

b)

Figure 30 - Storage modulus and Tan δ versus temperature for epoxy resin and composite with 1% wt of MMT-A1120 obtained by sonication (a) and sonication and ball-milling (b).

The storage modulus at 25°C of nanocomposites with both the modified and unmodified clays decreases of about 10-20% if compared to the neat epoxy, except for the pristine Na-MMT-based composite, whose modulus are quite

similar to that of relative neat epoxy matrix. This results is comparable with that reported by Triantafyllidis et al [16] for rubbery epoxy matrix filled with inorganic and organo-modified clays. They attributed that mechanical behaviour to the high organic modifier content and the negative effect of the modifier's dangling chains on the interfacial adhesion between clay and organic matrix. The interfacial interactions of polymer chains to the clay layer affect mainly the properties of epoxy polymer in the glassy region. In our case, the crosslinking reaction between the amino groups of silylated clays and epoxy monomers, which probably takes place during the sonication mixing, affects negatively the optimal stoichiometric ratio between monomers and hardeners. As a matter of fact the epoxide network exhibits a reduced cross-linking density and consequently the elastic modulus of composites in the rubbery region reduced with respect to that of the neat epoxy resin (Figure 30).

As far as the Tg's and the elastic modulus at 150°C values are concerned, the Epoxy/MMT composites filled with 1% and 3% wt/wt of pristine Na-MMT clay exhibit a marked reduction of both the characteristics compared to those ascribed to the epoxy matrix. The same properties increase for the Epoxy/MMT composite obtained with silylated clays, approaching the values of the neat epoxy matrix. In particular the enhancement in terms of Tg and elastic modulus is quite evident for the epoxy-clay composite prepared through the sonication procedure (S method). Here, as WAXS analysis showed, the extent of epoxy monomers intercalation in the silicate galleries is more pronounced and then the presence of amine groups grafted on the silicate layers act as coupling agents to improve the compatibility between the inorganic and the epoxy network. The elastic modulus at 150°C represents a key property very sensible to the interactions between inorganic filler and organic matrix. The higher the elastic

modulus at 150°C the better the interaction between polymeric matrix and the inorganic filler.

The results confirm that the silylation reaction of Na-MMT with aminosilanes is a valuable approach to enhance the interactions between the epoxy matrix and the fillers. This enhancement could be ascribed to the interaction established between amine groups and epoxy resin by means of both the covalent bonds due to the cross-linking reaction and the hydrogen bonding with the hydroxyl groups of opened oxirane rings. The reduction of the epoxy-clay composite Tg with respect to the pristine epoxy matrix may be ascribed to a poor interfacial compatibility in the case of unmodified Na-MMT and to the interfacial plasticization and/or disrupting of the polymeric network arising from the alteration of the competitive reactions, i.e. homopolymerization of epoxy rings and cross-linking, during the curing process [17]. The sonication process likely enhances the base catalyzed homopolymerization reaction due to the catalytic role of the silicate layers [18], leading to the formation of a network with greater chain mobility. In fact a portion of epoxy groups could be reacted during sonication and consequently an excess of curing agent (MXDA) remains unreacted to form free ends which causes the increase of free volume and consequently makes the Tg lower [19]. Finally cannot be excluded the possibility that the effects observed for Epoxy/MMT composites can be attributed to organic molecules (i.e. amino silanes) released from the clay to the matrix and plasticizing the systems which would off-set the effect of the improved compatibility between epoxy matrix and clay particles.

In the case of epoxy-clay composites prepared through the combination of sonication and ball-milling procedures, the amine groups grafted onto the surface of the silicate layers are not able to markedly improve the materials' properties

with respect to the composite realized with unmodified Na-MMT. Probably the compacting effect of the silicate layers due to the ball-milling process as well as the aggregation of the tactoides counteract the improved interfacial compatibility, and they result detrimental on the mechanism of loading transfer between the filler and the polymeric matrix. Finally the Tg reduction with increased amount of clays, more evident for the Epoxy/MMT composite prepared through sonication and ball-milling procedure, can be explained in terms of increased free volume. As the clay concentration is increased a larger amount of tactoids-tactoids aggregates form, creating additional free volume for the mobilization of the epoxy resins.

Similar results in terms of reduction of both Tg values and elastic modulus at 150°C, were obtained by RA Pethrick et al [18] for epoxy matrix filled with Cloisite 6A, a dimethyldehydrogenated tallow, quaternary ammonium chloride modified clay. In that case the discussed detrimental effect was associated to the organic moieties present inside the modified clay which in view of the authors resulted chemically not compatible with the epoxy resins and easily released, plasticizing the epoxy network.

Samples	Tg [°C] (S)	Bending Elastic modulus [GPa] (S)	Elastic modulus at 150°C [MPa] (S)	Tg [°C] (SB)	Bending Elastic modulus [GPa] (SB)	Elastic modulus at 150°C [MPa] (SB)
Epoxy resin	124	2.6	28.1	124	2.6	28.1
Na-MMT 1%	117	2.3	15.3	110	2.5	16.9
MMT-A1100 1%	123	2.4	21.4	108	2.3	11.6
MMT-A1120 1%	127	2.3	26.0	111	2.3	16.6
Na-MMT 3%	104	2.6	11.6	91	3.3	3.0
MMT-A1100 3%	117	2.3	23.4	98	2.9	11.0
MMT-A1120 3%	122	2.3	23.1	99	2.1	5.7

Table 8 - Bending elastic modulus at 25°C and 150°C and Tg for neat epoxy and epoxy-clay composites.

5.2.3 Tensile test

Figure 31 a) and b) show the stress–strain curves of pristine epoxy resin and Epoxy/MMT composites filled with 1% and 3% wt of modified and unmodified clay. The shown curves are the most representative, namely those whose average values in terms of elastic modulus, ultimate tensile strength and elongation at break approach the values reported in Table 9.

The elastic modulus was determined by measuring the slope in the beginning of the linear region in the stress-strain curve. The ultimate tensile strength and the strain at break were determined as the values at breaking point of the sample.

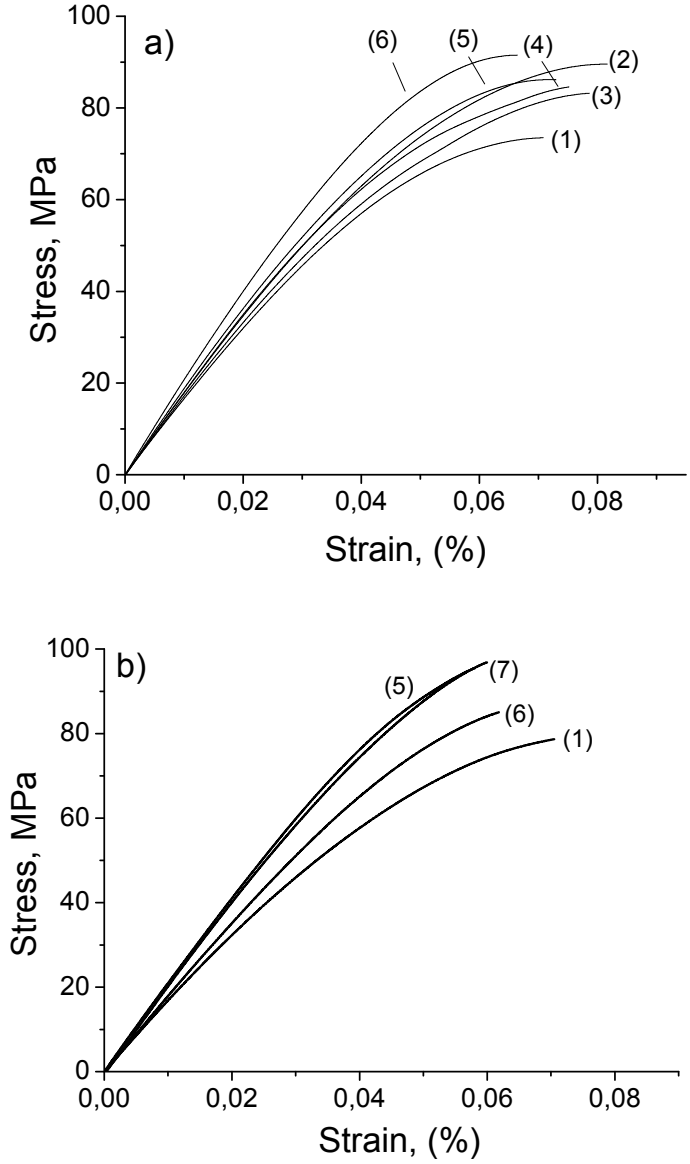

Figure 31 - Stress-Strain curves of pristine epoxy matrix and of Epoxy/MMT composites a) with 1% wt and b) 3% wt (silicate basis) of various clays: 1) pristine epoxy resin, 2) Na-MMT S, 3) MMT-A1120 S, 4) MMT-A1100 S, 5) MMT-A1120 SB, 6) Na-MMT SB and 7) MMT-A1100 SB. S stands for sonication method and SB for sonication-ball milling method. (In the Figures are reported only the stress-strain curves for the samples more comparable with the average values reported in Table 9)

Samples	Tensile strength [MPa] (S)	Elastic modulus [MPa] (S)	Strain at break [%] (S)	Tensile strength [MPa] (SB)	Elastic modulus [MPa] (SB)	Strain at break [%] (SB)
Epoxy resin	76.5 (2.3)*	1670 (20)	7 (0.5)	76.5 (2.3)	1670 (20)	7 (0.5)
Na-MMT 1%	87.0 (2.5)	1760 (20)	7.7 (0.6)	87.4 (4.4)	1710 (20)	6.6 (0.5)
MMT-A1100 1%	84.3 (4.5)	1800 (20)	7.9 (0.3)	87.5 (5.2)	1780 (20)	7.2 (0.5)
MMT-A1120 1%	83.2 (2.5)	1850 (20)	7.8 (0.6)	88.0 (4.0)	1805 (20)	7.5 (0.6)
Na-MMT 3%	77.7 (1.5)	1785 (20)	6.3 (0.5)	84,5 (1.9)	1825 (20)	6.3 (0.8)
MMT-A1100 3%	80.5 (4.5)	1930 (20)	6.0 (0.3)	90.0 (2.6)	1842 (20)	6.7 (0.5)
MMT-A1120 3%	79.0 (2.4)	1935 (20)	6.5 (0.3)	89.0 (2.5)	1866 (20)	6.5 (0.5)

Table 9 - Tensile properties of pristine epoxy resin and epoxy-clay composites (*In the brackets are reported the error range).

It is worth noting that the Epoxy/MMT composites prepared with 1% and 3% wt (silicate basis) of modified and unmodified clays exhibit improved tensile strength and elastic modulus compared to the pristine epoxy matrix. The strain at break decreases for all the samples containing 3% wt of clay whereas it slightly increases for composites at 1% wt in comparison to the epoxy resin. Moreover it is evident that since the inorganic layers are poorly intercalated with epoxy resins (as showed by WAXS analysis), the slight improvements in mechanical properties derive mainly from the better interfacial interactions between the epoxy matrix and the clays grafted with organic moieties. In fact the Epoxy/MMT composites filled with silylated clays show a further enhancement of the mechanical properties compared to the composite filled with unmodified clays, for which the reinforcing effect is due mainly to the presence of stiffer inorganic particles. Similar results were obtained by Rhee et al. [20] for epoxy

nanocomposite where the clays was modified by silylation with 3-aminopropyltriethoxysilanes (A1100). The simultaneous increase of elastic modulus and ultimate tensile strength with the clay loadings was ascribed to the better dispersion of the filler and the improved interfacial strength, which restrained the epoxy matrix cracking.

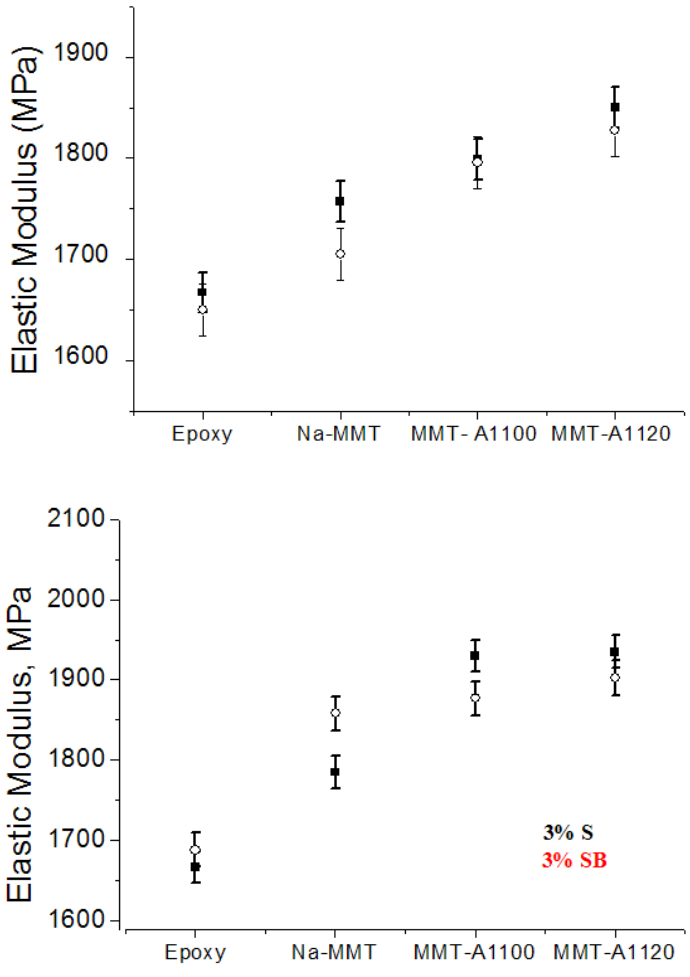

Figure 32 - Elastic modulus of the epoxy-clay composites at various clay content: a) 1% wt and b) 3% wt (silicate basis).

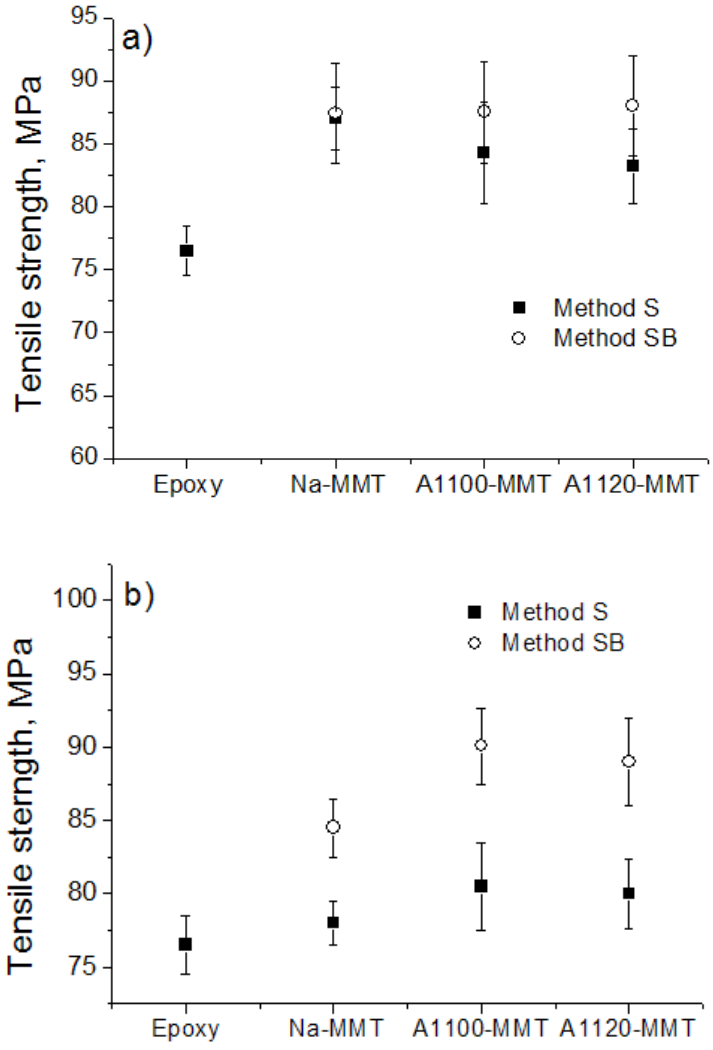

Figure 33 - Tensile strength of the epoxy-clay composites at various clay content: a) 1% wt and b) 3% wt (silicate basis).

The variation of the elastic modulus and tensile stress as a function of nature of the organic moieties grafted on the surface of the clay layers are reported in

Figure 32 a) and b) and Figure 33 a) and b) respectively for composite filled with 1 and 3wt% (silicate basis).

The results show that the elastic tensile modulus of the epoxy-clay composites increases with the clay content in either processing procedures (i.e. S or SB method). This response is characteristic of composite materials reinforced with particles stiffer than the neat matrix. Furthermore the elastic modulus of composites containing 1wt% of clays increases with increasing the chain length of organic molecules used for the silylation reaction. Regardless the aminosilanes used to functionalize the MMT, improvements of about 10% and 15% are observed respectively with the addition of 1 and 3wt% of organo-modified fillers. This behaviour is superior to that exhibited by conventional composites, where low concentrations (i.e. lower than 10%) of the inorganic filler induces no or negative effects to the tensile mechanical properties [21]. An improvement of the elastic modulus of 10% with respect to the pristine epoxy resin has been obtained by Triantafyllidis et al [16] only through the complete exfoliation of the inorganic layered filler. This result confirms the advantage in using the silylation approach to improve the interfacial polymer/filler interactions respect to both the simple dispersion of microsized fillers and the intercalation/exfoliation of organo-modified clays. Recently Giannelis et al [22] showed that in polysiloxane/layered silicate nanocomposites the edges interactions between the ended OH groups of polysiloxane and the oxydrilic groups present onto layers, affect the reinforcement of composites more than the exfoliation. These edge-interactions can also contribute to restrict the mobility of polymer chains during the mechanical tests [23]. The ultimate tensile strength of epoxy-clay composites is higher than that of the pristine epoxy matrix. In particular, the dispersion procedure seems to not affect the ultimate tensile

strength values in samples at 1%wt of filler, whereas it is in the case of 3%wt Epoxy/MMT composites. In fact, in the 3wt% samples the combination of sonication and ball-milling assures the highest ultimate tensile strength.

The stress-strain curves in Figure 31 were also used to estimate the toughness of the pristine epoxy resin and the Epoxy/MMT composites, since the area under the curves corresponds to the toughness of the materials in kJ/m^3 units. The toughness estimated for the pristine epoxy matrix is equal approximately to 3300 kJ/m^3, whereas it increases markedly (around $4000kJ/m^3$) for the 1%wt composites. In fact, the 1wt% Epoxy/MMT composites exhibit higher ultimate tensile strength and similar or slightly increased strain at break compared to the pristine epoxy matrix. On the other side the composites containing 3%wt of filler, exhibit reduced toughness (around $3000kJ/m^3$) since the strain at break is lower compared to that one of pristine epoxy resin.

Therefore, the above results suggest that the presence of reactive organic moieties (i.e. grafted amine groups) at the edges or onto the surface of the layers could represent a feasible approach to overcome the negative effect of the presence of micro-sized inorganic particles, i.e. tactoides or aggregates of tactoides.

5.2.4 SEM analysis

Figure 34 shows the fracture surface of MMT-A1120 3% S and MMT-A1120 3% SB composites. For clarity the micrograph image related to the neat epoxy resin has also shown.

The pristine epoxy system shows a wrinkled fracture surface typical of a slightly ductile behaviour. Each composites materials shows a smoother fracture surface than that of pristine epoxy evidencing a fragile fracture behaviour. Probably the presence of clay aggregates, which are well detectable as light spots in the SEM images, act as a crack initiation sites and cause the failure of the samples at lower strain at break compared to the epoxy resin (as shown in the stress-strain curves of Figure 31 b)). Comparing the fracture surfaces of the epoxy-clay composites, it is evident that composite sample MMT-A1120 3% SB prepared by the combination of sonication and ball-milling method shows considerable less roughness than the sample MMT-A1120 3% S prepared by sonication method. The more brittle behaviour of *SB* sample can be tentatively ascribed to the presence of larger tactoides aggregates.

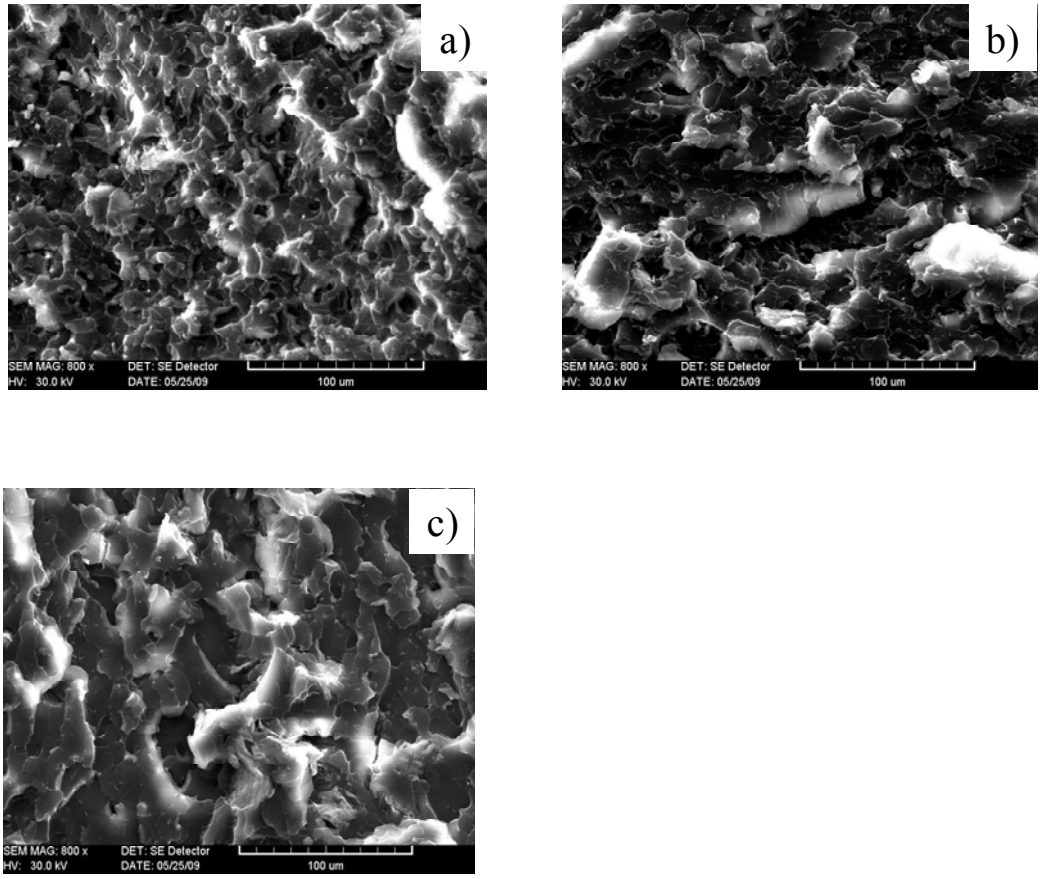

Figure 34 - Typical fracture surfaces of epoxy resin (a), MMT-A1120 3% SB (b) and MMT-A1120 3% S (c) samples at 800 x magnification.

5.2.5 Nanoindentation analysis

Although the fracture and mechanical behaviour of the epoxy-clay composites and nanocomposites materials has been extensively investigated over the past years, less attention has been spent to the study of stress transfer mechanism between clay interacting with epoxy polymer. In this respect Shen et al. [24] verified the ability of the nanoindentation technique to evaluate the time dependent mechanical properties of epoxy nanocomposites. In particular they showed that a clay content of about 2.5wt% maximized the creep resistance. At

higher clay loadings, the creep resistance decreases because of the plasticization effect of the alkyl ammonium chains, which reduces the cross-linking density near the silicate layers.

Typical loading-hold-unloading profiles under a maximum load of 100mN, are showed in Figure 35 for pristine epoxy and composite containing 3wt% of clay, prepared by sonication method. Similar profiles have been obtained for the composite prepared through the combination of sonication and ball-milling procedure. Pristine epoxy resins possesses the lowest resistance to indentation force and the highest maximum indentation depth, respectively, before and after the holding segment. For the Epoxy/MMT composites an higher force has been necessary to indent and consequently the load-displacement curves result shifted upward. Additionally the MMT-A1120 based composites highlights the highest indentation load at depths higher than 2000nm. It is noticed that the slope of the load-displacement curve at the initial unloading portion, related to the material's elastic modulus, increases only slightly for the composites in comparison to the pristine epoxy system. This result shows that at the nanometer scale the elastic modulus of Epoxy/MMT composites is not significantly modified by the presence of functionalized clay.

The holding load segment in the load-hold-unload cycle has been used to explore the creep behavior of the pristine epoxy and epoxy-clay composites. The increase in the creep resistance observed for the composites obtained through sonication method, could be ascribed to the presence of grafted organic moieties onto the clay surface and at the layer edges as well as to the extent of epoxy monomer intercalation which, as confirmed previously, reduce the molecular mobility of the segments in the epoxy network [24]. The composites obtained by the combination of sonication and ball-milling dispersion procedure, exhibit a lower

creep resistance which can be related to the worse dispersion of clay tactoides and to the dramatic reduction of the Tg values due to the lowering of the cross-linking density.

In Table 10 are reported the elastic modulus, the creep displacement at 60 s and the hardness values measured from indentation tests for pristine epoxy and Epoxy/MMT composites. It is worth noting that the composites hardness increases with respect to the pristine epoxy resin, and it seems to depend on *(i)* the adopted dispersion procedures, *(ii)* the clay content as well as *(iii)* the clay silylation. In particular the composites prepared through sonication method show an increase of the hardness of about 35 and 50% with respect to the pristine epoxy, for the composite filled with MMT-A1100 and MMT-A1120, respectively. This is probably due to the sonication method through which the clay tactoides are better dispersed within the matrix and better interacting with the epoxy resin. In the opposite case, the combination of sonication and ball-milling increases the agglomeration of clay tactoides additionally causing a poor interaction between tactoides and epoxy matrix in spite of the silylation.

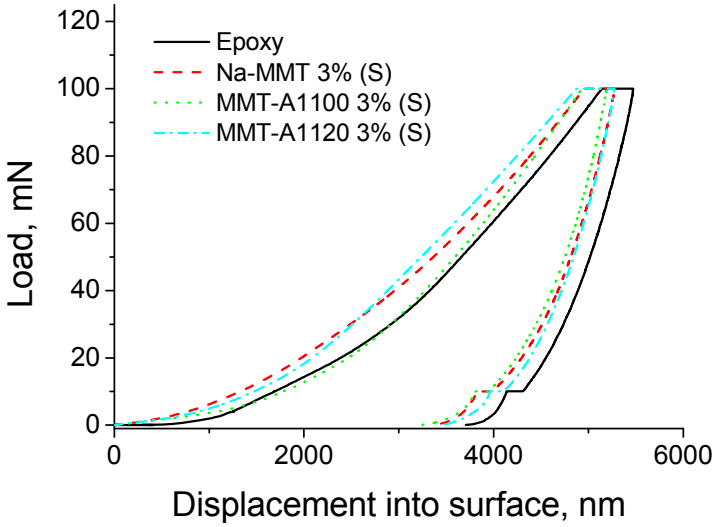

Figure 35 - Load–displacement relation of neat epoxy and epoxy-clay composite prepared by sonication method (method S).

Samples	Elastic Modulus [GPa]	Creep displacement at 60 s [nm]	Hardness [GPa]
Epoxy resin	4.01 ± 0.33	348.90 ± 12.40	0.145 ± 0.05
Na-MMT 3% (S)	4.10 ± 0.19	297.18 ± 15.46	0.162 ±0.02
MMT-A1100 3% (S)	4.30 ± 0.34	298.83 ± 13.73	0.195 ± 0.06
MMT-A1120 3% (S)	4.34 ± 0.23	336.65 ± 11.67	0.220 ±0.05
Na-MMT 3% (SB)	3.70 ± 0.32	352.53 ± 15.88	0.169 ±0.03
MMT-A1100 3% (SB)	4.20 ± 0.39	363.10 ± 16.07	0.178 ±0.04
MMT-A1120 3% (SB)	4.29 ± 0.15	347.91± 18.02	0.157 ±0.05

Table 10 - Mechanical parameters from indentation test.

It is worth noting that the values of elastic modulus obtained by nanoindentation tests are different from the values obtained by tensile measurements, although either techniques show that the modified or unmodified clays effectively stiffen the matrix. The difference in terms of absolute values can be ascribed to the different experimental conditions, i.e. applied loading rate [25].

5.2.6 Thermogravimetric Analysis

Thermal properties of pristine epoxy resin and Epoxy/MMT composites have been investigated by thermogravimetric analysis. In Figure 36 are reported the TGA curves of pristine epoxy resin and epoxy-clay composite obtained through the sonication and the combination of sonication and ball-milling dispersion methods.

Pristine epoxy resin shows a thermally oxidative degradation which occurs through a three step process with maximum rate at around 300, 410 and 520°C due respectively to the thermal degradation of the epoxy network, the charring formation and the complete oxidation of the char. The epoxy-clay composites undergo to an oxidative mechanism similar to that exhibited by the pristine epoxy suggesting that the presence of the clay filler does not significantly affect the thermal oxidative degradation mechanism of the matrix. This behaviour can be attributed to the relatively low clay loadings investigated which are not enough to affect significantly the thermal oxidative degradation of the epoxy matrix The temperatures of degradation were taken as the onset temperatures at which 3% wt mass loss occurs and are listed in Table 11.

Samples	**T_{id} (3% weight loss) [°C]**	
	S dispersion method	**SB dispersion method**
Epoxy resin	321	321
Na-MMT 1%	306	311
MMT-A1100 1%	316	316
MMT-A1120 1%	328	324
Na-MMT 3%	308	326
MMT-A1100 3%	309	324
MMT-A1120 3%	303	302

Table 11 - Initial decomposition temperatures from TGA test.

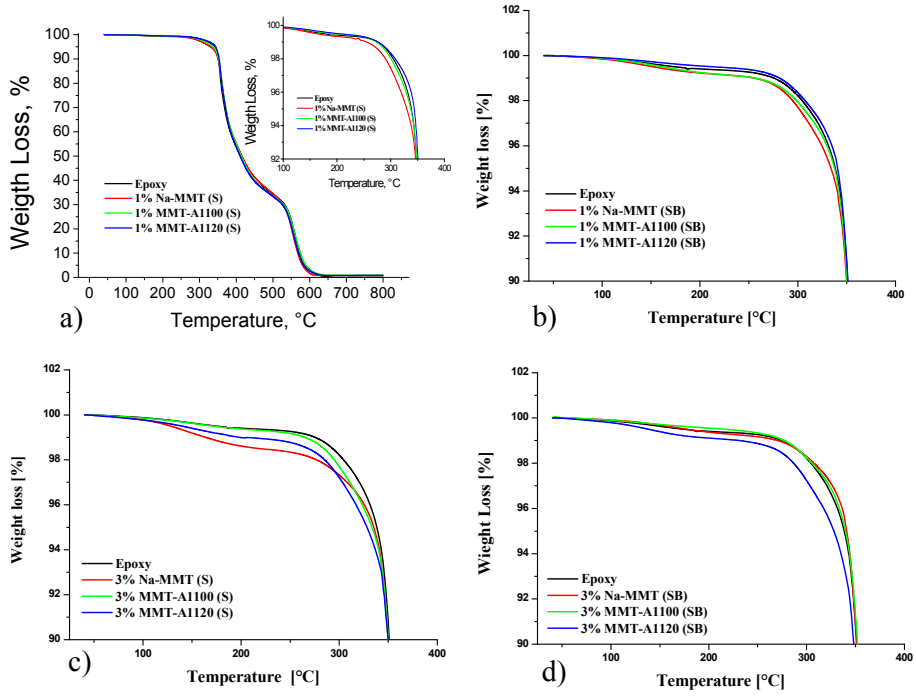

Figure 36 - TGA curve in air of pristine epoxy resin and composites with 1% wt (a-b) and 3%wt (c-d) of Na-MMT, MMT-A1100 and MMT-A1120 prepared with the S and SB method.

5.2.7 Cone calorimeter test

Flame retardant properties of the pristine resin and the Epoxy/MMT composites have been investigated by cone calorimetry. Figure 37 shows the average trend of the heat release rate as function of the time both for pristine epoxy resin and epoxy-clay composites.

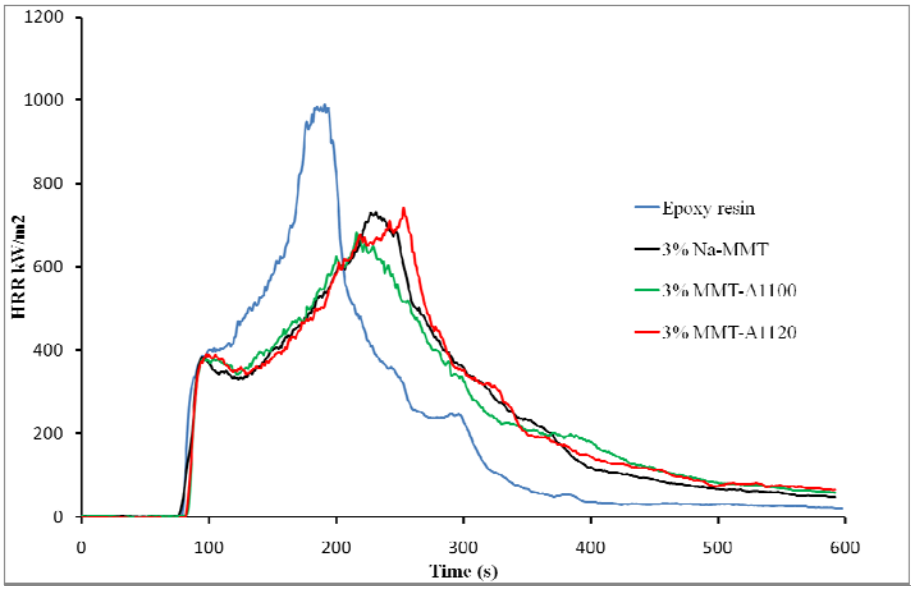

Figure 37 - Heat Release Rate from Cone Calorimeter test for pristine epoxy and composites materials prepared by sonication method.

Fundamental parameters in controlling flame propagation in a fire scenario are the maximum value of the HRR and the time corresponding to the peak. These parameters, together with the ignition time, are shown in Table 12.

The ignition time, t_{ig} slightly increases for the composites prepared by using silylated clays. Moreover the inclusion of 3%wt of clay in the epoxy resin causes a marked delay of the HRR peak and also a reduction of the intensity at maximum of HRR peak for both unmodified and silylated clays. The silylation of the clays with different aminosilanes slightly affects the mechanisms with which the material burns even though it does not cause significant changes in the fire properties.

	t_{ig}	HRR (peak)		
Sample	**(s)**	**Time (s)**	**HRR (max) kW/m^2**	**Percentage (%)**
Epoxy resin	80	191	990	100
Na-MMT 3% (S)	80	226	720	73
MMT-A1100 3% (S)	83	216	683	69
MMT-A1120 3% (S)	83	253	742	75

Table 12 - Comparison of time to ignition, t_{ig} and HRR of pristine epoxy and epoxy-clay composites.

The addition of clay modified with A1100 and A1120 aminosilanes produces two different effects in comparison to the Na-MMT filler:

1) the good dispersion of MMT-A1100 tactoides causes a further reduction of the HRR peak,

2) the presence of MMT-A1120 clays increases the necessary time to reach the HHR peak.

The slightly reduced flammability of composites with silylated clays compared to the pristine epoxy resin as well as to the Na-MMT composite can be explained through a more effective enrichment of layered silicates at the surface, which act as barrier for gases and heat. This is due probably to the cross-linking reaction between grafted amine groups and epoxy monomers. It is also worth noting that the HRR profiles of composite materials obtained by using silylated clays before the HRR peak are well superimposed to that one of pristine epoxy resin. This is an important results because in most of the epoxy composite with organo modified clays (i.e. clays modified with alkyl ammonium salts), which intercalate the epoxy resin or exfoliate during composite preparation, it is

possible to observe a faster degradation of the organic modifiers of the clay, which compromises the thermal and fire stability of the materials [12]. In this case the presence of silylated filler and the enhancement of the interfacial compatibility between the filler and the resin, increases the mechanical properties of the composites without affecting the fire resistance.

5.2.8 Conclusion

Nanocomposites with silylated MMT with aminosilanes were prepared employing two different dispersion methods, namely the sonication (S) and a combination of sonication and high energy ball-milling (SB). It can be found that contrary to what observed for the combination of sonication and ball-milling, the sonication technique alone allows to increase the basal spacing for organically modified clay. This result can be tentatively ascribed to the combined effect of ultrasound and mechanical movement, which probably make compact the interlayer spacing and destroy the original structural layer. This fact affects negatively the Tg values of composites that decrease about 20° C compared with neat epoxy. Moreover, the composites obtained by silylation reaction appear to be more resistant but brittle, according to tensile test too.

Finally, the hardness values of nanocomposites increase with the aminosilanes length.

In conclusion the results show that the sonication technique is a good method to obtain a well dispersed intercalated composites, without destructing the layer structure.

5.3 References

[1] C. Zhao; M. Feng; F. Gong; H. Qin; M. Yang; *J. Appl. Polym. Sci.*, 93, **2004,** 676.

[2] K. Endo; Y. Sugahara; K. Kuroda; *Bull. Chem. Soc. Jpn.* , 67, **1994,** 3352.

[3] T. Yankgisawa; K. Kurodo; C. Kato; *React. Solids*, 5, **1988**, 167.

[4] S. Okutomo; K. Kuroda; M. Ogawa; *Appl. Clay Sci.*, 15, **1999**, 253.

[5] I. K. Tonle; E. Ngameni; D. Njopwouo; C. Carteret; A. Walcarius; *Phys. Chem. Chem. Phys.*, 5, **2003,** 4951.

[6] E. Ruiz-Hitzky; J. M. Rojo; G. Lagaly; *Colloid. Polym. Sci.*, 263, **1985**, 1025.

[7] C. Wan; X. Bao; F. Zhao; B. Kandasubramanian; M. P. Duggan; *J. Appl. Polym. Sci.*, 110, **2008,** 550.

[8] S. Yariv; *Appl. Clay Sci.*, 24, **2004,** 225.

[9] H. He; J. Duchet; J. Galy; J. Gerard; *Colloid. Interface Sci.*, 288, **2005**, 171.

[10] Galimberti; *Polym. Adv. Technol.*, 20, **2009**, 135–142.

[11] T. Lan; P. D. Kaviratna; T. J. Pinnavaia; *Chem Mater*, 7, **1995**, 2144-50.

[12] G. Camino; G. Tartaglione; A. Frache; C. Manferti; G. Costa; *Poly Degrad and Stab*, 90, **2005**, 354-362.

[13] C. Kaynak; G. Ipek Nakas; N. A. Isitman; *Applied Clay Science*, 46, **2009**, 319-324.

[14] F. Piscitelli; P. Posocco; R. Toth; M. Fermeglia; S. Pricl; G. Mensitieri; M. Lavorgna; *J of Colloid and Interface Science*, 351, **2010**, 108-115.

[15] C. Zilg; R. Mulhaupt; J. Finter; *Macrom Chem Phys*, 200, **1999**, 661-70.

[16] P. I. Xidas; K. S. Triantafyllidis; *European Polymer Journal*, 46, **2010**, 404-417.

[17] H. Koerner; D. Misra; A. Tan; L. Drummy; P. Mirau; R. Vaia; *Polymer*, 47, **2006,** 3426-3435.

[18] J. Brawn; I. Rhoney; R. A. Pethrick; *Polym International*, 53, **2004**, 2130-2137.

[19] H. Liu; W. Zhang; S. Zheng; *Polymer*, 46, **2005**, 157-165.

[20] S. R. Ha; S. H. Ryu; S. J. Park; K. Y. Rhee; *Materials Science and Engineering A*, 448, **2007**, 264-268.

[21] O. Becker; G. P. Simon; K. Dusek; Epoxy layered silicate nanocomposites. In: *Inorganic polymer nanocomposites and membranes*. Berlin: Springer, **2005**, 29-82.

[22] D. F. Schimidt; A. P. Giannelis; *Chem Mater*, 22, **2010**, 167-174.

[23] C. L. Wei; M. Q. Zhang; M. Z. Rong; *Comp. Sci Teech.,* 62, **2002**, 1327-40.

[24] L. Shen; L. Wang; T. Liu; C. He; *Macromolecular Materials and Engineering*, 291, **2006**, 1358-1366.

[25] H. Lee; S. Mall; P. He; *Composite Part B: Eng.*, 38, **2007**, 58.

Chapter 6: Epoxy/silica Hybrids

This chapter is concerned with the main aspects of the siloxane epoxy hybrids research and the related experimental results, including their interpretation and evaluation in relation to the objectives. In particular, several efforts have been done to optimize the sol-gel process parameters and the amount of specific coupling agent to the aim to prepare Epoxy/silica Hybrids. Then the effect of the amine hardener on the hybrids final properties has been evaluated.

6.1 Functionalization of epoxy resin with APTES

Compatibility between silica and epoxy components is required in order to obtain hybrid materials with co-continuous phases. To the aim to improve the interactions between organic network and inorganic structures the aminosilane APTES was used as coupling agent and the functionalization reaction was carried out at 70°C in nitrogen flux.

During the functionalization reaction, in fact, it is essential to avoid the water to hydrolyze the SiOEt groups of the APTES molecules, because if the hydrolysis takes place, the SiOH groups could react with the C-OH epoxide groups of the opened epoxy ring and then condensate, by reducing the gelation time of the system [1-3]. Furthermore, according to the Scheme 5 [1] the amino groups of APTES molecules are able to react with the epoxide rings, forming secondary and then tertiary amines. Since only a portion of epoxide groups has to be functionalized with the aminosilane molecules, the tertiary amines can further react with the epoxide groups allowing the homopolymerization reaction to occur (Scheme 5).

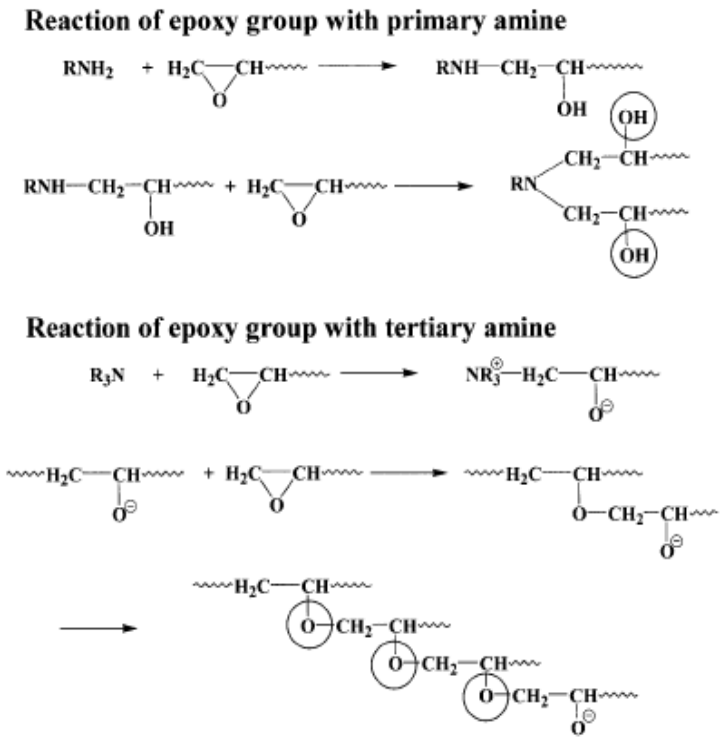

Scheme 5 - Possible reactions of epoxy groups with amines (primary, secondary and tertiary).

The functionalization reaction was monitored by FT-IR analysis and viscosity measures. In particular, the decrease of the absorption peak area of the reacting epoxide groups at 916cm^{-1} (see Figure 38) was used as index for the extent of functionalization reaction. The peak area has been measured at certain stages of the reaction and the degree of conversion (α) has been calculated as function of reaction time at 70°C. Since it does not change during the curing process the stretching of the aromatic rings at 1509 cm^{-1} has been used as internal reference, then the epoxide conversion degree has been calculated as:

$$\alpha = \frac{\overline{A}_0^{916} - \overline{A}_t^{916}}{\overline{A}_0^{916}} \quad \text{where} \quad \overline{A}^{916} = \frac{A^{916}}{A^{1509}}$$

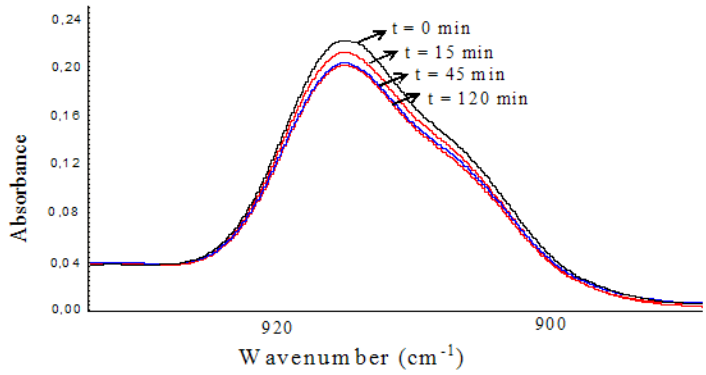

Figure 38 - FT-IR absorbance peak of epoxide groups during the functionalization reaction at 70°C with APTES.

In Figure 39 the epoxide conversion degree has been reported as function of reaction time at 70°C. In spite of the theoretical values of aminosilane used to functionalize, namely 5 or 10wt% pictured as straight-line in Figure 39, the 12 and 18 wt% of epoxide groups reacted, respectively. The higher value of conversion degree could be ascribed to the homopolymerization reaction which took place.

As previously mentioned, the evolution of functionalization reaction with APTES has been followed measuring the viscosity during the reaction at 70°C. The results highlight that the molecular weight increases with the reaction time since an increase of the viscosity can be observed (Figure 40), regardless the amount of aminosilane used to functionalize. Moreover, as the APTES content

increases, i.e. the 10wt% APTES reacting mixture, the viscosity reaches the plateau value early.

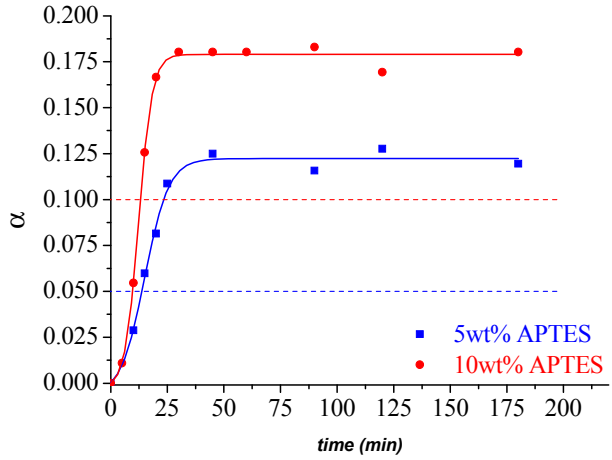

Figure 39 - Epoxide conversion degree with APTES as function of reaction time at 70°C.

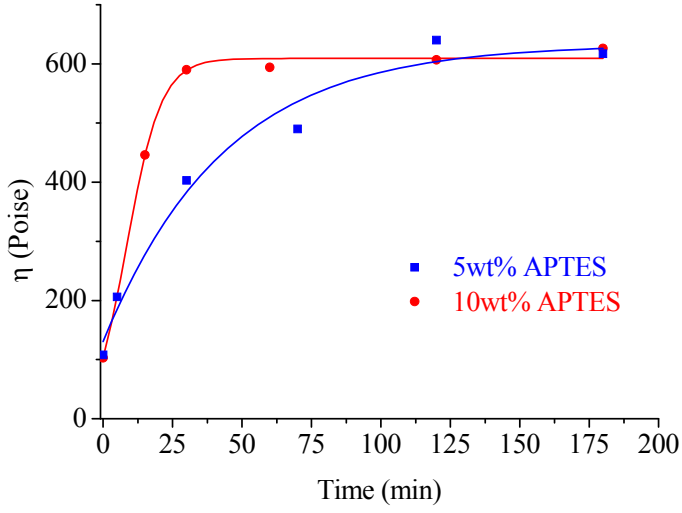

Figure 40 - Viscosity of epoxy resin during the functionalization reaction at 70°C as function of reaction time.

In order to study the homopolymerization effect on the final properties of the hybrid materials, films have been prepared by using the "sol-gel in-situ" procedure (Ep-5AP-Siy-IS sample), at different reaction time extends at 70°C. The cured samples have been characterized by DSC and DMA techniques (Figure 41 and Figure 42).

As shown in Figure 41 the Tg of samples decreases of about 16°C as the reaction time at 70°C increases from 5 to 90 minutes. Additionally, the DMA analysis (Figure 42) shows that the increase of the reaction time causes an increase in the loss factor ascribed to the increased viscous component of the modulus. Therefore a reduced number of cross-links caused by the homopolymerization reaction can be supposed. In fact, the increasing of the reaction time at 70°C in presence of tertiary amine formed during the functionalization reaction allows two synergic effect to happen.

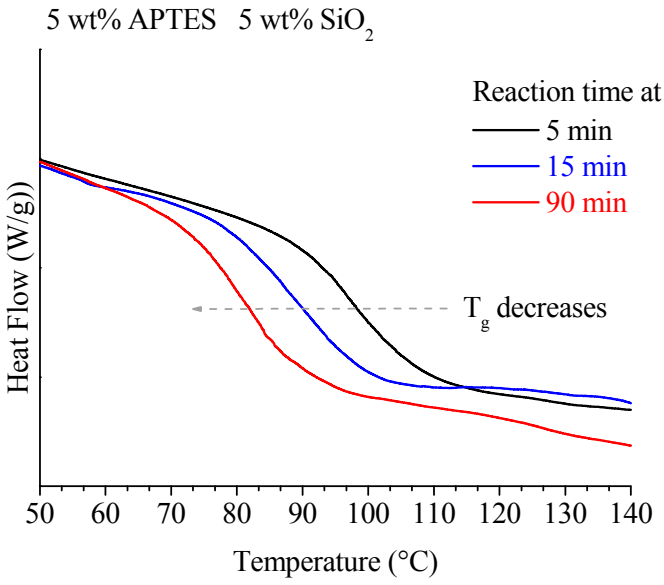

Figure 41 - : DSC analyses of Ep-5AP-Si5-IS samples obtained varying the functionalization reaction time at 70°C.

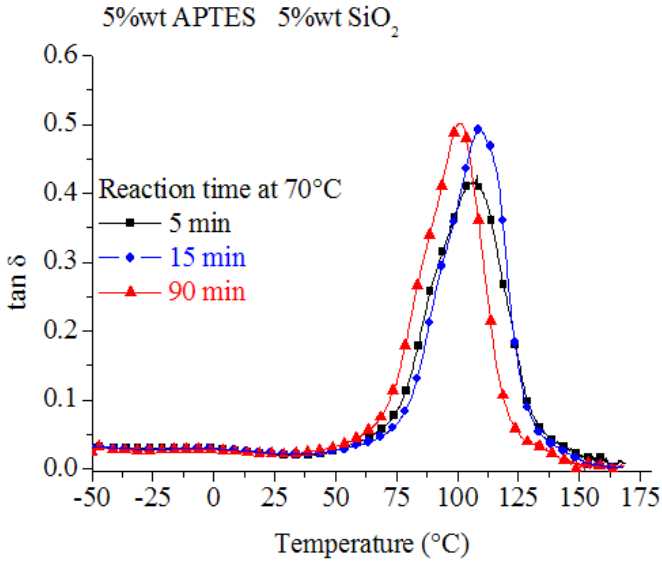

Figure 42 - DSC analyses of Ep-5AP-Si5-IS samples obtained varying the functionalization reaction time at 70°C.

On the one hand the homopolymerization reaction produces linear polymeric chains instead of a cross-linked network, which alone is sufficient to reduce the Tg. Otherwise the stoichiometric amount of hardener added becomes excessive if the homopolymerization reaction occurred, plasticizing the whole system. Taking into account the results obtained, the functionalization reaction of epoxy monomers was performed for 10 minutes at 70°C.

6.2 Sol-gel short hydrolysis (Ep-xAP-zSolv-ySi-Sh)

The effect of APTES and 1,6 hexanediol diglycidyl ether has been evaluated.

6.2.1 Effect of aminosilane content

In order to study the effect of the coupling agent APTES several samples namely Ep-xAP-10Solv-ySi-Sh with x ranging from 5 to 30, have been prepared. The

DSC results (Figure 43) show that the Tg increases with the APTES content, probably because of the improved interfacial interactions between the organic and inorganic moieties. So by increasing the aminosilane content a further improvement of the hybrid properties would be observed. Since the aminosilane molecules partially cross-link the epoxide groups they cause an increased viscosity of the epoxy mixture reducing its processability, hence the higher the aminosilane content the higher the viscosity of functionalized resin. To the end to reduce the viscosity of the functionalized epoxy resin, 1,6 hexanediol diglycidyl ether has been added and its effect on the final properties of hybrids systems has been studied.

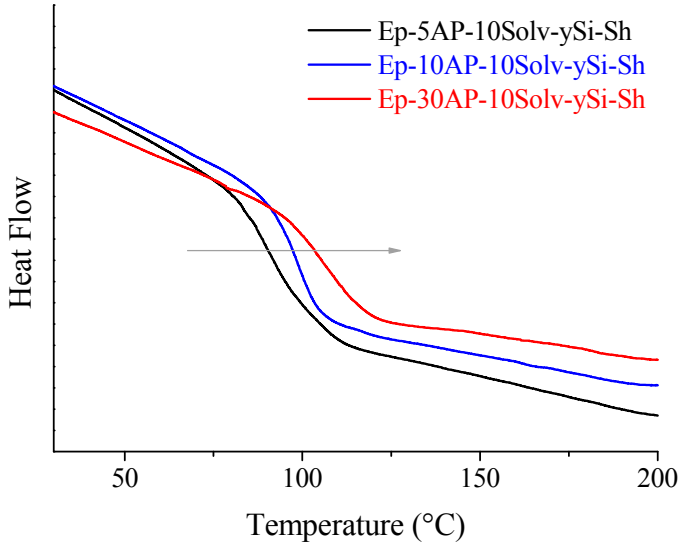

Figure 43 - DSC curves of Ep-5AP-10Solv-ySi-Sh, and Ep-10AP-10Solv-ySi-Sh and Ep-30AP-10Solv-ySi-Sh.

6.2.2 Effect of 1,6 hexanediol diglycidyl ether

In order to study the effect of 1,6 hexanediol diglycidyl ether content, two samples, namely Ep-5AP-0Solv-ySi-Sh and Ep-5AP-10Solv-ySi-Sh, have been prepared. The DSC results, shown in Figure 44, pointed out that the presence of 10wt% of 1,6 hexanediol diglycidyl ether causes the Tg to decrease of about 20°C, probably ascribed to the more flexible epoxide component inside the epoxide network.

In conclusion, in order to improve the interfacial interaction between the organic and inorganic moieties a large amount of coupling agent APTES has to be added. However, the increase of the reacting mixture viscosity requires the addition of the 1,6 hexanediol diglycidyl ether, which in turn reduces the Tg.

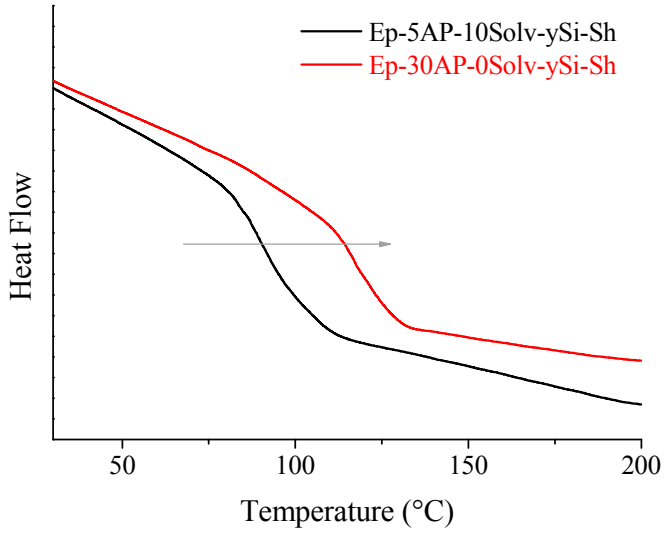

Figure 44 - DSC curves of Ep-5AP-0Solv-ySi-Sh and Ep-5AP-10Solv-ySi-Sh.

6.2.3 Effect of APTES as coupling agent

In the Ep-5AP-10Solv-5Si-Sh SEM image (Figure 45) several big aggregates of silica particles reaching micro-sized dimensions too, can be observed over the entire area of the hybrid materials. Furthermore, in spite of the functionalization with the aminosilane coupling agent, a poor interfacial interactions between the silica particles and the epoxy network can be observed since there is not continuity between organic and inorganic moieties. Furthermore, in spite of the functionalization with aminosilane APTES all the samples are not transparent.

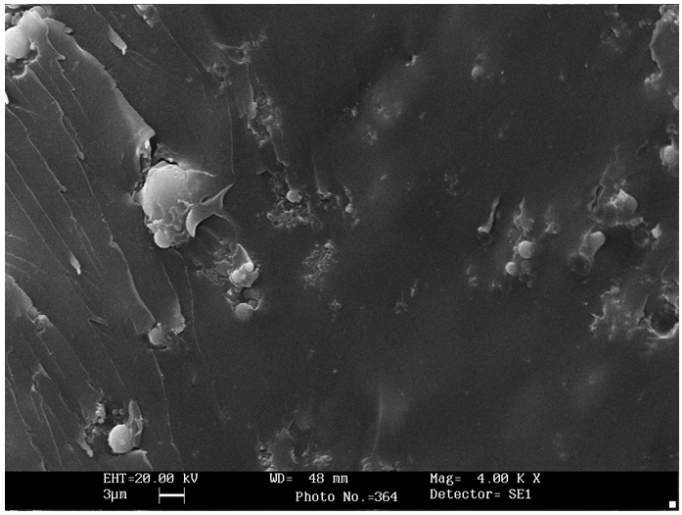

Figure 45 - SEM image of Ep-5AP-10Solv-5Si-Sh hybrid sample.

6.2.4 Small Angle X-ray Scattering characterization

Macromolecular scale structure is investigated by Small Angle X-ray Scattering method. As known, in addition to the size of the polymers or heterogeneity domains, the SAXS method also gives a geometrical description of the structures using the concept of fractal geometry, because random processes of polymerization or aggregation usually lead to the formation of fractal objects. In

Figure 46 the Ep-5AP-0Solv-3Si-Sh scattering plot, subtracted of the neat epoxy SAXS profile, is shown. It is well evident that siloxane domains isolated from SAXS spectra of hybrids show two discontinuities and three linear regions which account for an inorganic internal structure where smaller particles aggregate to produce larger fractal particles.

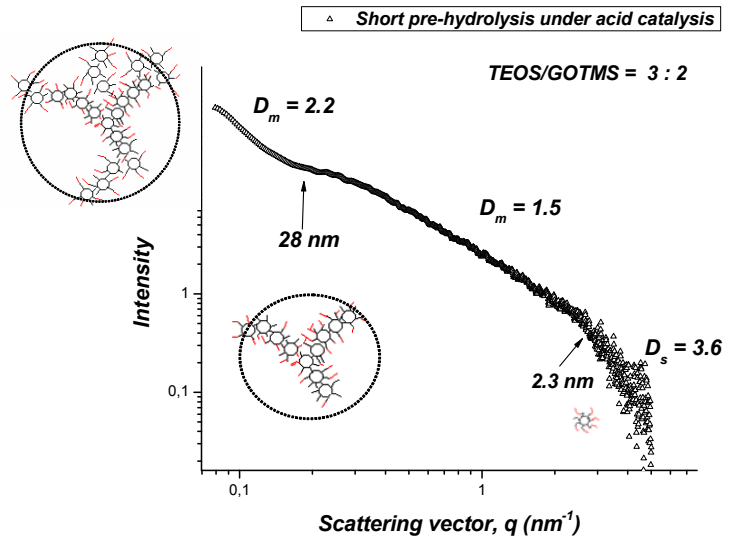

Figure 46 - Log-log plot of Ep-5AP-0Solv-3Si-Sh SAXS profile subtracted of the neat epoxy scattering contribute.

The presence of two discontinuities enables us to identify at least two structural length sizes which contribute to form the inorganic domains. At high q value the SAXS data are highly scattered because of the subtraction of the epoxy matrix scattering. However at q values of around 2.7nm^{-1} the first discontinuity can be observed, ascribed to small silica particle of 2-3nm sized. At lower q value it is well evident a linear segment whose fractal dimension D_m is equal to 1.5. This dimension corresponds to the presence of inorganic fractal domains characterised by a ramified structure due to the diffusion limited cluster-cluster aggregation

mechanism (DLCA) [4]. At q values of about 0.2nm^{-1} it is possible to observe another discontinuity which allows to determine the second characteristic size (28nm) of the multiple hierarchical siloxane structure. At lower q value the slope of the linear segment is 2.2 meaning that the corresponding inorganic domains, whose dimension are not determined because of the SAXS resolution, are characterized by an opened fractal structure. The SAXS analysis pointed out that the inorganic domains produced by the Ep-5AP-10Solv-ySi-Sh approach present a hierarchical structure characterised by a smaller siloxane units which aggregate to produce largest fractal domains. The latter are further aggregate to produce inorganic domains on the microscopic scale. A schematic picture of the hierarchical siloxane structure is proposed and reported in Figure 46.

In conclusion this approach pointed out the following issues:
the preparation procedure does not allow the solvents (water and ethyl alcohol; data not shown) to be eliminate;
the increased viscosity in epoxy systems with high content of APTES requires the addition of 1,6 hexanediol diglycidyl ether which in turn makes the Tg value lower;
since some big siloxane aggregates not bonded with the organic network can be detected, the functionalization of the organic moieties alone showed to be not enough to improve the siloxane domains dispersion.

6.3 Sol-gel long hydrolysis (Ep-xAP-Siy-Ol)

In order to improve the interfacial interactions between the two phases a second coupling agent, the GOTMS, has been used together with the APTES, by pursuing the idea to build-up a co-continuous organic-inorganic structure. A picture of final structure craved by using two coupling agents, namely the

APTES for the organic moieties and the GOTMS for the inorganic ones, has shown in Scheme 6. Moreover, to the aim to avoid the plasticizing effect due to the solvents of sol-gel process, their partial elimination in vacuum conditions at 50°C has been performed. According to Soucek approach [5] since an acidic catalyst has been used for the hydrolysis reaction, oligomers of linear siloxane backbone would be formed. In fact, as known, under acid catalysis, the terminal groups react preferably and the chain grows at the end to form linear sequences. As a consequence, an open network structure initially results. When the amine hardener for epoxy monomers is added to the mixture the ambient becomes sudden basic. Since the siloxane condensation reactions are favourites under basic catalysis the neighbouring SiOH groups sudden condensate by elimination of water molecules. A possible structure has been proposed in Scheme 7.

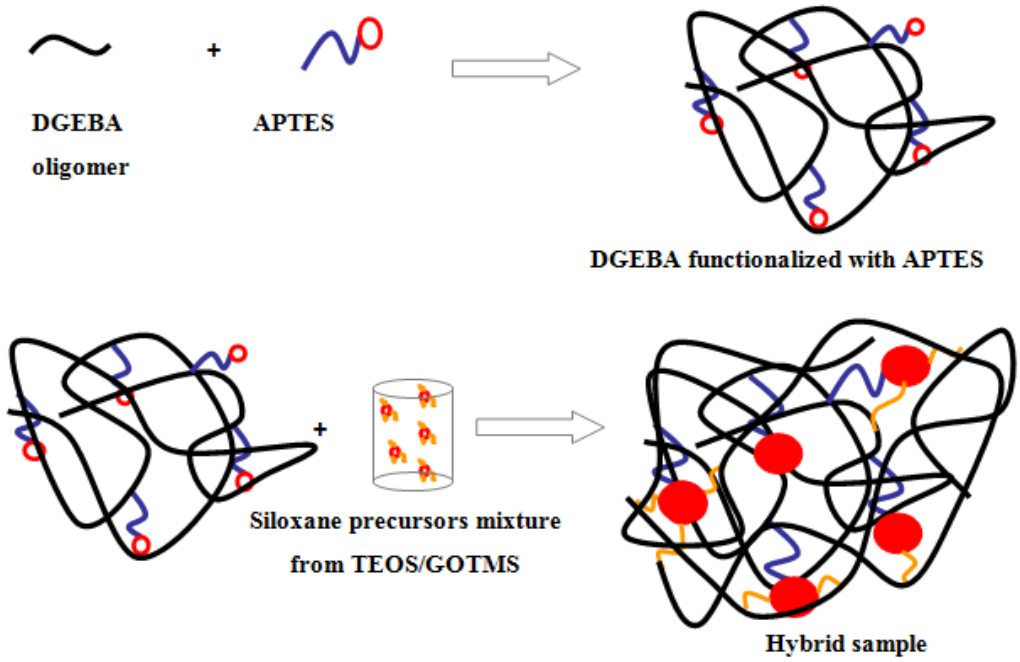

Scheme 6 - Role of coupling agents APTES and GOTMS in the hybrid formation.

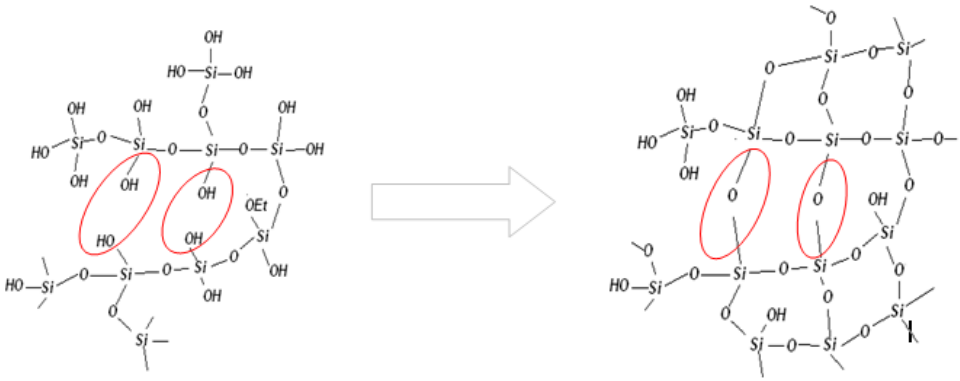

Scheme 7 - Schematic picture of the siloxane oligomers obtained in acidic catalysis (on the left) and their sudden condensation after the addition of the amine hardener (on the right).

6.3.1 Dynamic Mechanical Analyses (DMA)

The Dynamic Mechanical Analysis (DMA) has been performed to identify the glass transition temperature Tg of samples as maximum value of the loss factor tanδ, since usually, its position and intensity allows characterizing the reduction in mobility of the epoxide network [1]. Figure 47 shows, as example, the tan δ curves of Ep-5AP-3Si-Ol and the neat epoxy system (Ep-Mx). It is worth noting that the hybrid sample's Tg decreases with respect to the neat epoxy (Figure 47). Additionally, the hybrid sample curve broads and weakens with respect to that of the neat epoxy. The changing in the Tg value could be ascribed to the modified network arisen from the hybridization of epoxide samples, since the use of the two coupling agents probably modifies the fundamental structure of the organic network. Moreover, the glass transition temperature range related to the hybrid sample become larger than that of the neat epoxy. This means that the cross-linked network becomes poorly homogeneous when the hybridization occurs, causing the molecular relaxations to broad on a larger temperature range.

However, the loss factor shape retains quite symmetric and no multi-peaks are present.

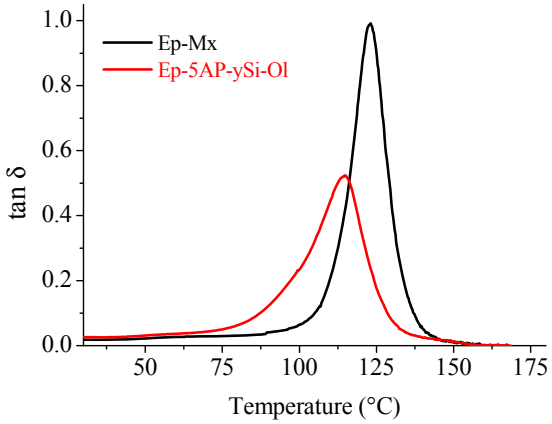

Figure 47 - Dynamic mechanical curves of Ep-5AP-3Si-Sh and Ep-Mx versus the temperature.

6.3.2 Small Angle X-ray Scattering (SAXS)

Figure 48 shows the scattering curve of the Ep-5AP-3Si-Ol hybrid sample after subtraction of the neat epoxy scattering profile. Again, the SAXS profile shows three linear region in the log-log plot with two discontinuity zones. At higher q values, namely $q>2\ nm^{-1}$, the slope of the linear regime is equal to 4.2, hence dense and smooth particles are formed. The discontinuity at $1.9nm^{-1}$ is attributed to a particles dimension of about 3nm. Furthermore, according to the hierarchical structure of fractal objects, these littlest particles aggregate to form larger structures whose compactness can be assessed by using the slope value of the linear region in the intermediate q values. In details, since the slope leads a D_m value of 1.2, a worm-like inorganic structures could be suggested. These opened inorganic structures, about 25-30nm dimensioned, aggregate to form more compact siloxane domains, with diffuse interface, since a power law of 4.8 is

detected at lowest q values. The proposed siloxane structures are pictured in Figure 48 for the sake of clarity.

The SAXS analysis has evidenced that the oligomeric inorganic domains produced according the Soucek method [5] present again a hierarchical structure characterised by a smaller siloxane units which aggregate to produce largest fractal domains.

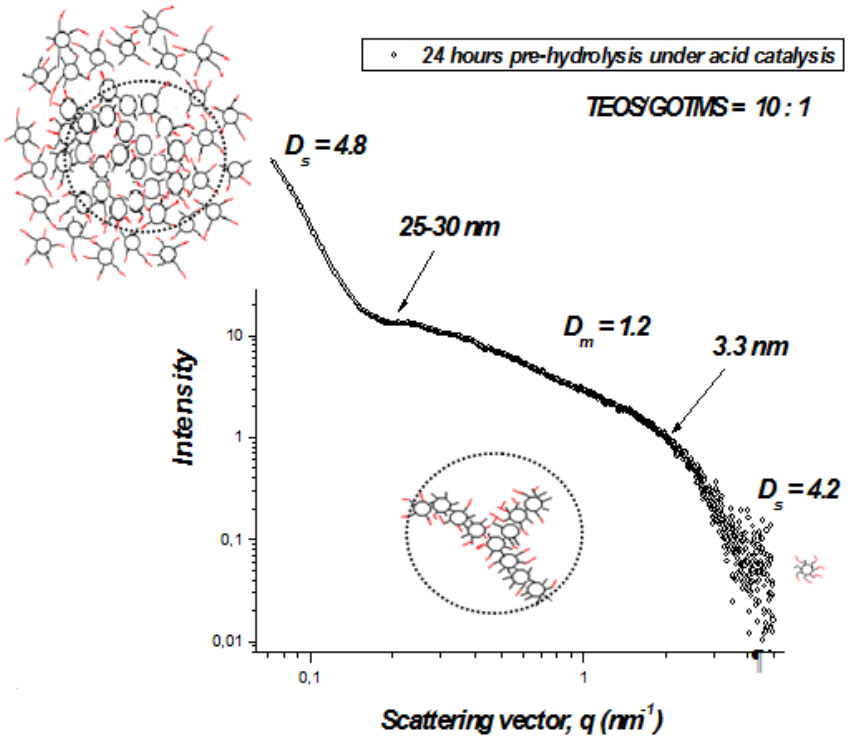

Figure 48 - Log-log plot of Ep-5AP--3Si-Ol SAXS profile subtracted of the neat epoxy scattering contribute.

6.3.3 *Scanning electronic Microscopy (SEM) and Energy Dispersive Scanning (EDS)*

In Figure 49 the cross-section micrograph of the Ep-5AP-3Si-Ol hybrid has shown. It is worth noting that some micro-sized aggregates, rich in silicium, embedded in the organic network can be detected. Analyzing the interface between the organic network and the inorganic aggregates, the absence of the free volume and a continuity between the two phases are evident. This continuity could be ascribed to the simultaneous use of the two coupling agent, namely APTES and GOTMS.

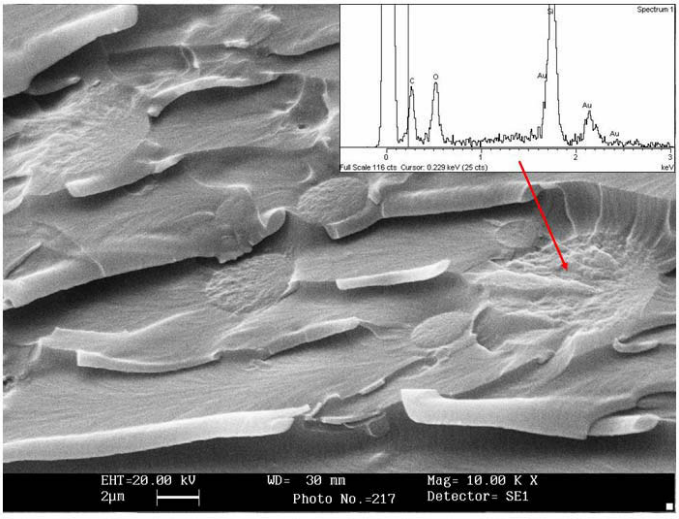

Figure 49 - SEM image of the Ep-5AP--3Si-Ol hybrid sample.

6.3.4 *Conclusions*

The dynamic mechanical analyses of Ep-xAP-Siy-Ol samples pointed out that the presence of the inorganic structures modifies the organic network producing a new structure with decreased Tg value. Furthermore, the broadening of the molecular relaxation attributed to the glass transition emphasizes the poor

homogeneity of the hybrid system. The tendency of the siloxanes structures to aggregate has been highlighted in the SAXS measurements too, since dense siloxanes structures larger than 20-30 nm in dimension are detected. Furthermore, the simultaneous presence of the two coupling agents for the two organic and inorganic network, respectively, allows the siloxanes structure to be inter-diffuse. The slope value of 4.2 in the lowest q range, in fact, speaks in favour of such a co-continuity between the two phases. This behaviour in the nanometer level is projected in a larger scale by the hierarchical structure. In fact, the co-continuity between the two phases and the absence of the free volume are evident in micro-size scale by the SEM micrograph. Hence, the use of the second coupling agent is essential to improve the interfacial interactions. Furthermore, too large siloxane aggregates are present. The aggregation in large separated domains could be ascribed to the particular procedure used to obtain the inorganic structure. In fact, the long pre-hydrolysis reaction in acidic ambient could be responsible of well hydrolyzed siloxane structures, hence numerous SiOH groups are present. However, the condensation is slow, and only oligomer products are formed at room temperature during 24h [6-8]. The sudden addition of the amine hardener causes the pH to abruptly increase and the hydrolysed Si-OH groups can easily condense to form large siloxane aggregates. In conclusion, this approach allows to obtain large siloxanes domains separated from the organic network, but having a good interface separation.

6.4 Sol-gel “in-situ” (Ep-xAP-Siy-IS)

To the aim to reduce the inorganic domains dimensions a so-called “one-step polymerization” [6-8] or “in situ” approach, in which all the organic and inorganic component are obliged to react altogether, has been attempted. In

detail, both the inorganic precursor TEOS and its coupling agent GOTMS, were directly added to the epoxy resin functionalized with APTES, forming an homogeneous mixture. Moreover, in order to allow the hydrolysis reactions to start, the water and catalyst (basic in this approach, being the amine hardener) were added at the end of the hybrid preparation. This procedure allowed to study the effect on the final siloxanes structures of both the procedure and the catalyst. As known, the latter governs the relative rates of hydrolysis and condensation, gelation of the system, and final morphology of the silica gels, including a possible phase separation. The acid promotes a fast hydrolysis, leading to oligomeric linear products, whereas in base catalysed reactions the rate and extent of hydrolysis is lower compared to acidic catalysis, and less hydrolyzed product prevail. Hence, highly cross-linked sol particles are obtained because of the tendency of hydrolysed SiOH groups to sudden condensate. Since in basic condition the condensation is faster than the hydrolysis reaction, a siloxane network schematically pictured in Scheme 8 could be obtained. Here, some Si-OR groups are not hydrolyzed and could retain as not reacted dangles in the hybrid system.

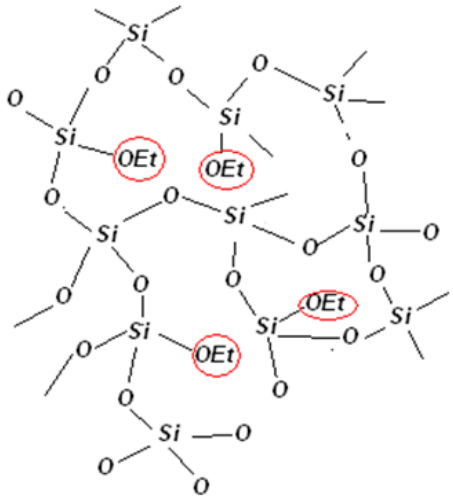

Scheme 8 - Schematic picture of the siloxane structures obtained by the "in situ" approach.

Furthermore, in the Ep-xAP-Siy-IS approach, the addition of the water and amine hardener together allows the two independent reaction mechanism to be simultaneously operative, i.e. the reaction of the epoxy and amine monomers to form the organic network, and the hydrolysis and condensation of TEOS/GOTMS to form the siloxane phase. Differently to previous approaches, here the hydrolysis of siloxane mixture occurs under basic condition and throughout the growth of the epoxy network. Hence, the two organic and inorganic networks are expected to be totally interpenetrated.

6.4.1 Dynamic Mechanical Analyses (DMA)

Figure 50 shows the tanδ curves related to the Ep-5AP-3Si-IS hybrid sample and the neat epoxy system (Ep-Mx). Again, the hybridization causes the Tg to decrease, and the loss factor curve to reduce and broaden, highlighting at least two different contributes, at about 90 and 107°C, respectively. Broadening of the loss factor peak evidences the wide spectrum of relaxation times typical of composite materials, whereas the separation in two contributes provides evidence

of a phase separation in the epoxy-silica hybrids, since several molecular relaxations could be detected. Phase separations which cause multi-peaks in the loss factor curves are frequently observed [6]. In fact, Matejka et al. [6] found that the neat epoxy system owns a narrow distribution of the molecular relaxation attributed to the glass transition, whereas in the epoxy-silica nanocomposites a new relaxation peak at higher temperature with respect to the neat epoxy system appears. The presence of two relaxation peaks is attributed to the phase separation between the epoxide and siloxane networks typical of composite materials. Furthermore, they attributed the new relaxation to the network chains immobilized by interaction with glassy silica domains, due to the strong interaction between the two phases caused by the use of coupling agents. Conversely what Matejka et al. [6] pointed out, even if the phase separation takes place, in the actual hybrid systems the maximum position occurs at lower temperature value with respect to that of the neat epoxy. However, as Yang et al. [9] pointed out silica nanostructures can play two different kinds of role in the epoxy matrix. If the interaction between the two phase is weak, the siloxane domains deteriorate thermal properties of epoxide system because they reduce its cross-linking degree. On the other hand, if a sufficient amount of coupling agent has been used, the interfacial interactions between the epoxide and siloxane domains can immobilize the polymer chains to some extent, and improve the thermo mechanical properties by increasing the storage modulus and the glass transition temperature. By taking into account those considerations, the DMA results (Figure 50) could be explained by considering that the amount of coupling agent is probably not enough to improve the interfacial interactions. In fact, the lowering of the epoxide Tg could be ascribed to the introduction of the siloxane domains poorly interacting with the epoxide network which in turn

partially destroy and make weaker the organic network. This could be the reason why the molecular transitions attributed to those of the epoxy network occurs at lower temperature values. Additionally, the presence of an additional peak at lowest temperature could be due to the interphase zone between organic and inorganic moieties. Again, in conclusion the approach Ep-5AP-3Si-IS leads to hybrid materials with poor viscous-elastic properties with respect to the neat epoxy system.

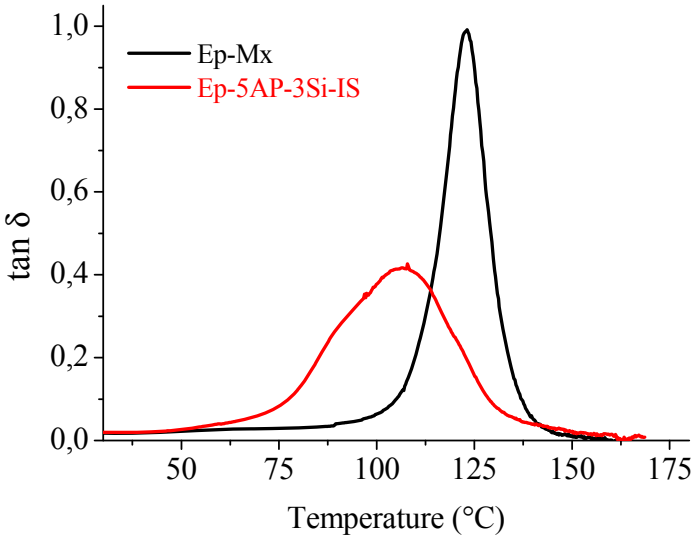

Figure 50 - Dynamic mechanical curves of Ep-5AP-3Si-IS and Ep-Mx versus the temperature.

6.4.2 Small Angle X-ray Scattering (SAXS)

The scattering profile of Ep-5AP-3Si-IS hybrid sample, subtracted of the epoxide contribute is shown in Figure 51. Again, the SAXS profile is characterized by three linear regions, in between two discontinuity zone can be detected. According to a hierarchical structure of siloxane domains, little spherical particles of 1.7nm dimensioned are supposed to interact forming open and

branched structures, since the fractal dimension in the middle q range is 1.6. The discontinuity at about 0.2nm^{-1} speaks in favour of a siloxane structure of intermediate dimension of 25-30nm, which in turn aggregates to form large siloxane domains with inter-diffuse morphology of inorganic chains in organic network.

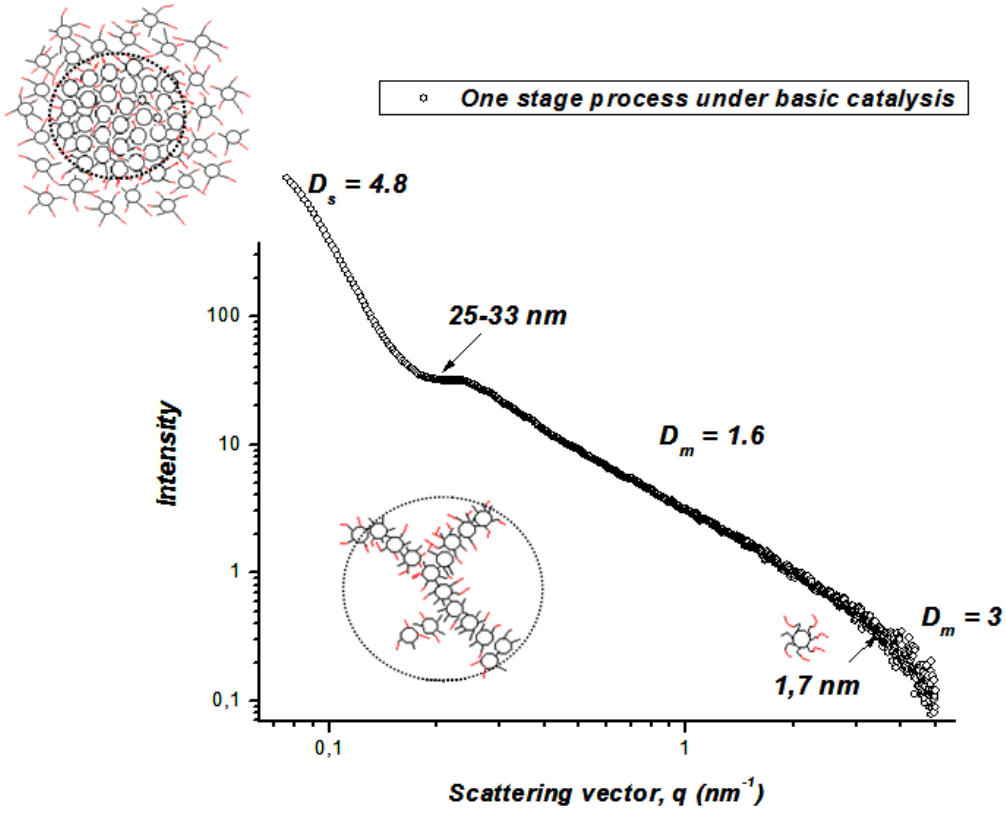

Figure 51 - Log-log plot of Ep-5AP-3Si-IS SAXS profile subtracted of the neat epoxy scattering contribute.

6.4.3 Scanning electronic Microscopy (SEM) and Energy Dispersive Scanning (EDS)

The morphology of the network synthesized by the Ep-xAP-Siy-IS method is the most homogeneous one obtained so far. In fact, as the Figure 52 shows, the

siloxane domains do not aggregate to form large inorganic phases as previously reported, but they are homogeneously distributed on the overall hybrid area. In fact, EDS analyses highlighted the presence of the silicium element everywhere. This morphology is probably due to the simultaneous growth of the two networks which avoided the siloxane structures to aggregate in inorganic domains, since the epoxy cross-linking and gelation reactions hindered it. Then opened and homogeneously distributed siloxane structures resulted (Figure 52) on the overall hybrid area.

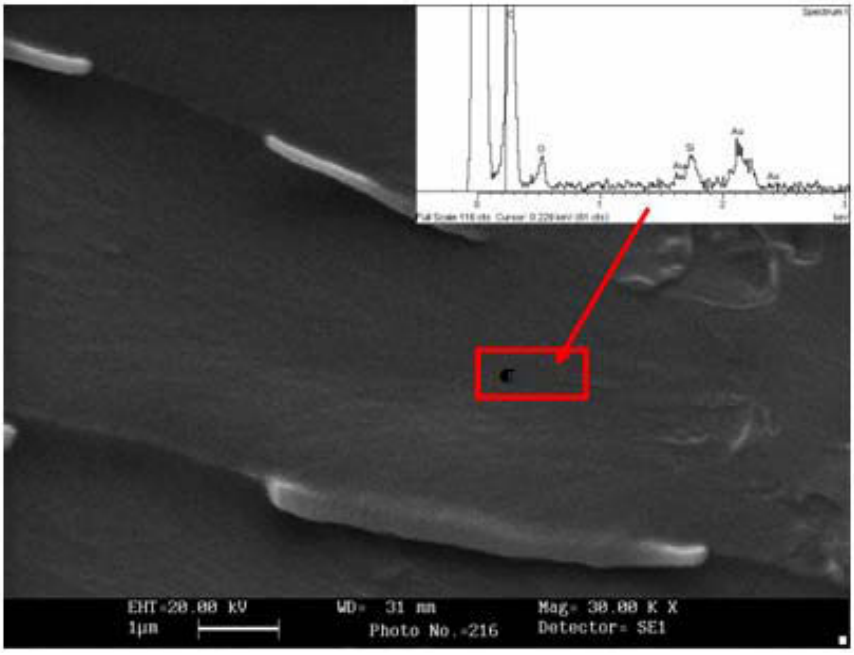

Figure 52 - SEM image of the Ep-5AP--3Si-IS hybrid sample.

The presence of gold is due to the metallization procedure used to make the measurement. This result appears to be in contrast with what Matejka et al reported [6]. In fact, the Matejka one-step procedure leads to the most heterogeneous morphology, involving large siloxane-silica aggregates 100-300nm sized, composed of smaller particles of 20-70nm in diameter.

6.4.4 Conclusion

By comparing the DMA curves of the Ep-5AP-3Si-Ol and Ep-5AP-3Si-IS hybrid samples (Figure 53) , and by taking into account their morphological features, it is worth noting that in spite of the same nanometric structure arising by the SAXS profiles, the dynamic mechanical behaviour and the final morphology are quite different. In fact, although both hybrids show a reduced Tg value with respect to the neat epoxy, the shape of loss factor curve changes markedly by modifying the synthesis approach. In fact, a further broadening and phase separation is observed in the Ep-5AP-3Si-IS sample with respect to the Ep-5AP-3Si-Ol ones.

The different behaviour of the hybrids could be explained by taking into account three effects which act in a synergistic way:

- The amount of coupling agents.

The same coupling agent amounts has been used to prepare the two hybrid samples. However, in the Ep-5AP-3Si-Ol approach the coupling agent amount seems to be enough to make compatible the two phase, since the inorganic phase is concentrated in some large domains. On the other hand, in the Ep-5AP-3Si-IS, the siloxane branched structures are homogeneously distributed in the organic network, making the coupling agent not enough to allow good interfacial interactions.

- The interaction between the siloxane structures and the epoxide network.

The more symmetric shape of the Ep-5AP-3Si-Ol loss factor could be due to the presence of a large amount of Si-OH groups which can interact with the OH groups of epoxide network. Whereas, in the Ep-5AP-3Si-IS approach probably

due to the presence of not hydrolyzed Si-OR groups, a poor interaction between the two phases is evidenced. The presence of Si-OH groups in the siloxane structure formed under acidic catalysis leads to a chemical grafting between phases by the reaction with C-OH of the epoxide network [1, 6, 10].

In both cases good interfacial interactions seems to be responsible of the higher Tg value of *Ep*-5AP-3Si-Ol sample and its more symmetric loss factor shape.

- The presence of developed solvents.

By using the Ep-5AP-3Si-IS approach, even if the addition of sol-gel solvents are avoided, little amount of solvents will be produced during the hydrolysis and condensation reactions, retaining into the reactive system. In the Ep-5AP-3Si-Ol procedure most solvents are subtracted during the treatment in the oven. The presence of these solvents could have a plasticizing affect, lowering further the Tg value of hybrids.

Finally, this approach pointed out that:

- the “in situ” approach for the production of hybrids weaken the epoxide network;
- the amount of coupling agent should be increased to further improve the interfacial properties;
- the solvents produced by the hydrolysis and condensation reactions retain into the reactive system, probably making a plasticizing affect.

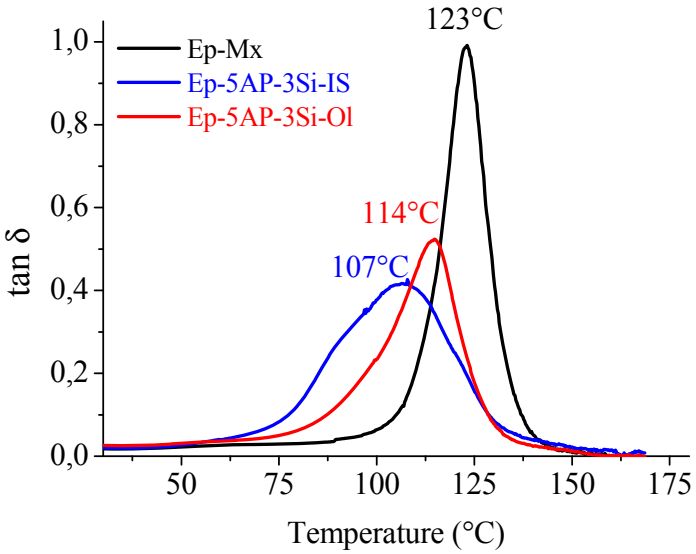

Figure 53 - Loss factor tanδ curves of Ep-5AP--3Si-IS and Ep-5AP--3Si-Ol versus temperature. The Ep-Mx curve is shown for comparison.

6.5 Sol-gel pre-hydrolysis MXDA-based hybrids (Ep-Siy-MX)

Hence, the pre-hydrolysis reaction under acidic catalysis has to be performed, in order to obtain structured inorganic domains and avoid the organic network to weaken. Previously attempts demonstrated that the properties of organic-inorganic hybrids depend to a great extent on both the interphase interaction and inorganic domains sizes. Aimed to reduce the inorganic size and make interactions stronger, the amount of coupling agent has to be increased. Moreover, in order to avoid an initial consumption of epoxy rings from APTES molecules, only GOTMS has been used from now on. The hybrid materials epoxy-silica obtained starting by GOTMS and epoxy resin, have been widely studied, since they can lead to materials with improved mechanical properties. In

fact, the GOTMS can undergo both the sol-gel polymerization of the alkoxy groups and curing of the epoxy functionality to form a hybrid network with covalent bonds between organic and inorganic phases. As Matejka et al. [11] demonstrated by size exclusion chromatography and ^{29}SI-NMR, GOTMS molecules are able to form epoxy functionalized cages, which in turn can further react by both the inorganic and the epoxy functionality. The self-assembling capacity of GOTMS molecules should produce numerous and nanometer sized cages chemically bonded to the organic network by the epoxide functionalities. Moreover, the excess of GOTMS coupling agent with respect to the TEOS amount, would assure the strong interactions between the two phases. But, though GOTMS is the most widely employed coupling agent [11-12] its slight negative effect has to be taken into account. GOTMS, in fact, is a monoepoxide agent, and its incorporation in the epoxy-amine network results in a decrease in organic cross-linking density worsening the polymeric mechanical properties, if some reactions involving either the organic or inorganic functionality did not occur. Consequently, it will be essential to obtain quite totally hydrolyzed Si-OH groups owing to the GOTMS molecules. Furthermore, to achieve this, the sol-gel co-solvent has been changed from ethyl in isopropyl alcohol. In fact, as known, the hydrolysis reaction become faster if the co-solvent used is not the same of that generated by hydrolysis of the alkoxide. Thus, to avoid the plasticizing effect of the sol-gel solvents, their extraction has been performed by using a rotavapor in vacuum condition. The new hybrids samples are named Ep-Siy-Mx. By using this protocol several formulations were prepared, as detailed in Table 13, to the aim to evaluate the siloxane content effect on the final properties of hybrid samples. The actual siloxane content has been evaluated as thermo-oxidative residual at 750°C by TGA analyses.

Samples	Siloxane content (wt%)
Ep-Mx	-
Ep-Si3-Mx	3.4
Ep-Si7-Mx	7.6
Ep-Si12-Mx	11.7
Ep-Si15-Mx	14.8
Ep-Si20-Mx	21

Table 13 - siloxane content of Ep-Siy-MX hybrid samples.

All hybrid samples also 2-3 mm in thickness dimensioned are transparent indicating that the larger dimension of inorganic inclusions is smaller than ~450nm, as shown for the Ep-Si12-Mx hybrid in Figure 54.

Figure 54 - Ep-Si12-Mx sample picture.

This appearance must be attributed to both the nanosized siloxane domains and the good interaction between them and the epoxide network, because of the high amount of coupling agent GOTMS.

6.5.1 Characterization by WAXS analyses

In order to investigate the modification of epoxide network caused by the introduction of siloxane structures, WAXS analysis has been performed. Figure 55 shows the scattering profiles of Ep-Si7-Mx and Ep-Si20-Mx hybrid samples.

The spectrum of the neat epoxy system Ep-Mx is also presented (Figure 55) for comparison. It is worth noting that the neat epoxy resin shows two characteristic broad bands with maximum located around 4.6 and 12 nm^{-1}, respectively, attributed to local density fluctuations of epoxy matrix [13]. The intensity of WAXD scattering profiles at low q values is attributed to the electronic density contrast between the siloxane and the organic phase [14], since the higher the siloxane content the higher the scattering intensity. It is worth noting that the siloxane domains affect the structure of the epoxide network, therefore a shift and intensity reduction of the broad band at $12nm^{-1}$ attributed to the epoxy network can be highlighted. Moreover, the band at $4.6nm^{-1}$ seems to disappear because of the superimposed siloxane scattering. The absence of peaks in the hybrids profiles demonstrated that no ordered organic-inorganic structures are formed [15].

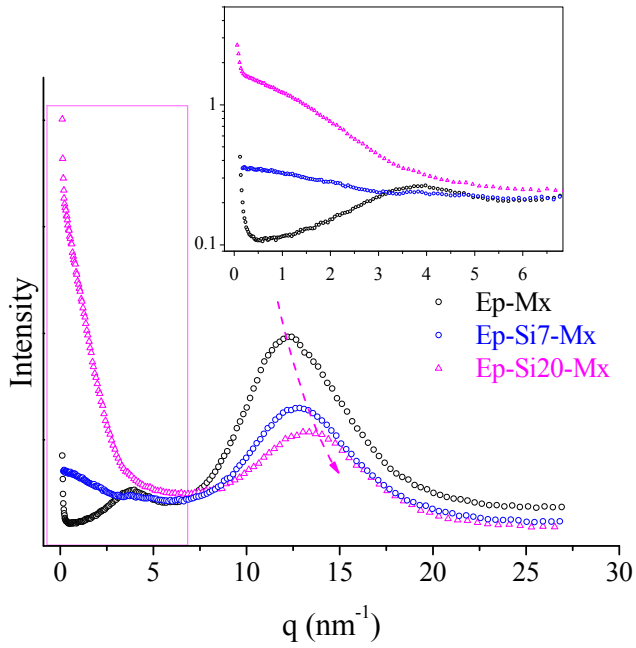

Figure 55 - WAXS analyses of Ep-Siy-Mx hybrid samples. In the inset an enlargement of the lowest q values is reported.

6.5.2 Characterization by ^{29}Si-NMR Spectroscopy

In Figure 56 the ^{29}SI-NMR spectra of Ep-Si12-Mx and Ep-Si20-Mx are shown, highlighting that the architecture of the inorganic domains in terms of Q and T arrangements changes with the siloxane content. In fact, in the Ep-Si12-Mx hybrid spectrum only T_2 and T_3 species can be observed, whereas in the Ep-Si20-Mx spectrum it is worth noting the presence of T_0 and T_1 peaks too. Hence, the siloxane amount affects the GOTMS condensation reactions since the inorganic structures originated from the trialkoxysilane change in terms of T*i* species. In details, since the T_0 species are detected in the Ep-Si20-Mx spectrum, it seems that no-bridged GOTMS molecules appears when the siloxane content increases. Moreover, the siloxane content seems not affect the inorganic structure arising from the TEOS molecules, since in both samples only Q_4 and Q_3 units are present. Furthermore, the higher the siloxane amount the higher the Q_4/Q_3 ratio, probably because of a higher siloxane content. By the knowledge of the peaks positions the percentages of T and Q species can be assessed by applying a deconvolution method of multi-peaks, as shown in Figure 57for the Ep-Si20-Mx spectrum.

Origin program has been used to perform the peaks deconvolution and calculate their area values. Since for the TEOS molecules only Q_4 and Q_3 units are present, the conversion degree of siloxane units can be assessed by the following formula:

$$q = \frac{T_1 + 2T_2 + 3T_3}{3} + \frac{3Q_3 + 4Q_4}{4}$$

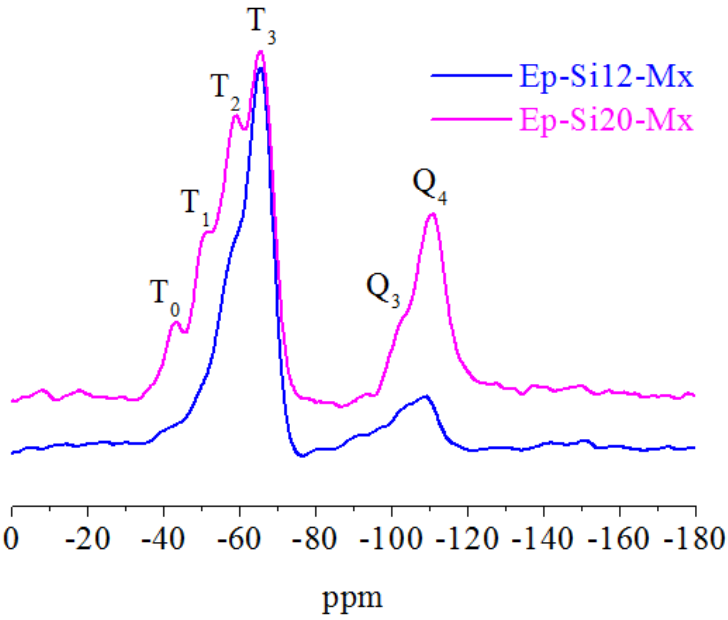

Figure 56 -^{29}Si-NMR spectra of Ep-Si12-Mx and Ep-Si20-Mx hybrid samples.

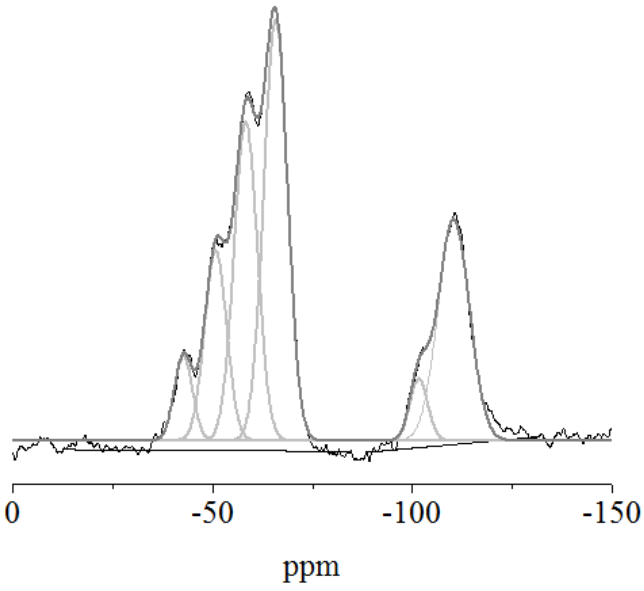

Figure 57 - Deconvolution of Ep-Si20-Mx 29Si-NMR spectrum.

The results, summarized in Table 14, show that as the siloxane content increases the q conversion decreases.

Table 15: q conversion degree of siloxane structures in the Ep-Siy-Mx hybrid samples..

Samples	q conversion (%)
Ep-Si7-Mx	88.5
Ep-Si12-Mx	85.6
Ep-Si20-Mx	77.3

Table 14 - q conversion degree of siloxane structures in the Ep-Siy-Mx hybrid samples.

These results could be tentatively explained by considering that the growth of both the orgabnic and inorganic networks can be mutually influenced. In fact, the amine hardener increases with the polysiloxane content, because of the higher content of GOTMS molecules to be cross-linked. The more basic conditions due to the higher amount of amine hardener allows the organic network to form more rapidly. Hence, the fast growth of the epoxide organic network could hinder the formation of the inorganic structure, limiting its extent probably because of the rapid gelation of the epoxide network. This is an interesting feature evidenced also by Davis et al. [16]. According to the authors [16], in fact, the inorganic network formation has proceeded to a greater extent in the materials that have a lower concentration of amine. This is contrary to what might be expected since the more basic conditions normally accelerate the inorganic condensation.

Finally, the NMR analysis points out that by using the Ep-xAP-Mx protocol, the formation of the two networks can be mutually influenced by the other one.

6.5.3 Characterization by Small Angle X-ray Scattering (SAXS)

In order to investigate the nanostructure of epoxy-siloxane hybrids and give information regarding hierarchical structures and particle size distribution the SAXS was employed [17-18]. Contrary to SAXS analyses performed previously, here the Ep-Siy-Mx spectra are not subtracted for the neat epoxy profile, because of the modification in the epoxide structure caused by its hybridization, as WAXS highlighted (Figure 55). Figure 58 shows the SAXS patterns on log-log plot for the hybrid samples as a function of siloxane content. The spectrum of the neat epoxy is also presented. It is worth noting that at low siloxane content, i.e. Ep-Si3-Mx, the typical epoxide broad band at $4.6nm^{-1}$ can be still observed, pointing out that the siloxane amount is not enough to modify entirely the organic structure. Whereas at higher siloxane content, the inorganic scattering superimposes that of the epoxide broad band. Moreover, the higher the siloxane content the higher the scattering intensity. Additionally, the Ep-Six-Mx spectra with x>3, exhibit typical Guinier plateau revealing the existence of a "diluted" hybrid system consisting of a few number of siloxane nanostructures dispersed in the epoxy matrix [19-20]. This behaviour is retained in hybrids at high siloxane content, i.e. Ep-Si20-Mx sample, which in turns does not show any correlation peak, underlining the dilution of siloxane structures embedded in polymeric matrix. The structure of siloxane phase in Ep-Six-Mx hybrids has been determined calculating their gyration radius (Rg), which gives a measure of the mean square distance of the scattering centers within inorganic domains from the center of gravity [21]. Therefore, Rg is related to sizes of inorganic siloxane domains, and could be calculated from the slope in the linear region of a plot of $ln(I(q))$ versus q^2, according to Guinier's relation [22]:

$$I(q) \propto \exp(-q^2 R_g^2 / 3)$$

Moreover, as done for the other hybrid samples, the slope in the log-log plot in the Porod region has been used to assess the fractal dimension D_m of the siloxane structures.

Samples	Rg (nm)	D_m
Ep-Si7-Mx	0.388	1.3
Ep-Si12-Mx	0.299	-
Ep-Si15-Mx	0.287	0.6
Ep-Si20-Mx	0.664	-

Table 15 - Rg and Dm values extracted from the SAXS patterns shown in Figure 58.

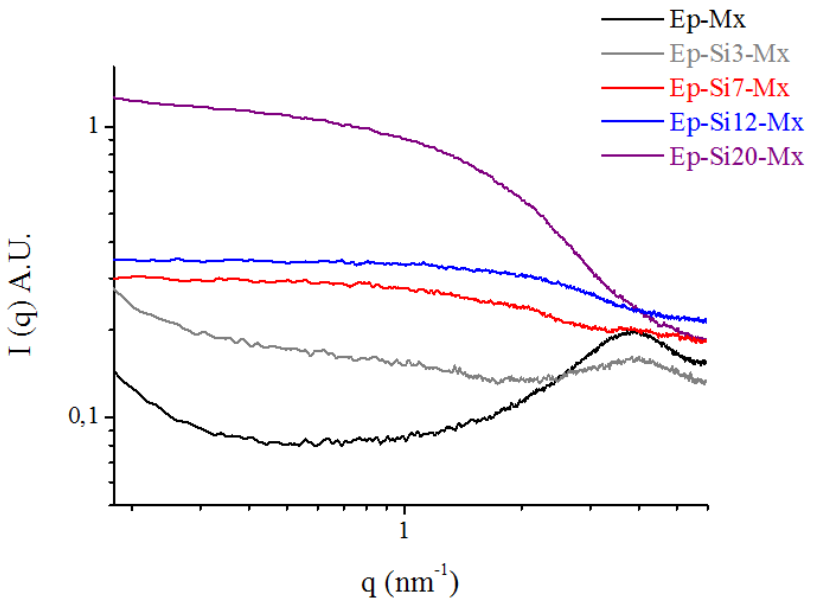

Figure 58 - SAXS scattering profiles for the Ep-Siy-Mx hybrid samples

In Table 15 the values of Rg and D_m have been reported. It is worth noting that the fractal dimension is quite low, if compared with those previously reported.

Thus due to the high GOTMS content the inorganic structures are finely dispersed in the organic matrix. Moreover, the size of the inorganic structures reduces slightly as the siloxane content increases up to 15wt%. However, the sample at highest siloxane content (i.e.Ep-Si20-Mx) exhibits a really high inorganic size, namely 0.664. Again this sample does not follow the trend.

6.5.4 Scanning Electronic Microscopy (SEM) and Energy Dispersive Scanning (EDS)

Fracture surfaces of the hybrid samples observed with Scanning Electron Microscopy, and silicium distribution mapping taken from an energy-dispersive analysis on the overall surface of the exposed surface, show how siloxane structures are dispersed in the epoxide matrix (Figure 59). In Figure 59 it is worth noting that the inorganic structure is quite homogeneous also at highest siloxane content, i.e. Ep-Si20-Mx and no silica aggregations are evident. This behaviour can be easily ascribed to the high percentage of GOTMS which can provide chemical bonds between epoxide network and inorganic structures, making better the compatibility between the two organic and inorganic phases. Additionally, the silicium is homogenously distributed on the overall area analysed. Furthermore, in the Ep-Si3-Mx hybrid sample, the appearance of black spots is due to the polymeric matrix.

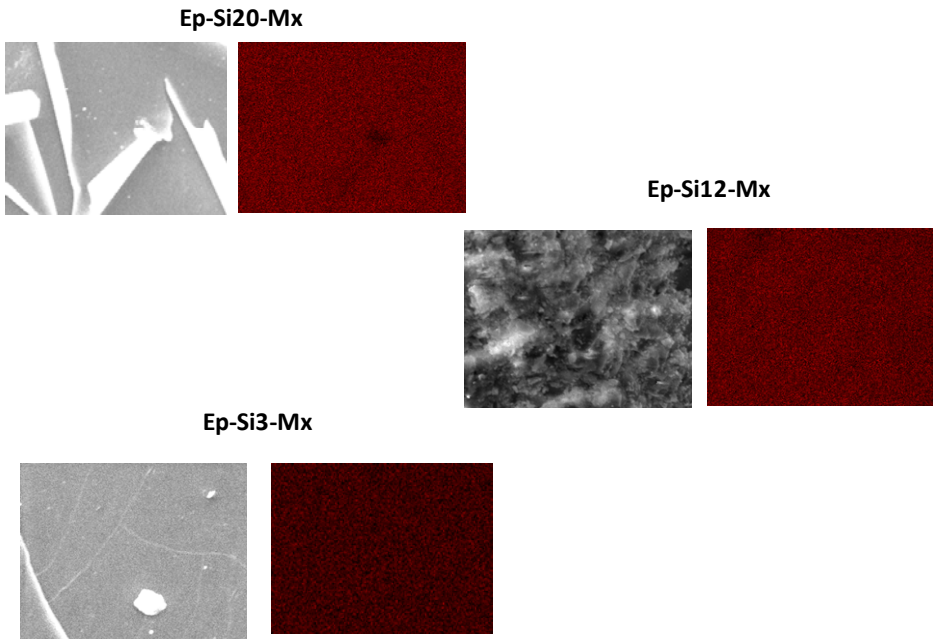

Figure 59 - SEM images of Ep-Siy-Mx with several siloxane content, namely y=3, 12 and 20. On the right of each micrograph, the silicium distribution mapping has shown as red spots.

6.5.5 Thermo-gravimetric Analysis (TGA) in air flow.

In Figure 60 the thermogravimetric analyses in air flow of hybrid samples Ep-Si12-Mx and Ep-Si20-Mx and neat epoxy Ep-Mx have been reported. In the inset, the temperature derivative curves DTA have been shown. It is worth noting that the thermo-oxidative stability of hybrid samples at temperature higher then 400°C is greatly improved with respect to the neat epoxy system. In fact, as evident in the inset of Figure 60, the maximum temperature of the second decomposition process increases of about 40°C in the hybrid samples. Moreover, as observed in other polymer silica nanocomposites [8, 23-26] the improvement efficiency in the thermal stability of the epoxy-silica hybrids increases with increasing the silica content. While being heated, the silica migrates on the surface of the hybrid materials, because of its relatively low surface potential

energy. Then the siloxane domains act as a heat barrier to protect the inner layer of polymer since they prevent the oxidation and thermal degradation of epoxide network. Furthermore, in spite of performed curing cycle at high temperature, it is worth noting a loss of sol-gel solvents at temperatures lower then 350°C. This behavior is found to be common in the epoxy-silica hybrid materials [27-28], probably because of solvents development at temperatures higher than of the curing cycle.

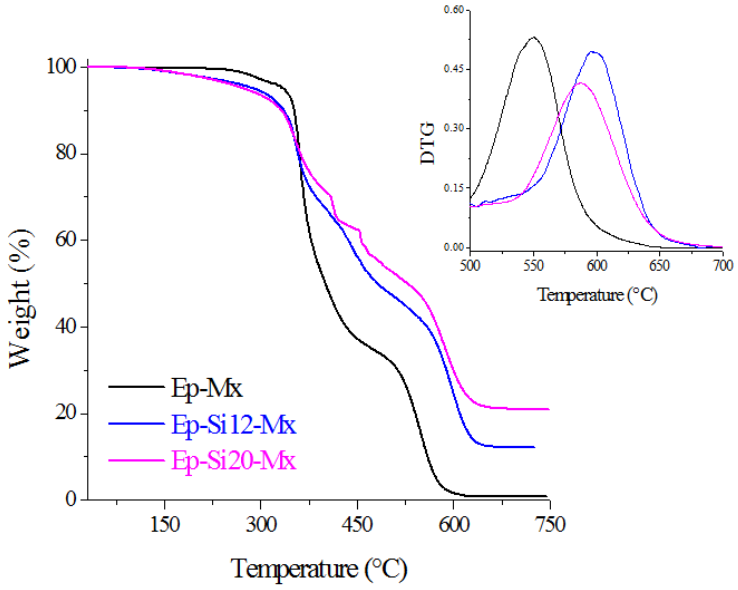

Figure 60 - Thermo-gravimetric analyses performed in air flow of both the hybrid samples Ep-Si12-Mx and Ep-Si20-Mx, and the neat epoxy Ep-Mx. In the inset the derivative curves with respect to the temperature has been reported.

6.5.6 Dynamic Mechanical Analysis (DMA)

Figure 61 shows the tensile storage modulus E' and loss factor tanδ (=E''/E') of both Ep-Siy-Mx hybrid and neat epoxy Ep-Mx systems as function of temperatures. The results pointed out that the introduction of siloxane structures into the epoxide network causes the glass transition temperatures to reduce with

respect to the neat epoxy system. The Tg values are shown in Figure 62 as a function of siloxane content. It is worth noting that its values retain quite constant when the siloxane content is lower than 15wt%, whereas it decreases drastically for the Ep-Si20-Mx hybrid sample.

As also Habsuda et al. [29] found changes in the glass transition temperatures of the hybrids are correlated with the siloxanes structures, in terms of T e Q values by ^{29}SI-NMR spectroscopy, and then with the molecular weight of the inorganic clusters. They found that condensed but brunched structures like Q_3 could be expected to lead to better molecular interactions and miscibility with respect to Q_4, resulting in greater chain constraint and thus higher glass transition values. Hence, an increase in Q_3 leads to better organic-inorganic molecular mixing and higher Tg values. In our case, the Q_4/Q_3 ratio increases with the siloxane content, as the Figure 56 showed, thus in the Ep-Si20-Mx sample the high Q_4 value could be responsible of the observed Tg value dramatically reduced with respect to the other hybrid systems. Additionally, the structural study by ^{29}SI-NMR spectroscopy highlighted that in the Ep-Si20-MX the T_0 content is extremely higher than that expected. Thus the contemporary presence of high Q_4 and T_0 siloxane structures act in synergistic way to cause a large decrease in Tg values at highest siloxane content. In fact, if the Q_4 structures can reduce the Tg because of the poor interaction between the two phase with respect to other more open siloxane structures, i.e. Q_3, on the other hand the no-bridged T_0 structures can cause a plasticizing effect reducing the cross-link density. All these effects could act together causing the low Tg value in the Ep-Si20-Mx sample.

In addition, it has been observed that the loss factor tanδ shape changes with the siloxane content, becoming weaker and broader as the siloxane content increases. As known [30], this is a typical behaviour of nanocomposites materials.

Moreover, the Ep-Si20-Mx shows a new damping peak which gives evidence of a phase separation in the epoxy-siloxane systems. Again the viscous-elastic behaviour could be explained by considering the inorganic structure distribution pointed out by the ^{29}SI-NMR spectroscopy. In fact, in the Ep-Si20-Mx sample the loss factor shape could be due to the simultaneous presence of T_0 and Q_4 siloxane structures. The broad siloxane species distribution could affect the molecular constraints and thus make large the region of molecular motion [9, 29].

Finally, as shown in Figure 61, the dynamic mechanical analyses pointed out that the elastic modulus E' of hybrid samples in the rubbery state increases with the siloxane content, meaning that the crosslinking density of elastically effective network νe increases, according to the equation [31]:

$$\nu e = E'/3RT$$

This beneficial effect can be due to the coupling agent effect of high GOTMS content, which improves the interfacial interactions between the two organic and inorganic phases providing chemical bonds between them, and then increasing the cross-linkers number. Also Yang et al. [9] found that the modulus in the rubbery region increases with the GOTMS content. Moreover, they demonstrated that the introduction of GOTMS in the silica-epoxy hybrid materials can enhance the interfacial interactions between silica and epoxy matrix and moreover it increases the cross-linking density of the final system. Additionally, according to our findings their results pointed out that the area of the tanδ peak decreased with an increase of the GOTMS content. Conversely, they found that the glass transition behaviour became indistinct as the GOTMS content increased.

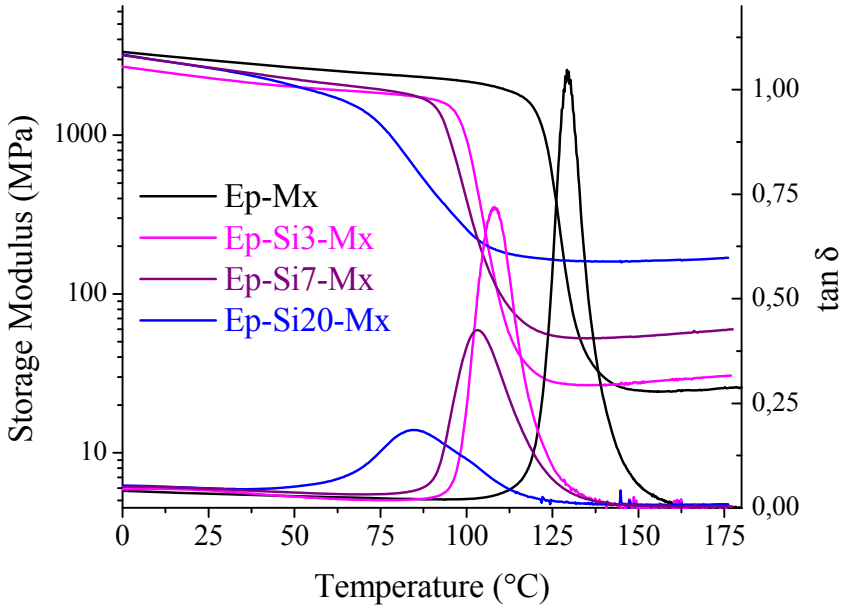

Figure 61 - Dynamic Mechanical properties of Ep-Siy-Mx hybrid and neat epoxy Ep-Mx samples as Storage Modulus E' and loss factor tanδ as a function of temperatures.

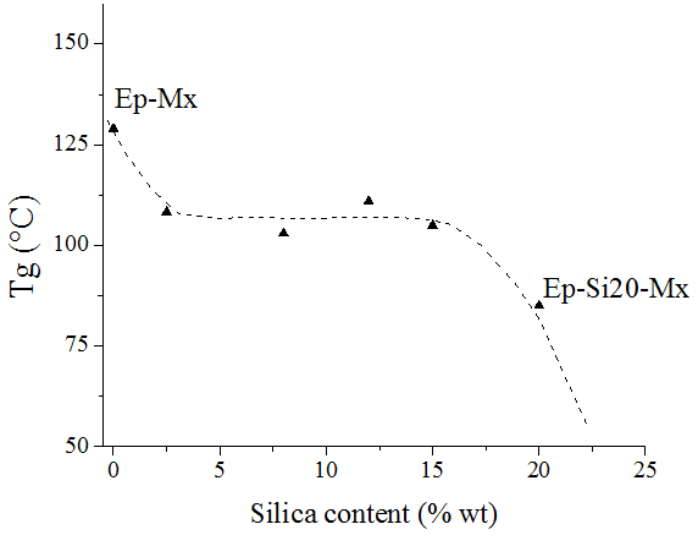

Figure 62 - Glass transition temperature of Ep-Siy-Mx hybrid and neat epoxy Ep-Mx samples as function of siloxane content.

6.5.7 Nanoindentation experiments

The mechanical properties of the hybrid materials are obtained by nanoindentation technique. Figure 63 shows the typical load-unload cycle for the pure epoxy resin (Ep-Mx) and the Ep-Si12-Mx hybrid sample.

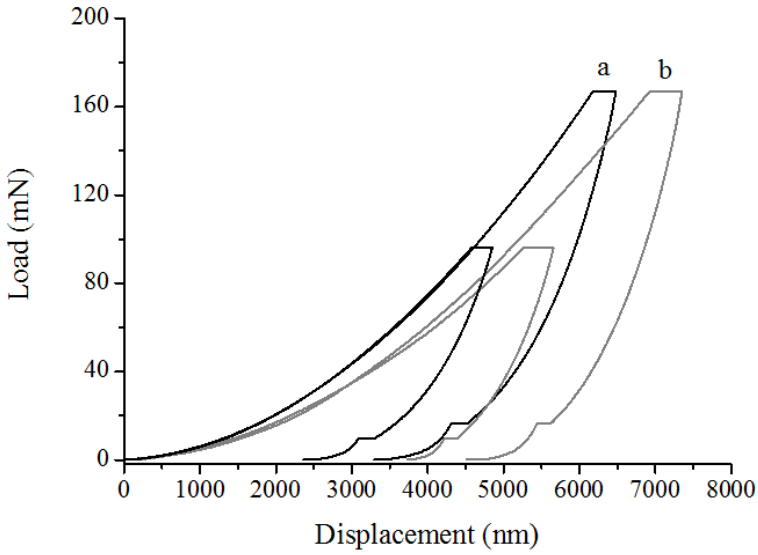

Figure 63 - Typical load-displacement curves of the hybrid Ep-Si12-Mx (a) and pure epoxy resin (b).

The hardness and the elastic modulus obtained by the nanoindentation measurements are shown in Figure 64 as a function of the siloxane content. It is worth noting that except the sample Ep-Si12-Mx, both the hardness and the elastic modulus decrease as the siloxane content increases. These results are in evident contrast to what previously reported. In fact, as known, [21, 32], the introduction of inorganic nanoparticles into a polymeric matrix usually allows the hardness and elastic modulus to enhance. Indeed, for instance, the silica addition by sol-gel method from TEOS in (γ-methacrylpropyl)trimethoxysilane (MPMS) results in harder structures containing silica SiO_2, which causes an

increase in the rigidity of the system [32]. However, the authors reported that if the TEOS content is higher than 20wt%, its introduction causes the hardness to reduce, because of the incomplete cross-linking and a looser final structure of the organic-inorganic hybrid. Together with the hardness, the elastic modulus decreases consequently. Additionally Xiong et al. [21] found that the process parameters of the sol-gel reaction drastically affect the hardness of the hybrid samples. They showed that the open and chain-like structures, the phase separation with a small size and the decrease in the cross-linking density cause the reduction of hardness and elastic modulus. Hence, the nanoindentation results suggest that in the Ep-Siy-Mx samples the siloxane structures are quite open, and the crosslinking density is lower than that of the neat epoxy system. Thus, as the siloxane content increases the epoxide network become more soft, since both the hardness and the elastic modulus decreases.

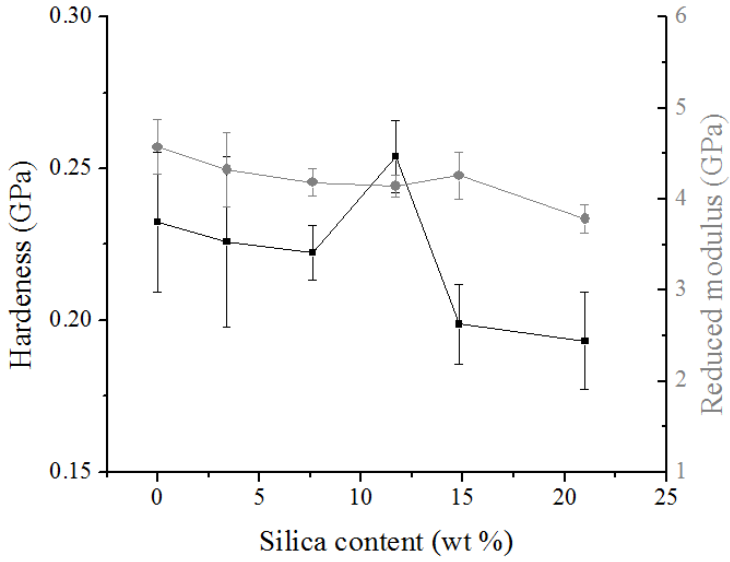

Figure 64 - Influence of siloxane content on the hardness and reduced elastic modulus of the Ep-Siy-Mx samples.

6.5.8 Conclusions

The Ep-Siy-Mx protocol provides samples transparent in appearance and whose morphology is homogeneous also at highest siloxane content. The absence of large inorganic aggregation can be easily ascribed to the high amount of coupling agent GOTMS, which displayed to be better than APTES to make compatible the two phases in the organic-inorganic hybrid materials production. Its use, in fact, allows to affect the intimate epoxide structure, as pointed out from the WAXS analyses, and produce nanosized inorganic clusters, as highlighted from the SAXS results. Therefore, in the last Ep-Siy-Je protocol, to the aim to study only the hardener amine effect, both the hybrid preparation procedure and the GOTMS amount have been retained the same of the Ep-Siy-Mx approach. Nevertheless, in spite of their good appearance and the little inorganic structures, the Ep-Siy-Mx samples show poor mechanical properties because their Tg's reduced with respect to that of the neat epoxy system. The ^{29}Si-NMR results pointed out that in our case, conversely to what Hsiue et al. [27] found, the total amount of siloxane bridges, namely the q conversion, decreases with the siloxane content, implying that as the amount of precursors increases a more open and poor siloxane structures are formed. It follows that when the siloxane content increases, more soft materials are obtained, as the decreasing hardness revealed from the nanoindentation measurements. Then the siloxane chain-like structure and the presence of the T_0 moieties in the Ep-Si20-Mx become responsible of the reduced value of hardness and Tg's in the hybrid materials, since the mobility of the epoxy chain is greatly enhanced by their plasticizing effect. In fact, as known [27], the silica is able to enhance the final mechanical properties of hybrid materials, only if complete silica network can be formed [33], causing a reduced

mobility of the epoxy chains and then producing relatively high Tg's [8, 24, 27, 34].

Therefore, to the aim to prepare hybrid materials with improved mechanical properties and to study the effect of the amine hardener on the inorganic structure formation, the Jeffamine D230 has been used instead of the MXDA in order to prepare the Ep-Siy-Je samples.

6.6 Sol-gel pre-hydrolysis D230--based hybrids (Ep-Siy-Je)

With the Ep-Siy-Je protocol several formulations were prepared, as listed in Table 16 The actual siloxane content has been evaluated as thermo-oxidative residual at 750°C by TGA analyses.

Sample	Siloxane content (wt%)
Ep-Je	0
Ep-Si7-Je	6.6
Ep-Si12-Je	12.3
Ep-Si18-Je	17.8
Ep-Si22-Je	21.5

Table 16 - Ep-Siy-Je hybrid samples. The actual siloxane contents are indicated.

These systems have been exhaustively characterized by following all the processes and modifications in the chemistry and morphology which happen during the preparation steps (see Scheme 9).

6.6.1 Characterization of siloxane precursors solution.

As previously discussed, the GOTMS/TEOS molar ratio and the sol-gel process parameters own to Ep-Siy-Mx approach provide hybrid samples with the desired final inorganic morphology. Therefore, a study of the inorganic network evolution during the sol-gel reaction has been done. To achieve this goal, the precursor solution has been characterized by using NMR and GPC techniques before and after the pre-hydrolysis reaction at 60°C.

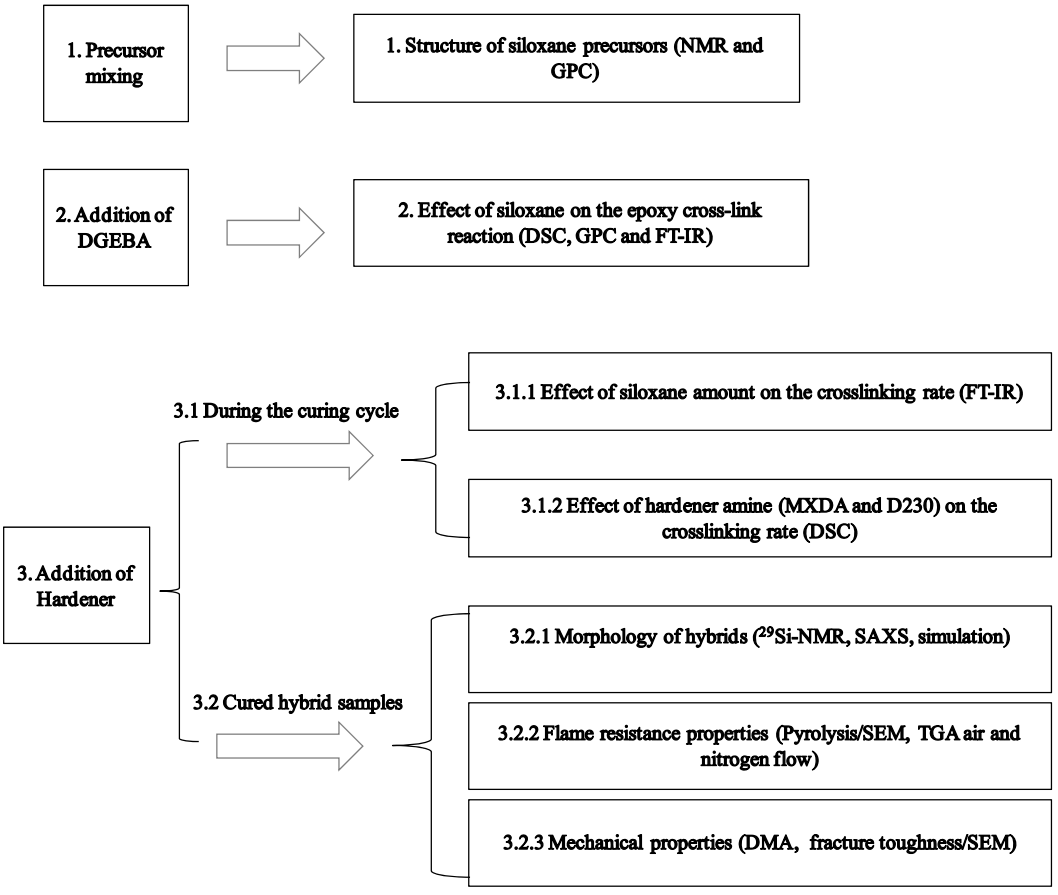

Scheme 9 - Schematic drawing of characterizations performed on the Ep-Siy-Je hybrids.

6.6.1.1 Nuclear Magnetic Resonance (NMR)

The ^{1}H, ^{13}C and ^{29}Si NMR provided information on both the hydrolysis and condensation degree of siloxane precursors and the stability of GOTMS epoxy ring during the pre-hydrolysis reaction at 60°C. As a matter of fact, as Matejka et al. [11] suggested, during the pre-hydrolysis step, a reaction of the GOTMS epoxy group could also occur. In particular, in our system, two kind of nucleophilic attach could theoretically take place, namely from OH of both H_2O and SiOH silanols groups. Since Hsu et al [35] found that H_2O does not appear to participate in epoxy ring opening reaction, in this work the OH attach from water molecules has not been considered. In Figure 65, the ^{29}Si NMR spectrum between -40 and -60ppm has been shown. According to what Hook et al found [36-39], assignments for the hydrolysis/condensation species formed during the pre-hydrolysis reaction have been done. Hence all the partially or totally hydrolyzed $Si(OH)_m(OCH_3)_n$ GOTMS peaks have been assignment, as indicated in Figure 65.

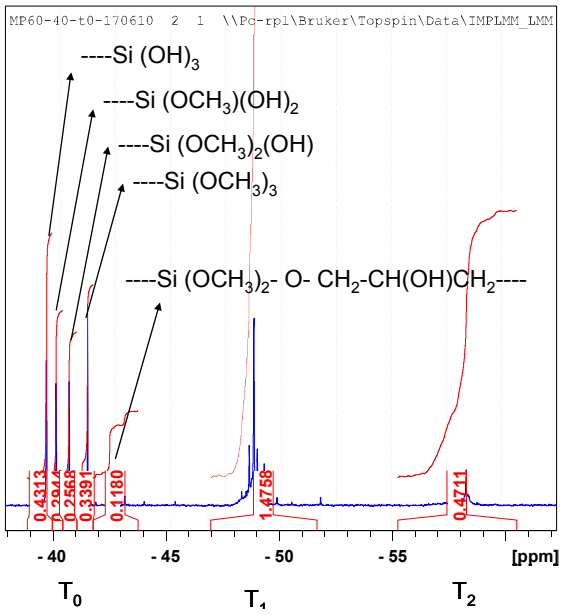

Figure 65 – ^{29} Si-NMR of reaction mixing before 4h at 60 °C.

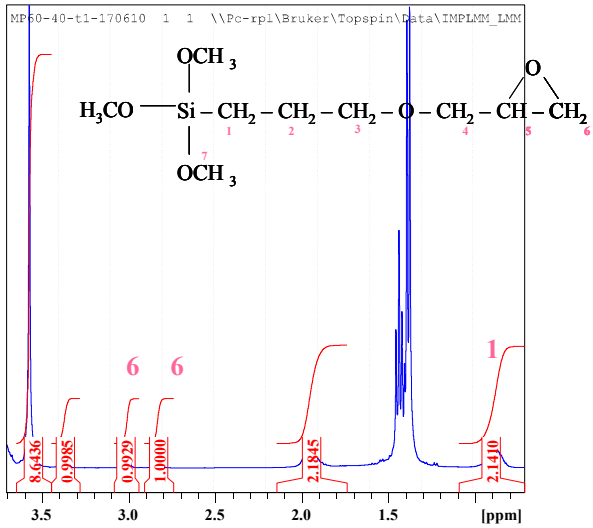

Figure 66 – ^{1}H NMR of reaction mixing after 4h at 60 °C

The peak at -43ppm could be tentatively ascribed to the –Si(OCH$_3$)-O-CH$_2$-CH(OH)CH$_2$- group, coming from the reaction between the Si-OH and the

GOTMS epoxy ring. This unexpected result highlights that the epoxy ring belonging to the GOTMS molecules is not quite stable, since the SiOH group is able to open it. Moreover, to the aim to quantify the extent of the GOTMS epoxy ring reacted, the evaluation of the ratio between the intensity of two H in position 6 and that in 1 has been done (see Figure 66). Since its value is 0.93 (see ^{1}H-NMR spectrum in Figure 66), [40] , the GOTMS epoxy ring has been considered to be stable versus the SiOH nucleophilic reaction.

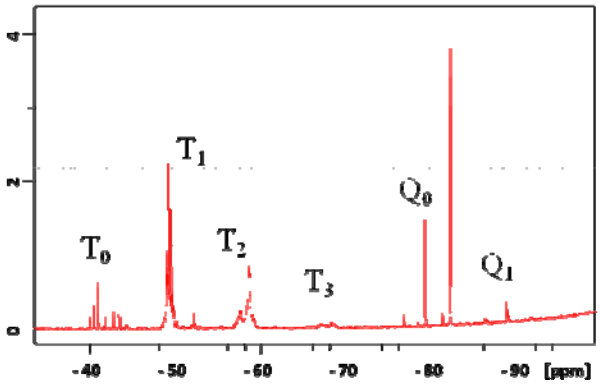

Figure 67 - ^{29}Si NMR of precursors mixing after the hydrolysis reaction at 60°C.

In Figure 67 the ^{29}Si NMR spectrum of the siloxane mixture after 4h at 60°C has been showed. It is worth noting that all the hydrolyzed and condensed moieties belonging to the GOTMS molecules are present, whereas the TEOS condensation seems to be negligible. ^{29}Si NMR spectrum (Figure 67) has been used to determine siloxane conversion degree in Si-O-Si groups defined as:

$$q = \frac{T_1 + 2T_2 + 3T_3}{3} + \frac{Q_1}{4}$$

since here only T_i and Q_1 species could be detected.

In spite of the DBTDL catalyst, after 4h at 60°C the siloxanes conversion degree q reaches a value of about 40%, hence open and poorly condensed siloxane

structures form after the pre-hydrolysis step. This is in contrast to what Matejka et al. found [11]. They stated, in fact, that no hydrolysed T_0 units are observed in a DBTDL-catalysed system because of their immediate condensation to branched T_2 and T_3 units, which rapidly form, becoming soon the dominant structures.

6.6.1.2 Gel Permeation Chromatography (GPC) of siloxane precursors mixture

In Figure 68 the GPC results related to the unreacted and hydrolyzed precursors mixture (after 4h at

60°C) has been shown. The two profiles (Figure 68) differ only for the presence of a broad peak at lower values of retention volumes for the reacted mixture. Since in GPC techniques molecules with larger size reach the end of the column before molecules with smaller size, hence the higher the molecular weight the lower the retention volume. Keeping in mind this statement, the appearance of the broad peak at lower retention volume value is a clear evidence of the slightly increased molecular weight during the pre-hydrolysis reaction at 60°C. These results confirm what the NMR analyses highlighted, that is the low tendency of siloxanes structure to condensate during the reaction at 60°C.

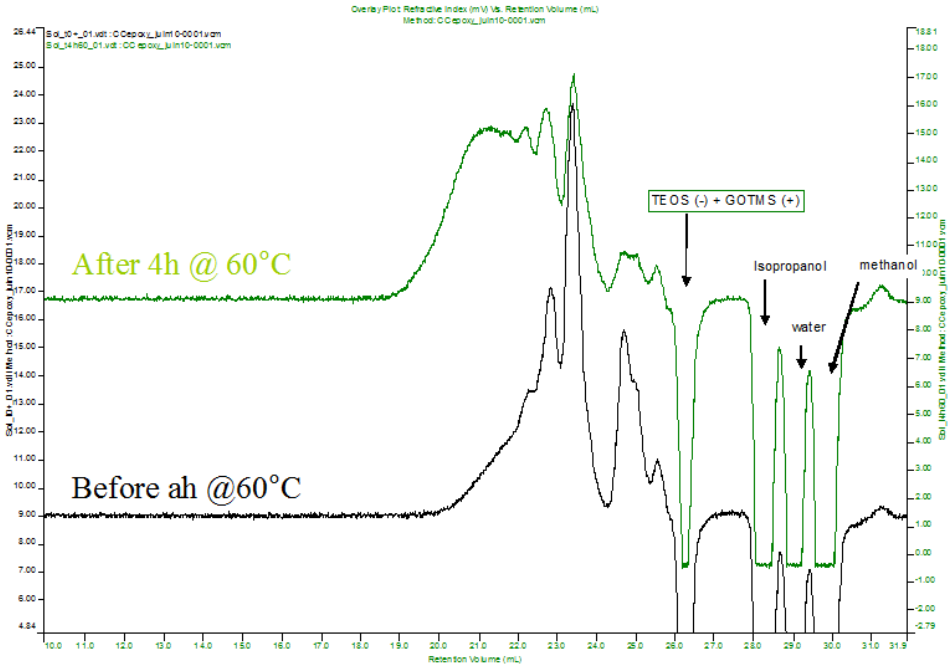

Figure 68 - GPC results of precursors mixing before and after the hydrolysis reaction at 60°C.

6.6.2 Cross-linking reaction of hybrid mixture without the addition of hardener.

As previously demonstrated by the ^{29}SI-NMR spectroscopy, the reaction between the GOTMS epoxy ring and silanols groups SiOH is possible to occur. Therefore, in order to evaluate the extent of the reaction between epoxy monomers and silanols groups, the hydrolyzed precursors and the DGEBA oligomers have been mixed to obtain an actual siloxane content of 22 wt% (Ep-Si22). The hybrid mixture (organic/inorganic moieties) has been heated by following the usual curing cycle (namely 4h at 80°C and 12h at 180°C), but in absence of the amine hardener. During the pseudo-curing cycle in several steps, i.e. after both 2 and 4h at 80°C, and after both 2 and 12h of post-curing at 180°C the samples have been analyzed by DSC, FT-IR and GPC.

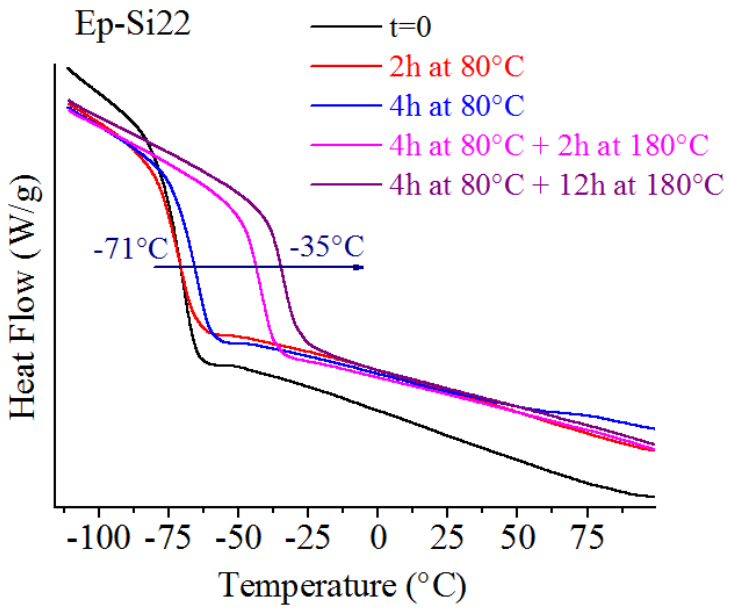

Figure 69 - DSC of hybrid mixtures without the addition of the hardener during the curing cycle.

6.6.2.1 Differential Scanning Calorimetry (DCS)

The DSC thermograms of the hybrid mixture at different curing cycle steps have been plotted in Figure 69. It is worth noting that after 4 hours at 80°C the Tg slightly increases from -71 to -66°C, whereas after the post-curing at 180°C the Tg increases visibly up to -35°C. The increase of the Tg during the curing cycle at 180°C without the addition of the hardener speaks in favour of an appreciable increased molecular weight, probably due to the effect of Si-OH groups as cross-linkers of epoxide groups. Moreover, it cannot be excluded the possibility that the Tg increasing could be due to the condensation reaction of siloxane which takes place at high temperature.

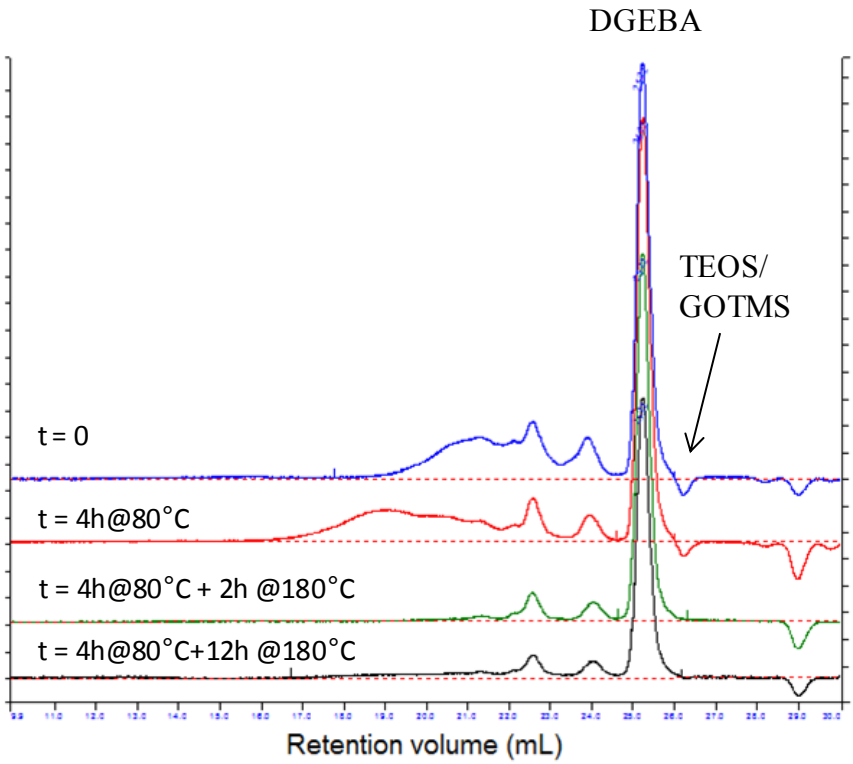

Figure 70 - GPC chromatograms related to the hybrid mixture at several step of the curing cycle without the addition of the hardener.

6.6.2.2 Gel Permeation and Cromatography (GPC)

The GPC chromatograms (Figure 70) show the presence of TEOS and GOTMS traces after 4h at 80°C, as the presence of the negative peaks at a retention volume value of about 20mL (red and blue curves) attests. Furthermore, the broad peak (ranging from 19 to 22mL) shits at lower retention volume values after the first step at 80°C. Since the lower the retention volume the higher the molecular weight, the shift of the broad peak suggests a slight increase of the molecular weight. Finally, after 2h at 180°C a disappearance of the broad peak at low retention volume values can be observed, pointing out the complete absence of soluble moieties in THF solvent. Additionally, from the intense peak at about

25.5mL the relative amount of unreacted DGEBA can be assessed. The results pointed out that after 12 hours at 180°C about the 30wt% of DGEBA has reacted.

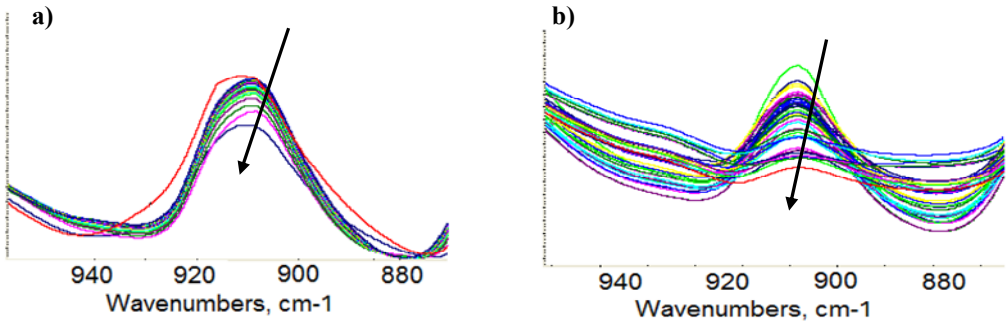

Figure 71 - FT-IR spectra of hybrid mixture (actual silica content 22 wt%) during the curing cycle at 80°C (a) and the post-curing at 180°C (b).

6.6.2.3 Fourier Transform-Infrared (FT-IR)

The Figure 71 shows the FT-IR spectra of the hybrid mixture thin film during the curing cycle at 80 (a) and 180°C (b), the arrows indicating the time evolution of the spectra. By using the following relationship (see chap 4)

$$(1) \qquad \alpha = \frac{\overline{A}_0^{916} - \overline{A}_t^{916}}{\overline{A}_0^{916}} \quad \text{where} \quad \overline{A}^{916} = \frac{A^{916}}{A^{1509}}$$

the conversion degree of epoxide groups has been assessed, and the resulting trend has been shown in Figure 72. The α estimation has been repeated twice. From the curves reported in Figure 71, it is worth noting that the cross-linking reaction at 80°C slightly allows the epoxide groups to react (Figure 71 a), whereas the post-curing at 180°C exhausts all the epoxide groups (Figure 71 b). In fact, according to the equation (1), the conversion degree reaches a value of

about 0.3-0.4 during the heating at 80°C, and become equal to 1 after few hours at 180°C (as showed in Figure 72). Furthermore, a possible catalytic effect of KBr on the cross-linking reaction of epoxy groups has to be considered. The first experimental data were not considered because of their apparent reduction, probably ascribed to the choice of the first absorbance value at 25°C. Anyway, after the curing at 180°C the overall consumption of epoxy ring is quite evident.

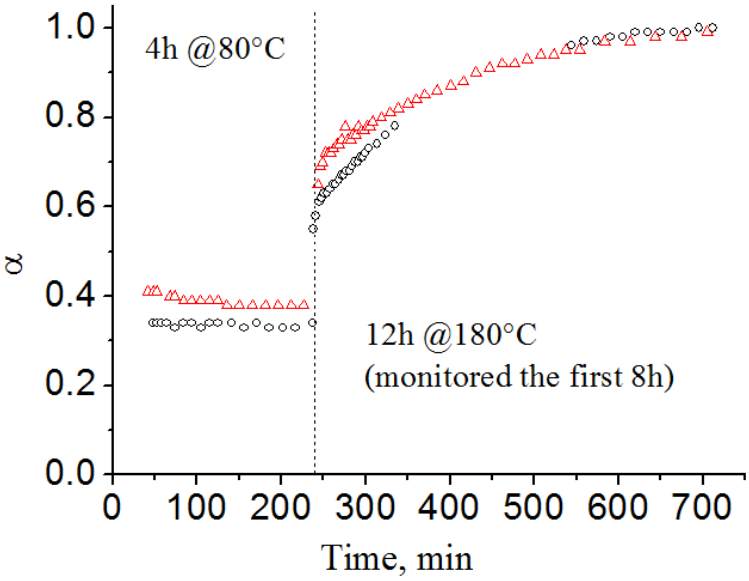

Figure 72 - Conversion degree of epoxide groups belonging to the hybrid mixture (without the addition of hardener) after the curing cycle at 80 and 180°C.

6.6.2.4 Conclusions

All the experimental results (GPC, FT-IT and DSC) suggest that in absence of the amine hardener the cross-link reaction of epoxide from SiOH groups starts at 80°C and becomes quite complete after the post-curing at 180°C. In particular, at 80°C the epoxide rings could be opened by the Si-OH groups causing the Tg to increase slightly. Instead the prominent increase of the Tg at 180°C could be explained with the concurrence of two phenomena, i.e. the cross-linking of both

the organic and inorganic species enhanced by the increased temperature. Concerning this, the cross-linking reaction of the organic moieties could be promoted by the silanols Si-OH groups which are able to open the epoxide rings. Furthermore, the reaction of nucleophilic addition of silanols on the epoxide groups would generate other hydroxyl groups, which could in turn act as catalyst of the epoxy cross-linking [41] and then form the tree-dimensional organic network. The increasing of Tg to -35°C and the unitary conversion degree strongly suggested that. Beside the increase of the temperature could enhance the condensation reaction involving the silanols groups to form the siloxane domains. Moreover, due to the high content of organosilanes GOTMS, the two reaction mechanism would act together to form a global organic-inorganic three-dimensional network. The reaction promoted by the silanols groups in the opening of epoxide rings could become competitive to that involving the diamine hardener.

Finally, it is worth noting the different estimation of conversion degree arising from the GPC and FT-IR results. This apparent mismatch could be explained by considering the different approach of the two techniques, that means by the GPC analyses only an estimation of the molecular weight could be done, whereas the FT-IR approach takes into account the consumption of functional groups, i.e. epoxide groups belonging to the both GOTMS and DGEBA species. In fact, if the heating at 80°C promotes the opening of the epoxide rings by Si-OH groups, without any other cross-linking reactions, then the FT-IR spectrum would show a consumption of epoxide groups, whereas the GPC analysis would not. Secondary, while the GOTMS molecules presence concurs to the absorbance of epoxide functional groups in the FT-IR analysis, the same ones are not considered in the estimation of conversion degree of DGEBA in GPC method.

6.6.3 Addition of hardener and characterization during the curing cycle

The influence of both the siloxane presence and the kind of amine hardener on the epoxide cross-linking reaction rate have been evaluated by FT-IR and DSC measurements.

6.6.3.1 Effect of siloxane amount on the crosslinking rate (FT-IR)

The Figure 73 shows the FT-IR absorption spectra in the range 880-970 cm^{-1} of the *Ep-Je* sample during the curing cycle. The arrow indicates the decreasing of the epoxy peak centred at 916cm^{-1} during the cross-linking reaction. By using the equation (1) the conversion degree α has been evaluated for both the neat epoxy system Ep-Je and two hybrids, namely Ep-Si12-Je and Ep-Si22-Je, in order to study the effect of Si-OH groups on the cross-linking reaction when the hardener amine is present. The α values as function of curing time are shown in Figure 74.

It is worth noting that the presence of Si-OH groups make the epoxy cross-link reaction faster, since the reaction rate $d\alpha/dt$ for the hybrids is higher than that of the neat epoxy. As previously shown, at 80°C the SiOH groups affect slightly the cross-link reaction of epoxy groups, promoting even if weakly the cross-link reaction. Moreover, the Si-OH group is able to catalyze the cross-link reaction of epoxy ring from the amine hardener [41]. These two effects contribute in a synergistic way to allow the hybrid samples gel faster than the neat epoxy. The same beneficial effect from SiOH groups on the cross-linking epoxy reaction has been found by Altmann et al [42]. They observed a catalytic effect in presence of high contents of micro-sized crystalline silica fluor in the cross-linking reaction of an epoxy matrix. In particular in presence of the filler, the reaction rate

increased rapidly especially at the beginning of the process and the gelation and vitrification times decreased [42]. Moreover, the high specific surface on nano-dimensioned siloxane structures is expected to influence significantly more the kinetics of the process due to the high content in silanols groups. In fact, it is well known that epoxy-amine reactions can be accelerated by compounds that stabilize the alkoxide ion intermediates, as OH belonging to silanols groups [43-44]. After the gelation time the cross-link reaction rate of hybrids slows down. As a consequence the hybrids reach α conversion degrees lower than the neat epoxy, because of the higher viscosity of reacting mixture due to faster gelation. Furthermore, it is possible noting that the higher the siloxane content the higher the plateau value of α conversion degree in the hybrid samples. This behaviour could be due to the higher amount of siloxane mixture which causes the viscosity to be longer low. The curing step at 180°C promotes the epoxide groups to cross-link quite completely in the Ep-Je and Ep-Si22-Je samples, whereas the conversion degree of EP-Si12-Je sample retains still lowest probably due to the vitrification which took place at 80°C.

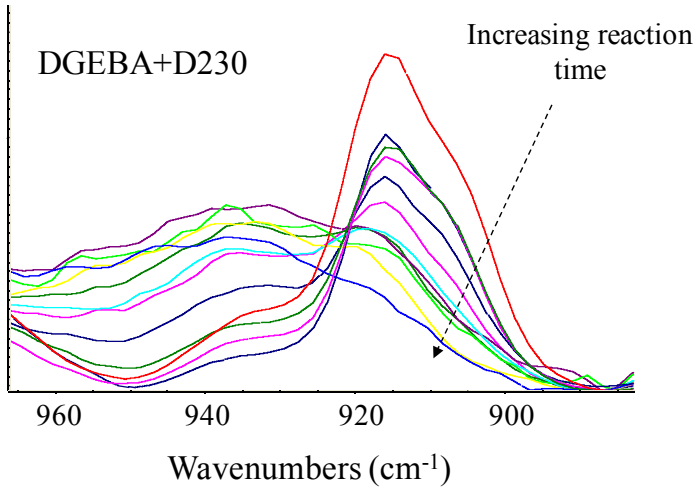

Figure 73 - FT-IR absorption spectra in the range 880-965 cm^{-1} of Ep-Je sample during the curing cycle.

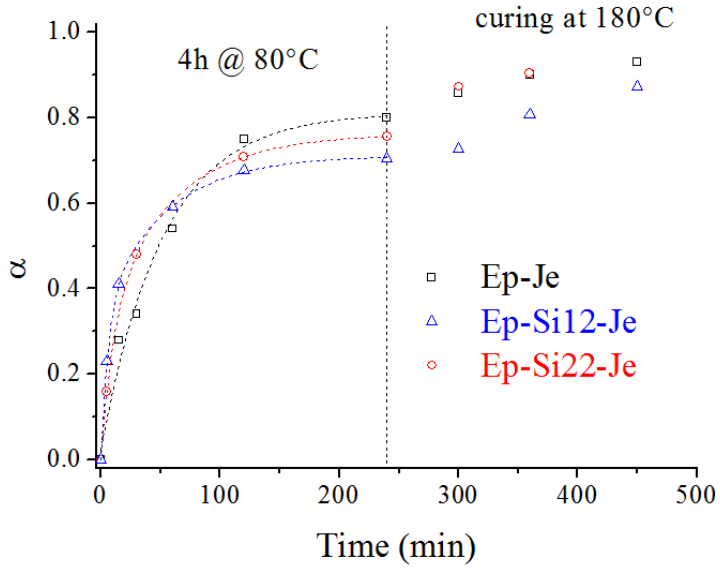

Figure 74 - Conversion degree of epoxide groups during the curing cycle with Jeffamine D230 of Ep-Je, EP-Si12-Je and Ep-Si22-Je samples.

6.6.3.2 Effect of hardener amine (MXDA and D230) on the crosslinking rate (DSC)

The synergistic effect of both the amine hardener and siloxane presence on the organic network building up has been evaluated by DSC measurements.

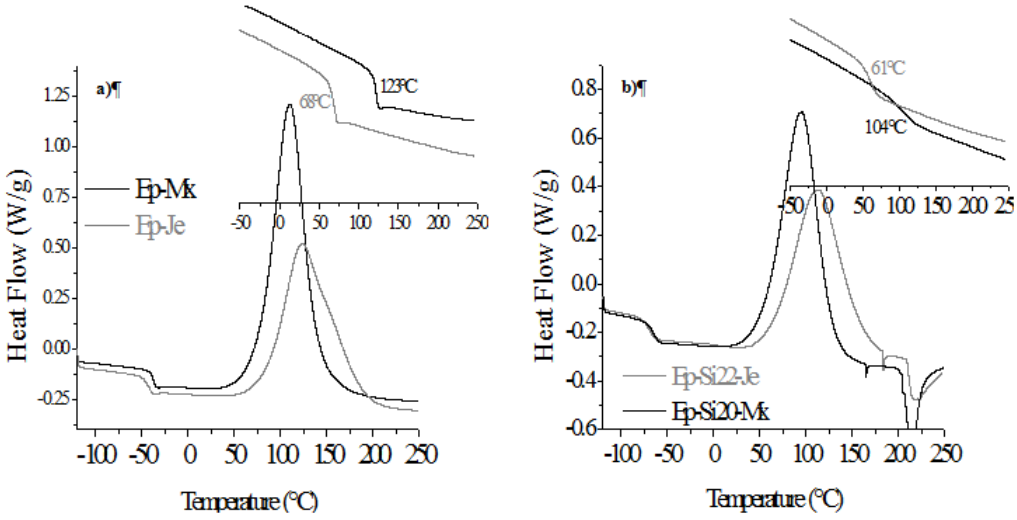

Figure 75 - DSC thermograms of both the neat epoxy resins and the hybrid samples upon the addition of the hardener (MXDA and Jeffamine D230).

To this end, two neat epoxy-hardeners systems, namely Ep-Mx and Ep-Je and two hybrids, Ep-Si20-Mx and Ep-Si22-Je, have been prepared. In particular, aimed to study the effect of amine hardener, namely MXDA and Jeffamine D230, a stoichiometric amount of the hardener has been added to neat DGEBA and suddenly a DSC measure has been performed from -120°C. Moreover, in order to study the influence of the SiOH silanols groups concurring to form the three-dimensional network, hybrid systems have been prepared with actual silica content of 20-22wt%, respectively. Then DSC thermograms have been suddenly performed after addition of amine hardener.

The Figure 75 a) shows the two thermograms related to the two neat epoxy systems prepared by using the two hardeners (MXDA and Jeffamine D230). In Figure 75 b) the curves related to the hybrid samples have been reported. The second DSC scan has been shown in the inset of Figure 75 a) and b). The shape of the thermogram and the position of the maximum would provide some knowledge about the amine reactivity, whereas the comparison with the corresponding hybrid provides information about the effect of silanols groups on the cross-linking reaction. The parameters extrapolated by the thermograms of Figure 75 a) and b) are reported in Table 17, where Tg_1 and Tg_2 are the glass transition temperature related to the first and second heating scan, respectively; T_t is the temperature value corresponding to the tangent to the exothermal curve in its increasing step (providing a measure of the cross-linking reaction beginning); T_{max} the temperature value corresponding to the maximum of the exothermal curve and finally ΔH is the total heat of cross-linking reaction, corresponding to the area under the exothermal peak. The results highlighted that the thermograms of both neat and hybrid systems MXDA-based are more reactive than those Jeffamine D230-based, because of the lower temperature T_t and T_{max} values. In practice, the overall curves of MXDA-based systems are shifted at lower temperature values if compared to those of D230-based ones. According to our results, Mijovic et al. [45] found that in the MXDA the electron-donating group enhances the reaction rate of attaching the epoxide groups and then lowers the relative activation energy. Additionally, the hybrid samples seem to be more reactive then the relative neat systems because of the lower values of both the T_t and T_{max}. This behaviour could be ascribed again to the catalytic effect of the SiOH silanols groups on the cross-link reaction of epoxy rings [43-44]. The SiOH groups affect the organic network building up

because they are able on the one hand to stabilize the epoxide intermediates during the cross-linking reaction and on the other hand they could contribute themselves to react with the epoxy rings, as previously demonstrated.

Moreover, the ΔH of hybrid samples is always lower than that of the corresponding neat epoxy system DGEBA-hardener, probably due to the occurrence of the inorganic endothermic condensation involving the siloxane groups overlapping to the exothermal cross-linking reaction. In conclusion, it is worth noting that not only the siloxane presence but also the kind of hardener could affect the crosslinking reaction rate leading probably to different hybrid properties.

Table 17 - Calorimetric parameters obtained by the DSC measures.

		Tg_1	Tg_2	T_t	T_{max}	ΔH (J/g)
D230	**Neat Epoxy**	-41.97	69.55	83.55	124.64	290.6
	Hybrid 60/40	-70.82	60.24	62.36	113.96	248.3
MXDA	**Neat Epoxy**	-37.31	122.61	76.10	110.89	370.7
	Hybrid 60/40	-63.42	104.66	53.65	95.66	286.8

In conclusion the DSC and FT-IR measurements were useful to understand that:

- SiOH has a catalytic effect of on the cross-linking reaction especially at the beginning of the reaction;
- MXDA is faster than Jeffamine D230 in building up the organic network;

- Silanols and hardener effects can act in synergistic way to make the reaction rate faster.

6.6.4 Characterization of cured hybrid samples (Ep-Siy-Je)

After addition of Jeffamine D230 in stoichiometric amount, the hybrid samples have been cured and then characterized in morphology, flame resistance and mechanical properties.

6.6.4.1 Morphology of hybrids (WAXS/SAXS, ^{29}Si-NMR and molecular dynamics simulations)

6.6.4.1.1 ^{29}Si-NMR spectroscopy

The structural features of the siloxane moieties are characterized by ^{29}Si solid state NMR spectroscopy. Figure 76 illustrates typical ^{29}Si-NMR spectra of the hybrid compounds, here represented by the samples Ep-Si12-Je and Ep-Si22-Je.

The results pointed out that the inorganic structure, in terms of *Ti* and *Qi* does not change with the siloxane content, but, as shown in Figure 76, all hybrids possess only T_3, Q_3 and Q_4 units. A little shoulder at about -55ppm can be assigned to not completely condensed T_2 units. Therefore since silicon by GOTMS has completely condensed as T_3 units and silicon by TEOS appears as Q_3 and Q_4 units, it follows that GOTMS and TEOS are completely condensed to form rigid cage-like clusters [46]. Therefore, contrary to what happened for the MXDA, the Jeffamine D230 causes the silicon to condensate also at highest siloxane amount, i.e. 20wt%.

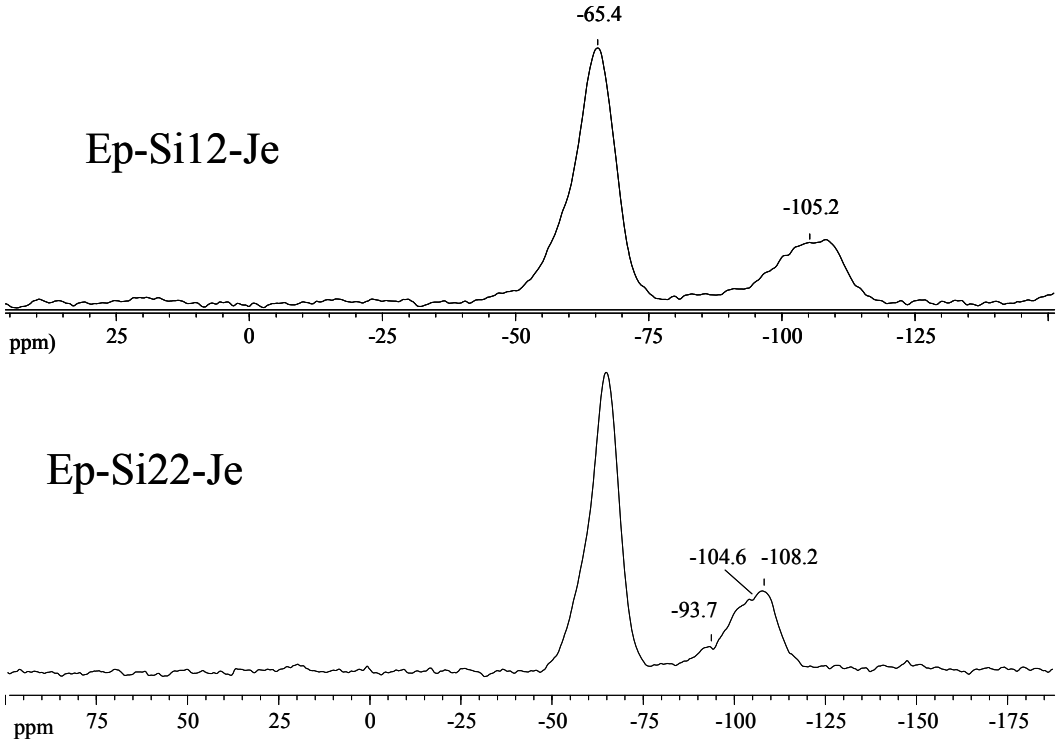

Figure 76 - ^{29}Si-NMR spectra for Ep-Si12-Je and Ep-Si22-Je hybrid samples.

6.6.4.1.2 Wide Angle X-ray Scattering (WAXS) characterization

The log-log WAXS spectra of Ep-Siy-Je hybrid samples and the corresponding neat epoxy system are shown in Figure 77. The spectra of the Ep-Siy-Je were not subtracted for the corresponding neat epoxy system spectrum.

Similarly to the Ep-Mx also the Ep-Je sample highlights two characteristic broad bands attributed to local density fluctuations of epoxy matrix centred at about 4 and 12nm^{-1} [13]. These two bands are characteristic of the epoxy component DGEBA, since their position, shape and intensity do not change by using different hardener, namely MXDA and Jeffamine D230. Therefore, the short range order of the epoxy resins is not changed with the amine cross-linker. On the other hand, it is worth noting that the introduction of the siloxane structures

modifies the inner structure of the epoxide network, since a modification in shape, intensity and position of the broad band at 12nm^{-1} have been observed. Finally, the epoxy band at about 4nm^{-1} seems to disappear under the high scattering intensity at low q values due to the siloxane domains [14]. The WAXS structural investigation points out that the inner structure of the epoxide network changes with the introduction of siloxane domains to form the Ep-Siy-Je samples, in the same way happened for the Ep-Siy-Mx hybrids. Therefore, this result strengthens the idea that it is the high content of GOTMS in the siloxane mixture to be responsible of the deep structural modification in epoxide network. To better understand the role of the GOTMS and siloxanes on the modification of epoxide network, WAXS measurements have been done on the neat Ep-Je and hybrid Ep-Si22-Je samples during the curing cycle.

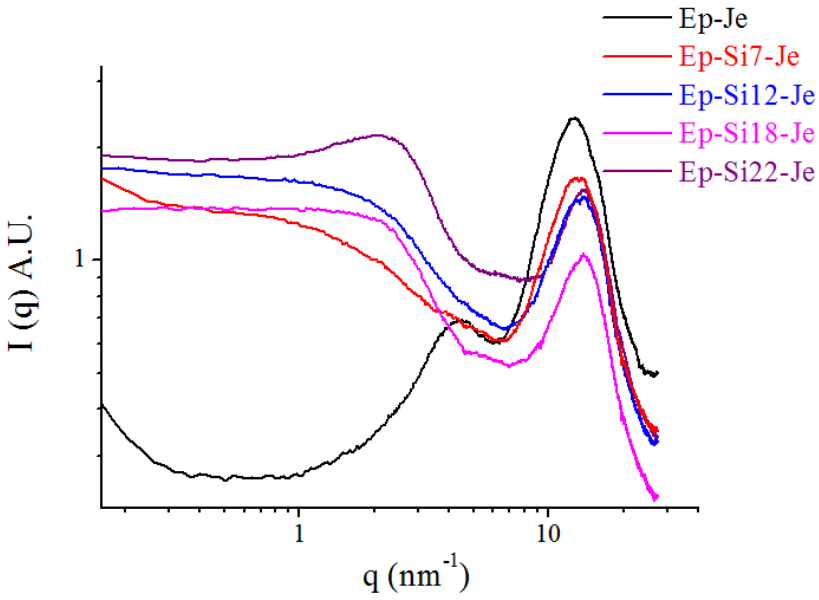

Figure 77 - WAXS spectra of Ep-Siy-Je hybrids and Ep-Je neat epoxy.

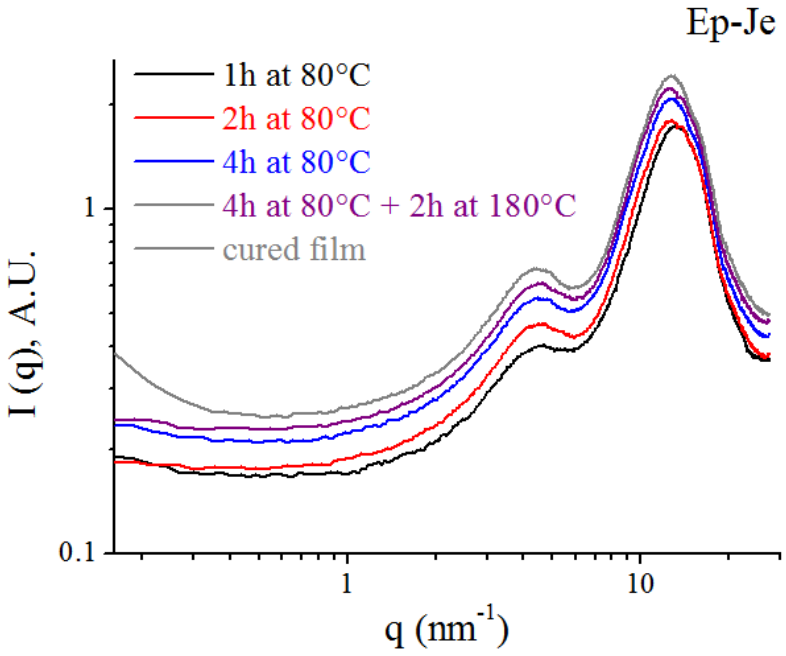

Figure 78 - WAXS spectra of Ep-Je neat epoxy acquired during the curing cycle.

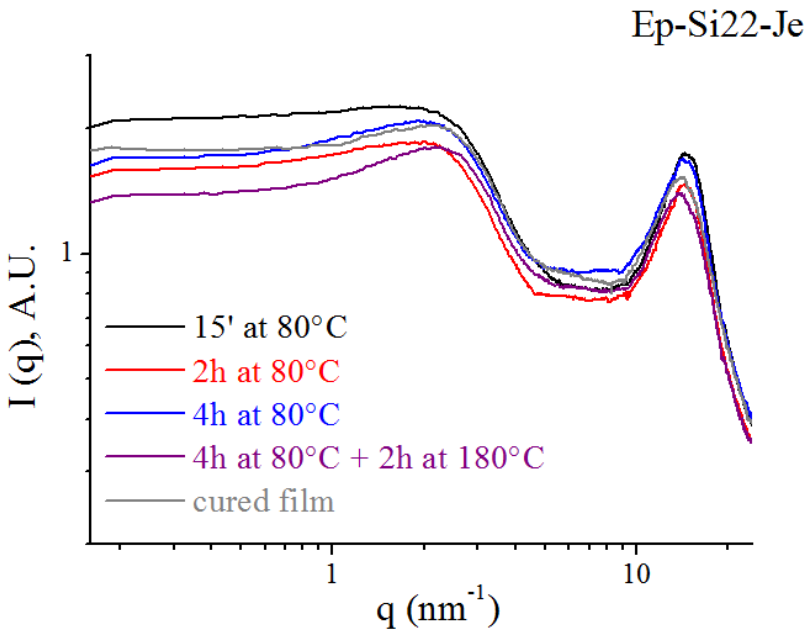

Figure 79 - WAXS spectra of Ep-Si22-Je hybrid acquired during the curing cycle.

Figure 78 shows the WAXS spectra related to the neat epoxy system Ep-Je acquired during the curing cycle. Here it is worth noting that the short range order of the epoxy resin has not been changing during the curing cycle, since the peaks centred at about 4 and 12nm^{-1} and attributed to local density fluctuations of epoxy matrix do not modify in position, shape and intensity during the organic cross-linking reactions. This important statement confirm that since these two peaks appear at the beginning of the cross-linking reaction, before the formation of the tridimensional network they are effectively due to very short range of density fluctuations and not to the whole epoxide network. This is the reason why the position, shape and intensity of these two peaks do not change by changing the amine hardener from MXDA to Jeffamine D230. Figure 79 shows the same sequences of scattering spectra during the curing cycle related to the Ep-Si22-Je hybrid. It is worth noting that the broad band at about 12nm^{-1} characteristic of epoxy short range fluctuation results to be modified just at the beginning of the cross-linking reaction. As a matter of fact, this peak is shifted to higher q values and highlights a lower scattering intensity if compared to the corresponding spectrum of the neat epoxy Ep-Je. Therefore, it follows that it is the simply introduction of siloxane molecules into the organic mixture to cause changing's in the local density fluctuation of epoxy oligomers.

6.6.4.1.3 Small Angle X-ray Scattering (SAXS) characterization and Molecular Dynamics Simulations

In order to study the siloxane structure the scattering at low q values in the log-log plot has to be considered. In Figure 77 the high scattering intensity al low q values is ascribed to the inorganic siloxane structures, since it does not appear in the neat epoxy Ep-Je spectrum. Moreover, the shape of the scattering intensity in

this region changes with the siloxane content, showing typical Guinier behaviour for the Ep-Si7-Je and Ep-Si12-Je samples and an overlapped peak at 2.33 nm^{-1} for the Ep-Si18-Je and Ep-Si22-Je spectra. The presence of a typical Guinier knee reveals the existence of a "diluted" hybrid system consisting of a few number of siloxane nanostructures dispersed in the epoxy matrix [19-20]. It is possible to assess the gyration radius Rg [21] as the slope in the linear region of the plot *ln(I(q))* vs q^2, in either Ep-Si7-Je or Ep-Si12-Je spectra, according to Guinier's relation [22]:

$$I(q) \propto \exp(-q^2 R_g^2 / 3)$$

The Rg has been evaluated to be 0.36nm. In the samples at high inorganic content, namely Ep-Si18-Je and Ep-Si22-Je, the correlation peak can be imaged overlapped to the characteristic knee shape of Guinier regime. Therefore, the same value of gyration radius has been attributed to the inorganic structures in the Ep-Si18-Je and Ep-Si22-Je hybrids. Matejka et al. [11] found that under particular reaction conditions the GOTMS polymerization could lead to formation of cage-like structures, the polyhedral oligomeric silsesquioxane POSS units with well established architecture. The tendency to build up the cage-like structures and their content depends on the catalyst used for the sol-gel process. In particular, cyclization is preferred under basic or neutral catalysis, namely with DBTDL [47]. This behaviour can be easily ascribed to the tendency of GOTMS to form condensate T_3 structures, which result preferred under basic reaction condition. This behaviour is evident in the ^{29}Si-NMR spectra (Figure 76) where the T_3 condensed units result to be the predominant structure, together to Q_3 and Q_4 units. In fact, it cannot be excluded the possibility for TEOS to participate in building up the POSS cages, as for Q_3 could replace the T_3 units,

whereas Q_4 units could tie two neighbouring cages. Additionally the length of a Si-O-Si edge in the cubic octamer POSS structure is about 0.3 nm (Figure 80), in agreement with the Rg value of 0.36 pointed out for the Ep-Siy-Je samples.

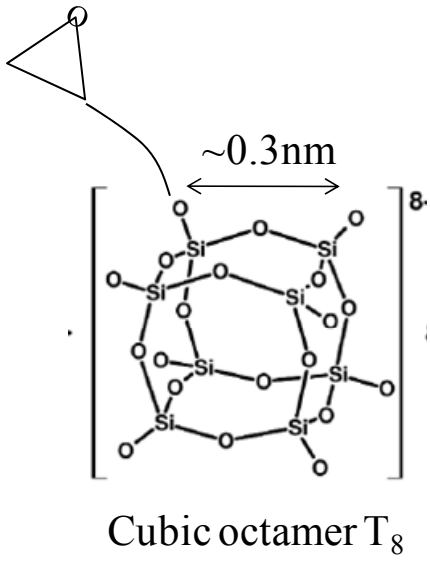

Figure 80 - Structure of a cubic octamer POSS

Therefore, in conclusion the SAXS results highlight the tendency of GOTMS molecules to form cage-like inorganic structures, whose dimension are about 0.3-0.4nm.

Moreover, the correlation peak in the Ep-Si18-Je and Ep-Si22-Je hybrids has to be ascribed to the distance between neighbouring inorganic domains or heterogeneity. These two systems are not diluted, but a great number of siloxane domains are present, since a peak correlation can be detected. As known [7, 21, 47], the position of the scattering peak can be used to estimate the average distance between the siloxane rich regions, by calculating the interdomain distance as $d=2\pi/q_{max}$, where q_{max} is the scattering vector at the peak maximum

[7, 21, 47]. Since q_{max} is 2.33nm^{-1}, the average distance between two siloxane domains is about 2.7nm. To the aim to investigate the nature of the interdomain distance peak and then to study the evolution of the inorganic structures, SAXS measurements of Ep-Si22-Je have been done during the curing cycle. The spectra are shown in Figure 82. Moreover, the same procedure has been followed by testing the Ep-Si12-Je sample, which did not show the correlation peak. The SAXS spectra have been shown in Figure 81.

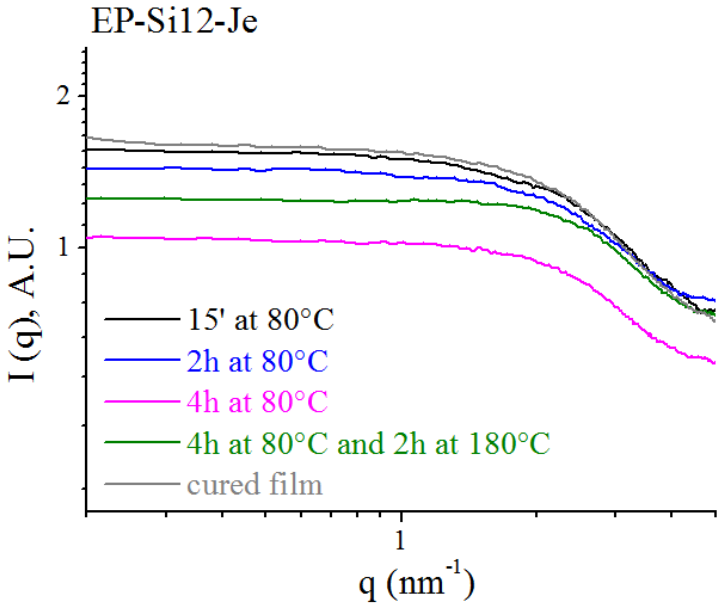

Figure 81 - SAXS spectra of Ep-Si12-Je hybrid acquired during the curing cycle.

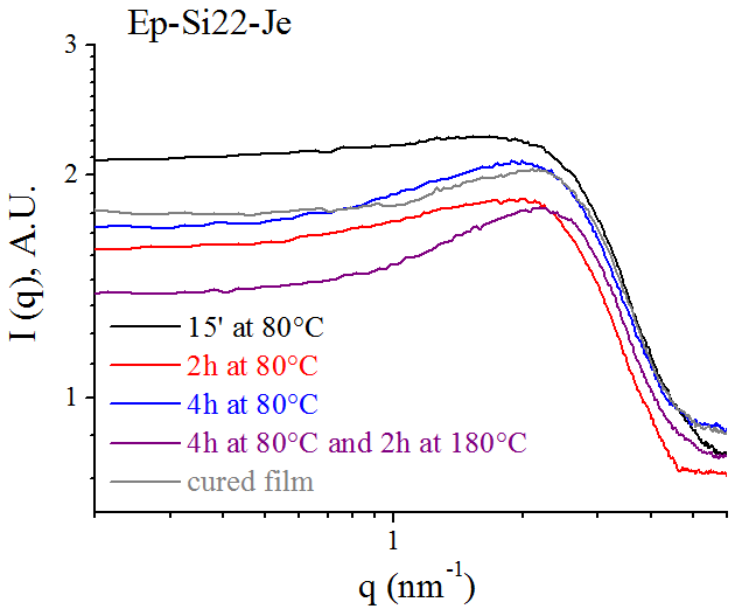

Figure 82 - SAXS spectra of Ep-Si22-Je hybrid acquired during the curing cycle.

The SAXS spectra of the Ep-Si12Je hybrid point out that the shape of the scattering curves does not change during the curing cycle and the characteristic Guinier knee shape appears at the beginning of the cross-linking reaction and retain up to complete the sample curing. Therefore in the Ep-Si12-Je sample, the final morphology, consisting of few number of siloxane domains dispersed in the epoxide matrix to form a diluted system, corresponds to that present at the beginning of the cross-linking reaction. On the contrary, in the Ep-Si22-Je sample, the correlation peak appears during the structural evolution at 80°C and become gradually more evident during the curing cycle. The comparison between the two hybrid having different behaviour demonstrated that the appearance of this correlation peak may be ascribed to the high siloxane content in the Ep-Si22-Je hybrid, which allows the formation of a higher number of particular kind of inorganic arrangement during the structural evolution of the organic/inorganic growth. As known the presence of such a peak speaks in

favour of some ordered organic-inorganic structures formed during the curing cycle [15]. Therefore, the results can be interpreted as follows: as Matejka et al [47] also suggested, hydrolysis and condensation of GOTMS molecules leads to a spontaneous self-organization to form cage-like inorganic structures, whose dimensions are determined by Rg value. Furthermore, since the dimension of these cages does not change, the number of cage-like inorganic structures increases with the siloxane content. Hence, at highest inorganic content, namely 18 and 22wt%, the distance between two neighbouring cages become little enough to be seen by using SAXS experiments, and consequently the correlation peak appears. Additionally, the distance between two neighbouring cages has been found to be about 2.7nm in both the Ep-Si18-Je and Ep-Si22-Je hybrids. Furthermore, since GOTMS molecules have been used as trifunctional siloxane, each edge of the cage-like structure has a γ-(glycidoxy)propyl organic pendant, which is able to further react with the amine hardener. Therefore, 2.7nm could be thought as the distance between the heterogeneity domains cages separated by pendant organic substituent γ-(glycidoxy)propyl group bonded by amine Jeffamine D230. Since the NMR results pointed out that the GOTMS preferentially form condensed cage-like structures, because of the high content of condensed T_3 units, hence the siloxane moieties of GOTMS react before the epoxy ring functionality, allowing the building up of cages which can tie later to give an interconnected organic-inorganic tridimensional network. A theoretical estimation of the length between two neighbouring cages bonded with Jeffamine D230 has been done by using molecular dynamics (MD) simulations. As known, the hardener Jeffamine owns two $–NH_2$ groups, on the opposite site of molecule, hence it is able to bond the epoxy ring by using either the same (head-head attach) or the opposite (head-tail attach) $–NH_2$ group. Moreover, average size

oxypropylene monomer unit is introduced (x=2 and x=3) for Jeffamine D230 [46]. Therefore, two different atomistic models are built chemically linking two alkyl POSS cages and using one Jeffamine D230 molecule; in the first scenario, the cages react with two opposite $–NH_2$ groups, namely head-tail attach, in the second with the same $–NH_2$ group, i.e. head-head attach. Furthermore, with the aim of creating more realistic models, each glycidoxy group is considered reacted with a Jeffamine D230 molecule and, in turn, with a DGEBA chain (green structures in Figure 83). These model systems are simulated at 80°C, when the correlation peak appears. From molecular dynamics (MD) calculation, it has been found that the average distance between two neighboring cages is equal to 3.1nm, if x=3 and 2.8 nm if x=2, when two cages are connected using head-tail $–NH_2$ groups; consequently, we can assume an average value of 2.9 nm; whereas the average distance between two neighboring cages is equal to 1.8nm, when two cages are bound through the same $–NH_2$ group, i.e. head-head attach. In Figure 83, snapshots extracted from Molecular Dynamics calculation of the POSS-epoxy resin systems, when x=3 have been shown. In particular, on the left two cages have been bonded by a head-tail attach, whereas on the left a head-head attach has been considered.

Hence the theoretical estimation of distance between two neighbouring POSS cages bonded by head-tail attach to the same Jeffamine D230 molecule is in agreement with the experimental result of 2.7nm by SAXS measurements. Therefore, as the siloxane amount increases the number of cages become high enough to make them bonded with the amine hardener. Thus the distance between two neighbouring cages will be determined only by the length of the amine hardener which links them.

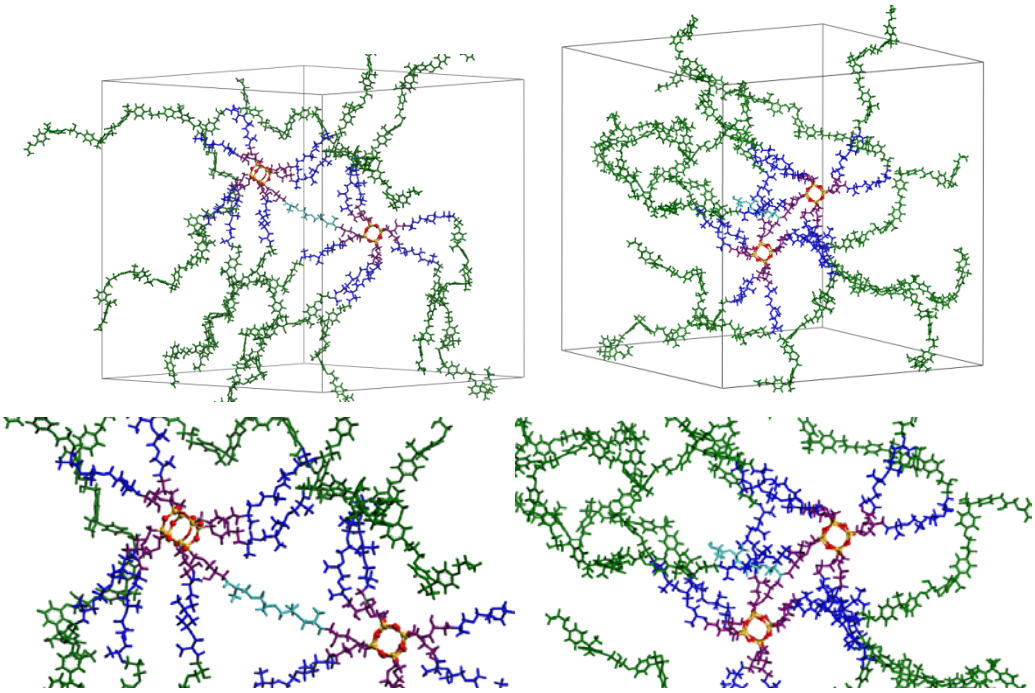

Figure 83 - Snapshots extracted from MD calculation of the POSS-epoxy resin systems, when *x*=3. (Top) Complete atomistic simulation box; (bottom) zoomed view; (left) different ammines; (right) same ammine. Color legend: cages are represented in stick and ball style; oxygen, red; silicon, orange; glycidoxy groups, purple; Jeffamine D230, blue; DGEBA, green.

Moreover, the results point out that the bonding between two neighbouring cages takes place after the complete formation of POSS inorganic structures, since the correlation peak appears only during the curing cycle whereas the Guinier knee is present also at the beginning of the epoxide cross-linking reaction. Therefore, as also Brus et al. [46] observed, no cleavage of oxirane rings occurs before thermal curing, and thus the whole process results to be well controlled.

In conclusion, the morphology study of Ep-Siy-Je hybrids revealed that highly condensed isolated polycyclic cage-like clusters are formed during the sol-gel reaction before their aggregation. The process parameters, i.e. DBTDL catalyst and the particular curing cycle associated to the Jeffamine D230 amine hardener,

promote cyclization of siloxanes and thus formation of highly condensed and rigid cage-like clusters. Subsequently, during thermal curing these star-like epoxy-functionalized building blocks react with Jeffamine D230, providing inorganic structures with high degree of regularity and self-ordering throughout the epoxide network.

The strong tendency of GOTMS molecules to arrange in POSS ordered cake-like clusters has been widely studied [46-47]. According to Matejka et al [47] the structural evolution of organo-trialkoxysilanes to build up POSS is controlled by the competition between intermolecular polycondensation and cyclization. They found that the tendency of organo-trialkoxysilanes to build up the polyhedral cyclic oligomers, mainly octamer cages and larger cage-like structures increases with the size of substituent R. As a result, long substituents prevent gelation of the trifunctional system and increase stability of POSS. Because of the incompatibility of the polyhedral POSS framework and pendant organic chains, microphase separation takes place and spontaneous self-organization occurs. Therefore, a micellar arrangement of compact POSS domains with correlation distance corresponding to the size of the substituent is formed, and the ordering is promoted by increasing length of the organic chain. Later, Brus et al. [46] found that the oxypropylene chains of hardener amine form phase which separates organic tails of siloxane cage-like clusters, uniformly dispersed in the polymeric matrix; the average distance between clusters being 1.8nm.

6.6.4.2 Flame resistance properties (Pyrolysis/SEM, TGA air and nitrogen flow)

The TGA curves performed in nitrogen flow (Figure 84) show that the thermal stability of the hybrids materials is improved compared to the neat epoxy resin at

temperature higher than 400°C, as far the char residual increases with the silica content. As observed in other polymer-silica nanocomposites [8, 24-26, 48-49] the higher the silica content in the epoxy-silica hybrids the higher the thermal stability, therefore the thermal stability of hybrids is enhanced proportional to the inorganic content. The protecting behaviour of siloxane domains can be observed in the air flow TGA curves at temperatures higher then 650°C (Figure 85). Here, it is evident that the higher the siloxane content the higher the thermo-oxidative stability of hybrids, since the TGA curves shift to higher temperatures (Figure 85).

In details, the thermo-oxidative curves of Ep-Siy-Je hybrids (Figure 85) show the typical three stage weight-loss behaviour, observed also for the Ep-Siy-Mx samples. It is worth noting that again the thermal decomposition onset temperature in the first decomposition process of the hybrids samples is slightly higher than that of neat epoxy, highlighting the improved thermal stability of hybrids. However, the maximum temperature of the second decomposition process changes a lot with the amount of siloxane and retains with the increasing amount of inorganic content, as previously observed for the *Ep-Siy-Mx* hybrids. The second process of weight loss could be due to the thermal oxidative degradation of the formed residuals which is inside the silica-rich domain. Thus, the thermal protection of the organic network occurs again with the formation of silica rich domains within the epoxide matrix, and the further degradation of epoxy network are prevented. These results demonstrate that the introduction of siloxane from GOTMS and TEOS into the epoxide network can definitively improve the thermal stability of the resulting hybrids, regardless the amine hardener used. Therefore, as Weng et al. [28] point out this enhanced behaviour

has to be ascribed to the coupling agent GOTMS, which could provide covalent bonding between the two phases and then improving the thermal resistance.

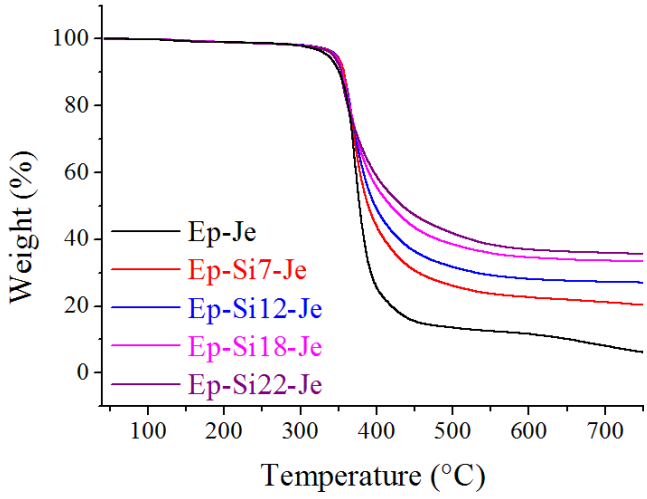

Figure 84 - Thermo-gravimetric Analyses in nitrogen flow of both the neat epoxy resin Ep-Je and hybrids samples Ep-Sit-Je.

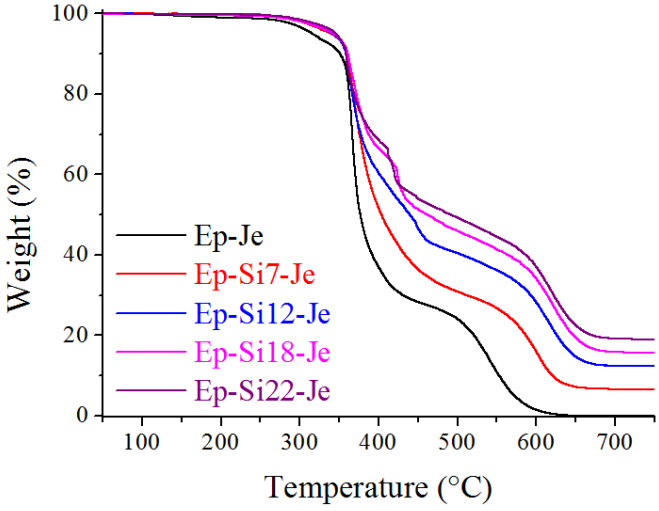

Figure 85 - Thermo-gravimetric Analyses in air flow of both the neat epoxy resin Ep-Je and hybrids samples Ep-Siy-Je.

In the air flow TGA curves (Figure 85) it is worth noting that at about 400°C an abruptly drop in the weight losses can be detected in the thermo-oxidative

degradation of hybrid with highest siloxane content, namely 18 and 22wt%. To the aim to explain this thermo-oxidative behaviour, a correlation between the shape of siloxane structures and the degradation of organic components must be done. In fact, at highest silica content, a cage-like structures of inorganic moieties bonded by means of GOTMS cross-linked epoxy groups, could be supposed. When the temperature increases the supposed cages condense in the outer sides of samples, protecting the inner organic components. At about 400°C, the cross-linkers between two cages could partially decompose, allowing the organic moieties to be directly exposed to oxidative environment and then abruptly degraded. Additionally, as expected, the thermo-oxidative residual increases with the siloxane content. To the aim to investigate the continuity of the siloxane structure, several hybrid samples in films shape were undergone to a step by step degradation in an oven at two fixed temperature (i.e. 300 and 400°C, respectively) in order to remove the organic moieties without destroy the inorganic network. In fact a continuous inorganic network provides a continuous film after the organic degradation. Therefore, the samples were left in the oven at a fixed temperature up to a constant weight value was reached. As shown in Figure 87, the samples were heated for 43h at 300°C, after that the weight losses were constant, then the temperature was arisen to 400°C and then left for 48h. At this point all the organic moieties was burned, as the thermo-gravimetric analyses in air flow pointed out (data not shown). The final weight value reached after the pyrolysis has been compared to that of the expected, i.e. the thermo-oxidative residual at 750°C obtained in air flow at a heating rate of 10°C/min, pictured with the corresponding colour straight line in Figure 87. The differences in siloxane contents obtained by heating in static (pyrolysis) or dynamic (TGA) conditions, could be tentatively ascribed to the different way to burn the sample.

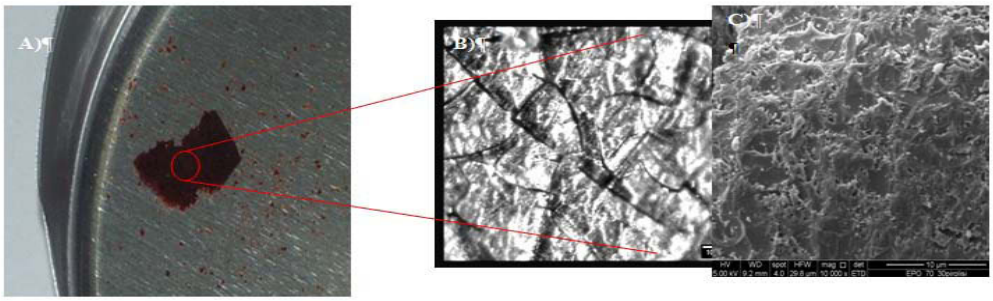

Figure 86 - A) photograph picture; B) optical microscope image and C) SEM image of burned hybrid sample after the pyrolysis cycle.

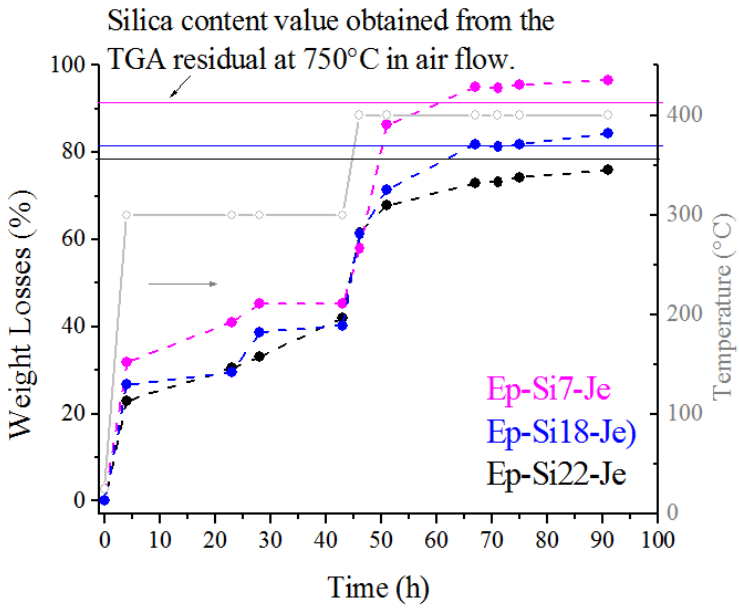

Figure 87 - Weight losses of several hybrid samples during the pyrolysis experiment. The straight line of the corresponding colour is related to the expected silica content values.

Finally, it is worth noting that after slow pyrolysis of the organic component, the inorganic residual appears as a film rather than a powder, highlighting the presence of a continuous and compact inorganic network (Figure 86). Since the micrograph SEM images of burned hybrid sample (Figure 86 b) and c)) shows

the formation of a foam structure, a co-continuous structure between the organic and inorganic moieties has to be supposed.

6.6.4.3 Mechanical properties (DMA, fracture toughness/SEM)

6.6.4.3.1 Dynamic Mechanical Analysis (DMA)

As known, valuable information on morphology and mainly on interface of the hybrid systems can be obtained from DMA analyses [8]. Figure 88 shows tensile Storage Modulus *E'(T)* and loss factor $tan\delta$ (=*E''/E'*) as function of temperature for studied Ep-Siy-Je hybrids, containing silica ranging from 7 to 22wt%. A significant reinforcement of hybrid samples with respect to the neat epoxy resin is evident, since the storage modulus E' increases with the hybridization of epoxide network, in both the glassy and rubbery regions. In particular, in the latter region the higher the siloxane content the higher the storage modulus probably because of an increased cross-linkers number due to the siloxane network formation. Moreover, it is well known [50] that the decrease in the modulus during the glass transition region is due to the micro-Brownian motion of the network chains. Therefore, the observed increased value of storage modulus in the rubbery regions points out that the micro-Brownian motion of the epoxy network is strongly restricted by the hybridization with siloxanes precursors [50]. The increasing in the storage modulus is accompanied by changes in the loss factor tanδ (Figure 88). In fact, the tanδ peak, which corresponds to the epoxy glass transition, decreases and broadens in the hybrid samples. This behaviour is typical of most nanocomposite systems and it is pointed out for the Ep-Siy-Mx hybrids too. Moreover, the decrease of the maximum height is proportional to the siloxane content, since it decreases as the siloxane amount increases. This behaviour could be explained taking into

account the presence of strong interactions between organic and inorganic components, which causes a loss in mobility of the macromolecules, according to what found by Landry et al. [51]. Furthermore, since all the tan δ peak do not show two separate transition region, the silica distribution into the samples can be supposed homogeneous [8]. Matejka et al. [8] stated that the absence of the high temperature new peak in the loss factor can give a proof of the absence of the immobilized interphase layer of epoxide network with the siloxane structures. But in our case, as the morphological study demonstrated, the siloxane cage-like clusters are homogenously dispersed within the epoxide matrix, hence neither separation phase nor discernable inorganic particles can be detected. Therefore, probably due to the high content of coupling agent GOTMS and then the particular siloxane structure formed within the epoxy matrix, the organic and inorganic moieties are intimately and covalently bonded. To this particular morphology and to the homogeneity of inorganic clusters distribution could be reasonably ascribed the narrow temperature range of the glass transition.

Additionally, the tan δ curves in Figure 88 highlight the important results that in the hybrid samples with highest siloxane content, i.e. Ep-Si18-Je and Ep-Si22-Je, the Tg increases if compared to the neat epoxy, since the tan δ peak shifts to higher temperatures.

In conclusion, as Ochi et al. found, [50] the dynamic-mechanical results show that the molecular motion of the epoxy network is effectively constrained by the presence of siloxanes structures dispersed and intimately and covalently bonded to the organic moieties. Moreover, at highest siloxane content, namely 18 and 22wt%, a neat increase on the glass transition temperature can be observed.

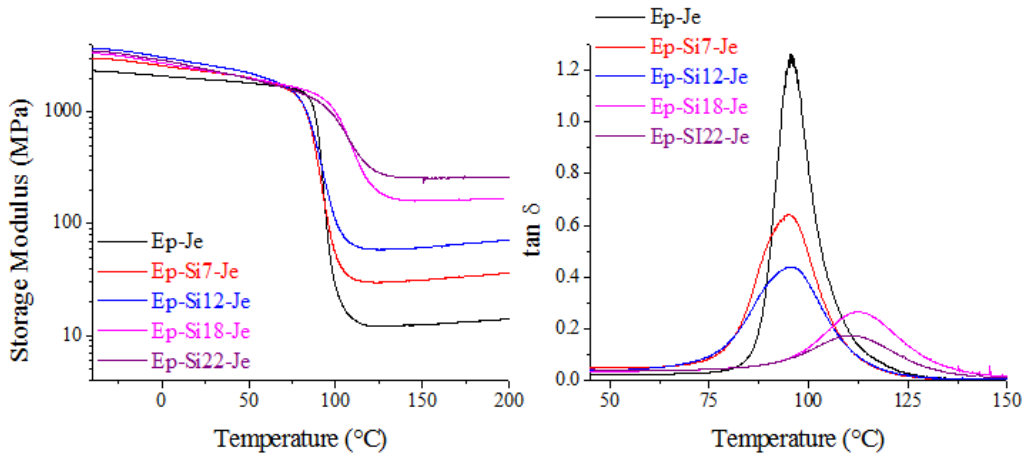

Figure 88 - Dynamic mechanical properties of Ep-Siy-Je hybrid samples, in terms of elastic moduli and tanδ as a function of temperatures.

Sample	Tg (°C)	Loss Factor	E' at 150°C (MPa)	SiO_2 (wt%)
Ep-Je	95.6	1.23	12.5	0
Ep-Si7-Je	95.5	0.64	31.4	6.6
Ep-Si12-Je	95.5	0.44	61.3	12.3
Ep-Si18-Je	112.6	0.26	160.0	17.8
Ep-Si22-Je	111.0	0.17	255.4	21.5

Table 18 - DMA extrapolated properties of Ep-Siy-Je samples.

6.6.4.3.2 Mechanical test

From the load-displacement curves the critical stress intensity factor (*Kc*) is evaluated as $K_c = Y\sigma\sqrt{a}$ a, where *a* is the indentation depth, σ the flexural stress and *Y* a parameter which accounts for the sample geometry [52]. The values of K_c and G_c so determined are reported in Figure 89 as a function of the siloxane content. These plots show that both K_c and G_c decrease significantly with the

addition of the siloxane structures. In other words the toughness reduces as the inorganic cluster content increases, according to Ragosta et al finding's [53] about mechanical performances of OctaGlycidyldimethylsilyl-POSS in DGEBA.

To further investigate the fracture behavior, the surface of fractured samples are examined by Scanning Electronic Microscopy (SEM). The Figure 90 shows the SEM micrographs taken near the crack tip of fractured surfaces for the neat epoxy system Ep-Je and the hybrid Ep-Si12-Je sample. No silica particles are discernible on the fractured surfaces of the specimens, even at very high magnification, confirming the absence of inorganic aggregates particles. The micrographs show two distinct regions of crack growth: a slow propagating crack area ahead the crack tip, and a fast fracture region (from right to left). The slow crack region is usually taken as a measure of the facture toughness because it represents the resistance of the material against crack propagation [52]. In Figure 90 the crack area is indicated with a red straight-line. It is worth noting that for the hybrid Ep-Si12-Je sample this region is markedly smaller with respect to the neat epoxy resin Ep-Je. This reduction in the propagating crack area ahead the crack tip is contrary to what previously observed [52]. Ragosta et al. [52], in fact, found that in epoxy-silica nanocomposites, the crack region increases with the silica content.

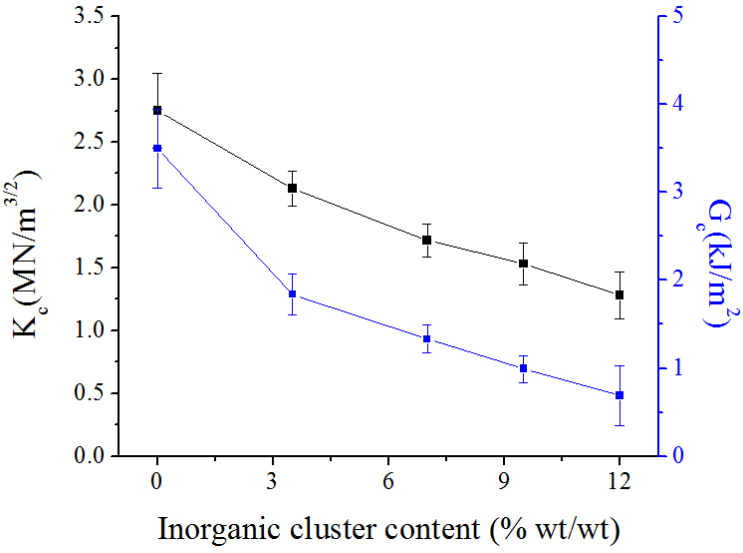

Figure 89 - Critical stress intensity factor, Kc, and critical strain energy release rate, Gc, as a function of the silica content.

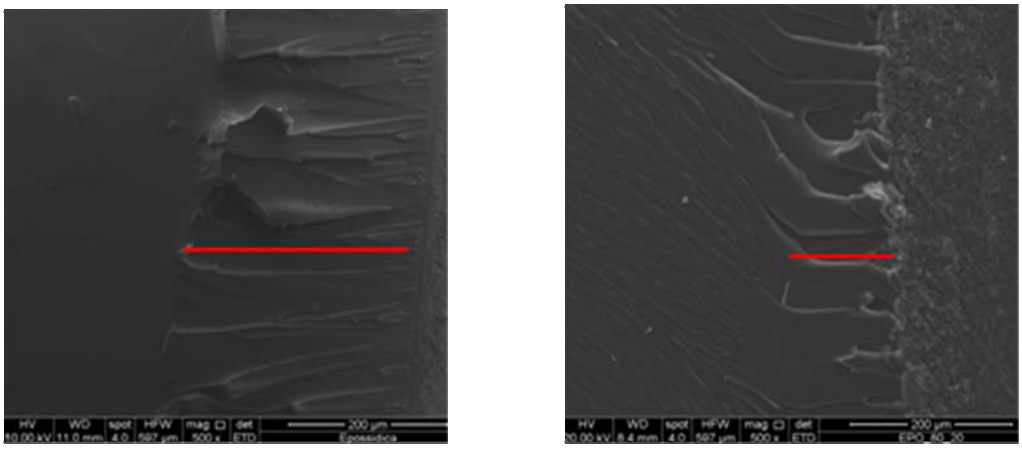

Figure 90 - SEM pictures of fractured surface: a) pure epoxy resin Ep-Je; b) hybrid Ep-12-Je.

6.6.5 Conclusions

We demonstrated that a suitable choice of functionalized siloxane monomers and reaction conditions leads to the formation of nano-heterogeneous networks with

well-organized cage-like structures, up to nearly homogeneous bicontinuous systems. In fact, the experimental results showed that under reaction conditions defined by the Ep-Siy-Je approach, GOTMS molecules are able to spontaneously arrange to form structures similar to polyhedral oligomeric silsesquioxane POSS units with well established architecture. Therefore, as the siloxane amount increases the number of cages become high enough to make them bonded with the amine hardener. Thus the distance between two neighbouring cages will be determined only by the length of the amine hardener which links them. This ordered arrangement highlights as distance correlation peak in the SAXS patterns profile of hybrids samples at high siloxane content becoming responsible of the improved thermal and mechanical properties. In particular, the co-continuous organic-inorganic structure is demonstrated with the achievement of films instead of powders in the pyrolysis experiments. It also affects the viscous-elastic behaviour causing both the Tg and the elastic modulus to increase. Moreover the symmetric shape of the loss factor peak speaks in favour of siloxane structure homogenously dispersed throughout the organic matrix. Whereas the increase of the Tg's value highlights the strong evidence of hindrance the polymeric chains movements during the glass transition. Hence, only the high siloxane content assures the clusters to be bonded highlighting the improved mechanical properties.

To the best of our knowledge it is the first time such cage-like clusters bonded by Jeffamine D230 molecules could be detected assuring the Tg to increase without any phase separation.

6.7 Ep-Siy-Mx and Ep-Siy-Je hybrids: effect of amine hardener on the hybrid structure.

The comparison between the Ep-Siy-Mx and Ep-Siy-Je hybrids allowed to state that:

1) The MXDA causes the high GOTMS content to not condensed, since high amount of T_0 units are present in the Ep-Si20-Mx hybrid. On the contrary the Jeffamine D230 assures the GOTMS to condensate at whatever siloxane contents.

2) Since the GOTMS molecules are not condensed at high siloxane content, the SAXS profiles appears as Guinier dilute system regardless the siloxane content. Moreover, the cluster dimensions change with the siloxane content. On the other hand, in the Ep-Siy-Je samples the Rg does not change with the siloxane content, but the number of defined size clusters increases as the siloxane content, up to the appearance of a correlation peak at highest siloxane content.

3) The Jeffamine D230 is able to bond two neighbouring siloxane cages, then building up a co-continuous organic-inorganic structure.

4) The presence of high T_0 units in the Ep-Siy-Mx samples is really detrimental causing a dramatic reduction of Tg value in the Ep-Si20-Mx hybrid. On the contrary, in the Ep-Si22-Je sample the Tg is markedly increased with respect to the neat epoxy due to its particular organic-inorganic morphology.

5) MXDA is an organic cross-linker faster than the Jeffamine D230, therefore in the MXDA-based hybrids the organic grows more rapidly than the inorganic

network, leaving out the GOTMS siloxanes monomers. A proof is the high content of T_0 units in MXDA-based hybrids.

6.8 References

[1] M. Ochi; R. Takahashi; *Journal of Polymer Science: Part B: Polymer Physics*, 39, **2001**, 1071.

[2] D. P. Fasce; R. J. J. Williams; F. Mechin; J. P. Pascault; M. F. Liauro; R. Petiaud; *Macromolecules*, 32, **1999**, 4757.

[3] I. E. dell Erba; D. P. Fasce; R. J. J. Williams; R. Erra-Balsells; Y. Fukuyama; H. Nonami; *Journal of Organometal Chemistry* , 686, **2003**, 42.

[4] L. Rozes; G. Fornasieri; S. Trabelsi; C. Creton; N. E. Zafeiropoulos; M. Stamm; C. Sanchez; *Progress in Solid State Chemistry* , 33, **2005**, 127-135.

[5] K. Zou; M. D. Soucek; *Macromol. Chem. Phys* , 205, **2004**, 2032–2039.

[6] L. Matejka; K. Dusek; J. Plestil; J. Kriz; F. Lednicky; *Polymer* 40, **1999**, 171.

[7] L. Matejka; J. Plestil; K. Dusek; *Journal of Non-Crystalline Solids* 226, **1998**, 114.

[8] L. Matejka; O. Dukh; J. Kolarik; *Polymer*, 41, **2000**, 1449.

[9] P. Yang; G. Wang; X. Xia; Y. Takezawa; H. Wang; S. Yamada; *Polymer Engineering and Science*, **2008**, 1214-1221.

[10] B. J. Bauer; D. W. Liu; C. L. Jackson; J. D. Barnes; *Polymer Advanced Technology*, 7, **1996**, 333.

[11] L. Matejka; O. Dukh; J. Brus; W. J. S. Simonsick; B. Meissner; *Journal of Non-Crystalline Solids*, 270, **2000**, 34-47.

[12] L. Prezzi; L. Mascia; *Advances in Polymer Technology* , 24, (2) **2005**, 91-102.

[13] L. A. S. A. Prado; M. Cascione; M. H. G. Wichmann; F. H. Gojny; B. Fiedler; K. Schulte; G. Goerigk; *Hasylab Annual Report*, **2005**, 945.

[14] K. Dahmouche; C. V. Santilli; S. H. Pulcinelli; A. F. Craievich; *Journal of Physical Chemistry B*, 11, **2001**, 3249.

[15] M. Spirkova; J. Brus; D. Hlavata; H. Kamisova; L. Matejka; *Journal of Applied Polymer Science*, 92, **2004**, 937-950.

[16] S. R. Davis; A. R. Brough; A. Atkinson; *Journal of Non-Crystalline Solids*, 315, **2003**, 197-205.

[17] A. Guinier; G. Fournet; *Small Angle Scattering of X-rays* , John Wiley & Sons, New York **1955**, p 268.

[18] O. Glatter; O. Kratky; *Small Angle Scattering of X-rays* , Academic Press, New York **1982.**

[19] S. Zaioncz; K. Dahmouche; B. G. Soares; *Macromolecular Materials and Engineering*, 295, **2010**, 243-255.

[20] G. Beaucage; *Journal of Applied Crystallography* , 29, **1996**, 134-146.

[21] M. Xiong; S. Zhou; L. Wu; B. Wang; L. Yang; *Polymer*, 45, **2004**, 8127-8138.

[22] S. Yano; K. Iwata; K. Kurita; *Mater. Sci. Eng.*, C 6, **1998**, 75.

[23] Y. Iami; H. Itoh; K. Naka; Y. Chujo; *Macromolecules*, 33, **2000**, 4343.

[24] A. Lee; J. D. Lichtenhan; *Journal of Applied Polymer Science* , 73, **1999**, 1993.

[25] Z. Wang; T. Lan; T. Pinnavaia; *Journal of Chemistry Materials* , 8, **1996**, 2200.

[26] J. B. Bauer; D. W. Liu; C. L. Jackson; J. D. Barnes;. *Polymer of Advanced Technology*, 7, **1995**, 1996.

[27] G. G. Hsiue; Y. L. Liu; H. H. Liao; *Journal of Polymer Science: Part A: Polymer Chemistry*, 39, **2001**, 986-996.

[28] W. H. Weng; C. C. Chang; H. Chen; *Composite Interface*, 11, n°8-9, **2005**, 631-641.

[29] J. Habsuda; G. P. Simon; Y. B. Cheng; D. G. Hewitt; D. R. Diggins; H. Toh; F. Cser; *Polymer*, 43, **2002**, 4627-4638.

[30] L. E. Nielsen; R. F. Landel; *Mechanical properties of polymers and composites*, New York: Marcel Dekker, **1994**.

[31] *Polymer*, 45, **2004**, 2967-2976.

[32] X. Zhang; L. Hu; D. Sun; *Acta Materialia*, 54, **2006**, 5469-5476.

[33] A. Morikawa; Y. Iyoku; M. Kamimoto; Y. Imrai; *Polymer Journal*, 24, **1992**, 107.

[34] W. Zhou; J. H. Dong; K. Y. Qiu; Y. Wei; *Journal of Polym er Science: Part A: Polymer Chemistry*, 36, **1998**, 1607.

[35] Y. G. Hsu; J. H. Huang; *Journal of Non-Crystalline Solids* , 208, **1996,** 259-266.

[36] R. J. Hook; *Journal of Non-Crystalline Solids*, 195, **1996,** 1-15.

[37] C. A. Fyfe; P. P. J. Aroca; *Phys. Chem. B*, 101, **1997**, 9504-9509.

[38] J. C. Pouxviel; J. P. Boilot; J. C. Beloeil; Lallemand; *J. Non-Crystalline Solids*, 89, **1987**, 345.

[39] L. Malier; F. Devreux; F. Chaput; J. P. Boilot; *Chemical Processing of Advanced Materials*, ed. L. L. Hench and J.K.West (Wiley, New York, **1992**), Chapter 6.

[40] B. Alonso; D. Massiot; M. Valentini; T. Kidchob; P. Innocenzi; *Journal of Non-Crystalline Solids*, 354, **2008**, 1615-1626.

[41] R. Mezzenga; L. Boogh; J. E. Månson; B. Pettersson; *Macromolecules*, 33, **2000**, 4373-4379.

[42] N. Altmann; P. Halley; J. Cooper; *Macromolecular Simposia*, 169, **2001**, 171-177.

[43] B. Ellis; *Chemistry and technology of epoxy resins* , Blackie Academic and Professional, London: Chapman and Hall, **1993**, 328p.

[44] E. Bugnicourt; J. Galy; J. F. Gerard; H. Barthel; *Polymer* 48, **2007**, 1596-1605.

[45] J. Mijovic; J. Wijaya; *Macromolecules*, 27, **1994**, 7589-7600.

[46] J. Brus; M. Spirkova; D. Hlavata; A. Strachota; *Macromolecules*, 37, **2004**, 1346-1357.

[47] L. Matejka; O. Dukh; D. Hlavata; B. Meissner; J. Brus; *Macromolecules*, 34, **2001**, 6904-6914.

[48] Y. Iami; H. Itoh; K. Naka; Y. Chujo; *Macromolecules*, 33, **2000**, 4343.

[49] G. H. Hsiue; J. K. Chen; Y. L. Liu; *J. Appl. Polym. Sci.* , 76, **2000**, 1609.

[50] M. Ochi; R. Takahashi; A. Terauchi; *Polymer*, 42, **2001**, 5151-5158.

[51] C. J. T. Landry; B. K. Coltrain; J. A. Wesson; N. Zambulyadis; *Polymer*, 33, **1992**, 1486-1495.

[52] G. Ragostra; M. Abbate; P. Musto; G. Scarinzi; L. Mascia; *Polymer*, 46, **2005**, 10506-10516.
[53] G. Ragosta; P. Musto; M. Abbate; G. Scarinzi; *Polymer*, 50, **2009**, 5518-5532.

Chapter 7: Conclusions and perspectives

The following conclusions can be drawn from the analyses of the experimental data.

7.1 Epoxy/MMT Composites

7.1.1 Silylation reaction of Na-MMT.

- ✓ The silylation reaction allows the aminosilanes molecules to be bonded on the Na-MMT surface, as proved by the presence of the organic moieties in the FT-IR spectra of silylated MMT.
- ✓ Regardless the aminosilanes and the process parameters, the silylation reaction causes the basal spacing between silicates layers to increase with respect to the pristine Na-MMT.
- ✓ The higher temperature and aminosilane concentration values lead to an increased amount of both chemically bonded silanes with respect to the intercalated species and aminosilanes interacting with the outside platelets.
- ✓ The process parameters affects not only the relative amount of aminosilanes interacting with the inside or outside platelets, but also the correlation between the aminosilane chain length and the basal spacing of MMT.

7.1.2 Silylated-MMT epoxy-based nanocomposites

- ✓ The sonication mixing procedure allows the interlayer spacing to increase (for the A1100-MMT clay) whereas the ball-milling dispersion method compacts the layered structure of the clays.
- ✓ The cross-linking reaction which probably takes place during the dispersion of modified MMT in the resin, prevents the intercalation of epoxy monomers in the silicate galleries. Thus retention of layer-layer correlations leads to micron scale reinforcing particles, not nano scale of individual layers.
- ✓ Silylated MMTs provide composites with improved mechanical properties with respect the pristine Na-MMT in terms of increased Tg and elastic modulus in the rubbery region. This improvements is more evident in the sonicated composites since the combination of sonication and ball milling makes compact the interlayer spacing and partially destroys the original layers structures.
- ✓ The Epoxy/MMT composites prepared with 1 and 3wt% of modified and unmodified clays exhibit improved tensile strength and elastic modulus compared to the pristine epoxy matrix. The strain at break decreases for all the samples containing 3wt% of clay whereas it slightly increases for composites at 1wt% in comparison to the epoxy resin. The elastic tensile modulus of the Epoxy/MMT composites increases with the clay content in either processing procedures (i.e. S or SB method). Moreover, in the composites at 1wt% it increases with increasing the chain length of aminosilanes.

- ✓ The hardness of composites increases with respect to the neat epoxy resin, and in the silylated MMT composites it increases with the aminosilanes length.
- ✓ The silylated clay composites highlight an increased fire resistance compared to the pristine epoxy resin as well as to the Na-MMT composite.

7.2 Epoxy/silica Hybrids MXDA based (Ep-Siy-Mx hybrids)

- ✓ The siloxane amount affects the GOTMS condensation reactions since the T0 species are detected in the Ep-Si20-Mx hybrid spectrum; in fact, the Si-O-Si condensed siloxane structures decreases as the siloxane amount increases.
- ✓ Regardless the siloxane amount, the morphology of hybrids can be ascribed to a dilute system of siloxane clusters embedded in the epoxide matrix.
- ✓ The Ep-Siy-Mx samples show poor mechanical properties because their Tg's reduced with respect to that of the neat epoxy system. Moreover, the hardness of hybrids decreases with the siloxane content. Additionally, as the siloxane content increases the loss factor tanδ shape changes, becoming weaker and broader, whereas the elastic modulus in the rubbery region increases.

7.3 Epoxy/silica Hybrids Jeffamine D230 based (Ep-Siy-Je hybrids)

- ✓ The inorganic structure, in terms of Ti and Qi does not change with the siloxane content, but, on the contrary all hybrids possess only T3, Q3 and Q4 units.
- ✓ GOTMS molecules are able to spontaneously arrange to form structures similar to polyhedral oligomeric silsesquioxane POSS units with well established architecture. As the siloxane amount increases the number of cages become high enough to make them bonded with the amine hardener.
- ✓ A correlation between an ordered arrangement of cage-like clusters and improved mechanical properties was found; the bonding between cage-like siloxane clusters causes improved mechanical properties, in terms of higher elastic modulus and glass transition temperature with respect to the neat epoxy resin. Moreover, the symmetric shape of the loss factor peak speaks in favour of siloxane structure homogenously dispersed throughout the organic matrix.
- ✓ The organic-inorganic structure is co-continuous, as demonstrated by the achievement of films instead of powders in the pyrolysis experiments.

7.4 Comparison between Epoxy/silica Hybrids prepared with Jeffamine D230 and MXDA

The effect of the amine hardeners MXDA and Jeffamine was studied highlighting the following:

- ✓ MXDA is an organic cross-linker faster than the Jeffamine D230, therefore in the MXDA-based hybrids the organic grows more rapidly than the inorganic network, leaving out the GOTMS siloxanes monomers, as the high content of T0 units in MXDA-based hybrids proved.
- ✓ The presence of T0 units is detrimental in the cured hybrids samples, since it causes a dramatic reduction in Tg values. On the contrary, in the Jeffamine-based samples the Tg is markedly increased with respect to the neat epoxy due to their particular organic-inorganic morphology.
- ✓ The Jeffamine is able to bond two neighbouring siloxane cages, then building up a co-continuous organic-inorganic structure, as the siloxane amount increases.

This research opens wide the doors to further studies on the correlation between the cage-like siloxane structures and the macroscopic properties of hybrids samples, enabling to tailor the siloxane inorganic morphology and then obtain nano-heterogeneous systems with desired and tunable properties.

Curriculum Vitae

Filomena Piscitelli was born in Caserta, Italy, on the 9th December 1976.

She received her master degree in Industrial Chemistry in 2004 with 110/110. Since 2004 she has been collaborating with Italian National Council, at Institute for Composite and Biomedical Materials (IMCB) working on epoxy based hybrids and composites.

Her main research interest field is the sol-gel process and SAXS characterization.

Selected publications

F. Piscitelli, G. Barra, L. Mascia, G. Mensitieri, M. Lavorgna, "Hybrid-nanocomposite materials: Effects of Nature of Epoxy resins and Siloxane Component", Special Topics on materials Science and Technology-The Italian Panorama, BRILL Leiden Boston **2009**, ISBN 9789004172241, 329-338, 2009.

M.Lavorgna, L.Fusco, F.Piscitelli, G.Mensitieri, P.Agoretti, A.Borriello, L.Mascia "Control of morphology of sulfonated syndio-polystyrene membranes through constraints imposed by siloxane networks", Polymer Engineering and Science, 48(12), **2008**, p 2389-2399.

G. Faiella, F. Piscitelli, M. Lavorgna, V. Antonucci, M. Giordano, "Tuning the insulator to conductor transition in a multi walled carbon nanotubes/epoxy matrix composite at sub statistical percolation threshold", Applied Physics Letters, 95, 153106, **2009**.

M.Lavorgna, F.Piscitelli, P.Mangiacapra, G.G. Buonocore "Study of the combined effect of both clay and 1 glycerol plasticizer on the properties of chitosan films" Carbohydrate Polymers .82(2), 291-298 **2010**

F.Piscitelli, P.Posocco, R.Toth, M.Fermeglia, S.Pricl, G.Mensitieri, M.Lavorgna "Sodium Montmorillonite silylation: unexpected effect of the aminosilane chain length", Journal of Colloid and Interface Science, 351, 108-115, **2010**.

Barra G., Lavorgna M., Mensitieri G., Piscitelli F. "Polimeri rinforzati con fibre, composizioni polimeriche a base epossidica e loro impiego" patent Mi2009a001980, 12/11/**2009**

Y. H. Zhan, R. Patel, M. Lavorgna, F. Piscitelli, A. Khan, H. S. Xia, H. Benkreira and P. Coates, "Processing of polyurethane/carbon nanotubes composites using novel minimixer" Plastics Rubber and Composites, vol 39, n° 9, 400-410, **2010**

Journal of Colloid and Interface Science 351 (2010) 108–115

Contents lists available at ScienceDirect

Journal of Colloid and Interface Science

www.elsevier.com/locate/jcis

Sodium montmorillonite silylation: Unexpected effect of the aminosilane chain length

Filomena Piscitelli [a,b,*], Paola Posocco [c], Radovan Toth [c], Maurizio Fermeglia [c], Sabrina Pricl [c], Giuseppe Mensitieri [a], Marino Lavorgna [b,d]

[a] Department of Materials Engineering and Production, University of Naples Federico II, Piazzale Tecchio 80, 80125 Naples, Italy
[b] National Research Council, Institute for Composite and Biomedical Materials, Piazzale E. Fermi, 1, 80155 Portici, Naples, Italy
[c] Molecular Simulation (MOSE) Engineering Laboratory, DMRN, University of Trieste, Piazzale Europa 1, 34127 Trieste, Italy
[d] IMAST Technological District on Polymeric and Composite Materials Engineering and Structures, Piazzale E. Fermi 1, 80155 Portici, Naples, Italy

ARTICLE INFO

Article history:
Received 25 May 2010
Accepted 24 July 2010
Available online 1 August 2010

Keywords:
Organosilane
Na-MMT silylation
Molecular dynamics simulations

ABSTRACT

In this work, the silylation of sodium montmorillonite (Na-MMT) was performed in glycerol using 3-aminopropyltriethoxysilane, N-(2-aminoethyl)-3-aminopropyltrimethoxysilane and 3-[2-(2-aminoethylamino)ethylamino]-propyl-trimethoxysilane. The effects on the *d*-spacing of sodium montmorillonite (Na-MMT) upon reaction with three aminosilanes of different chain length were studied in details by combining experimental and computational techniques. Infrared spectroscopy was used to monitor the grafting process, while the degree of grafting was calculated using thermogravimetric analysis. X-ray diffraction experiments were carried out to evaluate the shift of the (0 0 1) basal spacing. It was found that the degree of silylation of Na-MMT increases with increasing the length of the aminosilane organic moieties, the overall aminosilane concentration, and temperature. The same beneficial effects were observed on the silicate *d*-spacing, as its value increases with increasing silane concentration and reaction temperature. Remarkably, however, increasing the length of the organic chains in the silane modifiers resulted in decreasing values of the Na-MMT interlayer distance. A rationale for this behavior is proposed on the basis of atomistic molecular dynamics simulation evidences.

1. Introduction

Because of their unique structure, layered silicates are largely employed in the production of polymer nanocomposites with improved physical properties with respect to the pristine polymeric matrix [1–3]. Enhanced mechanical-, thermal- and gas-barrier properties can indeed be achieved by adding small amounts of clay (<5% by weight) to a given polymer, and this in fact opens new avenues in the design and synthesis of a plethora of new, high-performance materials for which an array of advance applications can easily be envisaged. Montmorillonite (MMT) is one of the layered silicates currently most widely employed in the production of polymer–clay nanocomposites [1–3]. The crystalline structure of MMT is based on a regular arrangement of silicon tetrahedra (SiO_4^{4-}) and aluminum octahedra ($Al(OH)_6^{3-}$), the unit cell containing two tetrahedral and one octahedral layers. MMT layer has permanent negative charge on the surface of its layers because of isomorphous substitutions of Mg^{2+} for Al^{3+} or, rarely, Al^{3+} for Si^{4+} [3]. These negative charges are counterbalanced by the presence of first-group cations such as sodium or potassium, which locate in the proximity of the clay platelets within the gallery space [1]. The presence of these net charges then confers to the pristine structure of, i.e., sodium MMT (Na-MMT) a highly polar nature, and this, in turn, renders this silicate quite incompatible with the vast majority of organic polymers [2,3]. Accordingly, a simple dispersion of Na-MMT in a polymeric matrix will not produce a composite with improved properties compared to the neat macromolecule, because of the poor interfacial interactions between the Na-MMT hydrophilic reaction sites and the highly hydrophobic polymeric chains. Therefore, chemical modification of internal and external Na-MMT platelets plays a crucial role in polymer/clay nanocomposite formation. Several efforts have been done in order to reduce the hydrophilicity of the Na-MMT internal platelets; in particular the cation exchange reaction with a quaternary ammonium salt (see for example the case of Cloisite 30B) represents the most commonly used method to modify clay surface. This modification increases the interlayer spacing and creates a more favorable organophilic environment. However, the thermal instability of conventional ammonium ion-modified clay is a strong limitation for melt-compounding of polymer/organoclay composites. In fact, most of the

* Corresponding author at: Department of Materials Engineering and Production, University of Naples Federico II, Piazzale Tecchio 80, 80125 Naples, Italy. Fax: +39 (0) 81 775 88 50.
E-mail address: Filomena.Piscitelli@imcb.cnr.it (F. Piscitelli).

0021-9797/$ - see front matter © 2010 Elsevier Inc. All rights reserved.
doi:10.1016/j.jcis.2010.07.059

alkyl ammonium surfactants are known to undergo a degradation process at temperature at which the plastics are commonly processed [4]. For this reason, the silylation approach involving direct grafting reaction by using a coupling agent has recently attracted much attention, and represents a viable method to make compatible inorganic platelets and organic matrix [5–10]. The presence of broken bonds on the platelet edges are common for layered silicates, and leads to the formation of hydroxyl groups, which can be utilized for chemical modification by silylation reaction. By using an organosilane, it is then possible to covalently bond the organic functional groups onto the layer surface. Importantly, the functionalization of clay minerals with organosilanes can take place at three different sites: at the interlayer space, at the external surface and at the edges [11,12].

In terms of performances of silane-modified MMT nanocomposites, Zhao et al. [13] found that the use of chlorosilane-modified clay allowed the improvement of the mechanical behavior of polyethylene (PE)-based nanocomposites determining an increase of both glass transition temperature and elastic modulus in the glassy region. In particular, after trimethylchlorosilane (TMSCl) modification, the OH groups at the edge of clay platelets were reacted and the wetting ability between PE and organoclay was subsequently improved. Moreover, the loss of hydroxyl groups resulted in a decrease of cation exchange capacity (CEC), which caused a reduction in the strength of interaction between the platelets. Both these effects favorably concurred to improve the intercalation of PE into interlayers.

So far the silylation reaction has been widely performed using (3-aminopropyl)trimethoxysilane (A1100), TMSCl and glycidyl-propyl-triethoxysilane (GPTS) [12] as coupling agents. Among several investigations, it is here mentioned the work of Wang et al. [14], which found that Na-MMT modified by a small amount of A1100 as coupling agent is able to promote a high extent of exfoliation for epoxy/clay nanocomposites. However, to the best of our knowledge, the effects of other aminosilanes on the MMT final basal spacing have not been evaluated yet.

Accordingly, in this paper the silylation reaction of Na-MMT with three aminosilanes, each bearing three functional groups but characterized by different lengths of the alkyl chains, has been studied. The functionalized clay has been characterized by Fourier transform infrared spectroscopy (FT-IR), thermogravimetric analysis (TGA) and X-ray diffraction. In order to understand the effect of reaction conditions (e.g., reaction temperature and aminosilane concentration), two different routes were followed in performing the Na-MMT silylation reaction by using the A1100 as a proof-of-concept. The results obtained in terms of modified Na-MMT *d*-spacing were correlated with the corresponding values predicted from atomistic molecular dynamics simulations, and a molecular rationale for these experimental evidences has been formulated on the basis of the molecular modeling results.

2. Experimental

2.1. Materials

Sodium montmorillonite (Na-MMT) with cationic exchange capacity (CEC) of 92 mequiv/100 g was purchased from Southern Clay Products Inc., USA. Prior to its use, the Na-MMT was dried over night at 90 °C in *vacuum* conditions. 3-aminopropyltriethoxysilane (A1100), N-(2-aminoethyl)-3-aminopropyltrimethoxysilane (A1120), and 3-[2-(2-aminoethylamino)ethylamino]-propyl-trimethoxysilane (A1130) were obtained from GE Advanced Materials. All trifunctional silylating agents had a purity of 98%. Glycerol was purchased from Fluka. All chemicals were used as received.

2.2. Silylation reaction

To perform the silylation reaction of Na-MMT by aminosilanes, two different reaction conditions were used, in which both the reaction temperature and the amount of the aminosilane were varied, respectively. These two experimental routes, referred to, in the following as *Procedure 1* and *Procedure 2*, are summarized in Table 1.

Dried Na-MMT (1 or 5 g) were added to 100 ml of glycerol, and the resulting suspension was stirred at 60 °C for 30 min in nitrogen atmosphere. The same procedure was used to dissolve the aminosilane in glycerol. In this work glycerol was selected as the solvent, since, recently, Shanmugharaj et al. [11] verified that, using high surface energy solvents, the interaction between aminosilanes and the edges of the clay platelets is reduced due to low wetting phenomena and, hence, the silane molecules can diffuse and react more efficiently in the mineral galleries.

The resulting Na-MMT dispersion and aminosilane solutions were then mixed, and the grafting reactions were carried out at 80 or 130 °C, under constant stirring for 3 h under nitrogen. After cooling, the reaction product was recovered by centrifugation at 13,000 rpm, and stabilized at 100 °C for 5 h in *vacuum* condition. Excess glycerol was removed by washing each reaction product with water under stirring at 60 °C for 1.5 h followed by centrifugation. This washing procedure was repeated three times, and the quantitative elimination of the solvent was confirmed by thermogravimetric analysis. Each resultant product was dried at 80 °C under *vacuum* and then ground to a powder. Procedure 1 was performed on all three aminosilanes, whereas Procedure 2 was carried out only in the case of A1100. In order to study the effect of the two silylation conditions on the final products, the interlayer spacings of the A1100-modified Na-MMTs obtained from the two procedures, were compared.

In order to determine the degradation temperatures of the silylated Na-MMT, two pastes with water and glycerol as dispersing agents were prepared to be tested by thermogravimetric analysis. In details, the Na-MMT/water paste (Na-MMT–H_2O) was obtained by dispersing Na-MMT powder in glycerol at 60 °C and then following the same procedure illustrated previously for the silylation reaction but without the addition of the aminosilane. The paste with glycerol (Na-MMT–Gly) was prepared by dispersing Na-MMT in glycerol at 60 °C. After centrifugation, the paste was kept in the oven for 22 h at 60 °C in *vacuum* condition.

2.3. Instrumental analyses

2.3.1. Fourier transform infrared analysis

Fourier transform infrared (FT-IR) spectra were performed by using a Nicolet FT-IR Fourier transform infrared spectrometer on KBr pressed disks containing 1% w/w of inorganic samples. FT-IR spectra were collected over the range 400–4000 cm^{-1} with a resolution of 4 cm^{-1}.

2.3.2. Thermogravimetric analysis

Thermogravimetric analysis (TGA) was carrying out on a TGA 2950 thermobalance (TA Instruments). Samples were heated from

Table 1
Reaction conditions adopted during the silylation process.

Procedure	Amount of Na-MMT in 100 ml of glycerol (g)	Amount of aminosilane in 100 ml of glycerol (g)	Reaction temperature (°C)
1	1	1	80
2	5	20	130

30 to 750 °C at a heating rate of 10 °C/min under nitrogen flow. The amount of grafted and intercalated aminosilanes was calculated using the following relationship [6]:

$$\text{Silane grafted amount (mequiv/g)} = \frac{10^3 \times W_{200-600}}{[100 - (W_{200-600})] \times M} \quad (1)$$

where $W_{200-600}$ corresponds to the mass loss between 200° and 600 °C and M (g/mol) is the molecular weight of the grafted silane molecules. The percentage of grafted amount, which corresponds to the percentage of organic aminosilane moieties with respect the total inorganic mass, was calculated as follows:

$$\text{Silane grafted amount (\%)} = \frac{100 \times W_{200-600}}{100 - W_{200-600}} \quad (2)$$

2.3.3. Wide angle X-ray diffraction analysis

The intergallery space between the clay platelets is defined as the basal spacing, and is usually denoted as d_{001} since it is derived from the (0 0 1) diffraction peak by using Bragg equation. The displacement of the (0 0 1) diffraction peak upon silylation was followed by WAXD measurements. To this end, an Anton Paar SAXSess diffractomer operating at 40 kV, 50 mA and equipped with a Cu Kα radiation (λ = 0.1542 nm) source and an image plate detector was used. The spectra were collected in the transmission mode. The scattering data were dark current and background subtracted, and normalized for the primary beam intensity.

2.3.4. Molecular dynamics analysis

All molecular dynamics (MD) simulations were performed using *Materials Studio* (v.4.4, Accelrys, San Diego, USA). The starting structure of Na-MMT was taken from previous work [15–19]. The main object of the computational part of this study was the prediction of the basal spacing in the aminosilane functionalized MMT. Since the quantities affecting the MMT basal spacing are highly sensitive to the non-bonded components of the force field (FF) employed (e.g., atomic charges and van der Waals parameters), the *ad hoc* FF developed by Heinz and coworkers [20,21] was adopted for the optimization of the initial MMT structure and in all subsequent calculations. As demonstrated by Heinz et al. [20,21] for Na-MMT and other phyllosilicates, this accurately derived FF is able to describe, among many other properties, the thermodynamics of surface processes more reliably by reducing deviations of 50–500% in surface and interface energies to less that 10%, thus constituting a fundamental step towards a quantitative modeling of interface processes involving layered silicates.

Accordingly, the resulting lattice of the optimized MMT model was monoclinic, with space group C2/m, and characterized by the following lattice parameters: a = 5.20 Å, b = 9.20 Å, c = 10.13 Å, and $\alpha = 90°$, $\beta = 99°$, $\gamma = 90°$, in excellent agreement with the available literature [21–24].

According to the computational recipe adopted, the molecular models of the aminosilane compounds considered (see Scheme 1) were built and geometry-optimized following a well-validated MD-based protocol [15–19,32].

The optimized MMT unit cell model was then modified by grafting the layers with a suitable number of aminosilane molecules [15]. For each aminosilane, three possible options were considered for creating covalent bonds between the silicon (Si) atoms of the aminosilane and the MMT surface oxygen (O) atoms, as illustrated in Scheme 2.

The new equilibrium position of the Na^+ counterions on the aminosilane-modified MMT sheets were determined following the procedure suggested by Heinz et al. [21]. Accordingly, half of them were placed 1 nm away on one side, and the remaining half 1 nm from the other side of the MMT layer in 10 different arrangements. Molecular mechanics energy minimizations were then performed to convergence, keeping all other MMT atoms fixed, and the structure with the lowest energy was finally selected for further simulations. In this configuration, the Na^+ ions were found at about 1.8 Å from the center of the surface oxygen atoms, or

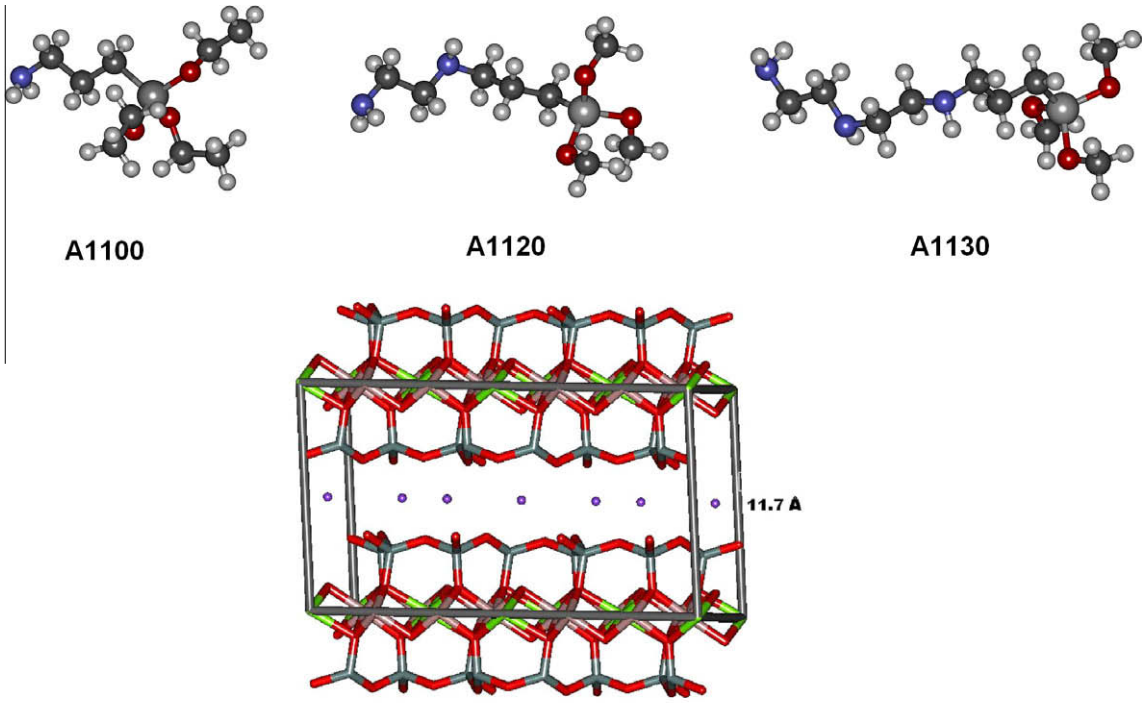

Scheme 1. Chemical structures of the considered aminosilanes and crystallographic unit cell of MMT. The atom color code is as follows: gray, C; light gray, Si; blue, N; red, O, white, H; purple, Na; green, Al; pink, Mg. (For interpretation of the references to color in this figure legend, the reader is referred to the web version of this article.)

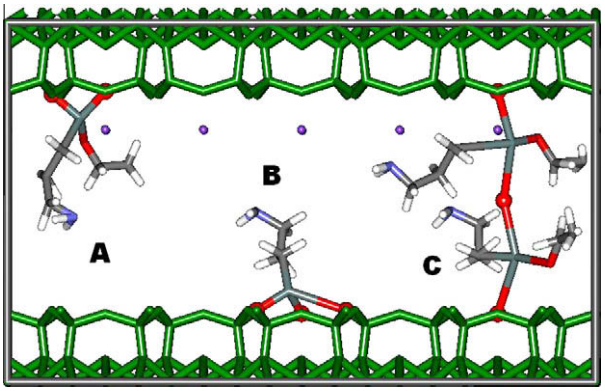

Scheme 2. Schematic representation of possible covalent bonds formation between the Si atoms of the aminosilane molecules and the MMT surface O atoms. A: two covalent bonds on the same MMT surface; B: three covalent bonds on the same MMT surface; C: two covalent bonds bridging two MMT layers.

about 4.8 Å from the central plane of the metal atoms, in excellent agreement with previous simulations [33] and experimental NMR data [34].

Lastly, each aminosilane-MMT unit cell was replicated four times in the *a* direction, and three times in the *b* direction, thus yielding a final simulation supercell for each aminosilane modifier with the following lattice parameters: $a = 20.80$ Å, $b = 27.60$ Å, and $\alpha = 90°$, $\beta = 99°$, $\gamma = 90°$. The *c* values in the initial model of aminosilane-MMT supercells were prolonged according to a bi-layer arrangement of each aminosilane molecules.

Molecular mechanics (MM) and molecular dynamics (MD) simulation protocols were then applied, consisting of a preliminary cell energy minimization procedure followed by isobaric-isothermal (NPT) MD runs at 300 K. To avoid crystal structure deformation during minimization, initially both MMT layers were treated as rigid bodies by fixing all cell dimensions except the *c* axis, whilst all atoms in the interlayer space including the cations were allowed to move without any constraint. Then, in a second minimization round, also movement along the *c* axis was allowed, leading to a suitable starting interlayer distance for each model. Subsequently, 1 ns NPT MD experiments were performed at 300 K for each system, using the Verlet algorithm and an integration step of 1 fs. Again, both MMT layers were treated as rigid bodies by fixing all cell dimensions except the *c* axis, leaving all remaining atoms in the interlayer space free to move without any constraint. The Ewald summation method [35] was applied for treating both van der Waals and electrostatic interactions, while temperature was controlled using the Nosé thermostat [36].

The final basal spacing values for each aminosilane-MMT system were extracted from the final part (0.5 ns) of the equilibrated MD trajectory.

3. Results and discussion

3.1. Fourier transform infrared analysis

Infrared spectroscopy was performed in order to verify the silylation process and to identify the presence of the organic moieties on the Na-MMT platelets due to silylation. As pointed out by Zhao et al. [13], the main evidence for the successful intercalation/silylation of the aminoalkylsilanes in the Na-MMT galleries is the presence of C–H and N–H absorbance peaks in the corresponding IR spectra. Fig. 1 shows an enlargement of the IR between 3800 and 2500 cm^{-1} for the A1100-MMT sample using the two different procedures described above. In the same figure, the spectra of the

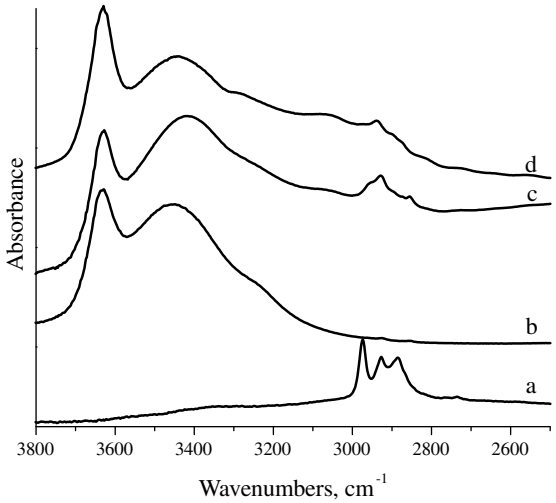

Fig. 1. Infrared spectra of: (a) A1100; (b) pristine Na-MMT; (c) A1100-MMT obtained from Procedure 1; (d) A1100-MMT obtained from Procedure 2.

A1100 silane molecule and the pristine Na-MMT are also shown for comparison.

Compared to the neat Na-MMT spectrum, the two functionalized powders show additional peaks which can be attributed to the asymmetric and symmetric stretching vibrations of the methylene groups at 2936 and 2885 cm^{-1}, respectively, thus confirming the presence of the organic moieties on the Na-MMT surface [25–27]. A shoulder at ~3290 cm^{-1} in Fig. 1 may be assigned to the stretching of the NH_2 group [28]. It is worth noting that, by increasing the aminosilane concentration and the reaction temperature, both methylene and NH_2 adsorption peaks in Fig. 1 become progressively more pronounced, suggesting the presence of a larger amount of intercalated/grafted silane modifiers. No evaluation was performed on the relative intensity of the peaks related to the stretching vibration of isolated or hydrogen bonded OH groups (at 3620 cm^{-1} and 3440 cm^{-1}, respectively), because the possible presence of adsorbed water cannot be ruled out [29].

3.2. Thermogravimetric analysis

Thermogravimetric analysis (data not shown) was carried out on the Na-MMT powders prior and after the silylation reaction performed by Procedure 1. The mass losses in the range between 200° and 600 °C were used as entry parameters in Eqs. (1) and (2) to evaluate the grafted aminosilane amounts, and the corresponding results are displayed in Table 2. Interestingly, by the application of Procedure 1 the grafted aminosilane amounts increase with increasing of the aminosilane alkyl chain.

Table 2
Thermogravimetric analysis of functionalized MMT.

		Mass loss[a] (%)	Grafted amount[b] (mequiv/g)	Grafting amount[c] (%)
A1100-MMT	Procedure 1	8.8	0.4 (I = 68%; S = 32%)	9.6
	Procedure 2	11.4	0.6 (O = 21%; I = 38%; S = 41%)	12.8
A1120-MMT		14.6	0.8	17.1
A1130-MMT		18.8	0.9	23.2

[a] Mass loss between 200° and 600 °C.
[b] Determined by using Eq. (1).
[c] Determined by using Eq. (2).

In order to identify the degraded species, two pastes obtained by dispersing the Na-MMT in water and glycerol, respectively, were analyzed. The results are displayed in terms of first derivative mass loss in Fig. 2.

The pristine Na-MMT shows two Fig. 2 peaks at 50 and 630 °C corresponding to the physically adsorbed water and the dehydroxylation of the clay, respectively [30,31]. The curve related to the Na-MMT–H_2O paste shows a peak at 50 °C related to the loss of physically adsorbed water, whereas the two other peaks at 270 and 358 °C (Fig. 2) can be sensibly ascribed to the loss of intercalated water. By analogy, the intense Fig. 2 peak at 215 °C in the Na-MMT–Gly curve could be assigned to the loss of physically adsorbed glycerol, whilst the weak Fig. 2 peak at ~350 °C could refer to the intercalated glycerol. As for the Na-MMT–H_2O paste, the Fig. 2 peak at higher temperature is due to MMT dehydroxylation. The DTG curves of the A1100-MMT system shows the mass loss of physically adsorbed water at 50 °C, and other two Fig. 2 peaks at 418 and 540 °C, respectively. The first one is ascribable to the intercalated aminosilanes, whereas the broad Fig. 2 peak at 540 °C could be linked to the decomposition of the chemically bound aminosilanes [9]. Due to the consumption of hydroxyl groups belonging to the platelet edges, the Na-MMT dehydroxylation Fig. 2 peak at 630 °C nearly vanishes for this system. Lastly, the absence of the Fig. 2 peak at 215 °C related to the physically adsorbed glycerol speaks in favor of the reliability of the applied washing procedure.

With the goal of evaluating the effect of the reaction parameters (i.e. temperature and aminosilane concentration) on the silylation process, the amount of intercalated and grafted aminosilane was assessed by performing TGA analysis on the A1100-MMT systems obtained by using the two different reaction routes summarized in Table 1. To eliminate the different contributes due to dissimilar adsorbed amounts of water, the curves shown in Fig. 3 A were normalized assigning to each curve the value of 100 to the mass achieved at 150 °C. It is worth noting that, as we will discuss later, by increasing both temperature and aminosilane concentration, the quantity of aminosilanes able to penetrate into the Na-MMT gallery platelets slightly increases. Moreover, the grafted aminosilane amount increased by using the Procedure 2 compared to Procedure 1 (see Table 2). The DTG analysis performed on the A1100-MMT product obtained by Procedure 1 (Fig. 3 B)) shows the presence of two peaks at 418 and 540 °C, ascribed to the intercalated aminosilanes and chemically bounded aminosilanes, respectively [9].

Interestingly, the A1100-MMT product prepared following Procedure 2 displays a third Fig. 3B peak at 310 °C, which could be attributed to the aminosilane interacting with the outer surfaces of the clay platelets.

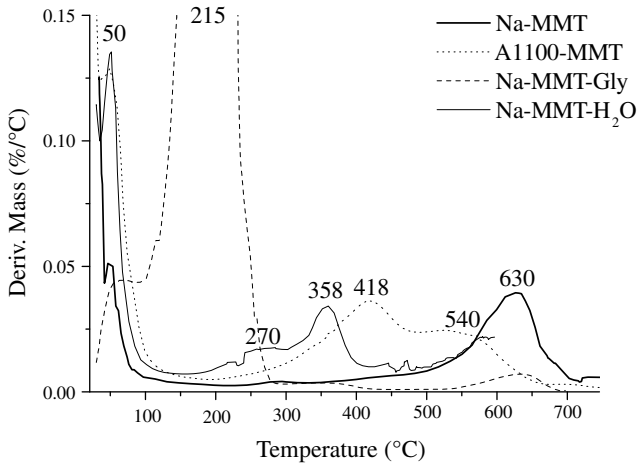

Fig. 2. DTG curves of pristine Na-MMT, functionalized Na-MMT powders, and Na-MMT/water and Na-MMT/glycerol pastes.

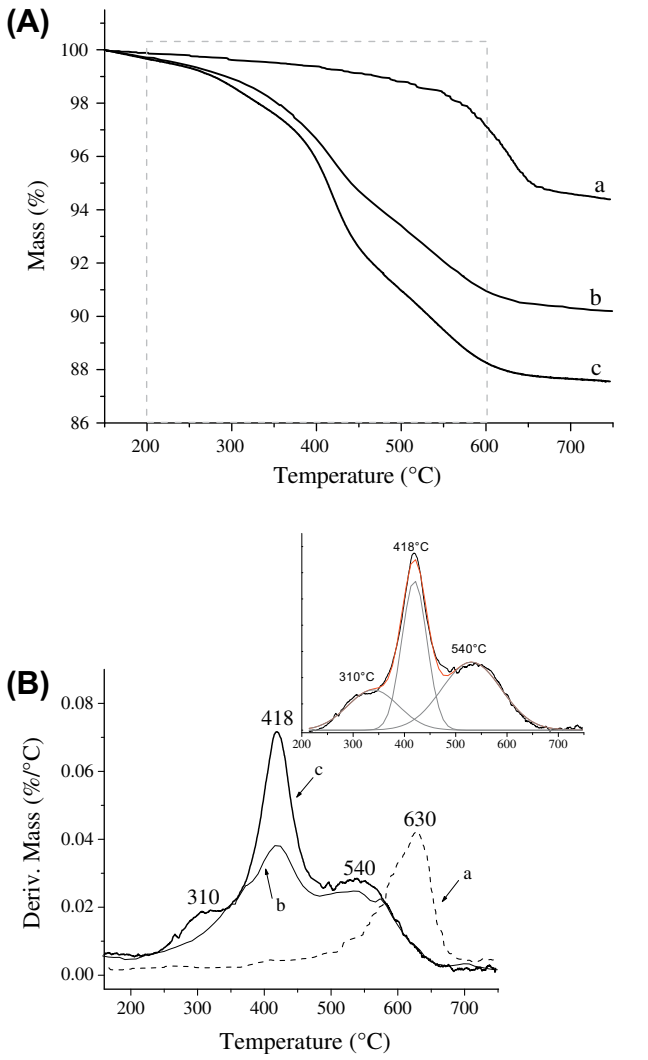

Fig. 3. Thermogravimetric analysis of Na-MMT before and after silylation reaction using two different process parameters: (A) mass losses curve; (B) first derivative of mass losses curve. The inset shows the peak deconvolutions: (a) pristine Na-MMT; (b) A1100-MMT obtained from Procedure 1; (c) A1100-MMT obtained from Procedure 2.

With these peaks assignments in mind, it was possible to quantify each degraded moieties using the deconvolution method of the Origin program. The results of these deconvolutions are summarized in Table 2, where *O* indicates the aminosilane interacting with the outside platelets, and *I* and *S* are the intercalated and chemically bonded aminosilanes, respectively. The results show that higher temperature and aminosilane concentration values lead to an increased amount of chemically bonded silanes with respect to the intercalated species. Moreover, and perhaps more interestingly, only the A1100-MMT obtained by Procedure 2 displays aminosilanes interacting with the outside platelets.

3.3. Wide angle X-ray diffraction results and molecular dynamics predictions

To quantify the effect of the length of the aminosilane alkyl substituents on the Na-MMT basal spacing, silylation reactions were performed using the three different aminosilanes A1100, A1120 and A1130, and adopting Procedure 1. The X-ray diffraction

patterns related to the (0 0 1) basal spacing, displayed in Fig. 4, show that the introduction of any aminosilane type into the Na-MMT gallery shifts the peak at lower 2θ values compared to the pristine Na-MMT.

This increase of basal spacing is a clear signal that each aminosilane species has been grafted/intercalated in the inter-platelets space of Na-MMT. In detail, the neat Na-MMT shows a Fig. 4 peak at 2θ equal to 7.5°, corresponding to a *d*-spacing value of 11.7 Å, whereas the aminosilane-modified MMTs show Fig. 4 diffraction peaks at 2θ values between 5.3° and 5.9° (Table 3). Concerning the effect of the alkyl chain length, the A1120-MMT and A1130-MMT systems show lower basal spacing values, 15.3 and 15.0 Å, respectively, compared to the A1100-MMT, for which d_{001} = 16.7 Å. A major, important conclusion which can be drawn from the analysis of data shown in Table 3 is that the longer the organic chain on the aminosilane molecules, the smaller the *d*-spacing in the relevant modified MMT.

To try to find a molecular rationale for the somewhat counter-intuitive behavior reported above, molecular dynamics (MD) simulations have been performed on model systems.

Table 4 shows the values of estimated aminosilane-MMT interlayer spacing for all model systems considered (see Scheme 1) as obtained from 1 ns NPT MD simulations. From these values, and the inspection of the relevant MD trajectories, we can draw some useful considerations.

First of all, independently of the aminosilane chain length, aminosilane molecules bridging two MMT layers (i.e., option C in Scheme 2) result in the lowest *d*-spacing values (see Table 4). From the viewpoint of further employment of aminosilane-MMT systems for polymer intercalation and/or exfoliation, this is the worst case possible, as the distance between MMT sheets is not only practically coincident with that of unmodified MMT (i.e., 11.7 Å), but also the aminosilane molecules act as 'anchoring points", counteracting any eventual macromolecular intercalation/exfoliation. Fig. 5 shows an equilibrated MD snapshot of the A1100-MMT/option C system as an example.

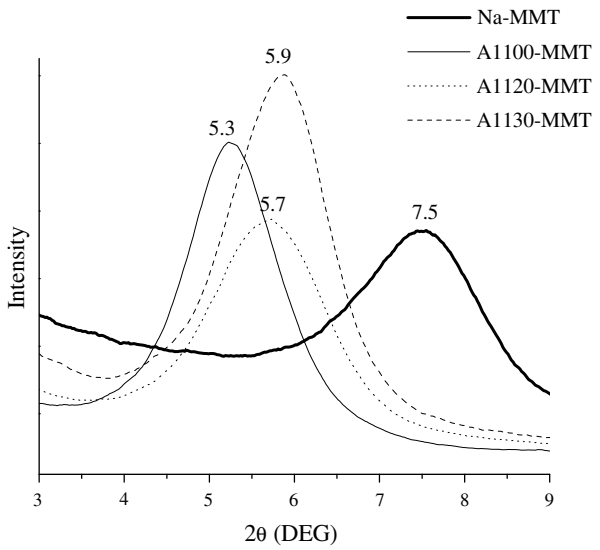

Fig. 4. X-ray diffraction patterns of Na-MMT before and after silylation reaction with different aminosilanes.

Table 3
d-Spacing values for aminosilane-modified MMT estimated by XRD analysis.

System		2θ (°)	*d*-Spacing (Å)
Pristine Na-MMT	Procedure 1	7.5	11.7
A1100-MMT	Procedure 2	5.3	16.7
		4.0	22.2
A1120-MMT		5.7	15.3
A1130-MMT		5.9	15.0

Table 4
d-Spacing values for aminosilane-modified MMT estimated by MD simulations.

System	*d*-Spacing (Å)			
	Option A[a]	Option B[a]	Average A and B	Option C[a]
A1100-MMT Procedure 1	17.0	16.2	16.6	11.7
A1100-MMT Procedure 2	21.9	21.7	21.8	11.7
A1120-MMT	15.9	15.3	15.6	11.9
A1130-MMT	15.1	14.8	14.9	11.9

[a] For the meaning of Options A–C, please refer to Scheme 2.

The results obtained for the two alternative bonding options (i.e., A and B in Scheme 2), expressed as average *d*-spacing values (see 3rd column in Table 4), are in excellent agreement with the experimental evidences discussed above. Notably, however, in contrast to common observations during the intercalation of small molecules between the silicate layers, where longer organic chains normally result in higher interlayer spacing, for aminosilane-MMT systems a reverse trend is observed. Indeed, longer aminosilane molecules yield lower *d*-spacing.

A sensible explanation for this coupled experimental/simulation evidence could be hypothesized, keeping in mind that the organic tail of each aminosilane molecule features not only $-CH_2$ groups, which are hydrophobic, but also one or more $-NH_2$/NH– groups, which are endowed with hydrophilic character, and capable to originate both intra- and inter-molecular hydrogen bonds (see Scheme 1).

Following these lines of reasoning, for the smaller aminosilane molecule A1100, characterized by the presence of a short chain and only one terminal $-NH_2$ group, a mechanism quite similar to that observed for quaternary ammonium salt-modified MMT can be envisaged. Accordingly, the A1100 aminosilane chains are attracted by the surface of clay and, while flattening onto it, provide a screening between the charges of the MMT layers ultimately favoring the weakening of interlayer attraction and, hence, a larger *d*-spacing value.

On the other hand, the other two aminosilane molecules (A1120 and A1130), featuring longer, more mobile chains with one and two –NH groups, respectively, have a strong tendency to interact among themselves (*via* both intermolecular hydrogen bonding and hydrophobic interactions). As a result, their flattening onto the MMT surface is reduced, the charge distribution on the MMT

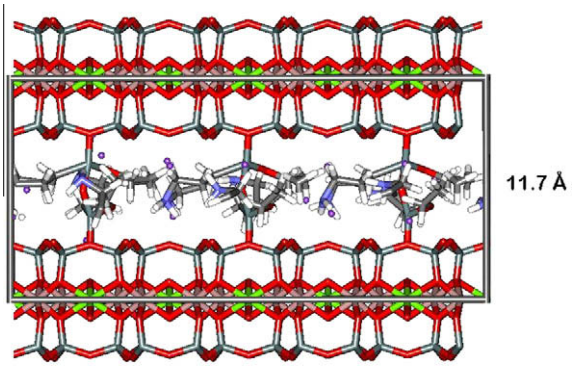

Fig. 5. Equilibrated MD snapshot of the A1100-MMT/option C system (see Scheme 2).

surface is less screened, and the clay sheets do not tend to separate as much as in the case of A1100 chains. Fig. 6a and b show a comparison between two equilibrated MD snapshots for A1100-MMT and A1120-MMT, respectively, in which the different degree of interactions between the aminosilane chains, resulting in a smaller *d*-spacing, is well evident.

The A1100-MMT system was further selected to check the effect of the preparation procedure adopted. Fig. 7 shows the diffraction patterns related to the A1100-MMT obtained by using the two procedures summarized in Table 1.

For the sake of comparison, the diffraction pattern of the pristine Na-MMT is also reported. In details, the silylation reaction with A1100 by Procedure 2 resulted in a further shift of the (0 0 1) diffraction peak up to $2\theta = 4.0^{\circ}$, corresponding to a *d*-spacing value of 22.2 Å, with respect to that obtained with the silylation by Procedure 1 (16.7 Å). It is worth noting that the highest reaction temperature and aminosilane concentration (i.e. Procedure 2) allowed obtaining a higher enlargement of the basal spacing. Moreover, the broader Fig. 7 (0 0 1) diffraction peak reflects the variety of platelets gallery heights due to the grafted/intercalated products.

In harmony with the experimental findings, the MD simulations reveal that, upon increasing the number of aminosilane molecules within the clay galleries indeed results in a larger value of the estimated *d*-spacing, which, in turn, is in excellent agreement with the corresponding experimental evidence (see values in Tables 2 and 3). Fig. 6c yields pictorial evidence in support to the numerical value. As can be easily seen by comparing Fig. 6a and c, when more aminosilane molecules are grafted/intercalated into the clay galleries the surface of the MMT layers is better screened by the silane hydrocarbon chains. Accordingly, the attraction forces among the layers are weakened, and the resultant distance between them is higher. Not only, but, in the presence of higher silane concentration, the hydrocarbon chains of neighboring molecules grafted/physical bounded to the same clay layer tend to interact more among themselves than with those laying on the opposite sheet. And this factor further concurs to lessen the overall attraction between facing sheets and, hence, a higher d_{001} value.

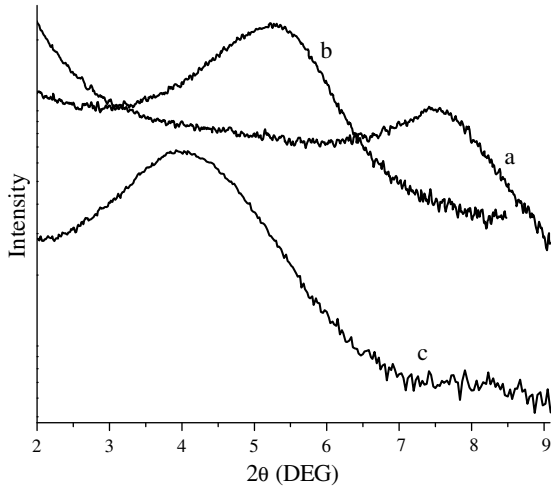

Fig. 7. XRD analyses performed on the Na-MMT before and after silylation reaction carried out using two different process conditions. (a) pristine Na-MMT; (b) A1100-MMT obtained with Procedure 1; (c) A1100-MMT obtained with Procedure 2.

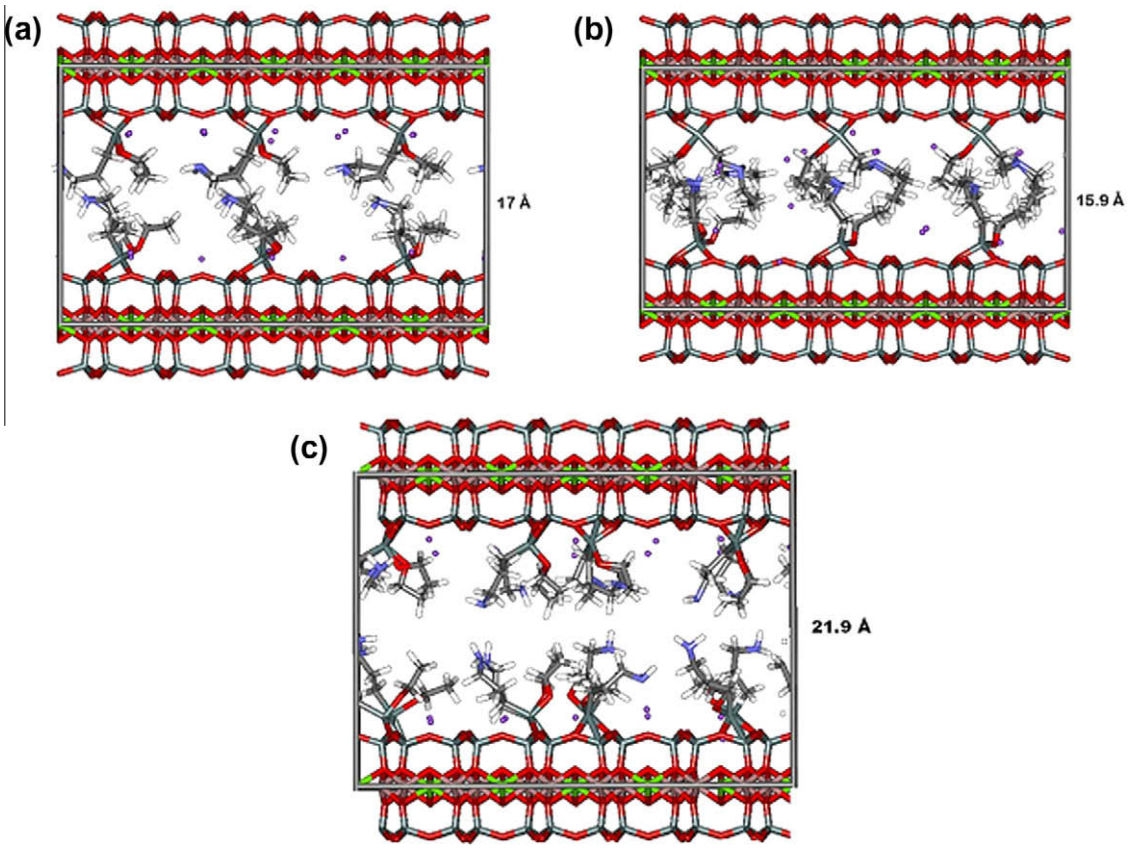

Fig. 6. Equilibrated MD snapshot of (a) A1100-MMT/option A, reaction Procedure 1, (b) A1120-MMT/option A, and (c) A1100-MMT/option A, reaction Procedure 2 systems (see Scheme 2).

4. Conclusions

Three aminosilanes (A1100, A1120 and A1130) characterized by different lengths of the alkyl chains are used to functionalize the Na-MMT, by following two different routes in terms of reaction temperature and aminosilane concentration. The appearance in the FT-IR spectra of additional peaks at 2936 and 2885 cm^{-1}, attributed to the asymmetric and symmetric stretching vibrations of the methylene groups, respectively, and a shoulder at $\sim$3290 cm^{-1} assigned to the stretching of the NH_2 group, confirm the presence of the organic moieties on the Na-MMT surface. The thermogravimetric analyses show that higher temperature and aminosilane concentration values lead to aminosilanes interacting with the outside platelets and an increased amount of chemically bonded silanes with respect to the intercalated species. The WAXD analyses show that the introduction of any aminosilane type into the Na-MMT gallery allows the basal spacing to increase with respect to the pristine Na-MMT, which is a clear signal that each aminosilane species has been grafted/intercalated in the inter-platelets space. Moreover, the WAXD analyses highlight the surprising result that the longer the organic chain on the aminosilane molecules, the smaller the *d*-spacing in the relevant modified MMT. The molecular dynamics simulation explains this result in light of the strong tendency of A1120 and A1130 aminosilanes to interact among themselves by both intermolecular hydrogen bonding and hydrophobic interactions because of the presence of one or two –NH groups in their organic chains. On the other hand the A1100 molecules, owing only one $–NH_2$ group, provide a better screening between the MMT layers ultimately favoring the weakening of interlayer attraction and, hence, a larger *d*-spacing value.

Acknowledgments

The authors thank IMAST and MIUR. This work was supported by the research project MACE coded MIUR n. DM24442.

References

[1] J. Zhang, R.K. Gupta, C.A. Wilkie, Polymer 47 (2006) 4537.
[2] H. Shi, T. Lan, T.J. Pinnavaia, Chem. Mater. 8 (1996) 1584.
[3] S. Yariv, H. Cross, in: Dekker M, (Eds.), Clays and Clay Minerals, New York, 2002. pp. 463–566.
[4] L.A. Utracki, Clay-containing Polymeric Nanocomposites, Rapra Technology Limited Press, Shrewsbury, 2004.
[5] P.A. Wheeler, J. Wang, J. Baker, L.J. Mathias, Chem. Mater. 17 (2005) 3012.
[6] N.N. Herrera, J.M. Letoffe, J.L. Putaux, L. David, E. Bourgeat-Lami, Langmuir 20 (2004) 1564.
[7] A.Y. Park, H. Kwon, A.J. Woo, S.J. Kim, Adv. Mater. 17 (2005) 106.
[8] N. Herrera, J. Letoffe, J. Reymondc, E. Bourgeat-Lami, J. Mater. Chem. 15 (2005) 863.
[9] H. He, J. Duchet, J. Galy, J. Gerard, Colloid. Interface Sci. 288 (2005) 171.
[10] M. Park, I.K. Shim, E.Y. Jung, J.H. Choy, J. Phys. Chem. Solids 65 (2004) 499.
[11] A.M. Shanmugharaj, K.Y. Rhee, S.H. Ryu, J. Colloid Interface Sci. 298 (2006) 854.
[12] A. Di Gianni, E. Amerio, O. Monticelli, R. Bongiovanni, Appl. Clay Sci. 42 (2008) 116.
[13] C. Zhao, M. Feng, F. Gong, H. Qin, M. Yang, J. Appl. Polym. Sci. 93 (2004) 676.
[14] K. Wang, L. Wang, J. Wu, L. Chen, C. He, Langmuir 21 (2005) 3613.
[15] M. Fermeglia, M. Ferrone, S. Pricl, Fluid Phase Equilib. 212 (2003) 315.
[16] R. Toth, A. Coslanich, M. Ferrone, M. Fermeglia, S. Pricl, S. Miertus, E. Chiellini, Polymer 45 (2004) 8075.
[17] G. Scocchi, P. Posocco, A. Danani, S. Pricl, M. Fermeglia, Fluid Phase Equilib. 261 (2007) 366.
[18] M. Fermeglia, M. Ferrone, S. Pricl, Mol. Simul. 30 (2004) 289.
[19] G. Scocchi, P. Posocco, J.W. Handgraaf, J.G.E.M. Fraaije, M. Fermeglia, S. Pricl, Chem. Eur. J. 15 (2009) 7586.
[20] H. Heinz, U.W. Suter, J. Phys. Chem. B 108 (2004) 18341.
[21] H. Heinz, H. Koerner, K.L. Anderson, R.A. Vaia, B.L. Farmer, Chem. Mater. 17 (2005) 5658.
[22] G. Brown, The X-ray Identification and Crystal Structures of Clay Minerals, Mineralogical Society Press, London, 1961.
[23] S.W. Bayley, Reviews in Mineralogy, Mineralogical Society of America Press, Chelsea, Michigan, 1988. <http://www.webmineral.com>.
[24] S.I. Tsipurski, V.A. Drits, Clay Miner. 19 (1984) 177.
[25] K. Endo, Y. Sugahara, K. Kuroda, Bull. Chem. Soc. Jpn. 67 (1994) 3352.
[26] T. Yankgisawa, K. Kurodo, C. Kato, React. Solids 5 (1988) 167.
[27] S. Okutomo, K. Kuroda, M. Ogawa, Appl. Clay Sci. 15 (1999) 253.
[28] I.K. Tonle, E. Ngameni, D. Njopwouo, C. Carteret, A. Walcarius, Phys. Chem. Chem. Phys. 5 (2003) 4951.
[29] E. Ruiz-Hitzky, J.M. Rojo, G. Lagaly, Colloid. Polym. Sci. 263 (1985) 1025.
[30] C. Wan, X. Bao, F. Zhao, B. Kandasubramanian, M.P. Duggan, J. Appl. Polym. Sci. 110 (2008) 550.
[31] S. Yariv, Appl. Clay Sci. 24 (2004) 225.
[32] R. Toth, D.J. Voorn, J.W. Handgraaf, J.G.E.M. Fraaije, M. Fermeglia, S. Pricl, P. Posocco, Macromolecules 42 (2009) 8260.
[33] E. Hackett, E. Manias, E.P. Giannelis, Chem. Mater. 12 (2000) 2161.
[34] D.K. Yang, D.B. Zax, J. Chem. Phys. 110 (1999) 5325.
[35] P.P. Ewald, Ann. Phys. 64 (1921) 253.
[36] S. Nosé, Prog. Theor. Phys. Suppl. 103 (1991) 1–46.